MODELING, DESIGN AND ENERGY MANAGEMENT OF FUEL CELL SYSTEMS FOR AIRCRAFT

A Dissertation
Presented to
The Academic Faculty

by

Thomas Heenan Bradley

In Partial Fulfillment
of the Requirements for the Degree
Doctor of Philosophy in the
School of Mechanical Engineering

Georgia Institute of Technology
December, 2008

MODELING, DESIGN AND ENERGY MANAGEMENT OF FUEL CELL SYSTEMS FOR AIRCRAFT

Approved by:

Dr. David E. Parekh, Advisor
School of Mechanical Engineering
Georgia Institute of Technology

Dr. William J. Wepfer
School of Mechanical Engineering
Georgia Institute of Technology

Dr. Dimitri N. Mavris
School of Aerospace Engineering
Georgia Institute of Technology

Dr. Yogendra Joshi
School of Mechanical Engineering
Georgia Institute of Technology

Dr. Thomas F. Fuller
School of Chemical and Biomolecular Engineering
Georgia Institute of Technology

Date Approved: August 01, 2008

ACKNOWLEDGEMENTS

This research was funded in part by the NASA University Research Engineering Technology Institute (URETI) grant to the Georgia Institute of Technology.

Thanks to my academic advisors David Parekh, Tom Fuller and Dimitri Mavris. I am grateful for all of your generosity in terms of resources and attention and for your dedication to a creative and collaborative learning environment. It was pleasure to be to able to engage with creative and knowledgeable people who work with such infectious enthusiasm. Thanks also to committee members Bill Wepfer and Yogendra Joshi.

Thanks to Blake Moffitt for his tireless collaboration and for providing my introduction to the world of aeronautical engineering. This work would have been impossible without his many contributions.

Thanks to the ASDL for making me one of their own. Thanks to the members of Dr. Fuller's lab for friendship and the inspiration that comes with the most interesting and cross-disciplinary lecture series on campus. Thanks to the GTRI Fuel Cell and Battery Technology faculty, Comas Haynes and Gary Gray for thousands of instances of teaching and research help.

Thanks to Kimberly, without whom none of this could have happened.

Atlanta, Georgia

July 25, 2008

TABLE OF CONTENTS

LIST OF TABLES

Page

LIST OF FIGURES

Page

LIST OF SYMBOLS AND ABBREVIATIONS

A	=	fuel cell active area, cm^2
a	=	sequential unconstrained minimization technique tuning variable
b	=	vector of control variables
C	=	sequential unconstrained minimization technique tuning variable
C_D	=	aircraft coefficient of drag
C_L	=	aircraft coefficient of lift
C_q	=	propeller coefficient of torque
C_{rr}	=	coefficient of rolling resistance
C_T	=	propeller coefficient of thrust
D	=	drag force, N
d	=	propeller diameter, m
D_{rr}	=	drag force due to rolling resistance, N
E	=	propulsive energy, J
$E°$	=	standard potential of the hydrogen oxidation reaction, 1.23V
F	=	Faraday number
f_{mount}	=	hydrogen tank mounting/bosses/tubing mass fraction
g	=	acceleration due to gravity, m/s^2
g	=	side constraint functional
g	=	cost functional
h	=	aircraft altitude, m
h	=	absolute constraint functional

I	=	fuel cell stack current, A
I_b	=	battery current, A
$I_{b\ max}$	=	maximum battery current, A
$I_{b\ min}$	=	minimum battery current, A
I_{sp}	=	specific thrust, N/N
J	=	propeller advance ratio
k	=	ratio of fuel cell stack active area to fuel cell stack mass, cm^2/kg
k	=	discrete index
k	=	slope of compressor performance map, rev/L
K_{flow}	=	feedforward control gain, rpm/A
K_v	=	motor voltage constant, rpm/V
L	=	lift force, N
m	=	aircraft mass, kg
$m_{airframe}$	=	mass of the aircraft airframe, which consists of all components of the aircraft excepting powerplant, kg
$m_{composite}$	=	hydrogen tank composite overwrap mass, kg
$m_{fuelcell}$	=	mass of the fuel cell stack, kg
m_{H2}	=	hydrogen mass, kg
m_{H2tank}	=	mass of the hydrogen storage tank, kg
m_{liner}	=	hydrogen tank liner mass, kg
m_{power}	=	powerplant mass including powertrain, fuel and tankage, kg
m_{reg}	=	regulator mass, kg
MW_{H2}	=	molecular weight of Hydrogen, g/mol

MW_{O2} = molecular weight of Oxygen, g/mol

n_{cells} = number of cells in the fuel cell stack

OEC = optimization overall evaluation criteron

P_{atm} = atmospheric pressure, Pa

P_{FC} = fuel cell power, W

P_{H2} = hydrogen pressure in fuel cell anode manifold, Pa

p_m = cathod manifold pressure, Pa

Q = propeller and electric motor torque, Nm

q_{H2} = flow rate of hydrogen, kg/sec

q_{H2} = cathode resistance limited flow rate of hydrogen, kg/sec

R = optimization objective function

R = universal gas constant

R_{cell} = fuel cell ohmic resistance, Ω

Re = Reynold's number

R_{FC} = pneumatic resistance of the fuel cell stack, Pa min/L

s = range, m

S = vector of states

SOC_i = initial battery state of charge

SOC_i = final battery state of charge

S_{w} = wing area, m^2

t = endurance, hr

t = time, sec

T = thrust force, N

t_{cmd} = throttle command

t_{liner} = hydrogen tank liner thickness, m

t_{PWM} = pulse width modulated throttle command

U = hydrogen utilization of the fuel cell system

u = vector of control variables

v = airspeed, m/s

$V°$ = Nernst potential of the hydrogen oxidation reaction, 1.23V

$v_{desired}$ = desired aircraft velocity, m/s

v_{error} = error in aircraft velocity, m/s

v_{purge} = volume of hydrogen purged in a purge cycle, L

$v_{consumed}$ = volume of hydrogen consumded in a purge cycle, L

V_{FC} = fuel cell potential, V

V_{im} = fuel cell input manifold volume, m^3

W = weight force, N

w = external inputs to optimization routine

W_f = aircraft weight without fuel, N

W_i = initial aircraft weight, N

x = vector of design variables

x_{fs} = hydrogen tank factor of safety to burst

y = vector of contributing analysis variables, vector of states

α = angle of attack, rad

α_{max}	=	stall angle of attack, rad
ΔG	=	change in Gibbs free energy
ΔH	=	change in enthalpy
ε	=	sequential unconstrained minimization technique slack variable
η	=	electrochemical potential, V
$h_{desired}$	=	desired aircraft altitude, m
h_{error}	=	error in aircraft altitude, m
η_{FC}	=	fuel cell efficiency
$\eta_{powertrain}$	=	powertrain efficiency
η_{util}	=	Hydrogen utilization of the fuel cell system
λ	=	bank angle, rad
λ_c	=	cathode stoichiometry
θ_{fc}	=	fuel cell temperature, C
ρ	=	air density, kg/m^3
$\rho_{composite}$	=	hydrogen tank composite overwrap density, kg/m^3
τ	=	time period of periodic optimal control, sec
τ_c	=	pneumatic time constant of cathode, sec
ω	=	propeller rotational speed, rad/sec
Ω	=	constraint function
ω_{fan}	=	fuel cell stack fan rotational speed, rad/sec
ω_{motor}	=	propulsion electric motor output speed, rad/sec

ζ	=	sequential unconstrained minimization technique penalty function
γ	=	aircraft flight path angle, rad

SUMMARY

Fuel cell powered aircraft have been of long term interest to the aviation community because of their potential for improved performance and environmental compatibility. Only recently have improvements in the technological readiness of fuel cell powerplants enabled the first aviation applications of fuel cell technology. Based on the results of conceptual design studies and a few technology demonstration projects, there has emerged a widespread understanding of the importance of fuel cell powerplants for near-term and future aviation applications. Despite this, many aspects of the performance, design and construction of robust and optimized fuel cell powered aircraft have not been fully explored.

This goal of this research then is to develop an improved understanding of the performance, design characteristics, design tradeoffs and viability of fuel cell powerplants for aviation applications. To accomplish these goals, new modeling, design, and experimental tools are developed, validated and applied to the design of fuel cell powered unmanned aerial vehicles.

First, a general sub-system model of fuel cell powerplant performance, mass and geometry is derived from experimental and theoretical investigations of a fuel cell powerplant that is developed in hardware. These validated fuel cell subsystem models are then incorporated into a computer-based, application-integrated, parametric, and optimizeable design environment that allows for the concurrent design of the aircraft and fuel cell powerplant. The advanced modeling and design techniques required for modern aircraft design (including multi-disciplinary analysis, performance optimization under

uncertainty and system performance validation), are applied at the fuel cell subsystem level and are linked to aircraft performance and design metrics. These tools and methods are then applied to the analysis and design of fuel cell powered aircraft in a series of case studies and design experiments.

Based on the results of the integrated fuel cell system and aircraft analyses, we gain a new understanding of the interaction between powerplant and application for fuel cell aircraft. Specifically, the system-level design criteria of fuel cell powerplants for aircraft can be derived. Optimal sub-system configurations of the fuel cell powerplant specific to the aircraft application are determined. Finally, optimal energy management strategies and flight paths for fuel cell and battery hybridized fuel cell aircraft are derived.

The results of a series of design studies are validated using hardware in the loop testing of fuel cell propulsion systems and field testing of a series of fuel cell powered demonstrator aircraft.

CHAPTER 1

INTRODUCTION

The focus of this dissertation is the modeling, design and energy management of fuel cell powerplants for aircraft. This chapter presents an introduction and motivational background to the topics of systems modeling and design, and fuel cell powerplants.

1.1 Systems Modeling and Design

The modeling and design aspects of this investigation build on the tools of multidisciplinary analysis and design as exercised in the aerospace design community.

Any non-trivial design process consists of numerous processes that exhibit varying degrees of interconnection and interrelation [1,2]. Traditionally, this design process had to be handled by a single expert designer who had enough experience in the entire problem domain so that the designer was able to guide the design through decision making. As the complexity of design has increased with increasing scale, increasing scope, incorporation of uncertainty, design for constraint robustness, and multi-stage decision making processes, the requirements of a designer have increased so that no one person can perform satisfactorily .

Multidisciplinary analysis and design have evolved to enable the analysis and design of complex systems. The tools of multidisciplinary design allow for the decomposition of a monolithic and integrated design/analysis problem into a series of independent sub-processes with defined inputs, outputs and interconnections between the sub-processes. The casting of a design problem into this multi-disciplinary analysis form is generally a subjective task, that must informed by knowledge of the information that is

required of the analysis. Analyses with the purpose of design, of validation, of decision support, of design space exploration must all have difference decomposition form. The determination and defense of the form of the multi-disciplinary analysis and design problem is a central problem in systems modeling and design.

Optimal design problems consist of choosing the design parameters of the multidisciplinary analysis so as to maximize a design objective subject to constraints [3]. The design then goes from conceptual design, where the design exists entirely in models, to detail design, where the physical, realizeable specifications of the components have been made [4]. The process of going from conceptual to detail design for complex and multidisciplinary systems is a developing field of system design.

1.2 Fuel Cell Introduction

Fuel cells are direct electrochemical conversion devices that convert the chemical energy in reactants to electrical energy and products. The primary fuel cell systems of near-term application interest for transportation applications are the polymer electrolyte membrane (PEM) fuel cell, the solid oxide fuel cell (SOFC), the alkaline fuel cell, and the phosphoric acid fuel cell. Of these technologies, the PEM fuel cell fueled by hydrogen is acknowledged to be the most technically mature fuel cell technology and the most well adapted to transportation-scale applications [5]. Despite this, all of these fuel cell technologies will need to be investigated in the future for applicability to the aviation application as they all have characteristics that may be advantageous. For instance, direct methanol and SOFCs are characterized by lower specific power than PEMFCs, but they can be fueled from liquid hydrocarbon fuels, which will allow for improved specific energy [6,7].

Only recently have the costs, reliability and specific power of mobile fuel cell powerplants improved to the point where the fuel cell can be considered for mass production and mainstream commercial applications [8,9].

Fuel cell powerplants are electric drive powerplants that convert the energy in fueling reactants mechanical output energy through an electrical pathway. The fuel cell system provides electrical power to an electric powertrain that consists generally of a power management device, a traction electric motor, and a motor controller.

The fuel cell system consists of several subsystems including water management, thermal management, hydrogen storage, hydrogen management, controls, etc. Each of these systems is made up of physical components that are assembled to construct the fuel cell system, as shown in Figure 1. These fuel cell subsystem components are assembled to make up the fuel cell system. The fuel cell system is a subcomponent of the powerplant for the aircraft. The powerplant is then a subsystem of the application, in this case a fuel cell powered aircraft. In this work, these distinctions define the application, powerplant, fuel cell system and fuel cell subsystem components.

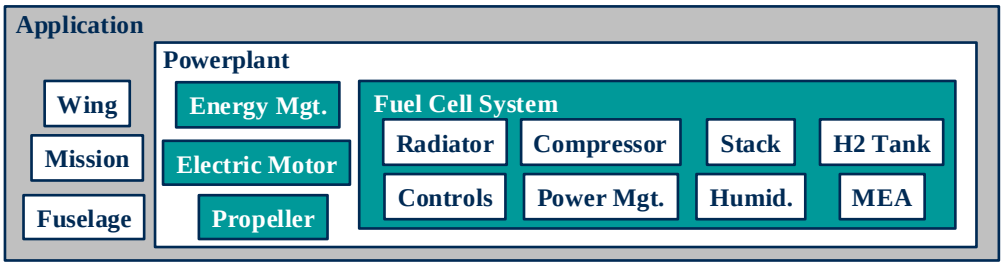

Figure 1. Decomposition of fuel cell aircraft modeling into application, powerplant system and subsystem modeling domains

1.3 Fuel Cell Flight Project Overview

This dissertation is a component of a larger research effort to work towards the development of design tools and analysis methods for fuel cell aircraft. In support of these goals, a fuel cell aircraft design and demonstration project was started in 2004 as a collaboration between the Aerospace Systems Design Laboratory at the Georgia Institute of Technology Daniel Guggenheim School of Aerospace Engineering and the Georgia Tech Research Institute. This research was funded in part by the NASA University Research Engineering Technology Institute grant to the Georgia Institute of Technology. The primary research objectives of this project are: the development of validated methodologies and tools for fuel cell aircraft design, the analysis of tradeoffs between the requirements of the fuel cell system and the requirements of the aircraft application, and the demonstration and experimental testing of a series of fuel cell unmanned aerial vehicles (UAVs).

The methods of investigation for this research effort evolved over its course. The research effort began with the conceptual design of a demonstration fuel cell powered aircraft. The initial design methods involved the development of empirical contributing analyses that described the set of commercially available technologies available to construct the aircraft and fuel cell systems. The contributing analyses were collected into a design structure matrix which is used to map aircraft performance metrics as a function of design variables over a defined design space. An exhaustive search within the design space was performed to identify optimal design configurations and to characterize trends within the design space so as to inform lower-level design decisions. These research efforts were documented in [10].

The optimal design configuration was translated into hardware with the development of an actual fuel cell powered demonstration aircraft. Bench and flight testing were used to validate the design methods and to develop new, scalable, physics based and validated subsystem contributing analyses. These research efforts were published in [11,12].

After the completion of the fuel cell flights in the summer of 2006, the focus of the project shifted towards generalization of the results, improvement of the design processes and exploration of the ultimate performance of fuel cell powered aircraft. The new fuel cell and aircraft contributing analyses were combined with a more sophisticated optimization-based design tool to allow for more rigorous and exhaustive design space explorations. These research efforts were published in [13,14].

These studies resulted in the introduction of the new project design goal of a fuel cell powered aircraft with 24 hour endurance and transatlantic range. Design studies were performed that integrated new validation and experimental techniques such as hardware in the loop, new design structure matrix decomposition forms and system sensitivity analyses. These research efforts were published in [15-17].

The last component of the project has involved both working towards the construction and demonstration of the 2nd generation of fuel cell powered aircraft and the generalization of the design and analysis methods. This dissertation presents the ultimate results of this latest research effort.

1.4 Outline of this Document

This chapter (Chapter 1) provides an introduction to the Fuel Cell Flight research project and presents the contributions of this dissertation.

Chapter 2 presents a literature survey of the design, environmental impact, and state of the field for fuel cell powered aircraft. In addition, a literature review of the fields associated with the research gaps addressed in this dissertation is included.

Chapter 3 presents the research questions and hypotheses that are the focus of this dissertation.

Chapter 4 presents the models developed for this research effort to describe the geometry, mass and performance of fuel cell system components. The construction of the design system matrix is described with the optimization methods used to define optimal configurations. Validation of the fuel cell system models is presented at the component level and system level. The function of the models within a design process is validated.

Chapter 5 presents a series of design experiments using the integrated fuel cell system and aircraft system design tools. Comparisons are made between conventional fuel cell balance of plant design rules and new (more optimal) design rules. Comparisons are made between the results of optimization of subsystems and optimization of complete systems. Finally a fuel cell UAV case study is conducted.

Chapter 6 presents methods and results for flight path optimization and optimal energy management strategies for hybrid fuel cell aircraft. A case study of a fuel cell powered long endurance optimized aircraft is presented.

Chapter 7 presents the design and development of the fuel cell demonstration aircraft that was developed for this study. Component and flight test results document the performance of the aircraft.

Chapter 8 presents the architecture and test result of a hardware in the loop simulator for a fuel cell powered UAV.

Chapter 9 provides conclusions to the study and a summary of future work.

Appendix 1 presents the detail design of the fuel cell powerplant for the fuel cell demonstration aircraft.

Appendix 2 presents the detail design of the fuel cell powerplant and test equipment for the fuel cell hardware in the loop simulation.

CHAPTER 2

LITERATURE REVIEW

This chapter reviews the state of the fields associated with fuel cell powerplants for aircraft. The first section reviews the general motivation for fuel cell powered aviation. Next is a review of the state of understanding of fuel cell aircraft design requirements and applications. The last section identifies the research needs for further development of fuel cell powered aircraft.

2.1 General Motivation for Fuel Cell Powered Aviation

The cited motivations for the development of fuel cell powerplants for aircraft are:

- Improved environmental compatibility relative to conventional technologies [18],
- Improved reliability relative to conventional technologies [18],
- Reduced detectibility due to lower noise and thermal emissions [19],
- Improved specific energy relative to other available technologies [19].

The environmental impact and specific energy benefits of fuel cell powerplants are reviewed in more detail in the following sections.

2.1.1. Environmental Impact of Aviation

For this discussion, environmental compatibility for aviation is broken down into metrics of pollution and energy sustainability, as these are where fuel cell technologies may have a beneficial impact. For the foreseeable future, aviation will be a contributor to

local and global atmospheric pollution in the forms of carbon monoxide, nitrogen oxides, hydrocarbons, particulate matter, sulfur oxides, hydrogen sulfide, carbon-dioxide, and water. Aviation is responsible for approximately 0.4% of the national nitrogen oxide inventory. Locally, the impact of aviation emissions can be larger. For the urban area of Dallas-Ft. Worth, Texas, United States, aviation is responsible for 6.1% of the local nitrogen oxide inventory in 1996. Aviation also has a significant impact on local noise pollution in the form of engine noise emissions during taxi and flight operations. Carbon-dioxide, nitric oxides and upper atmospheric water emissions are the primary globally active pollutants from aviation. By 2015 aviation is predicted to be responsible for roughly 5% of all athropogenic radiative forcing – a measure of climate change. Aviation is also a minor contributor to global petroleum depletion. For the United States in 2006, aviation consumed 4.8% of the nation's energy flow and 8.4% of its petroleum. In sum, the environmental impact of aviation is low relative to other applications such as automotive or stationary power generation, which suggests that adoption of fuel cells by the aviation industry may not be justified only by a desire for improved environmental compatibility. Despite this, in some aviation applications, fuel cell powerplants exhibit performance benefits that can justify further development and commercialization outside of any environmental benefits [20,21].

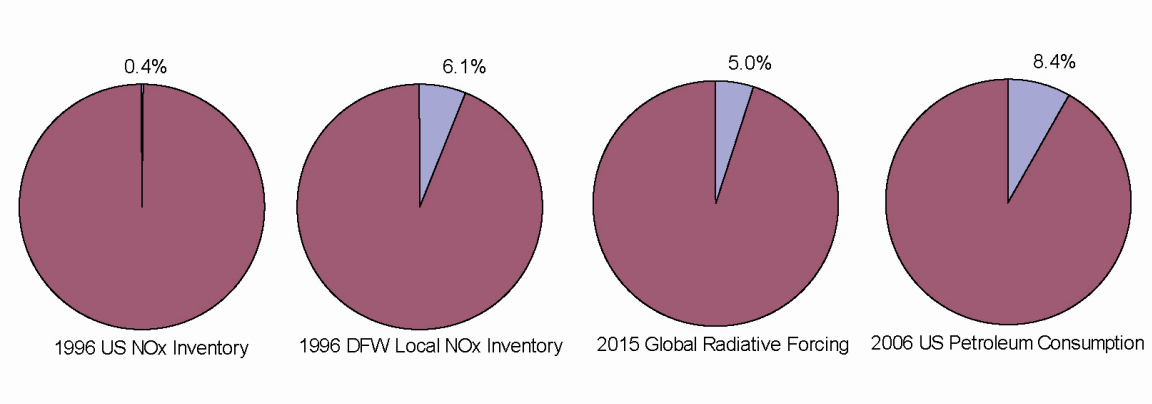

Figure 2. Environmental impact of aviation

2.1.2. Specific Energy Comparison Among Powerplants

Many studies have shown that, in certain application domains, fuel cell powerplants can exhibit greater specific energy than comparable internal combustion and electrochemical battery powerplants. Still, there has not been a study that compares the energy density of fuel cell and conventional powerplants at the variety of power and energy scales suitable for wide aviation applications.

This section proposes a conceptual comparison between the fuels and powerplants that are available for fuel cell powered aircraft. The powerplants under consideration are an internal combustion (IC) engine fueled by gasoline, a PEM fuel cell with gaseous hydrogen storage, a PEM fuel cell with liquid hydrogen storage, a SOFC fueled by propane, and a PEM fuel cell fueled by neat methanol.

All of the powerplants considered are composed of fuel storage and energy conversion components, which convert the energy stored as fuel to propulsive energy. The specific energy of the powerplant is therefore a function of the specific energy of the fuel and the mass and efficiency of the energy conversion components. These variables and therefore the specific energy of the powerplant are functions of the power required of

the powerplant and the energy required of the powerplant. For this study, the specific energy of the powerplant is the rotational mechanical energy output of the powerplant divided by the sum of the fuel, fuel tank, and energy converter (engine or fuel cell) mass.

For the IC engine, the analysis assumes that engine brake specific fuel consumption scales as shown in Figure 3 [22-24]. The engine weight scales at 1.7kW/kg [23], and the tank weight is 0% of the fuel weight.

For the hydrogen fueled PEM FC, the analysis assumes that the fuel cell system is 60% efficient with respect to the lower heating value of hydrogen at all scales [17]. The weight fractions of the gaseous [12,17,25] and liquid [26-28] hydrogen storage systems are scaled as shown in Figure 3. The hydrogen PEM system masses are scaled at 500W/kg [29], and the direct methanol PEM system mass is scaled (by its achievable current density relative to direct hydrogen) at 167W/kg [6]. The electric motor is assumed 90% efficient.

For the SOFC, the stack mass is scaled at 20W/kg for stacks less than 1kW [7], and at 70W/kg for stacks greater than 1kW [30]. The specific propane consumption of the stack is 287 g/kWh DC [7], and the electric motor is assumed 90% efficient.

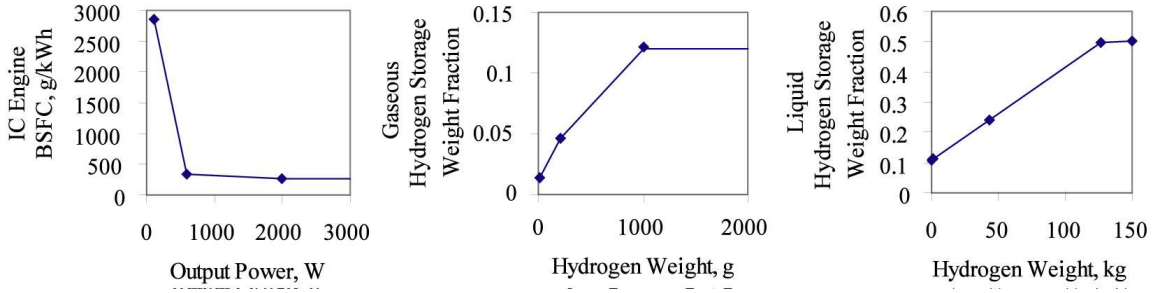

Figure 3. Scaling of key inputs to low order powerplant comparison

For each technology, the specific energy of the powerplant is calculated at endurances between 1 and 100,000 min. and powers between 10 and 100,000 W. The results are shown in Figure 4. A few points of interest are labeled in Figure 4.

Point 1 shows a condition of low power (10W) and multi-hour endurance (~1000 min). At this condition, the direct methanol fuel cell shows specific energy between 1000-2000 Wh/kg. This condition corresponds very well to the low-power, high energy, small scale applications that are of present interest to the direct methanol fuel cell community. These applications include hand-held electronics, small APUs and laptop computers [31,32].

Point 2 shows a point of small scale (100W) and long-endurance (>10,000 min) that is relevant to the small-scale UAV application. A comparison across technologies shows that at this scale the IC powerplant has a low specific energy of ~330 Wh/kg. This compares the specific energy of the hydrogen fuel cell powerplant of ~1800 Wh/kg. The specific energies of the liquid fueled fuel cell powerlants are higher still. This comparison suggests that for small scale UAV applications, the fuel cell powerplants exhibit higher specific energy than the IC powerplants. For comparison, the specific energy of commercially available lithium polymer batteries at this scale is 149 Wh/kg [33].

Point 3 shows the specific energy of the IC engine at long endurance and larger power. Under the conditions of point 2, the engine efficiency is low due to the small scale of the engine. Under the conditions of point 3, the efficiency of the internal combustion engine is nearly 31% based on the LHV of gasoline. Accordingly, the specific energy of the IC engine has increased to nearly 3700 Wh/kg. As the power

demands of the powerplant increase, the IC engine can show higher specific energy than the gaseous hydrogen and direct methanol PEM powerplants.

Finally, point 4 shows that at conditions of high power and long endurance, the liquid hydrogen PEM fuel cell can outperform the other available technologies. This is the application space that is of interest to designers of very long endurance high altitude UAVs [34].

In summary, fuel cell-powered aircraft show the potential to outperform conventionally-powered aircraft for a variety of missions and applications. At small scales and long endurance, compressed hydrogen PEM fuel cell powerplants can show significant improvements in specific energy relative to IC engine powerplants. At medium scales, SOFC and IC engine powerlants dominate the compressed hydrogen systems. At larger scales and endurances, IC engine powerplants dominate over all advanced technology powerplants, with the exception of liquid hydrogen fuel cells.

This analysis provides justification for the investigation of fuel cell powerplants for aircraft as there exists a number of applications spaces where fuel cell powerplants can outperform more conventional powerplant technologies.

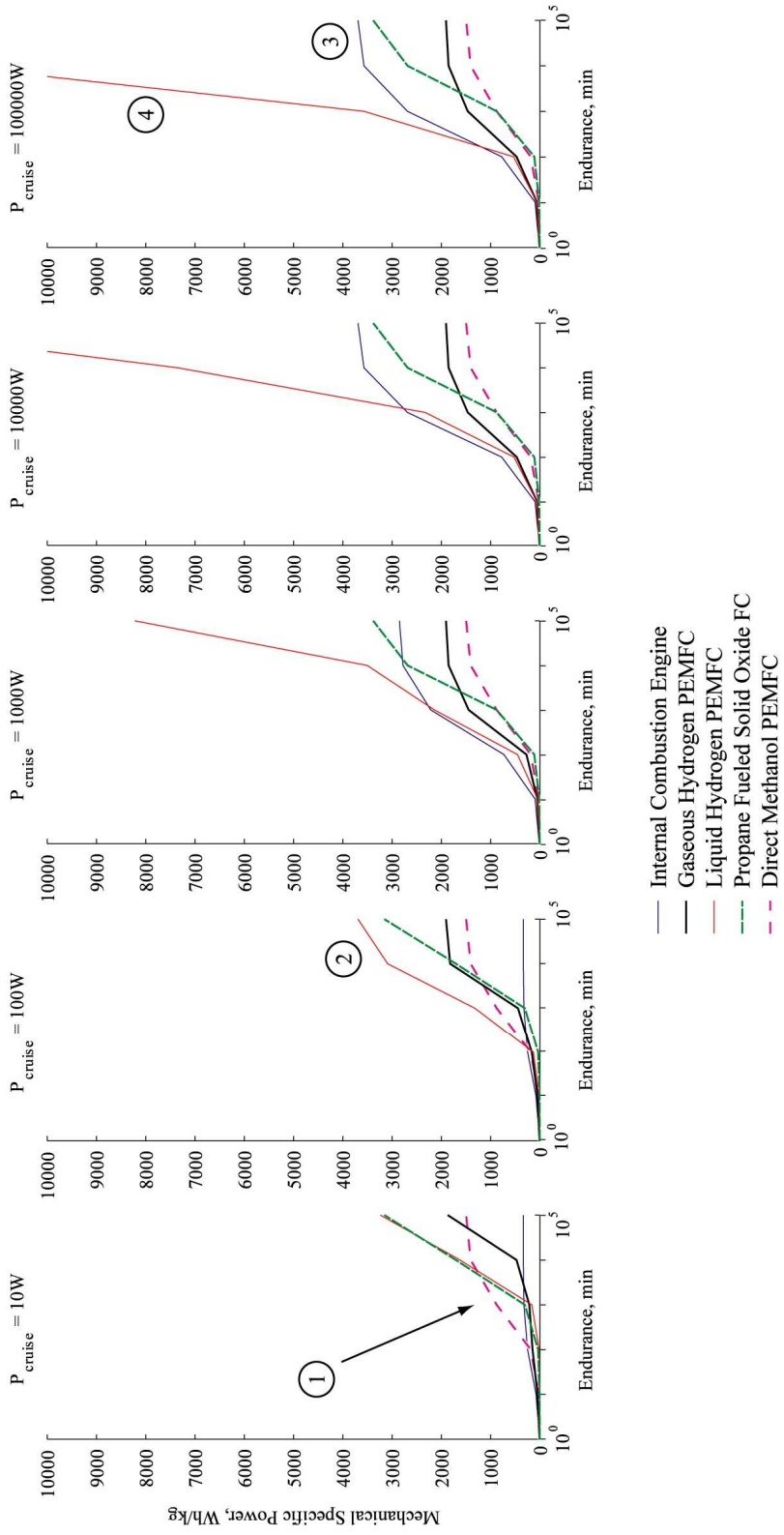

Figure 4. Results of low order powerplant comparison

2.2 Design Considerations for Fuel Cell Aviation Powerplants

Modern aircraft require integrated design processes which can allow tradeoffs between the design characteristics of aircraft subsystems [35]. Powerplants for fuel cell aircraft must incorporate compromises between the design challenges associated with aviation operating conditions, the characteristics of the environment and the fuel cell systems themselves.

Reactant storage is one of the primary design challenges for fuel cell aircraft of all types, but especially for those that consume hydrogen. Whereas hydrocarbon fuels can be stored in liquid form in irregular containers, distributed throughout the airframe, gaseous or liquid hydrogen must generally be stored in centralized spherical or cylindrical vessels. This necessitates an increase in aircraft frontal area, and an increase in wing structure, which both increase aircraft power consumption. Although all fuel cell aircraft that have incorporated chemical hydrogen storage media have used a centralized hydrogen storage unit, this is not necessarily an intrinsic feature of chemical hydrogen storage. The development of high specific energy hydrogen storage systems such as low pressure composite cylinders and chemical hydrogen storage systems will improve the performance of fuel-cell powered aircraft [25].

Aircraft must be able to operate efficiently at high altitude to improve the high-speed airframe efficiency and fly above atmospheric disturbances. The oxygen source for most fuel cell powered aircraft conceived to date has been the atmosphere so as to avoid carrying the weight and bulk of stored oxygen. At a cruising altitude of 10 km, the atmospheric pressure is only 0.26 atm and the oxygen partial pressure is 0.05 atm. For air-breathing fuel cells, this decrease in ambient oxygen partial pressure can cause the

fuel cell activation and mass transport overpotentials to increase [36]. A majority of fuel cell aircraft designs have incorporated compressors to maintain the cathode pressure at a fixed absolute pressure, but this solution has costs in terms of efficiency, weight and power output [37,38]. For example, for a fuel cell aircraft that operates at a 10 kW cruise, 0.7 V per cell, 10 km altitude with a cathode stoichiometry of 2.0, an 80% efficient compressor will consume 3.1 kW of power to maintain a constant 2 bar of cathode pressure. As the altitude increases, the power required to maintain the required cathode pressure will increase. This problem might be overcome by designing aviation specific fuel cells with compressor-expander modules, increased catalyst loadings, or higher active area.

The water and thermal management of the fuel cell system is also complicated by the aircraft altitude. Ambient humidity and temperature are very low at altitude. At 10 km altitude the standard atmospheric temperature is -50C and humidity is on the order of 0.2 g (kg dry air)$^{-1}$ [39], approximately 30 times less water content than summer desert air (42C, 10% relative humidity). To improve the performance of fuel cells in aviation applications, aviation-specific water and thermal management strategies must be incorporated into fuel cell powerplant design. These could include radiative heat rejection.

In automotive or portable fuel cell powerplants, hybridization of the powerplant with a battery or super-capacitor bank can improve the efficiency and performance of the system. These improvements are caused by isolating the low power, high energy fuel cell system from high power, low energy transients [40]. In a majority of aircraft applications the majority of power transients are high power, *high energy* input air heating, exhaust

water recirculation or transients such as takeoff, landing and acceleration. Because of this mismatch, only a few researchers have considered or constructed hybrid electric fuel cell aircraft powerplants, and in all the hybrid fuel cell aircraft constructed to date, the battery is indeed primarily used for high power takeoff [41]. A highly generalized comparison of automotive and aviation fuel cell systems and conditions of use is shown in Figure 5. Note the difference in the characteristics of the propulsive power requirements. The further study of the conditions of use of UAVs will define the role that hybridization can play in improving powerplant efficiency.

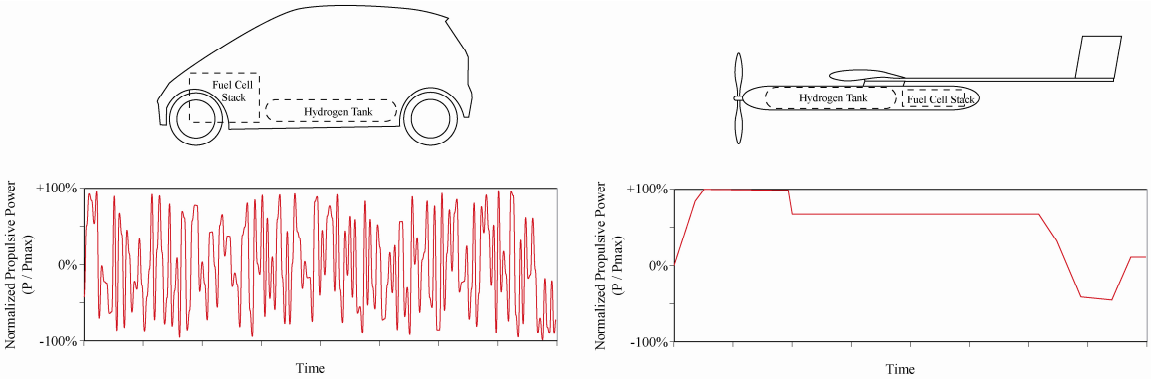

Figure 5. Generalized comparison of fuel cell systems and propulsive power requirements for (a) automotive and (b) aviation applications

2.3 Aviation Applications of Fuel Cell Powerplants

2.3.1. Small Scale UAVs

One of the primary drawbacks of conventional turbine and reciprocating combustion engines is that their efficiency cannot be preserved at very small scales because of issues such as combustion quenching, high surface area to volume ratios, and low reactant residence times [22]. As highly modular direct energy conversion devices, fuel cell powerplants have no such limitations and they are able to maintain high

thermodynamic efficiency and therefore high specific energy even at the sub-kilowatt scales. This scale of powerplant is of interest to the aviation community for applications such as long-endurance small- and micro-scale UAVs.

A comparison of potential small-scale UAV powerplants from the literature is shown in Table 1. Table 1 assumes that the airframe mass (m_{airframe}) is 5.1 kg, the electric motor mass (where appropriate) is 283 g, electric motor efficiency is 71%, propeller efficiency is 69% and each powerplant can produce 1560 Wh of propulsive energy at 70 W. Range and endurance for the internal combustion powerplant are calculated using the Breguet Range Equation:

$$s = vt = v\left(\frac{C_L}{C_D}\right) I_{sp} \ln\left(\frac{W_i}{W_f}\right) \tag{1}$$

Based on this comparison, the fuel cell powerplants have the ability to outperform other electrochemical storage media as well as conventional internal combustion powerplants at this scale.

Table 1. First order powerplant comparison for small scale aircraft

Powerplant Type	Powerplant Specification	$\left(\frac{E}{m}\right)$	$\left(\frac{E}{m^{3/2}}\right)$	Calculated Range	Calculated Endurance
Compressed Hydrogen PEM Fuel Cell	1000 DC Wh kg^{-1} [13]	186.4 Wh kg^{-1}	64.4 Wh kg$^{-3/2}$	1642 km	44.0 hr
Propane Fueled Solid Oxide Fuel Cell	660 DC Wh kg^{-1} [7]	157.2 Wh kg^{-1}	49.9 Wh kg$^{-3/2}$	1384 km	34.1 hr
Zinc Air Battery	350 DC Wh kg^{-1} [42]	108.0 Wh kg^{-1}	28.4 Wh kg$^{-3/2}$	951 km	19.4 hr
Lithium Polymer Battery	166 DC Wh kg^{-1} [31]	62.9 Wh kg^{-1}	12.6 Wh kg$^{-3/2}$	554 km	8.6 hr
Small Internal Combustion Engine	0.3 kg hr^{-1} @105W [43]	125.5 Wh kg^{-1}	35.6 Wh kg$^{-3/2}$	1509 km	38.6 hr

Because of these performance advantages, fuel cells have found their first aviation applications as powerplants for small-scale UAVs. In 2003, AeroVironment Inc., a vehicle design and manufacturing company in Monrovia, California, built and flew the

first fuel cell powered aircraft [44]. Its monopolar fuel cell system consumed hydrogen from a sodium borohydride reaction vessel. Between those first flights and the present, a number of researchers and commercial entities have developed fuel cell powered UAVs with increasing size and scale, as shown in Figure 2. To date, most small-scale UAV powerplant systems have been designed with PEM fuel cell systems, which are self-humidified or passively humidified, unhybridized, and with compressed or chemical hydride hydrogen storage. Demonstration of an SOFC UAV fueled by propane has also been accomplished by Adaptive Materials Inc [7]. In all of these demonstrations, the fuel cell powerplants were designed for high specific energy, so as to maximize endurance and range, and for high specific power, so as to allow for easy handling and controllability. It is anticipated that small-scale UAVs with endurances of >24 hrs and ranges of >2000 km will be developed in the near future. These aircraft will have significant value as low-altitude, low-cost, autonomous reconnaissance and remote sensing platforms for both commercial and military applications.

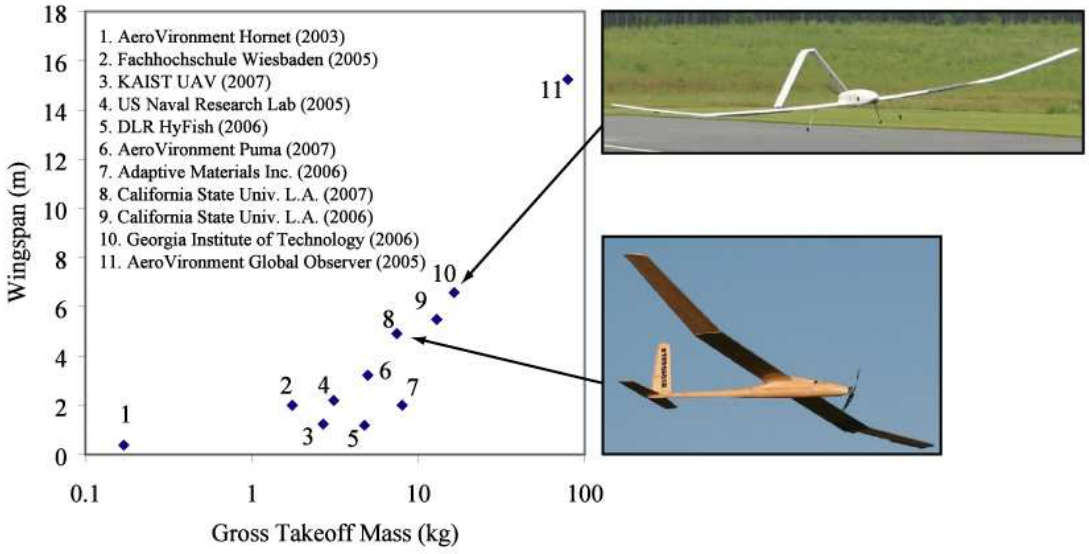

Figure 6. Scale comparison of small-scale fuel cell powered UAVs constructed to date

Table 2. Chronological list of published unmanned fuel cell powered UAV demonstrations

Organization (date) [Ref.]	Fuel Cell Type	Reactant Storage Type	Endurance (est.)
AeroVironment (2003) [44]	PEM	H_2 Sodium Borohydride	0.2 hr
AeroVironment (2005) [45]	PEM	H_2 Cryogenic	24 hr
FH Wiesbaden (2005) [46]	PEM	H_2 Gaseous	90 s
Naval Research Lab (2006) [47]	PEM	H_2 Gaseous	3.3 hr
Adaptive Materials Inc. (2006) [7]	SOFC	Propane	4 hr
Georgia Inst. of Tech. (2006) [11]	PEM	H_2 Gaseous	0.75 hr
CSU Los Angeles (2006) [48]	PEM	H_2 Gaseous	0.25 hr
DLR/HyFish (2006)[49]	PEM	H_2 Gaseous	0.25 hr
CSULA/OSU (2007) [41]	PEM	H_2 Gaseous	12 hr
KAIST (2007)[50]	PEM	H_2. Sodium Borohydride	5 hr
AeroVironment (2007) [51]	PEM	H_2. Sodium Borohydride	9 hr

2.3.2. Commercial Jet APU

NASA and various aerospace companies have performed research on the development of a solid-oxide based fuel cell auxiliary power unit (APU) for passenger aircraft [52]. Aircraft APUs are gas turbine generators that generate electric power during ground operations to power aircraft electrical loads such as lighting, cabin environmental conditioning and main engine startup. Conventional APUs are fueled by the onboard jet fuel. The systems that are proposed to replace these APUs consist of a hybrid solid-oxide fuel cell and gas turbine system with onboard jet fuel reformation. Whereas a conventional APU achieves approximately 15% electrical energy generation efficiency, the hybrid solid-oxide fuel cell system should achieve between 41% and 60% efficiency. In addition to these fuel savings, the solid-oxide fuel cell APU would offer lower nitric oxide emissions, longer service intervals, and power conversion at cruise. Disadvantages might include higher upfront costs and a longer startup time.

Fuel cell APUs will also be an enabling technology for the More Electric Airplane Architecture. The More Electric Airplane Architecture is an aviation industry-wide development concept wherein the hydraulic and pneumatic systems of conventional aircraft are replaced with electrical servo-actuated systems of higher reliability and lower cost. The More Electric Airplane Architecture would enable functions that would be powered by the APU including motor-powered ground taxi, electrically redundant controls, and high bandwidth control surface optimization [53].

2.3.3. Solar Regenerative Aircraft

Regenerative PEM fuel cell systems have been proposed as an enabling technology for a new class of aircraft with unlimited endurance. Using electricity

generated from solar cells and composite pressure vessels to store reactants, a rechargeable, high efficiency, high specific energy aircraft powerplant can be constructed. This powerplant could be a component in an airship or gossamer aircraft. To compare rechargeable systems for a long endurance application, we can again compare their energy density. For rechargeable systems though, the energy of interest must be the electrical charging energy, so that the figure includes both charging and discharging efficiencies. Advanced batteries can reach electrical discharging specific energies of 200 Wh kg^{-1} at the module level [54] and have charge efficiencies of nearly 100% at low current [55]. A rechargeable fuel cell/electrolyzer energy storage system with compressed reactant storage can have a discharging specific electrical energy of >800 Wh kg^{-1}, and a charging efficiency of 80% [25,56,57]. This results in a round trip, specific electrical energy of >640 Wh kg^{-1}. So, in comparison to advanced battery technologies, compressed hydrogen regenerative fuel cells can exhibit significantly higher specific energy.

A majority of research on regenerative fuel cell systems for very long endurance aircraft has concentrated on conceptual aircraft and powerplant system design. The NASA ERAST project and its Pathfinder test aircraft are notable exceptions. A planned fuel cell powered flight by the Pathfinder aircraft was halted only by the catastrophic failure of the aircraft in 2003 [44,58]. The NASA Glenn Research Center has developed and tested a laboratory version of a regenerative fuel cell for aviation applications [59]. No functional regenerative fuel cell powerplants have been demonstrated in aviation applications to date.

2.3.4. General Aviation

General aviation is a subset of aviation consisting of chartered passenger aircraft, private aircraft, and other components of civil aviation that are not regularly scheduled airline flights. The purpose of developing fuel cell power general aviation powerplants is to demonstrate fuel cell technology in a manned application, and to mitigate the noise and air pollution of general aviation. This would allow for 24 hour operations from urban airports with noise and/or pollution abatement regulations.

A number of groups have proposed these projects and completed feasibility studies, battery powered test flights and laboratory tests [60-63]. These projects have generally utilized fuel cell systems and components derived from automotive applications. The first manned fuel cell powered aircraft was developed by Boeing from a converted glider airframe. This aircraft uses a custom fuel cell stack and a hybrid electric powertrain. The fuel cell is sized to primarily provide the power required for cruise. A ~20 minute flight demonstration was performed in 2008 [64].

2.3.5. Long Term Applications

In the longer term, many envision fuel cells as a primary powerplant for advanced aviation concepts. These might include SOFC-powered liquid hydrogen aircraft with ~20 days endurance [34], distributed onboard accessory power generation, and multi-functional fuel cells that generate power and make up the skin of the aircraft. Some researchers have proposed fuel cell powerplants for large-scale passenger and commercial aviation applications . Because commercial aircraft are very high power, high energy applications, it is estimated that a fuel/propulsion system specific power of 2

kW kg^{-1} would be required, many times the performance of currently available technology [18,61,62].

2.3.6. Applications Literature Review Conclusions

It is anticipated that fuel cell powerplants for small-scale UAVs will be the first commercially available fuel cell aviation application. These powerplants will replace advanced batteries to allow for long-endurance and long-range missions. Fuel cell powerplants may have a larger effect on the entire aviation industry in the far future as the development of fuel cells and hydrogen storage media advance.

2.4 Design and Implementation Challenges for Fuel Cell Aircraft

Based on the results of the studies of fuel cell aircraft performed to date, the primary challenges for modeling, design and implementation of fuel cell systems in aircraft are:

- integrated fuel cell systems modeling,
- definition of design methodologies and design requirements and
- energy management and system supervisory control.

The following sections review the literature for these topics.

2.4.1. Fuel Cell Systems Modeling

This section reviews the literature associated with fuel cell system modeling and design. Fuel cell systems are divided into two primary subsystems: the fuel cell stack and the fuel cell balance of plant. Each fuel cell stack is made up of a number of fuel cells. The fuel cell balance of plant is made up of the other components of the fuel cell system including water and thermal management, hydrogen storage and management, controls,

power distribution and more. This dissertation is primarily concerned with the design and modeling of fuel cell systems at the systems level. This section of the literature review will concentrate on the literature associated with fuel cell system modeling where the fuel cell stack and balance of plant are all included in the performance model. Lower level fuel cell modeling that attempts to characterize the fuel cell performance at the cell or sub-cell level is not included in this review.

Models for fuel cell systems have been proposed at a variety of levels of fidelity and purposes. For the purposes of fuel cell systems design, fuel cell system models would ideally be able to deterministically describe the steady state performance, dynamics, subsystem energy flows, geometry, cost and mass of the system parametrically and with computational efficiency. No such model exists to date that achieves all of these goals although many attempts have been made to develop models that describe more than one of these characteristics.

Many researchers have proposed mathematical systems of equations that characterize the steady-state performance of fuel cell systems using a static polarization curve [65-68]. These models use experimentally or theoretically derived parameters to describe the polarization performance of the fuel cell system at well characterized steady-state conditions. Although static polarization-curve–based models are useful for describing the performance of the fuel cell system, they are not useful for design of fuel cell systems because they are system-level models and they are not parameterized. The subsystem performance can not be specified or evaluated on the basis of the system polarization curve and the performance parameters that are used to fit the system experimental data are specific to the experimental stack.

Dynamic models of fuel cell systems often do model the fuel cell systems at a subsystem level using the framework of dynamic system modeling. Models for describing the dynamics of fuel cell systems have included modeling of the thermal dynamics [69-71], air management system dynamics [72-76], water transport dynamics [77,78], and control system dynamics [72,79]. These models are unsuitable for fuel cell system design as they are not parameterized and they are computationally very expensive.

Fuel cell system models that have been developed for conceptual design and optimization must be parameterized and more computationally efficient than the more common descriptive models described above. A fuel cell model scalable by the fuel cell active area has been used to optimize fuel cell system cost [80]. Fuel cell models scalable by the number of cells have been proposed and applied to automotive systems to determine an optimal degree of hybridization [81]. Parametric PEM fuel cell models have been developed for multi-objective optimization of system performance versus cost [82-84]. These fuel cell system models are not integrated into specific applications, and as such they are optimized for fuel cell system design requirements rather than application-specific design requirements. The primary example of a fuel cell system design tool that is application integrated is Argonne National Laboratory's GCTool. GCTool is a dynamic and scalable fuel cell model for automotive applications, but the model is of high complexity and is focused on automotive technologies and applications [85]. A similar tool is under development at the University of California – Davis [86]. Neither of these tools is suitable for multidisciplinary optimization or computational design. There are no simulations of fuel cell vehicles that allow for physics-based,

scalable, parametric design of the fuel cell system suitable for multidisciplinary design [40].

In the field of fuel cell systems modeling there exists a considerable knowledge gap because of the lack of fuel cell sub-system models appropriate for construction of multidisciplinary, optimizeable fuel cell models. This is complicated in many applications (including automotive) because, in general, the modeling of fuel cell systems is complex and computationally demanding. Many of the aspects of fuel cell system design are proprietary and are not published in open literature. The small scale of the powerplants considered for the fuel cell powered UAV application may be particularly amenable to sub-system component modeling and design under multidisciplinary optimization. In order for these fuel cell models to be a component of a multidisciplinary design process, parametric models of the fuel cell system must be developed, validated and they must be shown to be of value in a real-world design process.

2.4.2. Fuel Cell Aircraft Design Methodology

Aircraft are historically designed using a requirements-driven design process: the required performance of the aircraft is known and components are assembled to meet the performance goals [87]. Design of fuel cell aircraft up to the present has been performed by using aircraft performance requirements to determine the theoretical performance requirements of a fuel cell system. The primary means of scaling the performance of fuel cell systems that has been proposed for fuel cell aircraft design is scaling based on fuel cell output power [18,88-94]. This method ignores the interactions among the fuel cell subsystem components and does not provide information about the fuel cell system proposed to the design and implementation tasks.

NASA performed a number of early studies on the feasibility of fuel cell powered aircraft [90,92,93]. For the fuel cell powered aircraft designed in these studies, the state of technology is not developed enough to be able to design or construct aircraft that can accomplish the desired missions and payloads. This leads to fuel cell performance requirements that are not technologically available. Other researchers have performed studies on fuel cell powered aircraft and concluded that the efficiency of fuel cells required for their mission of interest is >90% [95]. This efficiency requirement is greater than the ideal reversible efficiency of a fuel cell operating on pure hydrogen and oxygen at STP ($\eta_{FC}=\Delta G/\Delta H$=237/286=83%), making this result theoretically infeasible [36].

To avoid the specification of unavailable or infeasible fuel cell system designs, fuel cell systems must be modeled at a subsystem level using physics-based modeling techniques. NASA has applied a scalable high-fidelity solid oxide fuel cell (SOFC) model to design of aircraft fuel cell powerplants [34], but the analysis was only weakly coupled to the aircraft application.

Fuel cell systems are generally highly modular systems that can be designed for a wide range of performance goals including efficiency, power density (W/L), energy density (Wh/L), specific power (Wh/kg), specific energy (Wh/kg) and/or lifetime. What combination of these metrics should characterize fuel cell powerplant design for aircraft is under dispute. Some studies have suggested that for long endurance missions, the specific energy of the powerplant should be maximized [34]. Results associated with this dissertation and research effort suggest that a compromise between specific power and energy must be maintained to meet aircraft performance constraints [13]. For aviation applications, modeling of fuel cell systems for energy consumption prediction generally

assumes that ambient pressure changes, ambient temperature changes, and balance of plant heat transfer are negligible [18,88]. Only a few studies have investigated the effect of altitude on fuel cell system operation [37,38].

In summary, the design studies of fuel cell aircraft to date have been performed with the goals of understanding technological feasibility, technology sensitivity, or global sizing and synthesis. No design studies in the literature have made development of fuel cell aircraft their goal.

2.4.3. Energy Management and Supervisory Control

Simulations of the energy consumption of fuel cell powered aircraft generally assume steady flight conditions and no active energy system management [13,34]. This despite that during flight of a hybrid fuel cell aircraft, there are 3 means of reversible energy storage available (potential, kinetic, electro-chemical). Fuel cell hybrid aircraft simulations to date have assumed a default energy management strategy without consideration of its effect on system optimization and aircraft performance [94].

Studies of other types of aircraft powerplants have shown that there exist optimal energy management trajectories that can increase range, endurance or decrease fuel consumption [96-99]. These studies generally are interested in periodic efficiency optimal flight profiles where the aircraft performs a climb-glide-climb flight pattern. These flight patterns exist because the point of peak propulsive efficiency of the powerplant is not achieved at the point of peak flight efficiency of the airframe. By climbing at peak propulsive efficiency and gliding near peak endurance efficiency, the resulting endurance of the aircraft can be increased. This behavior is characteristic of

almost all internal combustion and gas turbine powerplants for aircraft. No research has performed similar analyses for fuel cell powered aircraft.

Studies in hybrid electric ground vehicles have shown that there are significant fuel economy gains to be realized through optimal energy management [40,81,100,101]. For conventional internal combustion powerplants, these studies can derive energy management strategies for the hybrid powerplant that uses the energy storage capability of the batteries to improve the overall efficiency of the powertrain. These studies also take advantage of the regenerative braking ability of hybrid automobiles to improve the drive cycle efficiency of the study vehicle. For hybrid fuel cell automobiles, studies have shown that the primary use of the hybrid energy storage system is to 1) recapture braking energy through regenerative braking and to 2) isolate the fuel cell powerplant from vehicle transients that can degrade the fuel cell and reduce fuel cell efficiency. Neither of these conditions exists in the fuel cell powerplants that have been considered for fuel cell UAVs. Regenerative braking through propeller wind-milling is dismissed in the literature as inefficient [18], and the conditions of use of an aircraft are such that the aircraft transients are much slower than those of the automotive application.

Based on these observations, there exists a considerable gap in the understanding of the broader design space around hybridized fuel cell powered aircraft. No research has defined the contribution of hybridization to fuel cell powered aircraft. Similarly, no research has considered flight path optimization for fuel cell powered aircraft.

CHAPTER 3

RESEARCH QUESTIONS AND DEFINITION OF RESEARCH SCOPE

3.1 Primary Research Question

Based on the research challenges outlined in the previous chapter, a primary research question can be posed:

Primary Research Question: Can fuel cell and aircraft system models be developed and integrated to facilitate global and sub-system performance analysis, design and optimization for near-term-realizeable fuel cell powered aircraft?

To answer this question, this research effort will establish the methods and framework for physical and empirical parametric modeling of fuel cell aircraft components at a level appropriate for conceptual and preliminary design. These models will be validated individually, as a system and as a component in an aircraft design process. The validated system design and optimization environment will be used to derive design sensitivities, to test sub-system performance criteria, and to derive high-performance aircraft configurations. Energy management strategies for fuel cell and hybrid electric fuel cell powered aircraft will be derived and tested.

The primary research question can be further broken down into research questions of smaller scope. The work required to answer each research question is broken down

into Tasks. Each Task provides outputs which contribute to answering the primary research question and to accomplishing subsequent Tasks.

3.2 Research Question 1 – Fuel Cell Systems Modeling and Validation

The fuel cell engineering community would like to be able to use the tools of modern design to design complex fuel cell systems from models of their subsystem performance and models of the interactions between the subsystems. This first research question asks whether fuel cell systems are amenable to subsystem modeling, and whether the design results can be validated.

Research Question 1*: Can the geometry, performance and mass of fuel cell systems be represented parametrically within an integrated, validated, optimizeable powerplant and propulsion system model?*

There are a number of challenges that are associated with answering this research question. As noted in the literature review, there exist only a few fuel cell multidisciplinary optimization models. It is unclear whether components of the fuel cell system should be modeled empirically, physically or both. The interactions between the components of the fuel cell system are complex, multi-domain and time dependent. Validation data within the fuel cell system literature is primarily based on automotive-scale fuel cell systems instead of <1kW systems. Modeling of small-scale fuel cell system components is dominated by nonlinear and non-ideal behavior.

It is hypothesized that the way to develop scalable fuel cell models is to model the fuel cell system at the sub-system component level. Combining the models of the components into a multidisciplinary modeling and design environment will allow for the

uncertainty associated with the subsystem models to be understood and managed during design and validation.

Hypothesis 1*: The development of sub-system level fuel cell powerplant models will allow for validated, scalable, optimizeable performance simulation for fuel cell system conceptual design.*

There are two tasks that are associated with the testing of this hypothesis.

Task 1.1*:* Develop models of fuel cell sub-systems that can be integrated into a scalable and parameterized fuel cell system model.

Models are needed to describe fuel cell systems at a sub-system level so as to allow scalability of system performance, parameterization of component specifications and physics-based modeling of performance and component interactions. These models will be constructed based on experimental testing of a constructed fuel cell stack, and based on data sets from the literature.

Task 1.2*:* Validate the developed subsystem models for sub-system performance prediction, system performance prediction, and utility within the fuel cell aircraft design process.

This task will investigate the validation of the fuel cell system modeling at three levels. First the models will be validated individually from experimental data. Second, this task will involve qualitative validation of the behavior of the models when assembled into a fuel cell system. Finally the utility of the models as a design tool will be established by validating the applicability of the modeling to the conceptual stage of a fuel cell aircraft design process.

Upon completion of these tasks, the hypothesized validity and scalability of the model will be supported if the subsystem models developed for one fuel cell system can be used to predict the performance of another fuel cell system. If the fuel cell system design model can be used within a design process to design and develop a fuel cell powerplant that meets design requirements, then the optimizeability and design process utility of the model will be supported.

3.3 Research Question 2 – Fuel Cell Aircraft Integrated Design Studies

With design models there exists a fundamental tradeoff between the fidelity of the design model and its usability in a computational design process. If the model is too refined, then the computational cost becomes too great for use in early stages of design. If the model is computationally efficient, but cannot predict the relevant design tradeoffs, then the model is of no value to designing among those tradeoffs. The design model must be of the correct scale in order to capture relevant design characteristics, but must not be bloated with unimportant contributing analyses. This research question asks whether fuel cell aircraft must be designed with a multi-level design tool (that includes subsystem and system and application models) or whether more simplification of design requirements can maintain acceptable design performance.

Research Question 2*: Is the extra complexity and cost of a multilevel design tool (that includes subsystem-level, system-level and application-level models) justifiable for optimization and design of fuel cell powered aircraft? What are the costs to the design performance of replacing either the application model or subsystem models with the surrogate design rules that have been proposed in literature?*

This research question is a common question for modelers of complex systems. What are the borders of the problem and where do the upsides of increasing model scale overtake the downsides? The development of subsystem models for fuel cells and their integration into the aircraft design process has increased the complexity and scope of the fuel cell aircraft design process. This increase in complexity has monetary and computational costs and should be justified.

The tasks associated with this research question attempt to trim the model from the two directions to quantify the benefit of the new models. Task 2.1 compares the performance of the fully integrated multi-level fuel cell aircraft design tool to a design tool where the fuel cell subsystem models and optimizers have been replaced by conventional fuel cell system design rules. Task 2.2 compares the performance of the fully integrated multi-level fuel cell aircraft design tool to a design tool where the aircraft models and aircraft level-design criteria have been replaced by approximations. These tasks are compared visually in Figure 7 and Figure 8. Both hypotheses state that the integrated design tool will outperform these simplifications.

Hypothesis 2.1*: Disintegration of the powerplant design rules allows for empirical, unbiased optimization of the system design that shows improvement over conventional powerplant design rules*

In order to allow the optimization schemes to design the fuel cell powerplant system to meet the requirements of the aircraft application the design rules and design constraints for the powerplant component interactions must be minimized. As described in the literature review, in previous fuel cell system design studies the powerplant component sizing relations are determined from design rules. For

instance, in many studies, the fuel cell air management system is sized causally by the number of fuel cells and their maximum current output. By removing these types of constraints and allowing the fuel cell system components to be specified by the optimization routine, unexpected configurations that are application optimized can result.

Task 2.1*:* Apply complex system optimization techniques to derive the high-level system specifications and design criteria for fuel cell powerplants in the fuel cell aircraft application.

The first task then is to remove the conventional design constraints from the fuel cell powerplant system contributing analysis and allow the designer and optimizer to "discover" unexpected application-specific configurations. These new design configurations should then be compared to the conventional design configurations to see what tradeoffs are being made by the fuel cell system optimizer.

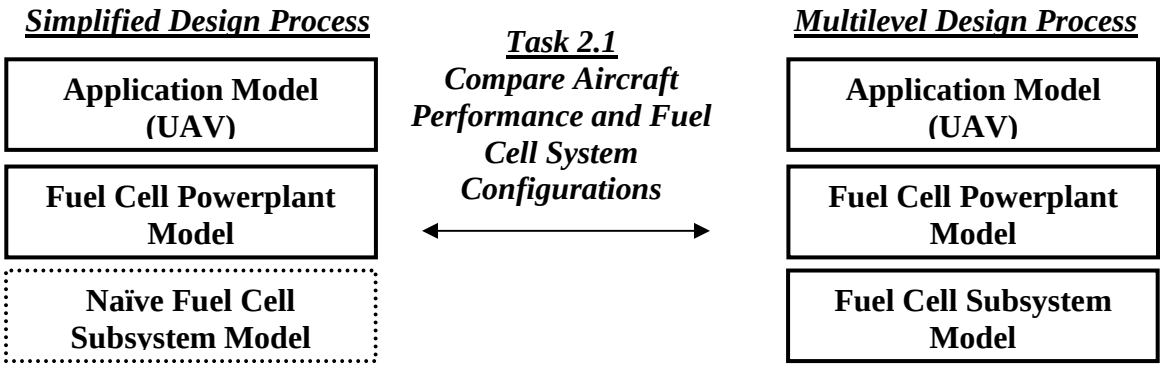

Figure 7. Visual representation of design methods comparison associated with Hypothesis 2.1

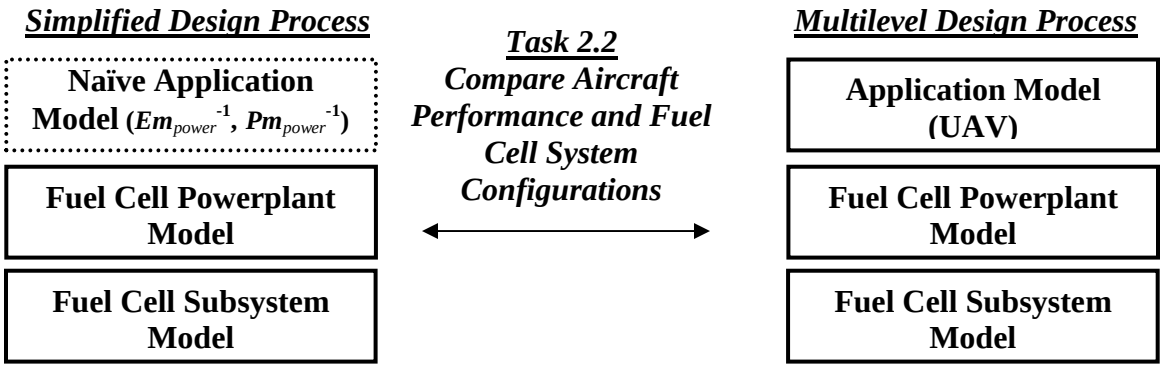

Figure 8. Visual representation of design methods comparison associated with Hypothesis 2.2

Hypothesis 2.2*: Fuel cell systems designed using an application-integrated design process can improve the performance of the aircraft system relative to the state of the art surrogate design metrics*

To date, the designers and developers of fuel cell powerplants have been primarily responsive to the needs of the automotive and stationary power generation applications. The primary fuel cell system design criteria for these applications are: powerplant power density (WL^{-1}), powerplant energy density (W hrs L^{-1}), lifetime (hrs or start-stop cycles) and powerplant system cost ($\$ W^{-1}$).

For aviation some primary aircraft-level performance metrics might include range, endurance, cargo capacity, maximum speed and rate of climb. To maximize these aircraft performance metrics, fuel cell powerplants will have to be designed and built to meet aviation-specific design criteria. This may involve significant departures from the conventional automotive or stationary fuel cell design. One primary design metric that has been suggested for fuel cell aviation powerplants is specific energy, $E\ m_{power}^{-1}$, the ratio of the energy stored in the aircraft E (W hrs) to

the sum of the fuel and powerplant mass m_{power} (kg). Another primary design metric of interest for fuel cell aviation powerplants is specific power, $P\ m_{power}^{-1}$, the ratio of the power output from the powerplant to the sum of the fuel and powerplant weight. In steady flight, the aircraft cargo weight, maximum speed and rate of climb are proportional to $P\ m_{power}^{-1}$.

Task 2.2: Compare system optimization results for fuel cell airplane system design between sub-system optimized designs and system optimized designs

The second task then is to compare the performance of aircraft that are designed towards design criteria that are formulated at the aircraft level (Range, Endurance, Climb Rate) to the performance of aircraft that are design towards design criteria formulated at the powerplant level ($E\ m_{power}^{-1}$, $P\ m_{power}^{-1}$).

Upon completion of these tasks, the hypotheses can be tested by comparing the performance of the simplified models to the fully integrated multilevel aircraft design models. Each task is directly a test of each hypothesis.

3.4 Research Question 3 – Energy Management Studies for Fuel Cell Hybrid Aircraft

As stated in the literature review of design for fuel cell powered aircraft, all of the fuel cell aircraft design methods that have been proposed to date are static designs. No dynamics of energy management or flight dynamics have been considered in the literature of fuel cell powerplants for aircraft. This despite the fact that a number of the demonstrated fuel cell powered aircraft are hybridized and that flight path optimization has been used to design and build long endurance conventionally powered UAVs.

This research question seeks to understand what the broad applications of hybridization and flight path optimization might be for fuel cell powered aircraft.

Research Question 3*: What are the conditions where optimal fight path management and hybridization can improve the design performance of fuel cell powered aircraft? Does the aircraft simulation structure as proposed enable the prediction of maximum aircraft endurance?*

There are two primary goals of this research question. First, we would like to understand, in general, whether there is an application for fuel cell powered hybrid aircraft. It could be that the hybrid aircraft that exist in practice use battery power as a design "band-aid" to cover up inadequacies in the fuel cell system design. Second, we would like to understand whether the static design methods developed in over the course of this research effort are adequate to describe the maximum endurance of the aircraft. If not, the scope of the research effort will have to expand to include the hybridization and flight path management of the fuel cell powered aircraft.

Hypothesis 3*: Dynamic energy management of a fuel cell powered aircraft will not improve the performance of fuel cell powered aircraft.*

Task 3.1*:* Characterize the conditions of use of a small aircraft including turbulence, wind variability, thermals etc. Synthesize meta-models of the fuel cell aircraft energy storage systems and perform nonlinear programming analyses to determine strategies for optimal energy management. Propose conditions of use (flight regimes, battery states of charge, flight profiles, battery power to fuel cell

power ratios, etc.) where fuel cell powered hybrid aircraft can provide performance benefits compared to conventional fuel cell powered aircraft.

Task 3.2: Synthesize meta-models of the fuel cell aircraft energy storage systems and perform nonlinear programming analyses to determine strategies for periodic optimal flight. Compare the optimal flight paths of fuel cell powered aircraft to those of conventional fuel cell powered aircraft and internal combustion powered aircraft.

Completion of these tasks will provide direct tests of the hypothesis. If there are no regimes of foreseeable flight where the fuel cell hybrid powerplant can outperform a non-hybrid fuel cell powerplant, then the hypothesis is supported. If there are no conditions where periodic flight paths enable more endurance than conventional flight paths, then the hypothesis is supported. If the hypothesis is not supported, then the present non-dynamic structure of the long-endurance UAV design algorithm must be abandoned.

3.5 Research Questions Summary and Development Tasks

Completion of the research tasks will result in the development of a new methodology for the design of fuel cell powerplants for unmanned aerial vehicles. The fundamental models will have been constructed at the fuel cell subsystem level. This allows the model to guide the design, development and construction of fuel cell systems at a level of detail that has not been attempted before. The model will have been validated at the component level, at the system level, and as a component of a fuel cell aircraft design process. The design model will be used to construct a series of fuel cell

powered aircraft and powerplants for technology demonstration, validation and testing. The complexity and scope of the modeling effort will be defended through comparison to other fuel cell aircraft design methods that exist in the literature. The design space around fuel cell hybrid aircraft will have been explored and integrated into the design model.

A summary of the research questions, associated tasks and research challenges is shown in Figure 9. The research challenges that are associated with each research question often require the gathering of new information that does not exist in literature and requires significant developmental and experimental effort to obtain. The details of these development tasks are shown in Figure 10. Each development task is not necessarily associated with a research question, but instead provides the information, experience and baselines required to address the research challenges for each research question.

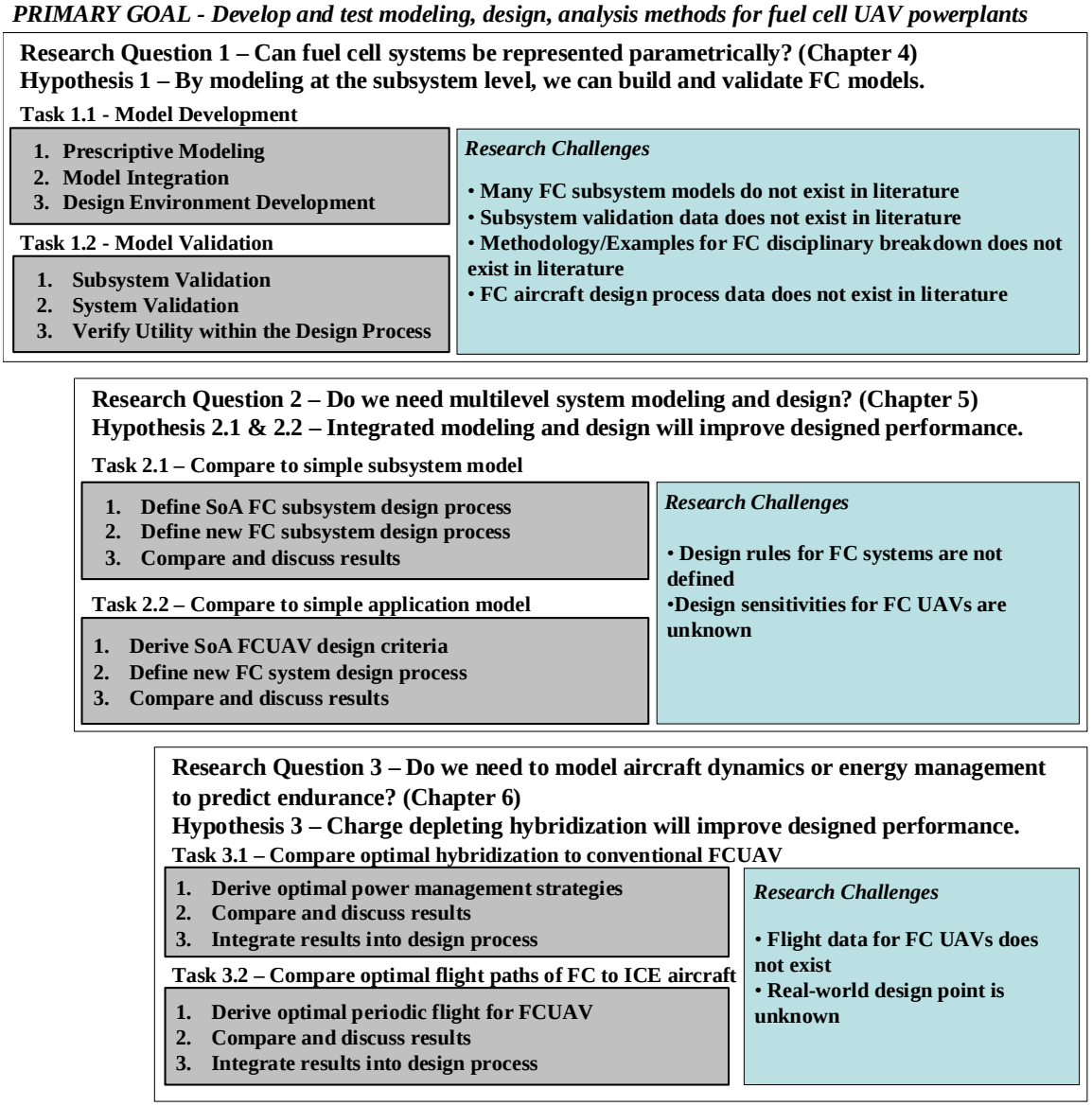

Figure 9. Summary of research questions and tasks associated with this dissertation

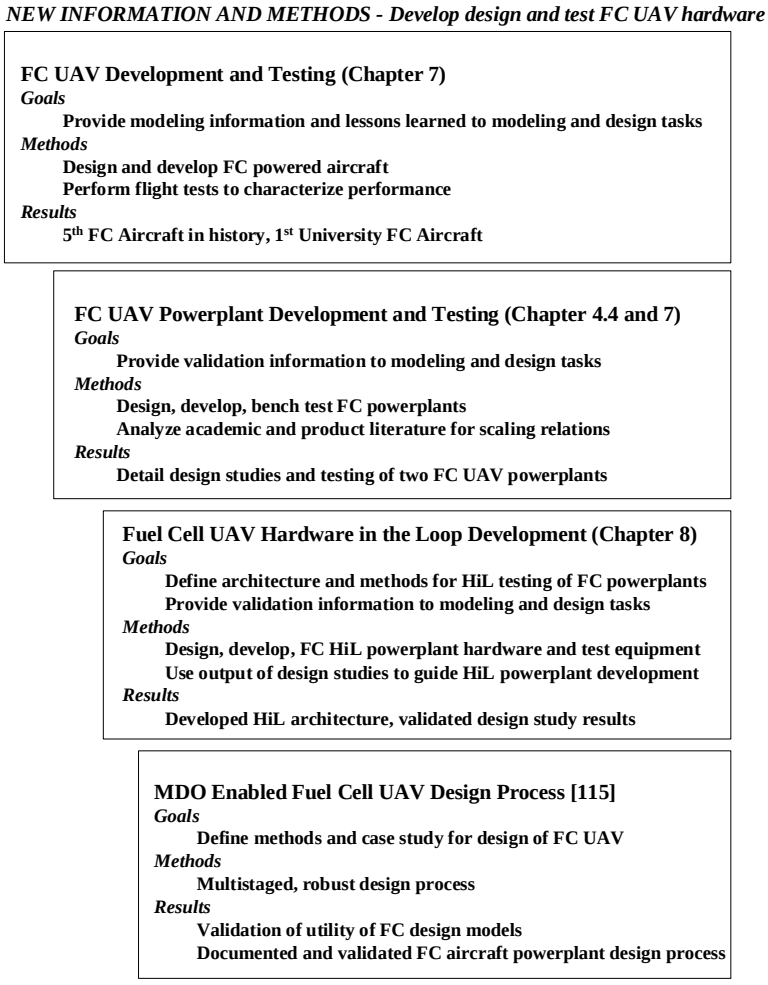

Figure 10. Summary of development tasks associated with this dissertation

3.6 Definition of Research Scope

The research effort will be concentrated on near-term realizeable fuel cell powered aircraft. The most technologically ready fuel cell powered aircraft is the small scale, polymer electrolyte membrane (PEM) fuel cell powered unmanned aerial vehicles. The methods, case studies and models developed for this research will reflect the performance and requirements of this application. The methods developed for this research effort are more general and have wider applicability.

3.7 Definition of Research Plan

The global layout of the research effort is shown in Figure 11. The first section (Chapter 3) of the dissertation deals with the development of fuel cell subsystem and system models. The modeling information from this effort is passed to the remaining tasks. Chapter 4 uses the models and tools developed in the Fuel Cell System Modeling task to perform design studies for fuel cell powered aircraft. The conceptual design results that are the output of these design studies are passed to the next tasks. Chapter 5 presents studies of the energy management of fuel cell and fuel cell hybrid aircraft. Experimental fuel cell UAV hardware studies including demonstration and hardware in the loop studies of a fuel cell aircraft follow in Chapters 6 and 7. There are a number of ways that the information from these later tasks are included in the earlier tasks. The information from the experimental studies are used for validation of the design models. The information regarding energy management of fuel cell hybrid aircraft is used with the tools from Chapter 4 to design a hybrid fuel cell powered UAV in Section 5.5.

Design sensitivity information from the conceptual design tasks are used to determine the fidelity needs for the fuel cell models.

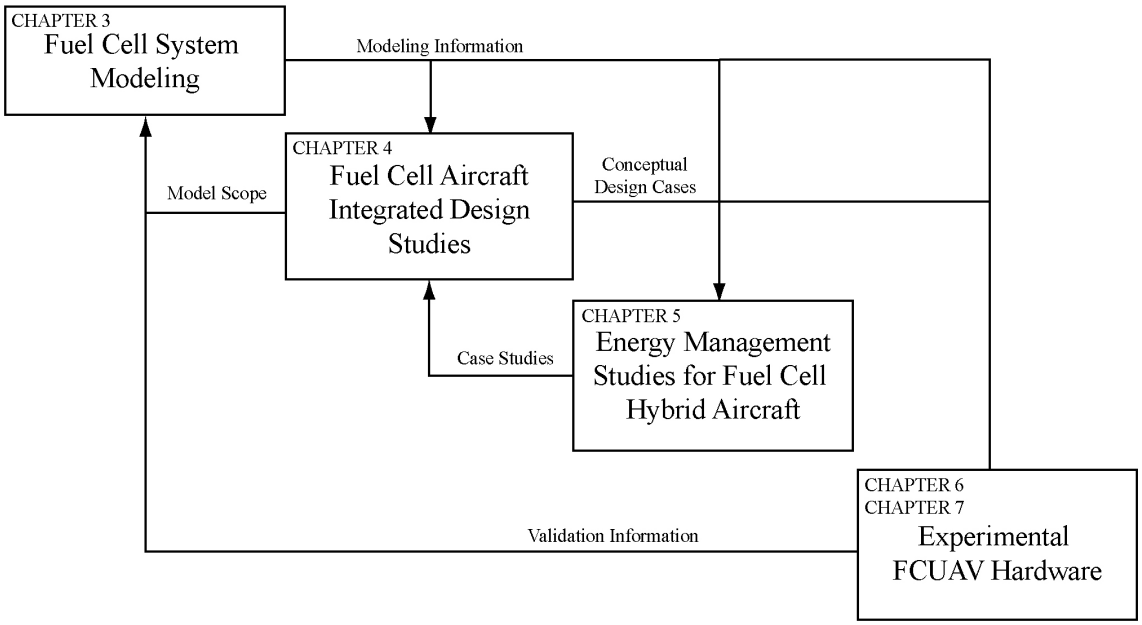

Figure 11. Information flow within the dissertation research effort

CHAPTER 4

MODELING OF FUEL CELL POWERPLANTS FOR SYSTEM DESIGN FOR AVIATION APPPLICATIONS

This study begins at the stage of conceptual aircraft design. Conceptual design synthesis begins with definitions of the systems of interest, the modeling and simulation structure, and the system objectives for evaluation and optimization.

The goal of conceptual design is to define the subsystem interactions, configuration, layout, dimensions and performance of the integrated airframe and powerplant system. For this study, we are primarily interested in the synthesis and comparison of near-term available, small-scale, low altitude fuel cell powered UAVs that are able to accomplish the generic, long-endurance mission profiles. These restrictions of design scope place requirements and limitations on the models used to represent the performance of the aircraft systems.

For instance, the airframe model is designed to be able to model the static performance of highly generic UAVs at low Mach number, at a scale of between 5 kg and 50 kg of gross takeoff weight. As such, the baseline airframe is a conventional high wing monoplane, with rear empennage, driven by tractor propeller. To model the airframe, this study includes parametric model representations of the airframe aerodynamics, structures, mass, stability, geometry, mission performance, payload, and propulsion. Details such as airframe dynamics, rigorous aerodynamic optimization, manufacturability, and costs are left for later stages of design.

The powerplant model is designed to be able to model the steady-state performance of a PEM fuel cell powerplant delivering DC electrical power to a propulsion electric motor and payload. The PEM fuel cell technology is chosen for this study because of its high technology readiness factor, relatively high specific power and robustness in mobile applications. To model the powerplant, this study includes parametric model representations of the powerplant electrochemical performance, static control, mass, geometry, and component power consumption. Again, low-level implementation challenges are left for later stages of design.

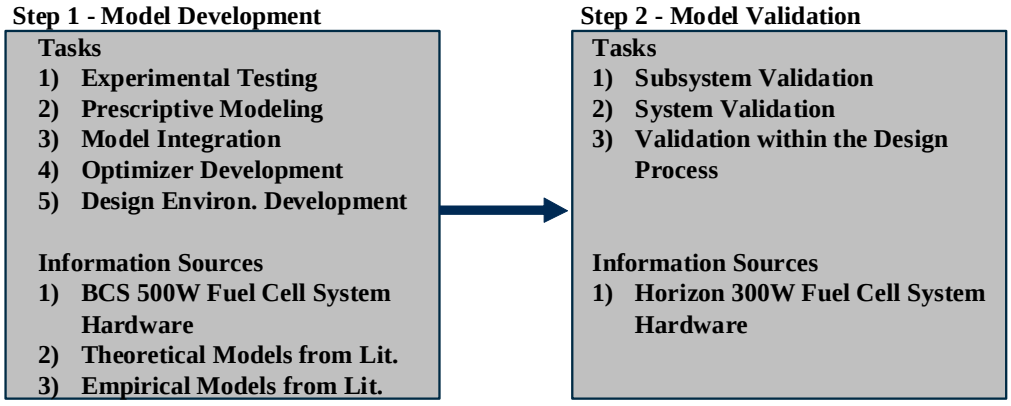

Figure 12. Description of information sources and tasks for the modeling of fuel cell systems for aircraft

Figure 12 shows the layout of the information sources and tasks for the modeling of fuel cell systems and for this chapter. The models developed in this chapter are derived from a variety of information sources including experimental data from testing of developed fuel cell systems, theoretical models of fuel cell performance, and empirical models from the literature. Two fuel cell systems are used to provide input data to the model development and validation tasks. These two systems were constructed by the author for this project at the GTRI Center for Innovative Fuel Cell and Battery

Technology. The first system is based on a 500W 32-cell fuel cell stack whose MEAs and bipolar plates are manufactured by BCS Fuel Cells of Bryan, TX. The second system is based on a 300W 62 cell fuel cell stack manufactured by Horizon Fuel Cells of Singapore. In general, the fuel cell models are based on experimental data from the BCS fuel cell system. Validation of the fuel cell models is based on experimental data from the Horizon fuel cell system. Breaking up the development and validation tasks allows for the validation exercise to provide information regarding the scalability of the models.

4.1 Model Development Tasks

This section describes the characteristics of the mathematical and conceptual contributing analyses (CAs) that are used to describe the geometry, mass and performance of the components of the fuel cell powered aircraft.

4.1.1. Experimental Testing of Fuel Cell Hardware

The experimental methods and results for the development, testing and evaluation of the fuel cell powerplants are presented in other parts of this dissertation including Chapter 7, Appendix I and Appendix II.

4.1.2. Fuel Cell Contributing Analyses

Fuel cells are a direct electrochemical conversion device that generates electricity from a reaction with atmospheric oxygen and stored hydrogen gas. The fuel cell powerplant is divided into the fuel cell stack and the fuel cell balance of plant.

Stack Modeling - The electrochemical, geometric and mass characteristics of the fuel cell stack are scaled by the number of fuel cells in the fuel cell stack and the electrochemically active area of each fuel cell. The fuel cell stack electrochemical

performance is modeled at the cell level using a static polarization curve fit from literature [68].

$$\frac{\eta}{b} = \phi\left(\frac{f_\lambda \bar{j}}{j_*}\right)\ln\left(\frac{f_\lambda \bar{j}}{j_*}\right) - \ln k_0 - \ln\left(1 - \frac{f_\lambda \bar{j}}{j_{D0}}\right) \tag{2}$$

$$f_\lambda = -\lambda_c \ln\left(1 - \frac{1}{\lambda_c}\right) \tag{3}$$

$$V_{cell} = V_0 - \eta - R_{cell}\bar{j} \tag{4}$$

The quantities b, V_0, R_{cell}, $\ln(k_0)$, and j_{D0} are fit in a least squares sense using a pattern search optimization approach. The efficiency of the fuel cell system is defined by the equation:

$$\eta_{FC} = \frac{V_{FC}}{n_{cells}E_0} \tag{5}$$

Based on the fuel cell characteristics and the required output power, the mols of hydrogen required to complete the flight can be calculated based on Faraday's Law:

$$\dot{W}_{H_2} = \frac{n_{cells}I}{2F\eta_{util}} \tag{6}$$

This model of fuel cell performance was derived and verified using the BCS fuel cell, whose performance is shown in Figure 13.

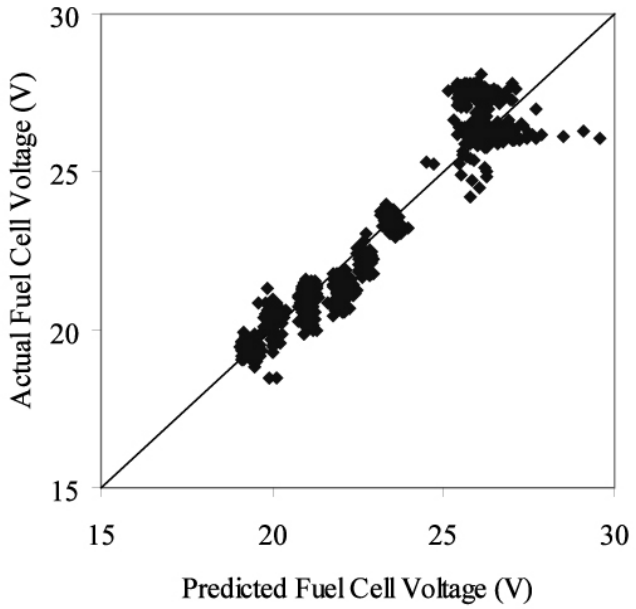

Figure 13. Actual versus predicted performance of the fuel cell model using the data from the BCS fuel cell

The performance of the individual fuel cells used for subsequent conceptual design tasks is equivalent to the published stack performance of the Gore 58 series membrane electrode assembly [102]. This membrane electrode assembly is chosen as representative of the state of the art for self-humidified, low-pressure PEM fuel cells. The maximum current density achievable from the fuel cell stack is 1200mA cm^{-2} $cell^{-1}$ and the maximum specific power is 0.6W cm^{-2} $cell^{-1}$, as shown in Figure 14.

0.028251 0.0090847 1.443 0.17242 0.76728

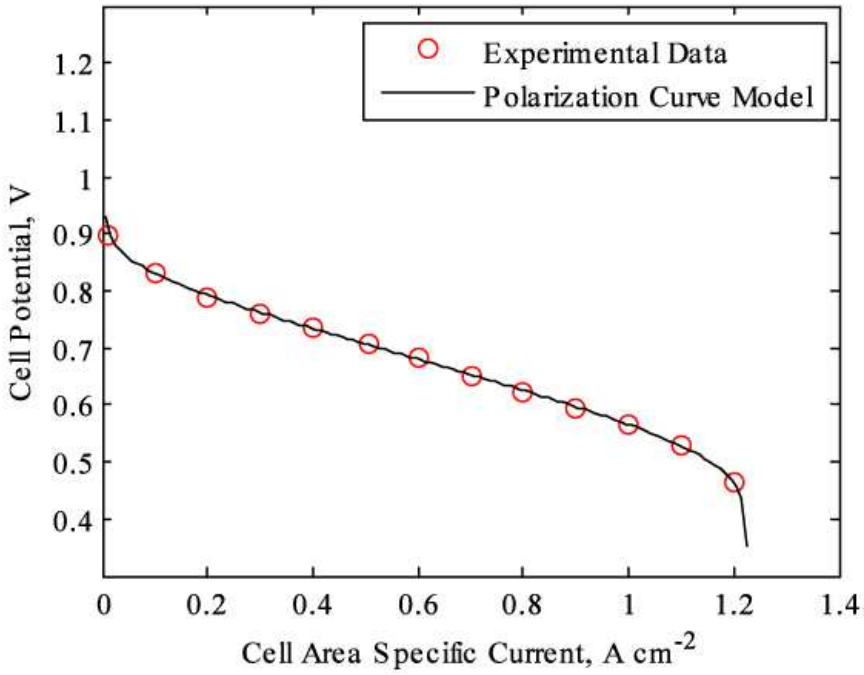

Figure 14. Fuel cell unit cell performance

The stack size and mass scaling factors are based on the characteristics of the BCS prototype stack with 0.48cm (3/16in) graphite bipolar plates, aluminum endplates and aluminum through-bolts. The weight of the fuel cell stack is the sum of the weight of the bipolar plates, current collecting endplates, and through bolts.

$$m_{stack} = m_{BP} + m_{EP} + m_{Bolts} \tag{7}$$

The dimensions of the bipolar plates and endplates are based on the active area of the fuel cell MEA.

$$\begin{aligned} x_{EP} &= y_{EP} = x_{BP} = y_{BP} = 1.2 \cdot \sqrt{A_{FC}} \\ z_{BP} &= 0.48cm \\ z_{EP} &= 0.96cm \end{aligned} \tag{8}$$

The bolts are assumed to be made of alumimum at ¼" diameter and a length (z_{Bolts}) of

$$z_{Bolts} = n_{cells} x_{BP} + 2x_{EP} \tag{9}$$

Balance of Plant Modeling - The fuel cell balance of plant represents the air delivery, hydrogen delivery and regulation, water cooling and power management and distribution subsystems of the fuel cell. The electrical power consumption and mass of the fuel cell balance of plant are based on the characteristics of the developed 500W BCS self-humidified, low-pressure fuel cell system. The compressor power consumption and mass are scaled at 1.76 W min/L and 37.75 g/L of air required, values representative of the tested performance of a low pressure (34 kPa) diaphragm compressor, as shown in Figure 15. The water pump consumes 0.05 W of DC electrical power per watt of heat rejected continuously and the radiator weighs 2.1 g/W of fuel cell heat rejected at peak fuel cell power.

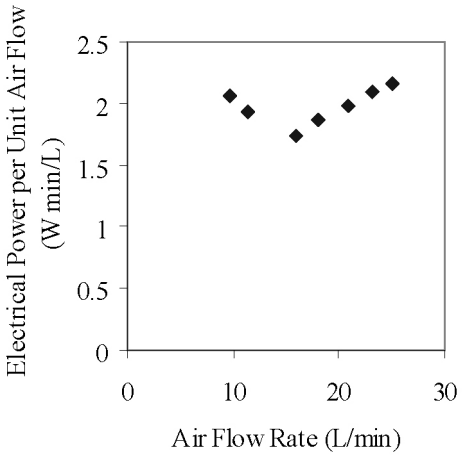

Figure 15. Performance of a single diaphragm compressor at 5 psi gage pressure

4.1.3. Hydrogen Storage Contributing Analyses

The compressed hydrogen storage system is modeled as a composite over-wrapped pressure vessel using empirical data from the literature and mechanics of materials. The hydrogen tank is of cylindrical geometry with hemispherical end caps. The tank is subjected only to loading due to the uniform pressure difference between the internal hydrogen pressure and the external atmospheric pressure. The aluminum tank liner is assumed to be of constant thickness and does not contribute to the strength of the tank, but does contribute to its weight. In general, composite hydrogen tanks require metallic or polymeric liners to reduce the hydrogen leak rate. The thickness of the composite overwrap is specified to resist the hoop stress and the axial stress due to the pressure loads. The total composite thickness is equal to:

$$t_{composite} = x_{fs} \cdot \left[\frac{r(P - P_{atm})}{\tau_{\text{maxcomp}}} + \frac{r(P - P_{atm})}{2\tau_{\text{maxcomp}}} \right] \tag{10}$$

and the total tank mass is calculated using the formula:

$$m_{\text{tank}} = (1 + f_{mount}) \cdot (m_{\text{liner}} + m_{\text{composite}}) + m_{\text{reg}} + m_{H_2} \tag{11}$$

Table 3. Characteristics of conceptual compressed hydrogen storage system

Hydrogen Storage Design Parameter	Value	Notes
Composite Overwrap Maximum Stress ($\sigma_{maxcomp}$)	1.9GPa	Kevlar-49/epoxy at 55% translation [103,104]
Liner Density (ρ_{liner})	2700 kg/m^3	Aluminum 6061 [105]
Regulator Mass (m_{reg})	0.35 kg	[12]
Composite Overwrap Density (ρ_{comp})	1530 kg/m^3	[103]
Liner Thickness (t_{liner})	0.762 mm	Aluminum 6061 [106]
Liner Load Sharing	0%	
Factor of Safety to Yield (x_{fs})	2.5-4.0	
Tank Mounting/Bosses/Tubing Mass Fraction (f_{mount})	10%	[107]

The volume (V) required by this amount of hydrogen stored at a pressure (P) is calculated using the Redlich-Kwong equation [108]:

$$P = \frac{RT}{V-b} - \frac{a}{T^{1/2}V(V+b)}$$
$$a = 0.1425\ K^{1/2} \cdot m^6 \cdot Pa \cdot mol^{-2}$$
$$b = 1.817 \cdot 10^{-5}\ m^3 \cdot mol^{-1} \qquad (12)$$

4.1.4. Aircraft Contributing Analyses [16]

For conceptual design calculations, the wing airfoil used is a Selig-Donovan 7032. This airfoil is a highly efficient, low-Reynolds number airfoil and is used for all of the aircraft configurations considered. The aerodynamic contributing analysis was conducted using both offline and online calculations. Wings2004, a potential flow analysis code, was used offline to calculate induced drag, lift, and interaction effects between the wing and tail [109]. The parasite drag of the wing was also calculated offline using profile drag numbers tabulated versus Reynold's number based on wind tunnel tests of the Selig-Donovan 7032 airfoil [110].

Online, the Aerodynamic CA estimates the fuselage lift and drag characteristics and uses this information with the offline values to estimate the parasite drag of the aircraft and develop a drag polar of the aircraft. Most of the online calculations are based on the methods and equations of Roskam [87]. The fuselage models take into account the geometric properties of each of the powerplant components so as to size the fuselage appropriately. Example designs, shown in Figure 16, illustrate that the geometry of the components of the powerplant influence the geometry, mass, and aerodynamic properties of the fuselage.

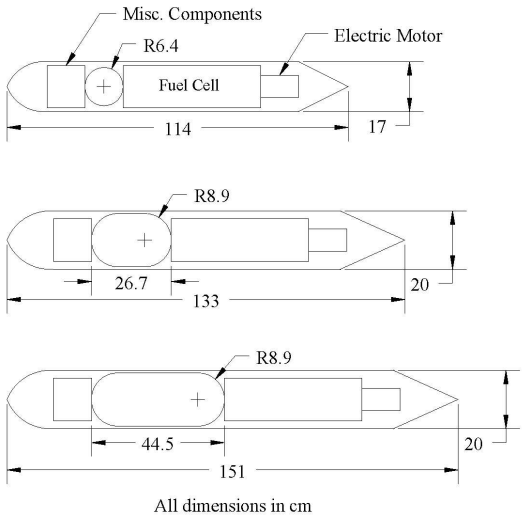

Figure 16. Example fuselage specifications and packaging diagrams

Empennage sections were analyzed assuming a NACA 0009 airfoil. Sizing of the empennage is based on maintaining a static margin (scaled by the wing chord) of 20% and an aircraft yawing moment coefficient of 0.15. Sizing of the tail is accomplished using an offline iterative method involving Wings2004 [109] and was scaled online using the resulting tail volume coefficients. Aircraft thrust, cruise airspeed and maximum climb rate at cruise airspeed are calculated at standard atmospheric conditions at the elevation of Atlanta, Georgia, USA.

The propeller performance contributing analysis is based on Goldstein's vortex theory of screw propellers using the Betz condition [111]. The propeller geometries used in this analysis are derived from measurements of several commercially available small-scale propellers. To account for propellers of varying diameter and pitch, the baseline propeller aerodynamic pitch distributions and the planform blade shapes are appropriately scaled while assuming that the airfoil shape distribution along the blade span remains consistent with the baseline propeller. Propeller/fuselage interference is modeled using the method from Lowry [112]. Variable pitch is modeled by allowing the optimizer to determine the optimal propeller pitches for both climb and cruise configurations.

For this conceptual design study, the aircraft follows a two part flight path consisting of climb and cruise, shown in Figure 17. The optimal flight conditions of the aircraft for each mission component are determined independently during the flight simulation and optimization.

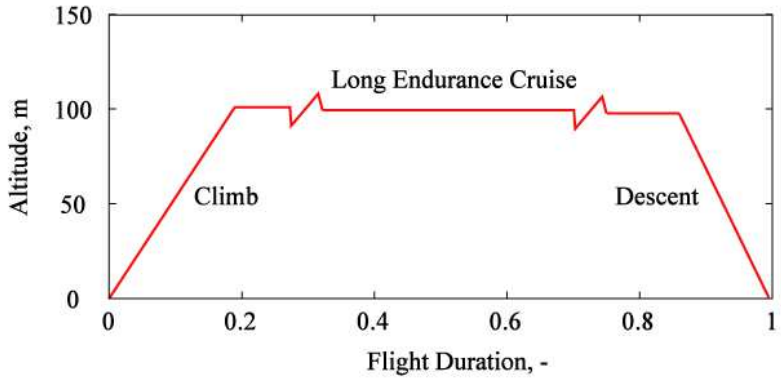

Figure 17. Prototypical long endurance flight profile

4.2 Model Integration into System Analysis and Design Environment

The fuel cell aircraft analysis and design problem that is addressed in this study is cast in the form of a canonical multidisciplinary design and optimization (MDO)

problem, as shown in Figure 18. The design point is specified by a number of design variables that are inputs to a multidisciplinary analysis (MDA) or design structure matrix (DSM) which is capable of analyzing the complex system at the system level. The performance of the aircraft design is improved by embedding the DSM inside of an optimization routine, which varies input design variables to minimize a cost function (*OEC*).

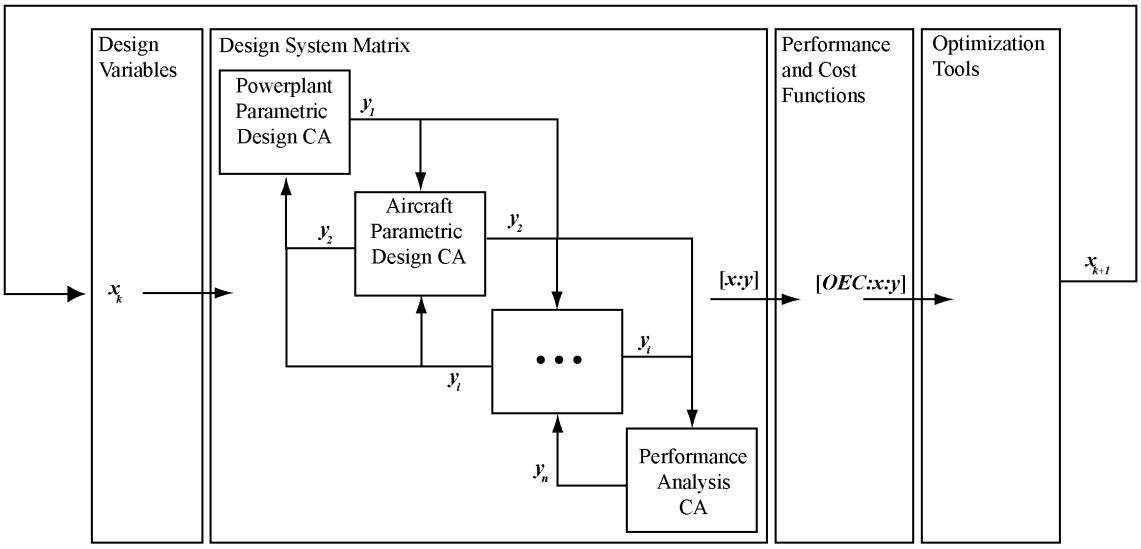

Figure 18. Canonical multidisciplinary design and optimization problem structure

The 45 CAs that are used for the fuel cell airplane design problem are connected into the DSM shown in Figure 19. The problem contains 108 CA variables and 28 design variables. The DSM is primarily upper triagonal, with only a few feedback signals. For solution purposes, the feedback loops are eliminated by defining compatibility constraints and introducing guess design variables. A converged solution of the DSM for a given design variable input vector x is then found using Newton's method. The design variables that are used to specify the aircraft configuration are provided in Table 4.

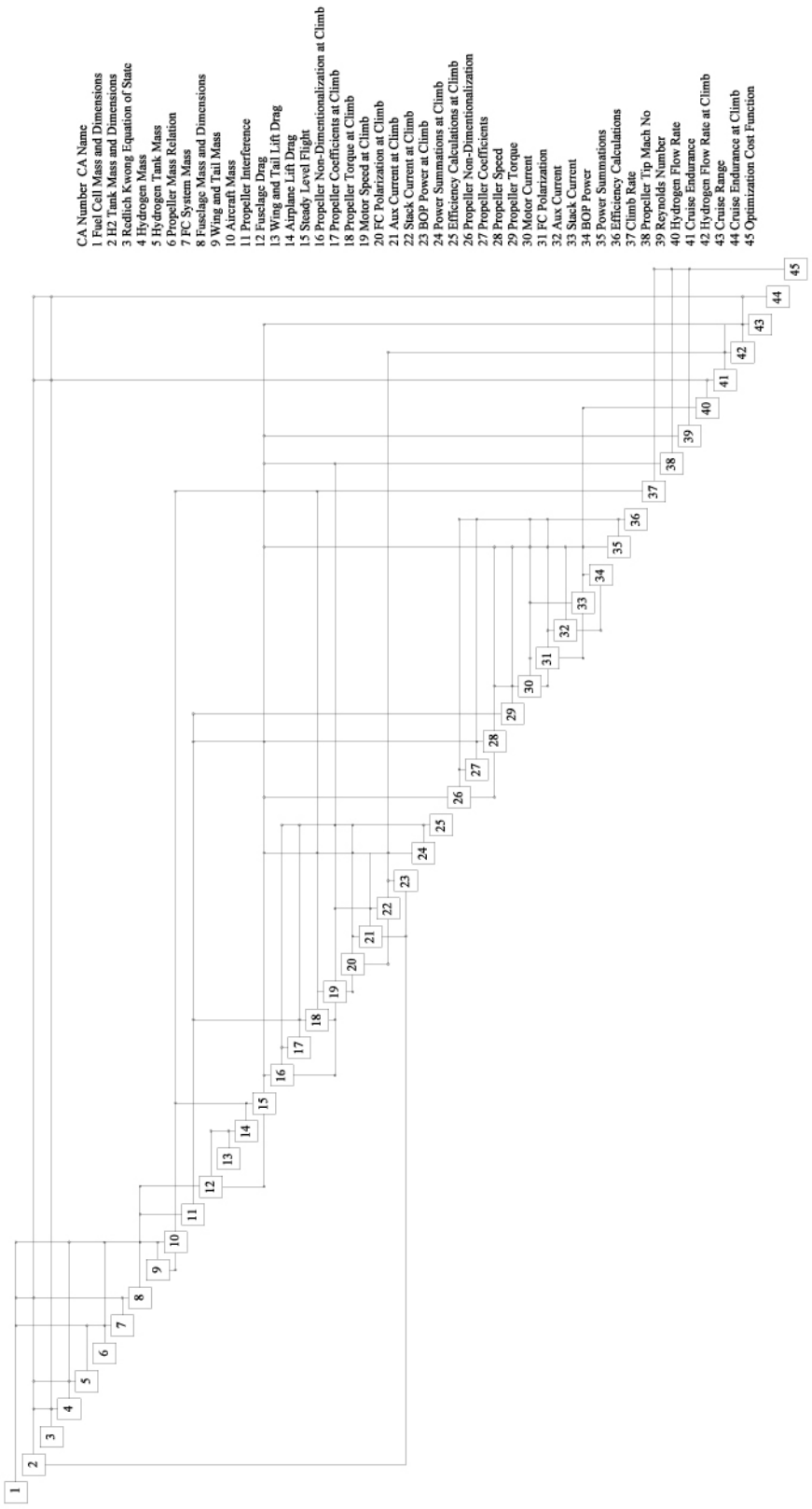

Figure 19. Default design structure matrix for fuel cell UAV design problem

Table 4. Primary design variables and side constraints for conceptual design of a fuel cell UAV

Design Variable	Minimum Value [units]	Minimum Value [units]
Electric Motor Scaling Parameter	1 [-]	12 [-]
Number of Propellers/Motors	1 [-]	4 [-]
Number of Fuel Cells	1 [-]	∞[-]
Fuel Cell Active Area	1 [-]	∞ [-]
Hydrogen Tank Radius	0 [m]	∞ [m]
Hydrogen Tank Length to Diam. Ratio	1 [-]	4 [-]
Hydrogen Storage Pressure	0 [MPa]	∞ [MPa]
Propeller Diameter	0 [m]	∞ [m]
Wing Area	0 [m^2]	∞ [m^2]
Wing Aspect Ratio	1 [-]	20 [-]
Propeller Pitch at ¾ Span at Cruise	0 [m]	∞ [m]
Propeller Pitch at ¾ Span at Climb	0 [m]	∞ [m]
Motor to Propeller Gear Ratio	0.1 [-]	20 [-]

4.3 Design Optimization Methods

Varying the values of the design variables changes the performance of the aircraft model. In order to design aircraft that can meet the design goals of interest, the MDA is wrapped in an optimization routine that controls the design variables so as to improve the design of the aircraft by minimizing an overall evaluation criterion (*OEC*) function, subject to constraints (*g*).

$$\begin{aligned} &\text{Minimize}: OEC\left(\vec{y}\left(\vec{x}\right)\right) \\ &\text{Subject to}: \vec{0} \geq \vec{g}(\vec{x}) \end{aligned} \tag{13}$$

A negative number for any of the side constraints can occur when a design variable is outside of the ranges shown in Table 4. Many of the physics-based CAs will produce an error if a design variable is outside of the physically feasible ranges (ie a Hydrogen Tank Radius of < 0). Unfortunately, many constrained optimization schemes cannot guarantee

that side constraints will not be violated during the solution process. To avoid side constraint violations, a sequential unconstrained minimization technique (SUMT) was used. The SUMT requires that the objective function to be reformulated as:

$$\Phi = OEC\left(\vec{y}(\vec{x})\right) + \lambda\zeta\left(\vec{x}, \vec{y}(\vec{x})\right) \tag{14}$$

where λ is a scalar multiplier and $\zeta_{(x,\, y(x))}$ is an imposed penalty function dependent on the design variables (x) and the CA output variables (y). In order to force the optimization procedure to favor feasible designs and to avoid possible discontinuities caused by the introduction of the penalty function, the following definition for $\zeta_{(x,\, y(x))}$ was used:

$$\zeta\left(\vec{x}, \vec{y}(\vec{x})\right) = \sum_{j=1}^{n} \tilde{g}_j(\vec{x}) \tag{15}$$

$$\tilde{g}_j(\vec{x}) = -\frac{1}{g_j(\vec{x})} \quad \text{if} \quad g_j(\vec{x}) \le \varepsilon \tag{16}$$

$$\tilde{g}_j(\vec{x}) = -\frac{2\varepsilon - g_j(\vec{x})}{\varepsilon^2} \quad \text{if} \quad g_j(\vec{x}) > \varepsilon \tag{17}$$

$$\varepsilon = -C \cdot (\lambda)^a \tag{18}$$

The variable array $g_j(\vec{x})$ represents the absolute and side constraints, where n is the total number of absolute and side constraints. The scalar values of C = 0.246 and a = 0.417 were used in all calculations based on preference weighting of the design criteria [113]. For the first stage of the optimization, λ = 0.006 was used. The converged

solution of the first stage optimization provides a better starting point for the next optimization stage. For the next stage λ is decreased to 10% of its previous value and the optimization routine is repeated using the previous solution as a starting point. This is continued until the acceptable convergence criteria have been met.

Figure 20 shows the result of a multi-objective tradeoff study performed using the tools described above. The multi-objective study is constructed by treating the climb rate as a constraint in the above formulation. By varying the value of the constraint, the Pareto optimal frontier can be constructed [113].

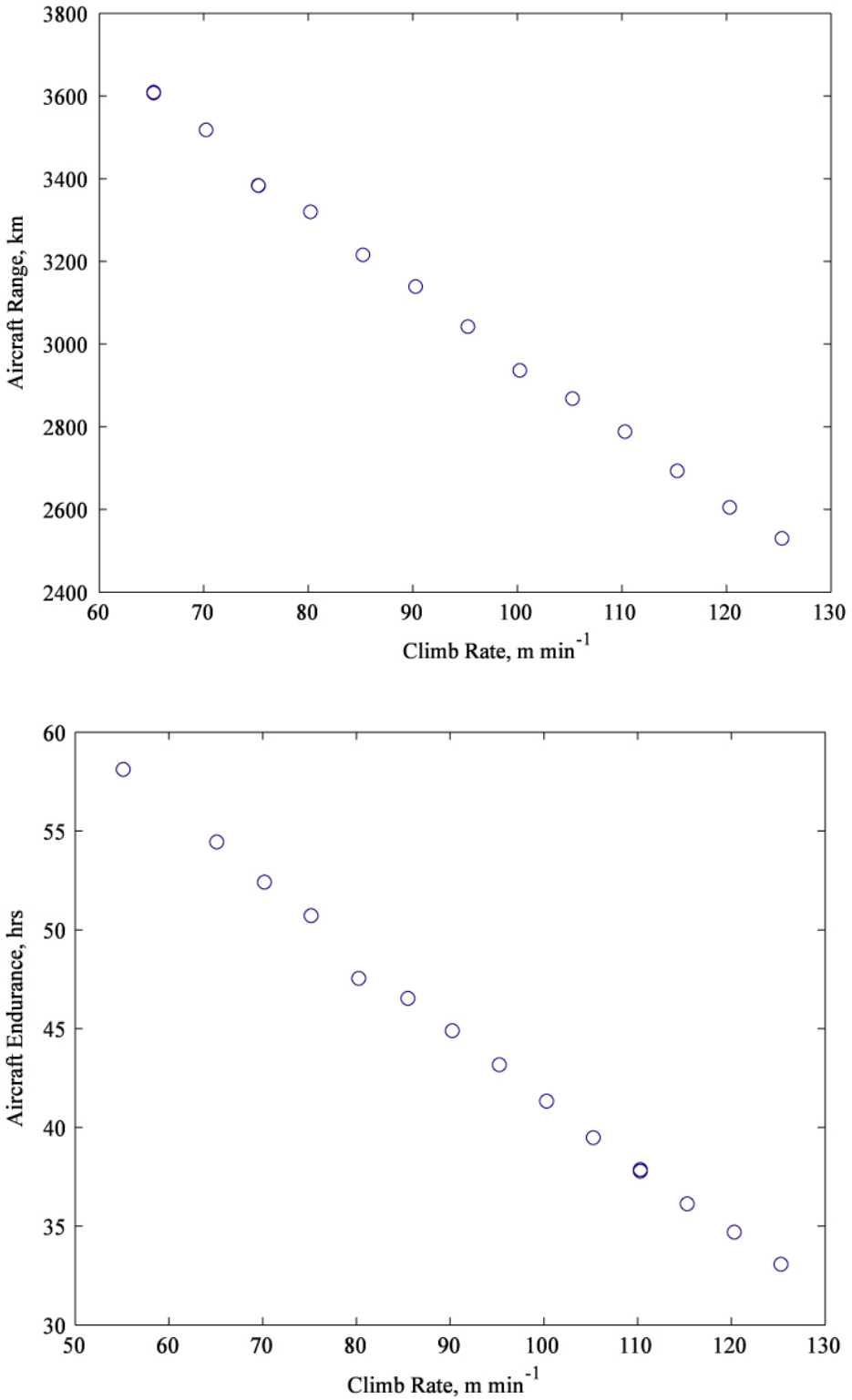

Figure 20. Multi-objective tradeoff study of fuel cell aircraft performance as a function of climb rate constraints and cost functions

4.3.1. Optimization Algorithm Performance

Figure 21 shows the performance of the optimization algorithm at finding the optimum configuration from three separate starting points. The three starting points represent different initializations of the optimization algorithm. As the iterations of the SUMT optimization scheme progress, the three aircraft designs converge to the same point in the design space.

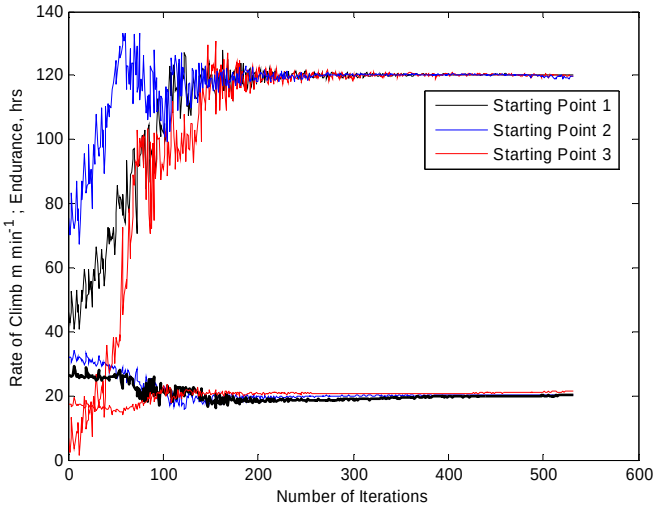

Figure 21. Optimization algorithm performance

4.4 Model Validation Tasks

The multi-disciplinary analysis framework for system design decomposes design problems into discrete contributing analyses with predefined interactions between the contributing analyses. Validation of systems models within the multi-disciplinary design framework therefore has three primary components:

1. Independent validation of the contributing analyses. This method theorizes that if each of the contributing analyses is trusted, the systems analysis built

from them can be trusted. This can be though of as a build-up approach to systems validation [114,115].

2. System-level validation of the system-level behavior. This method seeks validation of system level behavior of the model by comparison to system level behavior of the modeled system.
3. Validation for design decision utility. This step of validation ensures that the system model has a utility as a component in a design process. This type of validation is asserted by using the model for design and analyzing the outcomes [116].

These steps of the validation process are shown in Figure 22. The three components of the validation process are shown with their information inputs. For instance, the *subsystem validation* process consists of a comparison between the output of the contributing analysis and 1) the results of experimental tests of the actual component, or 2) the product specification literature. The *system level validation* makes a comparison between the results of thee detail design and the system test results. Any inconsistencies between these results show that the fuel cell system model does not capture all of the relevant interactions between the contributing analyses. The design process validation shows the comparison between the conceptual design and the system test results. If the performance as predicted during conceptual design and the performance as realized are substantially different, then the design process is not validated. If the values of the design variables from conceptual design and detail design are substantially different, then the design process is not validated. Ideally, the design process provides a direct decision

making path between the conceptual design and a more optimal detail design or similar performance and configuration.

Whereas a vast majority of aviation system design studies have incorporated contributing analysis validation, the scale, complexity and cost of most applications prevents system-level validations. This research effort attempts to perform an empirical contributing analysis validation, an empirical systems level validation, and a validation of the efficacy of the model within the proposed design scheme.

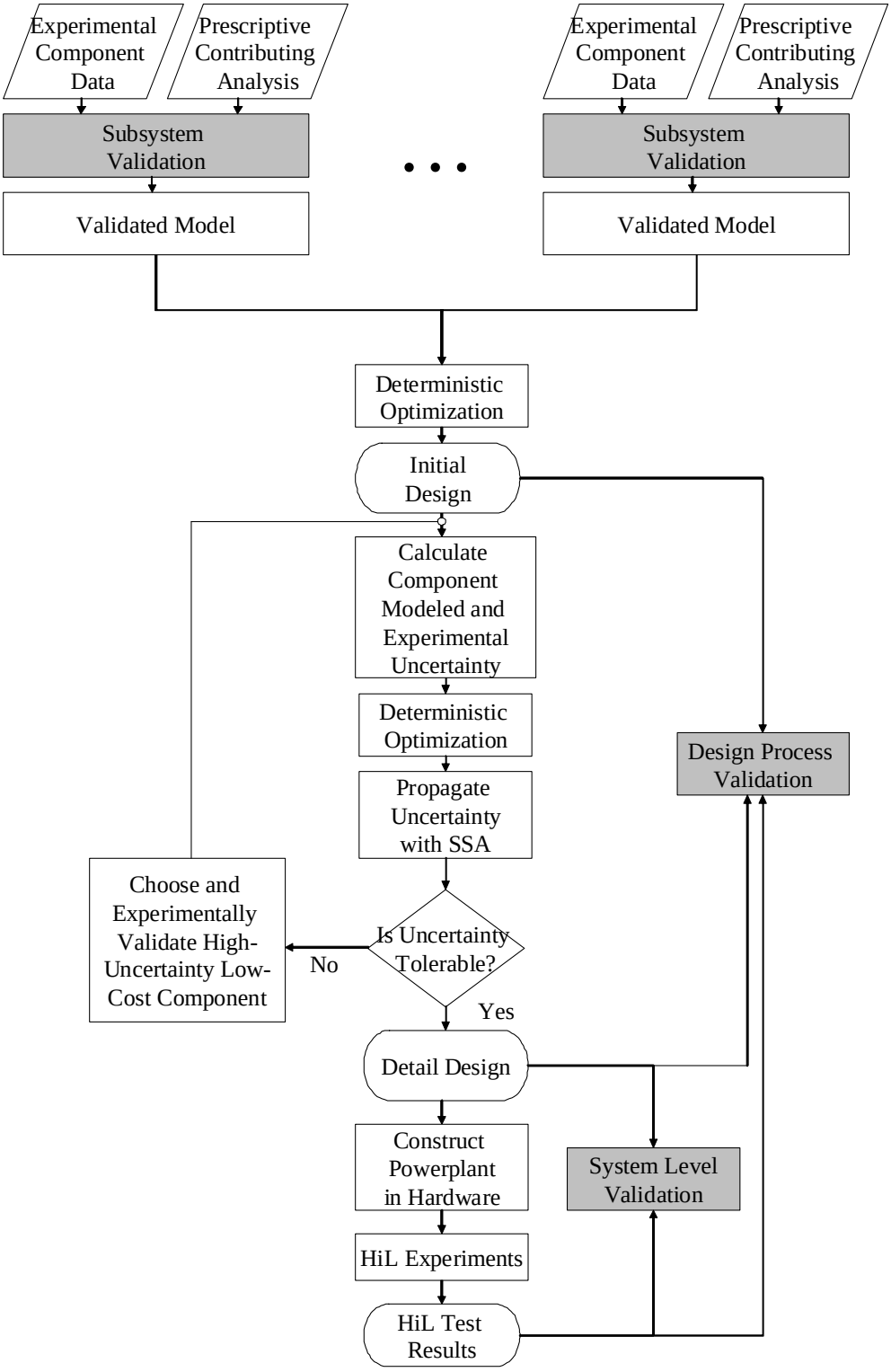

Figure 22. Flow diagram showing validation processes

4.4.1. Subsystem Validation

The following sections describe the empirical contributing analysis validation. The systems level validation is performed by comparing the system performance as modeled to the system performance of actual hardware [16].

Validation of the fuel cell system output voltage from the fuel cell CAs is performed by comparison to the Horizon H300 fuel cell hardware, shown in Figure 23.

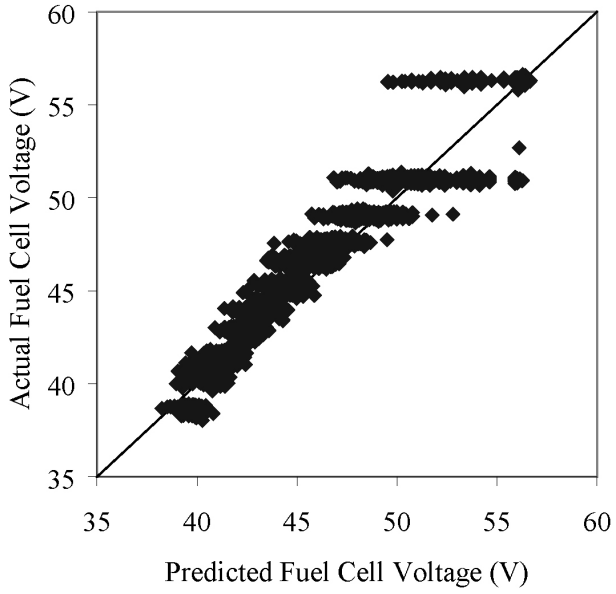

Figure 23. Actual by predicted plot for the Fuel Cell Voltage CA using the Horizon H300 fuel cell stack

Uncertainty in the steady state hydrogen flow rate output from the CA is calculated from comparison to the Horizon H300 fuel cell hardware, shown in Figure 24. The uncertainty in the CA is due to both aleatory and epistemic uncertainty. The aleatory uncertainty in the experimentally measured moment to moment hydrogen flow rate is 1.4% and the epistemic error in the model is 5.3%. The total uncertainty is calculated as

the Pythagorean sum of these component errors. It is notable that the Hydrogen Flow Rate CA slightly under-predicts the hydrogen flow rate.

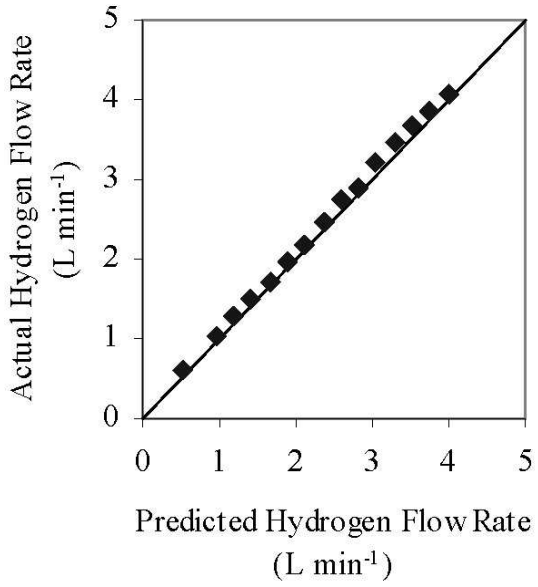

Figure 24. Actual by predicted plots for the Hydrogen Flow Rate CA

Uncertainty in the hydrogen utilization output of the fuel cell CA is calculated from comparison to the Horizon H300 fuel cell hardware, shown in Figure 25.

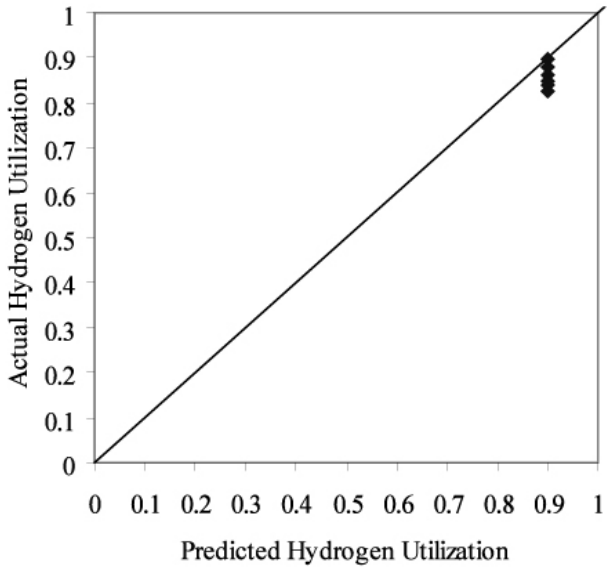

Figure 25. Actual by predicted plots for the Hydrogen Utilization contributing analysis

Uncertainty in the balance of plant power consumption output from the CA is calculated from comparison to the Horizon H300 fuel cell hardware, shown in Figure 26. Because of differences between the balance of plant assumed by the model and the balance of plant used in the H300 system, the model does not validate very well.

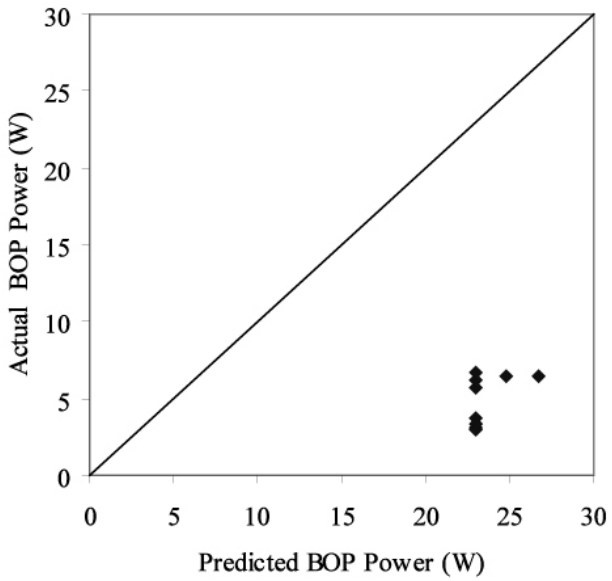

Figure 26. Actual by predicted plots for the balance of plant contributing analysis

Figure 27 shows the comparison between the predicted CA outputs and the actual hydrogen tank characteristics as provided by a commercial composite overwrapped cylinder manufacturer [117]. The uncertainties in the hydrogen tank CA outputs are primarily due to error in the model. Variability in the dimensions of the tanks as manufactured is approximately 0.6% and variability in tank mass is 2.1%.

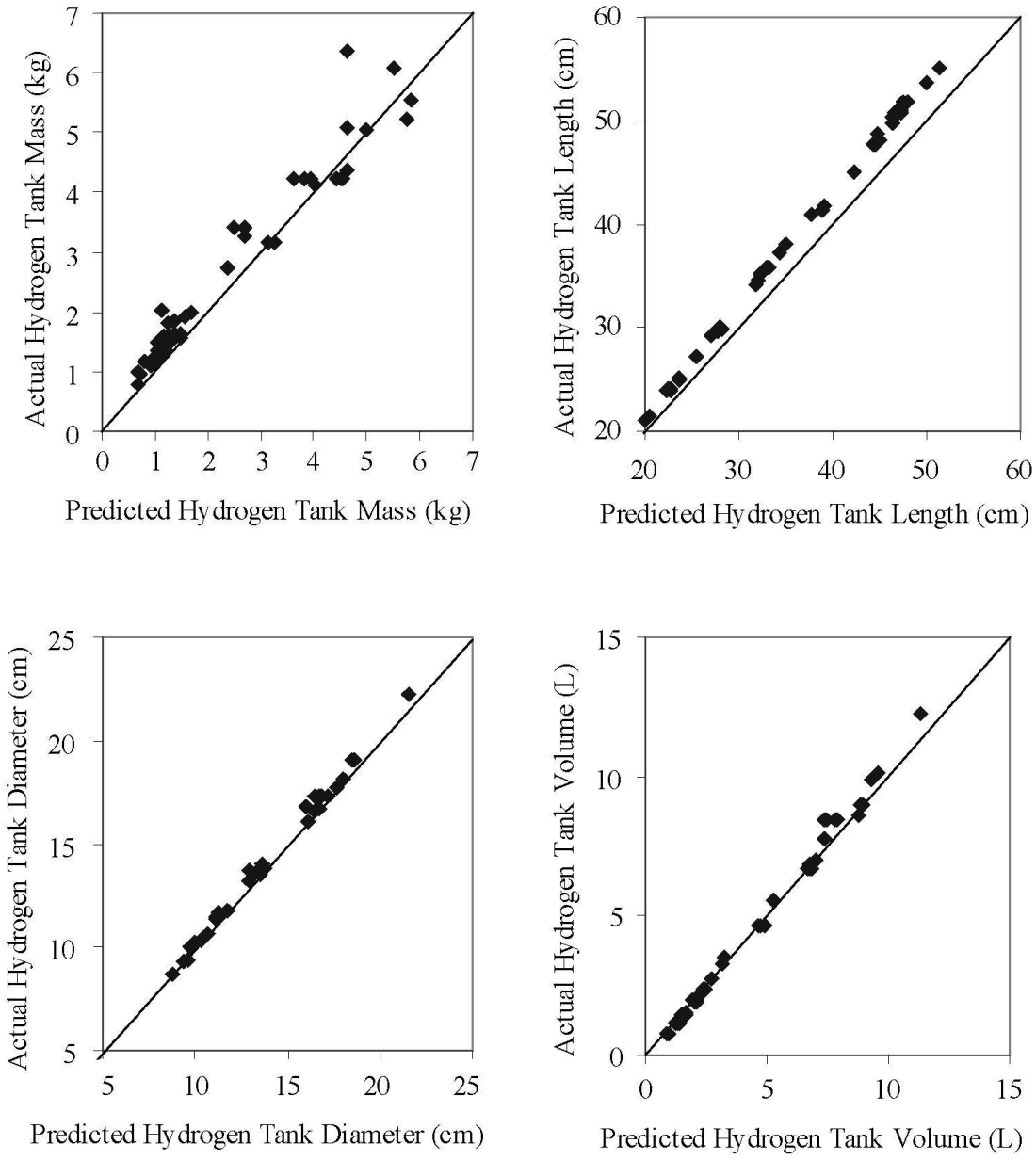

Figure 27. Actual by predicted plots for the Hydrogen Tank Mass and Dimensions contributing analysis

The uncertainty associated with the outputs of the Propeller CA is calculated based on comparisons between the calculated performance and actual wind-tunnel performance of three propellers. Aleatory uncertainty is assumed to be 0% because, for instance, the effect of manufacturing variability in terms of the values of the CA output

variables is negligible [118]. An actual versus predicted comparison for propeller coefficient CA is shown in Figure 28. The errors in the propeller CA are modeled as an epistemic uncertainty.

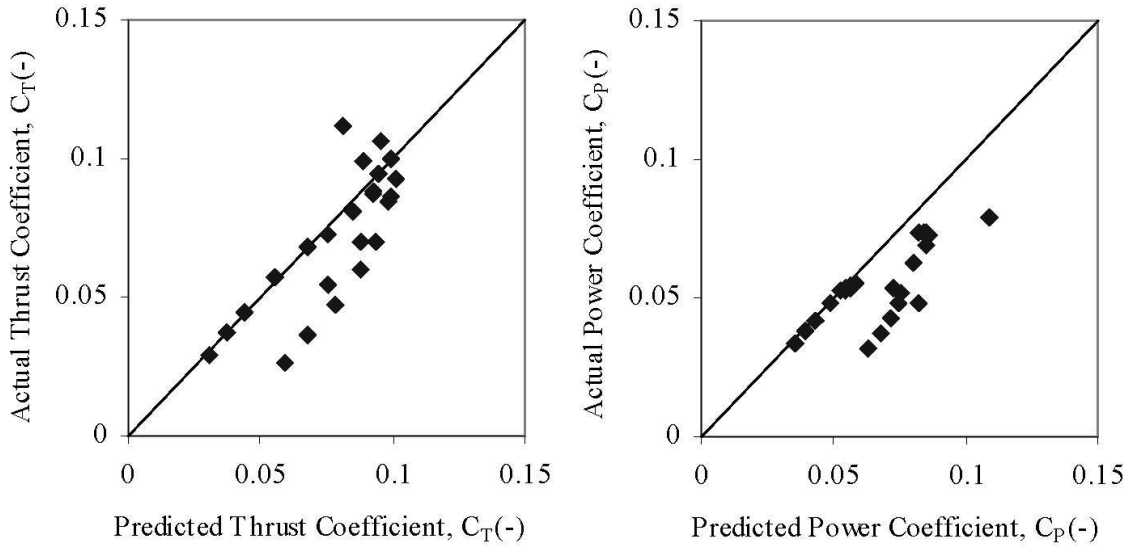

Figure 28. Actual by predicted plots for the Propeller CA

Data is not available to comprehensively validate the aircraft mass, lift and drag contributing analyses. For purposes of design, the modeling uncertainty associated with the aircraft contributing analyses is estimated to have zero mean and a standard deviation between 2% and 5% of the mean.

Table 5 summarizes the quantitative results of the subsystem validation efforts. The error in each subsystem contributing analysis is modeled as a Gaussian distribution of zero mean. The standard deviation of the modeling error is representative of the degree of fidelity of the models constructed for subsystem modeling.

Table 5. Statistical fits to error between contributing analyses and experimental data for fuel cell powerplant and aircraft models

	Design Variable or Contributing Analysis Output	Subsystem Validation Standard Deviation
Fuel Cell Powerplant Contributing Analyses	Hydrogen Flow Rate (L min^{-1})	3.4%
	Hydrogen Utilization (-)	3.3%
	Hydrogen Tank Mass (kg)	16.9%
	Hydrogen Tank Volume (m^3)	6.6%
	Hydrogen Tank Length (m)	7.1%
	Hydrogen Tank Diameter (m)	1.8%
	Hydrogen Equation of State (m^3 mol^{-1})	1%
	Fuel Cell Stack Potential (V)	17.9%
	Balance of Plant Power (W)	81.1%
Aircraft Contributing Analyses	Propeller Mass (kg)	1%
	Wing Mass (kg)	5%*
	Tail Mass (kg)	5%*
	Propeller/Fuselage Interference Coeff. (-)	5%*
	Fuselage Drag Coeff. (-)	5%*
	Wing Lift Coeff. (-)	2%*
	Wing Drag Coeff. (-)	5%*
	Propeller Power Coeff. (-)	10.4%
	Propeller Thrust Coeff. (-)	9.3%
	Motor Current at Full Power (A)	4.7%
	Motor Current at Cruise Power (A)	26.3%

*Estimated, all others are experimentally validated

4.4.2. System-level Validation

In order to validate the predictive performance of the design simulation at the system level, the predicted system performance can be compared to the experimental system performance. For this comparison the data that populates the contributing analyses are meta-models of the experimental performance of each powerplant component. For instance, for the fuel cell polarization model, the contributing analysis is a curve fit of the fuel cell stack polarization curve. For the electric motor model the contributing analysis is a neural network fit to experimental data of the electric motor performance. This assures that the contributing analysis models are very accurate (as shown in Figure 29) and that inconsistencies between the system performance of the

model and the hardware are due primarily to unmodeled system interactions. This experiment can validate the connections between the contributing analyses.

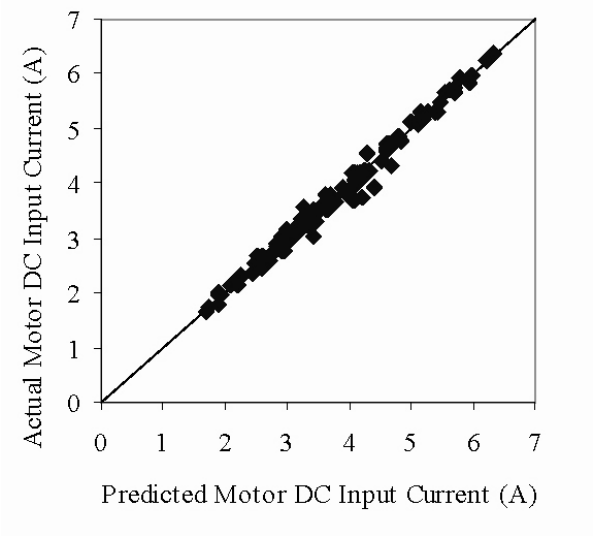

Figure 29. Actual by predicted plot for electric motor model

The design of a fuel cell powered aircraft was deterministically optimized for endurance using the design variables and constraints shown in Table 6 and the following side constraints.

$$\text{Climb Rate, } \dot{h} > 75 \text{ m min}^{-1} \tag{19}$$

$$\text{Propeller Mach Number, } M_{tip} < 0.85 \tag{20}$$

$$\text{Reynolds Number based on wing chord, Re<200,000} \tag{21}$$

Table 6. Design variables for system level validation study

Design Variable	Lower Bound	Upper Bound	Final Design Point	Units
Hydrogen Tank Length to Diameter Ratio	1	4	3.1	
Hydrogen Tank Radius	0	inf	0.026	m
Hydrogen Tank Pressure	0	inf	3.10E+07	Pa
Motor Series Number	2	15	10	
Planform Wing Area	0	inf	0.951	m^2
Number of Motor Winds	1.5	3	2	
Motor Gear Ratio	1	10	6.7	
Propeller Diameter	0	inf	0.6073	m
Propeller Pitch	0	inf	0.4976	m
Number of Fuel Cells	0	inf	62	
Fuel Cell Active Area	0	inf	20	cm^2

Table 6 also shows the design point that is the output of the fuel cell aircraft design process. The design cruise endurance of the aircraft at this point is 22.48±2.1 hrs and the design climb rate is 72.6±15.3 m min^{-1}. The powerplant hardware that is specified at this design point was bought, assembled and the performance of the aircraft powerplant was measured using an electric motor dynamometer, which is shown in Figure 30 and Figure 31.

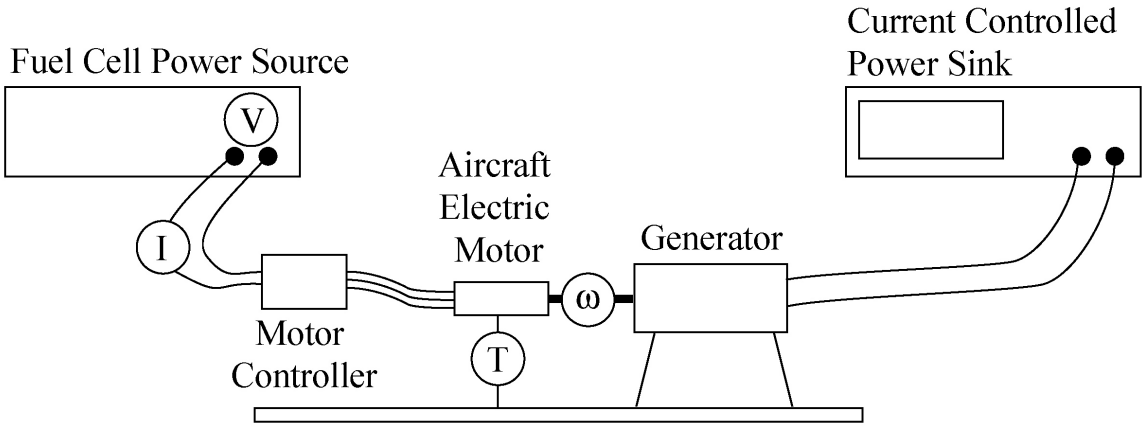

Figure 30. Schematic of powertrain testing dynamometer setup

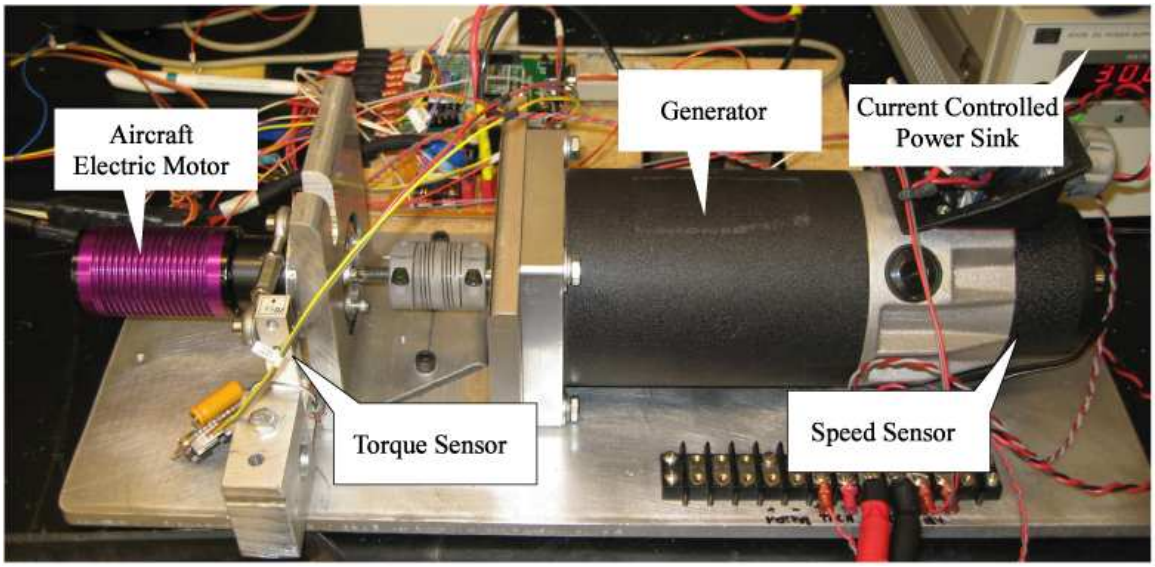

Figure 31. Photograph of powertrain testing dynamometer

The comparison results are shown in Table 7. The uncertainty associated with the hardware tests are experimental measurement uncertainties. The design study only incorporates uncertainty in the calculated endurance. As shown by these results, the performance of the fuel cell models can be qualitatively validated against the hardware performance of the H300 fuel cell powerplant.

These results show that the system performance of the fuel cell powerplant model is very close in comparison to the physical performance of the powerplant. This result supports the system level validation of the model by showing that there are no relevant system connections or relationships that are not captured by the model.

Table 7. Comparison between design point and hardware experiment

Signal Name (Units)	Hardware Bench Testing	Design Study	Simulated System Error
Hydrogen Flow Rate (L min^{-1})	1.71±0.05	1.70	-1%
Net Electrical Power (W)	142.65±8.5	134.48	-6%
Rotational Power (W)	101.24±1.7	99.97	-1%
Endurance (hrs)	22.48±0.62	22.35±0.61	-1%

4.4.3. Validation as a Component of a Design Process

Validation of this final point in the conceptual design was performed using a benchtop hardware in the loop simulator whose architecture and function are described in Chapter 8. The physical, assembled fuel cell UAV powertrain including the fuel cell, balance of plant, and electric motor are tested at the cruise condition derived from the conceptual design exercise. This experiment assumes that the rest of the aircraft is designed so that it performs at its deterministically optimized condition.

Figure 32 shows the design performance with estimated uncertainty bounds as a function of the stage of the design process. At both initial and detail design stages, the aircraft performance is shown with the estimated uncertainty that is due to the uncertainty in both the fuel cell powerplant models and the total uncertainty that is due to both powerplant and aircraft models. As might be expected, the uncertainty associated with the design points goes down as the design process progresses. The final condition shown in Figure 32 corresponds to the results of the hardware in the loop endurance tests. At this point, the uncertainty associated with the aircraft models is zero (by assumption) and the uncertainty associated with the powerplant is representative of experimental uncertainty.

The cruise endurance of the fuel cell UAV as bench tested is 22.35±0.6 hrs, including a standard deviation of experimental uncertainty. The bench test shows that the fuel cell UAV design as implemented is within the experimental uncertainty of the design point using the multidisciplinary analysis.

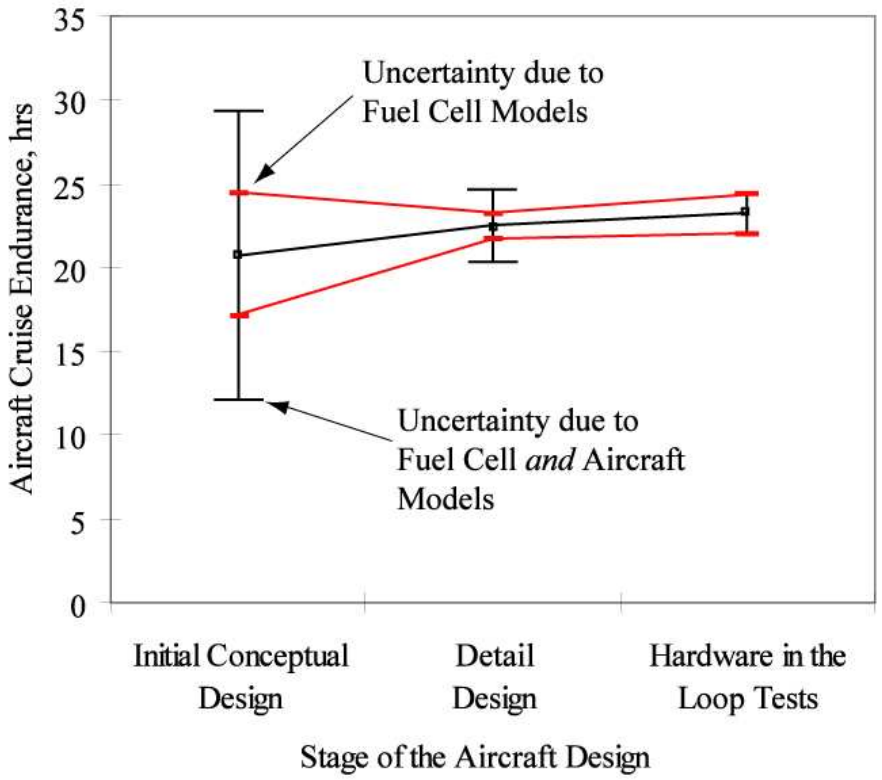

Figure 32. System-level validation of the fuel cell design tool for the design goal of endurance

Figure 33 compares the values of the design variables at the initial and detail stages of the design process. This comparison provides a degree of validation because of the similarity between values of the design variables at the initial and final design points.

More details of the design process and uncertainty propagation are presented in [16].

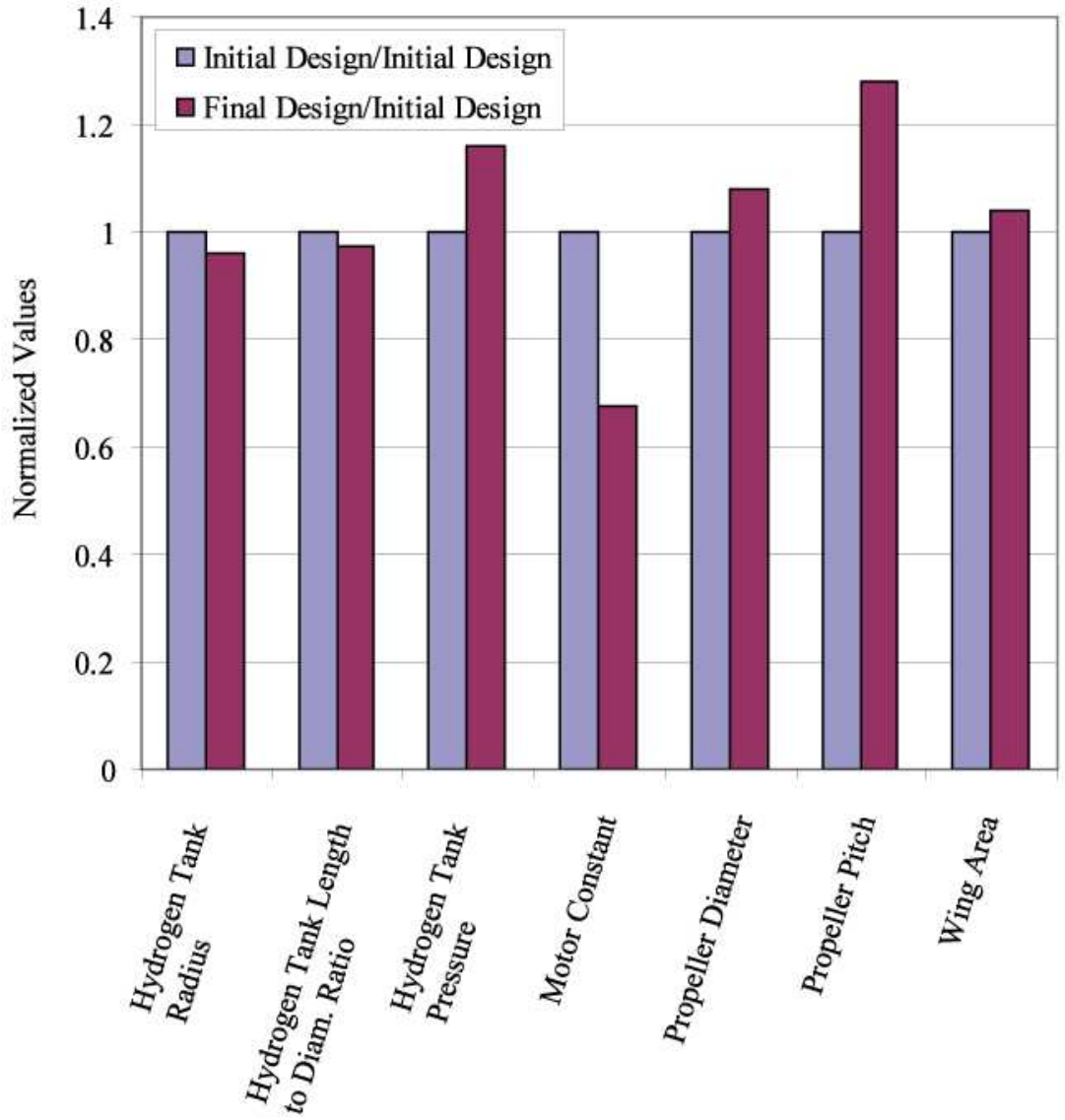

Figure 33. System-level validation of the fuel cell design tool for some of the design variables associated with the aircraft design

4.5 Chapter Conclusions

This section of the research effort has allowed us to address Research Question 1, which is restated here:

Research Question 1*: Can the geometry, performance and mass of fuel cell systems be represented parametrically within an integrated, validated, optimizeable powerplant and propulsion system model?*

Research Question 1 is associated with Hypothesis 1.1:

Hypothesis 1.1*: The development of sub-system level fuel cell powerplant models will allow for validated, scalable, optimizeable performance simulation for fuel cell system conceptual design.*

The research effort has provided support for this hypothesis. A subsystem-level model of the fuel cell powerplant has been proposed and developed. System component models are based on a variety of information sources including the fuel cell literature and experimental testing of relevant components. Validation of the models at the subsystem and system level has been performed using experimental data from the two constructed fuel cell systems. The validation is effective enough that the model does have utility in the fuel cell UAV design process described in [16]. This utility has been validated through the execution of an entire design process for a fuel cell UAV.

CHAPTER 5

DESIGN STUDIES FOR FUEL CELL POWERED AIRCRAFT

The design tools described above allow for the definition of optimal conceptual PEM fuel cell aircraft configurations that are subject to certain assumptions regarding proposed architecture, design constraints and optimization criteria. In this section we will quantitatively explore the effect of these assumptions on the conceptual design of fuel cell aircraft. Design tradeoffs among multiple constraints and objectives will be assessed.

5.1 Comparison of Fuel Cell System Design Rules

Conceptual fuel cell aircraft design studies that have been performed to date incorporate system-level models of fuel cell powerplants. These models describe the performance of the powerplant as a bulk system and are scalable by a variety of performance metrics including specific power (W/kg), specific energy (Wh/kg) and power density (W/L). These models are most often derived using sparse data from the automotive fuel cell literature. Intrinsic to these system models are assumptions about the structure and function of the fuel cell system that come from the automotive application.

For instance, the design method used in most other fuel cell design studies assumes that the air supply compressor is sized by the mass transport limited current of the fuel cell. This is a commonly used assumption [61,74,81] that states that the maximum airflow of the air supply compressor is proportional of the amount of air that the fuel cell stack requires to produce its peak, i.e. mass transport limited, current, and that the air supply rate should not be the limiting factor in developing fuel cell peak

power. This assumption is relevant for fuel cell powered automobiles where the performance of the automobile is highly dependent on the stack output power. We can use the tools developed for this study to understand the limitations intrinsic in this conventional design method, and to determine what more optimal balance of plant sizing laws might be for long-endurance fuel cell powered aircraft.

5.1.1. Methods for Fuel Cell System Design Rules Comparison

To conduct this comparison, we will design and compare two fuel cell powered aircraft under the two different sets of design constraints. The difference between these design assumptions is shown conceptually in Figure 34. Figure 34 shows the contributing analyses of the design structure matrix where the fuel cell and balance of plant are analyzed. Both aircraft have the same design variables (Fuel Cell Active Area, Number of Fuel Cells) input to this portion of the DSM, and both aircraft use the same contributing analysis modules. The difference between the design method for Aircraft A and Aircraft B is in the structure of the DSM and the inputs to the Balance of Plant Sizing contributing analysis.

Aircraft A is designed with the traditional design constraint that the balance of plant is sized as a function of the active area limited current. In Aircraft A, the output of the balance of plant sizing contributing analysis is passed forward to the Aircraft Performance contributing analysis to be sure that balance of plant mass and power requirements are taken into account in the aircraft performance calculation. Also, an output of the Balance of Plant Sizing contributing analysis is passed backwards to the Polarization Curve contributing analysis iteratively so as to assure that the current coming from the fuel cell represents both the current required by the aircraft and the current

required by the fuel cell balance of plant. The inputs to the Balance of Plant Sizing contributing analysis are the number of fuel cells and the active area limited current.

Aircraft B is designed so that the balance of plant is sized by the actual current required of the aircraft during climb. In order for the Balance of Plant Sizing contributing analysis to have that information accessible, the Aircraft Performance contributing analysis must have already been run. This requirement means that the aircraft performance code must be within the feedback loop between the Polarization Curve and Balance of Plant Sizing contributing analyses.

The conventional design rules used to design Aircraft A have a number of conceptual and computational benefits. Conceptually, Aircraft A is a simpler aircraft to understand and design. Where Aircraft A has weak links between the fuel cell contributing analyses and the aircraft performance contributing analyses, Aircraft B has feedbacks between the fuel cell design tasks and the aircraft design tasks. This structure makes the design structure matrix computationally more expensive to evaluate and converge. Also, the design process for Aircraft A is easier to partition into discrete and disciplinary fuel cell analysis tasks and aircraft performance analysis tasks.

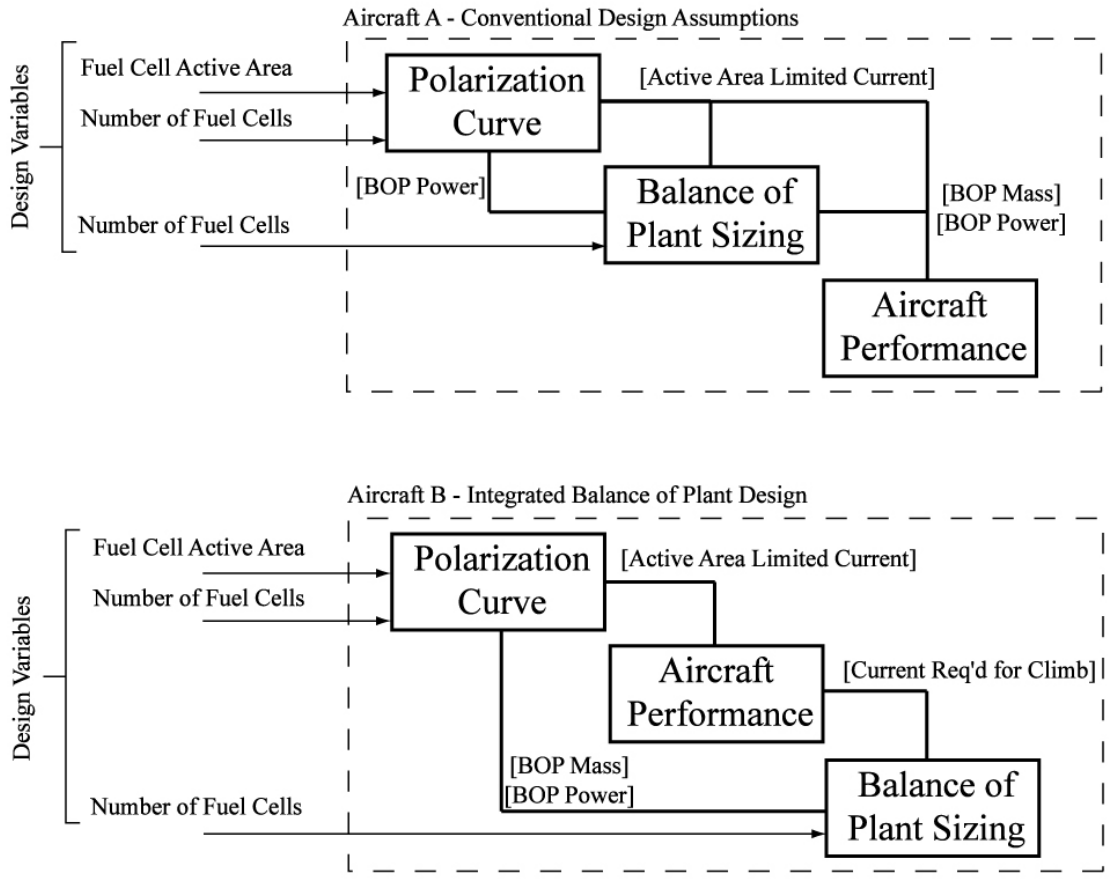

Figure 34. Conceptual design structure comparison between two fuel cell system design rules

5.1.2. Results and Discussion for Fuel Cell System Design Rules Comparison

The two aircraft are then designed to maximize on-station endurance, subject to a 125 m min^{-1} climb rate constraint and a maximum weight constraint of 30 kg. The design characteristics of the two aircraft are shown in Table 8 and Figure 35. Comparing the performance of the two aircraft shows that Aircraft B is a longer endurance, and therefore more optimal aircraft than Aircraft A, suggesting that the integrated balance of plant design is more effective than the conventional design assumptions. Figure 35 and Figure

36 provide some insight into the design tradeoffs that the optimizer is exploiting to improve the performance of Aircraft B. Figure 35 compares the subsystem weight breakdown for the two aircraft designs. Figure 36 shows the fuel cell stack polarization curves for the two aircraft designs. Three points per curve are indicated on Figure 36. The condition of the fuel cell is shown at the cruise and climb condition for each aircraft. Also Figure 36 shows the active area limited current, which represents the maximum current that the fuel cell stack could produce, given an unconstrained reactant flow.

Table 8. Comparison of aircraft characteristics for Aircraft A and Aircraft B

Aircraft Characteristics	Aircraft A "Conventional Design"	Design B "Integrated BoP Design"
On Station Endurance [hrs]	23.3	32.6
Hydrogen Tank Volume [L]	17.4	19.9
Number of Fuel Cells [-]	67	49
Fuel Cell Active Area [cm^2]	34.3	64.9
Fuel Cell Mass [kg]	20.9	21.3
Fuel Cell Output Power at Cruise [W]	333.4	300.1
Aircraft Climb Rate [m min^{-1}]	125.3	125.4
Fuel Cell Output Power at Climb [W]	1211	1189

Based on (14), the dual goals of the design optimization tool are to minimize the objective function and to satisfy the constraints. Although both the objective function (endurance) and many of the constraints (climb rate) are aircraft level metrics, these objectives force requirements of power and energy on the fuel cell powerplant. To meet the climb constraint, the optimization algorithm must add electrical output power to the fuel cell system by adding additional fuel cell active area or an additional number of fuel cells. To add additional endurance, the optimizer must either reduce the mass of the aircraft by shrinking the fuel cell and balance of plant mass, or improve the fuel conversion efficiency of the powerplant by adding fuel cell active area or an additional

number of fuel cells to reduce the fuel cell current loading. The mechanisms of efficiency improvement with decreasing current density are shown in Figure 14.

For Aircraft A, the optimizer handles the dueling requirements by designing a fuel cell with relatively small active area and a larger number of cells. The design rules for Aircraft A demand that the balance of plant be scaled by the active area limited current. In order to avoid a very weighty balance of plant, the fuel cell active area is kept small. This is shown in Figure 6 by the small peak current for Aircraft A and the close proximity of the climb condition operating point to the active area limited current point. Despite the small size of Aircraft A's fuel cell stack, Figure 35 shows that the balance of plant for Aircraft A is still heavier than the balance of plant for Aircraft B.

For Aircraft B, the design of the fuel cell balance of plant is decoupled from the scaling of the fuel cell, and the optimizer is able to discover a more optimal configuration. Figure 36 and Figure 37 show that because of this decoupling, the current required by the aircraft at climb is roughly half of the active area limited current. In other words, the fuel cell is roughly two times larger than is necessary to meet the power demands of the aircraft. This suggests that the optimizer is moving towards larger fuel cells in order to reduce the current density of the fuel cell stack, thereby improving its efficiency. Because the balance of plant sizing and fuel cell active area are decoupled, the balance of plant can be under-sized for the fuel cell stack, reducing its weight, while still allowing it to manage the fuel cell for all realizeable performance conditions. Of course, increasing the fuel cell size, makes it more massive relative to the fuel cell specified for Aircraft A, but this mass difference is made up for by the decreased mass of the fuel cell balance of plant.

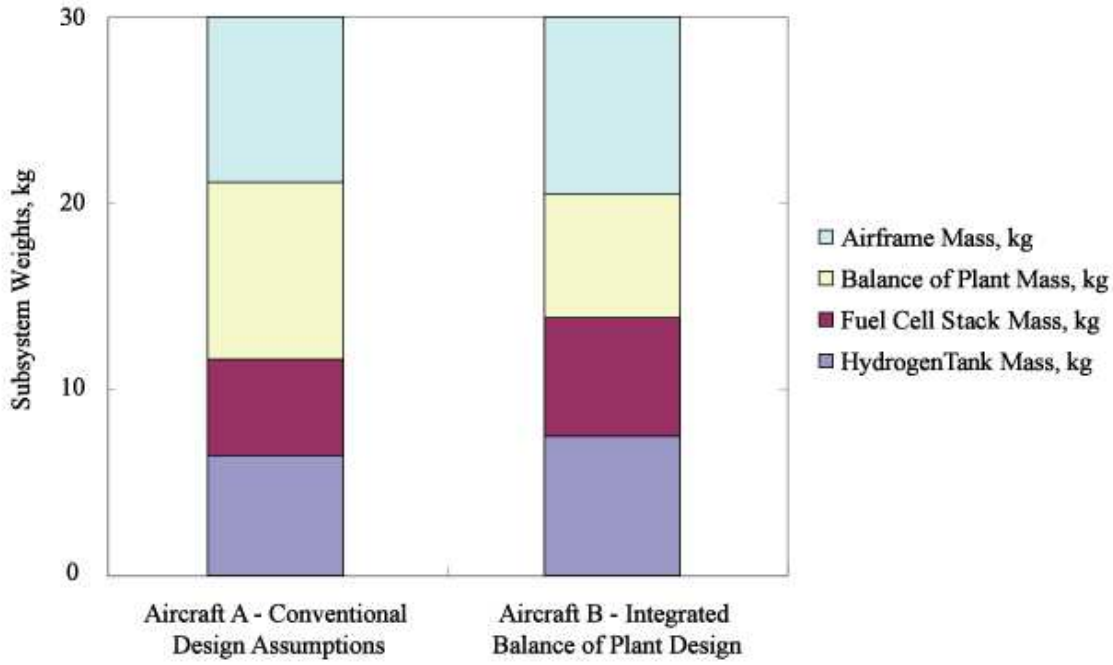

Figure 35. Weight breakdown among major subsystems for balance of plant design comparisons

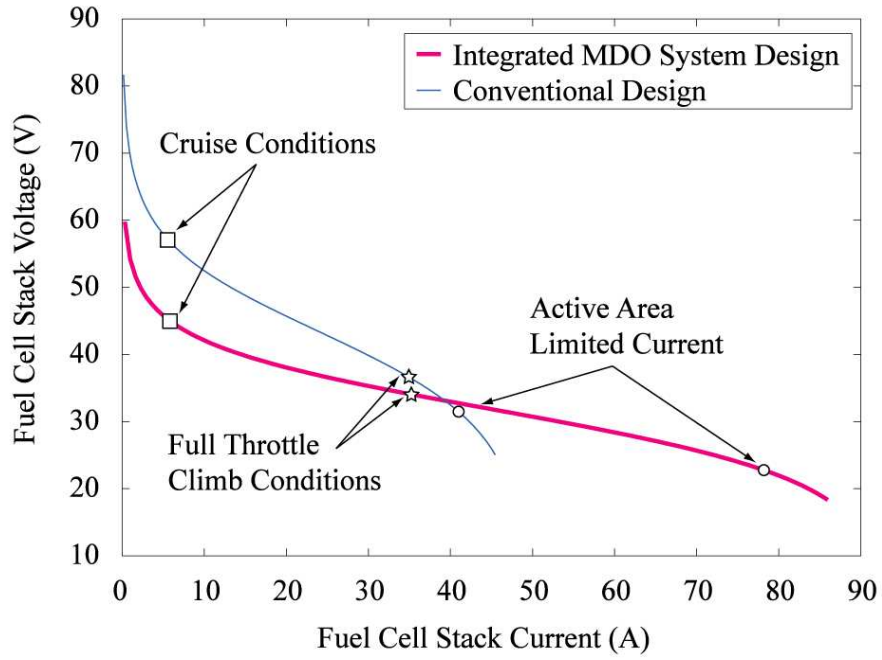

Figure 36. Comparison between rules based and integrated design of fuel cell powerplant

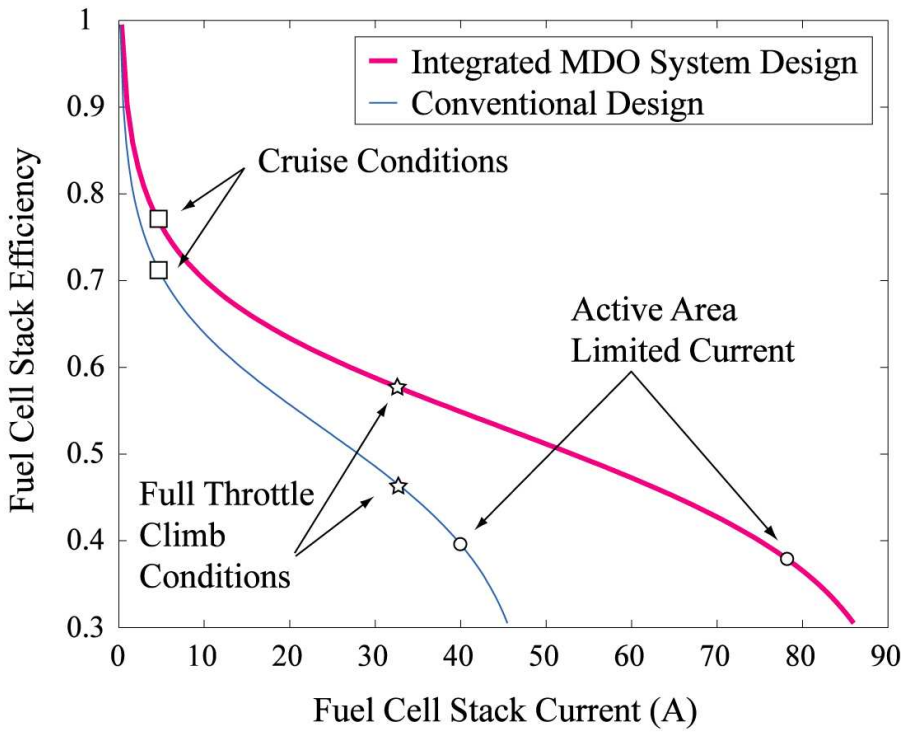

Figure 37. Efficiency-based comparison between rules based and integrated design of fuel cell powerplant

As shown in Figure 35, the fuel cell balance of plant is a significant portion of the fuel cell aircraft mass. In order to accurately design and implement fuel cell powered aircraft, the balance of plant must be considered as an important and optimizeable component of the design process. Whereas automotive design studies have determined that the fuel cell balance of plant should be sized to approximately 80-90% of the active area limited power, this study suggests that 45-50% is more optimal for long endurance fuel cell aircraft.

5.2 Application-level and Powerplant-level Design Metric Comparisons

Many researchers have proposed that aircraft design integrated MDO is perhaps not necessary and that the design of long-endurance fuel cell aircraft might be simplified

by designing the fuel cell system so as to maximize powerplant specific energy, independent of the aircraft propulsion sub-system performance or aircraft geometry [19,34,89]. These studies suggest that perhaps fuel cell systems could be specified for fuel cell powered aircraft based on powerplant-level design requirements such as powerplant specific energy, and powerplant specific power, instead of using more costly aircraft-integrated design methods. The goal of this section then is to compare the efficacy of fuel cell aircraft design towards application-level design metrics with design towards powerplant level design metrics. This section will derive powerplant-level design metrics of interest, propose and follow a design experiment so as to compare the design strategies, and will draw conclusions regarding the differences between the design strategies.

5.2.1. Derivation of Design Metrics for Fuel Cell UAVs

To date, the designers and developers of fuel cell powerplants have been primarily responsive to the needs of the automotive and stationary power generation applications. To maximize the performance of fuel cell powered aircraft, fuel cell powerplants will have to be designed and built to meet aviation-specific design criteria. These may involve significant departures from conventional automotive or stationary fuel cell design. For aviation, some primary aircraft-level performance metrics include range, endurance, rate of climb and maximum speed. These aircraft design requirements can be translated into first-order, powerplant-level design requirements for the fuel cell system by analyzing Newton's Laws for an aircraft in steady, level flight [1].

A simplified range equation for unconventional powerplants can be derived where aircraft weight is constant,

$$ds = \int \frac{dE}{T} \tag{22}$$

During steady level flight at small angles of attack, $T=D$ and $L=mg$,

$$s = \left(\frac{E}{D}\right) = \left(\frac{L}{D}\right)\left(\frac{E}{L}\right) = \left(\frac{E}{m}\right)\left(\frac{C_L}{gC_D}\right) \tag{23}$$

A similar approach can be followed to derive a simplified endurance equation for unconventional powerplants.

$$T = \frac{C_D}{C_L} W \tag{24}$$

$$L = \frac{1}{2}\rho v^2 S_w C_L \tag{25}$$

Rearranging (4) with $W=L$,

$$v = \left(\frac{W}{1/2\,\rho S_w C_L}\right)^{1/2} \tag{26}$$

The propulsive output energy is the integral of the propulsive output power. Under the assumption that the weight of the aircraft changes negligibly over the course of the flight,

$$E = \int_0^t \frac{C_D}{C_L} W \left(\frac{W}{1/2\,\rho S_w C_L}\right)^{1/2} dt = \frac{C_D t}{\sqrt{1/2\,\rho S_w}} \left(\frac{W}{C_L}\right)^{3/2} \tag{27}$$

Solving for the aircraft endurance,

$$t = \left(\frac{E}{m^{3/2}}\right)\left(\frac{\left(1/2\,\rho S_w\right)^{1/2} C_L^{3/2}}{g^{3/2} C_D}\right) \tag{28}$$

Under similar assumptions, the aircraft flight path angle can be expressed as,

$$\gamma = \frac{vL}{mg} = \frac{vT}{mg}\frac{C_L}{C_D} = \left(\frac{\dot{E}}{m}\right)\frac{C_L}{gC_D} = \left(\frac{P}{m}\right)\frac{C_L}{gC_D}, \tag{29}$$

and the aircraft airspeed as,

$$v = \left(\frac{P}{T}\right) = \left(\frac{P}{D}\right) = \left(\frac{P}{m}\right)\frac{C_L}{gC_D} \tag{30}$$

Based on these analyses, we can characterize the design metrics to be maximized so as to maximize fuel cell aircraft performance. To maximize the performance of the fuel cell powered aircraft we can maximize $\left(\frac{E}{m}\right)$ which is proportional to aircraft range, $\left(\frac{E}{m^{3/2}}\right)$ which is proportional to aircraft endurance, and $\left(\frac{P}{m}\right)$ which is proportional to flight path angle, climb rate, maximum speed and many other aircraft performance metrics.

Powerplant specific energy is defined for this study as:

$$\frac{E}{m_{power}} = \frac{P_{FC}t}{\left(m_{FC} + m_{H2} + m_{H2\text{tank}} + m_{BOP}\right)} \tag{31}$$

Powerplant specific power is defined for this study as:

$$\frac{P}{m_{power}} = \frac{P_{FC}}{\left(m_{FC} + m_{H2} + m_{H2\text{tank}} + m_{BOP}\right)} \tag{32}$$

5.2.2. Methods for Design Metric Comparisons

The design tools developed for this study allow for the comparison between a design optimized for these subsystem performance metrics, such as $\frac{E}{\left(m_{power}\right)^{3/2}}, \frac{E}{\left(m_{power}\right)}$ and $\frac{P}{\left(m_{power}\right)}$, and a design optimized for aircraft-level performance metrics, such as

endurance, range and climb rate. This comparison will be made by designing fuel cell powered aircraft for both aircraft-level and powerplant-level design criteria, and making comparisons between the performance of the resulting aircraft. The last step determines whether the aircraft optimal performance can be recovered through aircraft design once the powerplant design variables are frozen at the powerplant-level optimum.

The experimental method is described below and in tabular form in Table 9 and Table 10.

Let the vector of design variables, $\vec{x}$, be split into a set of design variables that control the powerplant and hydrogen storage design and a set of design variables that control the aircraft design.

$$\vec{x} = \left[\vec{x}_{power}^{T} \quad : \quad \vec{x}_{airframe}^{T}\right]^{T} \tag{33}$$

$$\vec{x}_{power}^{T} = \left[n_{cells} \quad A_{FC} \quad r_{H2} \quad AR_{\text{tank}} \quad P_{H2}\right] \tag{34}$$

$$\vec{x}_{airframe}^{T} = \left[X_{motor} \quad Y_{motor} \quad d \quad S_{w} \quad p_{\text{cruise}} \quad p_{\text{climb}} \quad R\right] \tag{35}$$

1. The aircraft is designed using all design variables for maximum endurance subject to side constraints: a 125 m min^{-1} climb rate constraint and a maximum weight constraint of 40 kg. This step ensures that the subsequent design steps occur in the neighborhood of a feasible point in the design space. This configuration also serves as the experimental control. Optimization towards other design criteria will move away from this aircraft-level optimized design configuration.

2. From this baseline, the powerplant is redesigned for maximum $\frac{E}{\left(m_{power}\right)^{3/2}}$ using only the powerplant and hydrogen storage design variables ($\vec{x}_{power}^{T}$). The aircraft-level side constraint on climb rate is replaced with a single powerplant-level constraint on $\frac{P}{\left(m_{power}\right)}$. This step allows the optimizer to seek out a sub-system optimum in terms of powerplant design metrics at fixed specific power. This approximates the action of a naïve designer working towards designing a fuel cell aircraft powerplant so as to maximize $\frac{E}{\left(m_{power}\right)^{3/2}}$ while maintaining a fixed specific power $\frac{P}{\left(m_{power}\right)}$.

3. The powerplant design is now fixed and the aircraft is designed using only the airframe design variables. Again, the aircraft is designed for maximum endurance subject to side constraints: a 125 m min^{-1} climb rate constraint and a maximum weight constraint of 40 kg. This step approximates the action of an aircraft designer who is given a fixed powerplant design and must maximize performance only using aircraft design variables.

This procedure is repeated for the similar study where the design goal is a maximum range aircraft. The procedure for the range study is shown in Table 10.

Table 9. Tabular summary of steps associated with the endurance design metric comparison experiment

	Step 1	Step 2	Step 3
Goal	Initialize Design at Aircraft Optimum	Move Towards Fuel Cell Optimum	Move Back Towards Aircraft Optimum
Cost Function	-Endurance	$-E_{FC}\, m_{power}^{(-3/2)}$	- Endurance
Constrained Variables	Climb Rate	$P_{FC}\, m_{power}$	Climb Rate
Active Design Variables	Fuel Cell and Aircraft DVs	Fuel Cell and Aircraft DVs	Aircraft DVs

Table 10. Tabular summary of steps associated with the range design metric comparison experiment

	Step 1	Step 2	Step 3
Goal	Initialize Design at Aircraft Optimum	Move Towards Fuel Cell Optimum	Move Back Towards Aircraft Optimum
Cost Function	-Range	$-E_{FC}/m_{power}$	-Range
Constrained Variables	Climb Rate	P_{FC}/m_{power}	Climb Rate
Active Design Variables	Fuel Cell and Aircraft DVs	Fuel Cell and Aircraft DVs	Aircraft DVs

5.2.3. Results and Discussion for Design Metric Comparisons

Figure 38 shows the trajectory of the design study as it progressed. The study begins at in the lower left corner of the figure, which is shown on axes of aircraft on-station endurance and $\frac{E}{\left(m_{power}\right)^{3/2}}$. As the first optimization progresses, the aircraft configuration improves in terms of both endurance and $\frac{E}{\left(m_{power}\right)^{3/2}}$. The optimizer reaches an endurance optimal solution with all constraints met at Point 1. Although configurations with higher endurance are explored by the design optimization scheme, these configurations do not meet the design constraints and are therefore not optimal with

respect to (14). Step 2 of the design study begins at Point 1. The design study then begins to optimize the fuel cell powerplant for the metric of $\frac{E}{\left(m_{power}\right)^{3/2}}$. As the $\frac{E}{\left(m_{power}\right)^{3/2}}$ of the aircraft powerplant increases, the endurance of the aircraft decreases. The optimization algorithm finds the configuration with the highest available $\frac{E}{\left(m_{power}\right)^{3/2}}$ and with all powerplant-level constraints met at Point 2. Step 3 of the design study begins from Point 2 and attempts to improve the endurance of the aircraft and meet aircraft-level performance constraints using only the aircraft design variables. In fact, the optimizer is unable to improve the endurance in order to meet the climb rate constraint. A similar progression is shown in Figure 39 for the same design study performed for optimal range and optimal specific energy $\frac{E}{\left(m_{power}\right)}$.

Step 1 of the design process has derived the optimal configuration for the aircraft level design metrics and aircraft level constraints that are appropriate for fuel cell aircraft design. From Figure 38 and Figure 39, we can see that for these fuel cell aircraft, aircraft endurance is roughly proportional to the powerplant performance metric of $\frac{E}{\left(m_{power}\right)^{3/2}}$ and aircraft range is roughly proportional to the powerplant performance metric of $\frac{E}{\left(m_{power}\right)}$. Figure 40 shows the same results as Figure 39 with the steps broken down into individual figures and with arrows showing the direction of motion of the optimization routine.

Steps 2 and 3 of the design process allows us to compare the effectiveness of integrated aircraft/powerplant design and disintegrated powerlant and aircraft design that uses subsystem-level design metrics to guide powerplant design. A comparison of the design point 1 to the design point 3 shows that design of fuel cell aircraft using the powerplant-level performance metrics of $\frac{E}{\left(m_{power}\right)^{3/2}}$, $\frac{E}{\left(m_{power}\right)}$ and $\frac{P}{\left(m_{power}\right)}$ are a poor substitute for an aircraft-integrated multidisciplinary optimization-based design process. The endurance of the $\frac{E}{\left(m_{power}\right)^{3/2}}$ optimized aircraft is 16.5% less than the optimum and the range of the $\frac{E}{\left(m_{power}\right)}$ optimized aircraft is 6.6% less than the optimum when aircraft weight is constrained at 40kg. These experiments are repeated for both range and endurance and at a variety of constrained aircraft weights. Results are shown in Table 11.

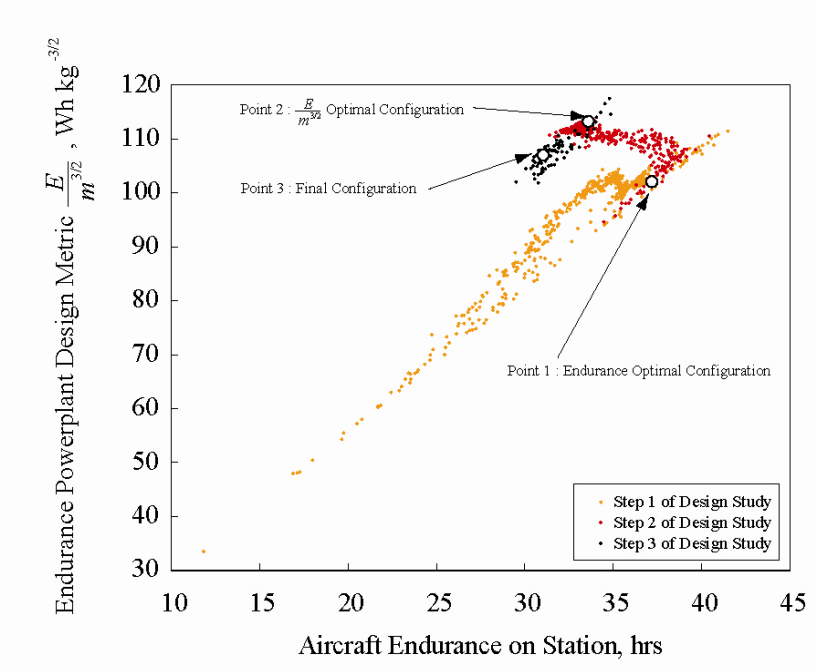

Figure 38. Results of design tradeoff study between endurance and powerplant level design metrics at aircraft weight = 40kg

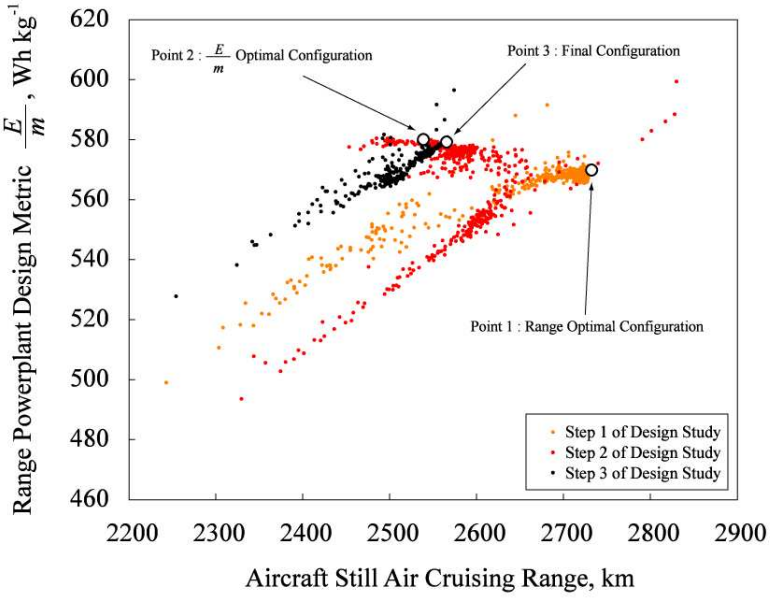

Figure 39. Results of design tradeoff study between range and powerplant level design metrics at aircraft weight = 40kg

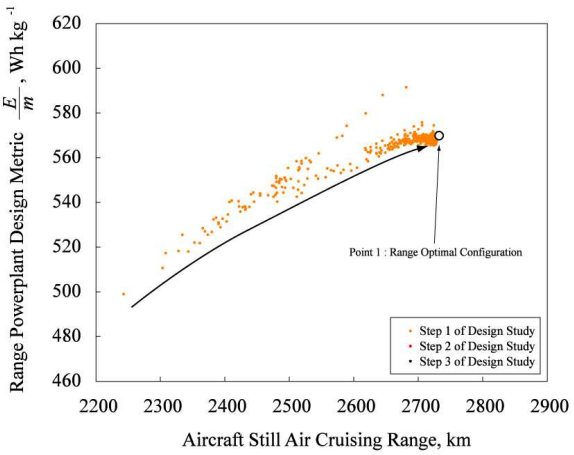

(a)

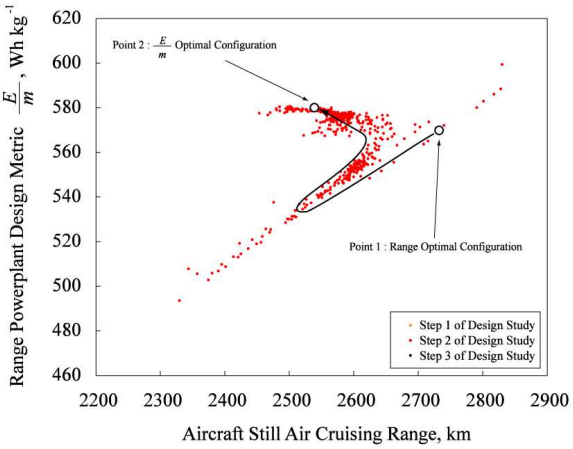

(b)

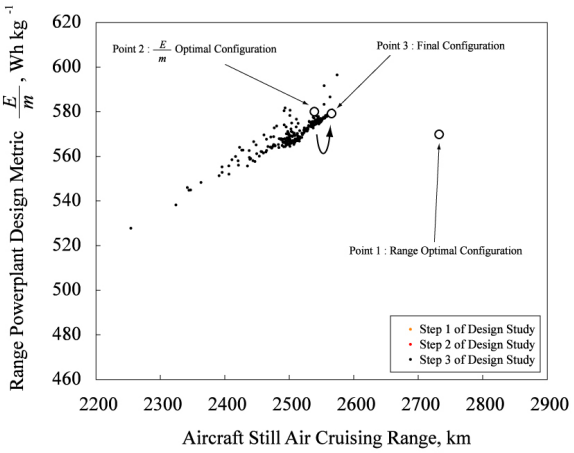

(c)

Figure 40. Breakdown of steps associated with Range optimal design study at aircraft weight = 40kg, (a) Step 1, (b) Step 2, (c) Step 3

Table 11. Design of experiment results for design metric comparison study with percentage improvement from aircraft level design metric optimization

Cost Function	Aircraft Weight Constraint	Percentage Improvement Using Aircraft Level Design Metric Optimization $\left(1-\frac{\text{Powerplant Optimal Cost Function Value}}{\text{Aircraft Optimal Cost Function Value}}\right)$
Range	50 kg	2.4%
Range	40 kg	6.6%
Range	30 kg	7.8%
Range	20 kg	11.4%
Endurance	50 kg	11.3%
Endurance	40 kg	16.5%
Endurance	30 kg	7.5%
Endurance	20 kg	5.6%

Conventional design rules for fuel cell powerplants that are derived from automotive design requirements or from design simplifications produce significantly sub-optimal results when applied to fuel cell aircraft design. Application-integrated design studies can be used to derive and design improved fuel cell powerplants for aircraft.

5.3 Fuel Cell UAV Design Case Study

In order to analyze the design of a fuel cell powered aircraft in detail, the aircraft design code was exercised with the goal of designing a more practical and tactically valuable long endurance fuel cell powered UAV. As such, the aircraft is designed to climb at 120 m min^{-1} and carry a 1 kg, 15W payload over a maximum endurance mission. The climb rate is comparable to the climb rate of small-scale UAVs [23]. The payload is representative of the power and mass requirements of a miniature synthetic aperture radar system for UAVs [119]. The mission profile is derived from a characteristic low-altitude base patrol mission.

A two view drawing of the aircraft concept is shown in Figure 41. The aircraft as designed has an on station endurance of >25 hours, a wingspan of 4.4m and a gross takeoff weight of 20 kg. The specific electrical energy and specific electrical power of the fuel cell powerplant including hydrogen storage and balance of plant is 340.3 Wh kg^{-1} and 55.5 W kg^{-1}. This can be compared to the specific energy of conventional rechargeable lithium ion batteries at 166 Wh kg^{-1} and 313 W kg^{-1} [33] or primary Zinc-air batteries at 300 Wh kg and 55 W kg^{-1}. [42] A comparison of the capability of the fuel cell powered UAV to a commercially available UAV is presented in Table 12.

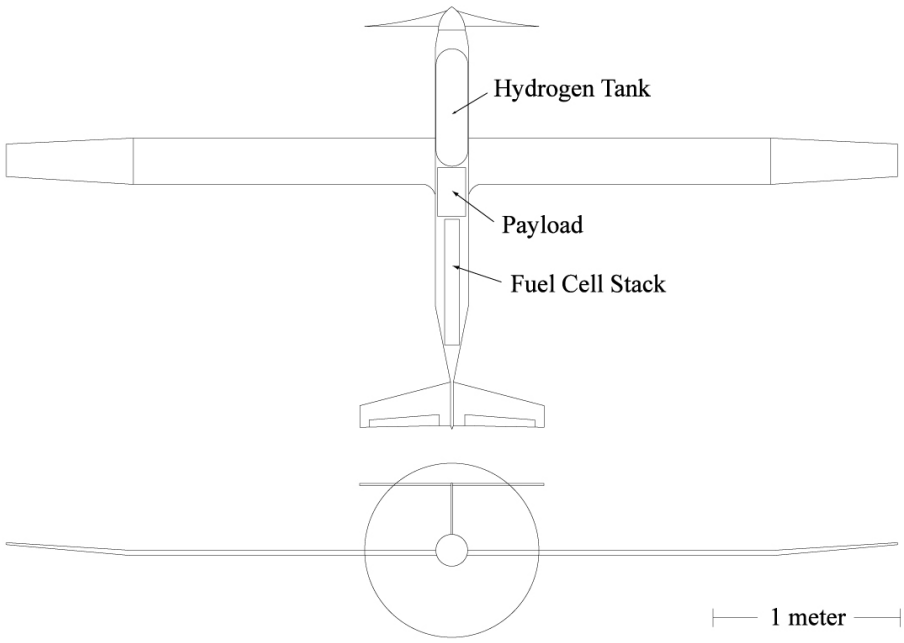

Figure 41. Two view drawing of fuel cell powered UAV design case study

Table 12. Comparison of fuel cell powered UAV case study to conventionally powered commercial UAV

Design Characteristic	*Aerosonde* Mk 1 [23]	Conceptual FCUAV
Empty Endurance	26.8 hrs	25.2 hrs
Climb Rate	120 m/min	120m/min
Gross Take off Mass	13.4 kg	20 kg
Wing Span	2.9 m	4.4 m

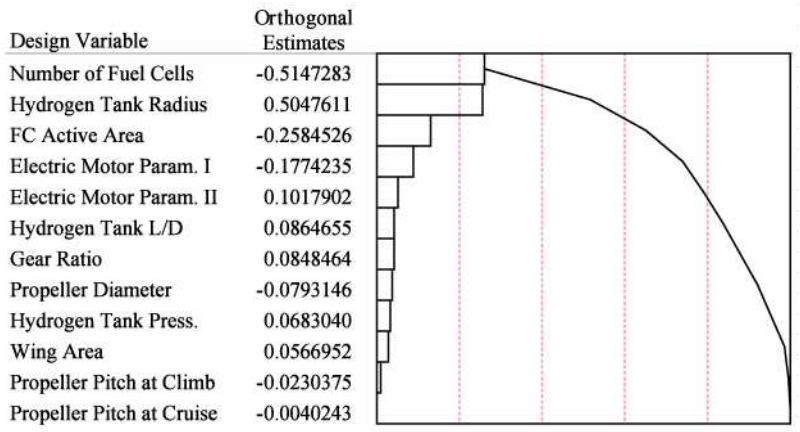

Figure 42. Pareto plot of Endurance response surface fitted to final design point of fuel cell UAV

A sensitivity analysis of the endurance-optimal configuration was performed by using a full factorial design of experiments (DOE) around the optimal design point for endurance.

An analysis of variance (ANOVA) was performed on the results of the DOE to generate the Pareto plot in Figure 42. Figure 42 tabulates the percent contribution of each of the design variables with respect to the overall range variability calculated from the DOE. Figure 42 shows that the aircraft endurance of the optimal design is most sensitive to the design variables associated with the fuel cell and hydrogen tank. Propeller pitch and aircraft wing area are the least influential design variables.

5.4 Chapter Conclusions

This section of the research effort has allowed us to address research question 2, which is restated here:

Research Question 2*: Is the extra complexity and cost of a multilevel design tool (that includes subsystem-level, system-level and application-level models) justifiable for optimization and design of fuel cell powered aircraft? What are the costs to the design performance of replacing either the application model or subsystem models with the surrogate design rules that have been proposed in literature?*

Research question 2 has two hypotheses associated with it. Each hypothesis is discussed in turn.

> ***Hypothesis 2.1****: Disintegration of the powerplant design rules allows for empirical, unbiased optimization of the system design that shows improvement over conventional powerplant design rules*

This section has presented a method for multidisciplinary design and optimization of a fuel cell powered unmanned aerial vehicle. The design tools developed as a component of this research effort allow for the comparison of the effectiveness of an integrated aircraft/powerplant design method versus a disintegrated powerplant and aircraft design method that uses subsystem-level design metrics to guide powerplant design. When compared to optimization towards pre-established powertrain performance metrics such as $\frac{E}{\left(m_{power}\right)^{3/2}}$, $\frac{E}{\left(m_{power}\right)}$ or $\frac{P}{\left(m_{power}\right)}$, the integrated design method allows for substantial improvement in the on-design performance of the aircraft.

***Hypothesis 2.2**: Fuel cell systems designed using an application-integrated design process can improve the performance of the aircraft system relative to the state of the art surrogate design metrics*

The design of fuel cell systems for automotive or stationary or stationary applications incorporate design rules that may or may not apply to the new application of aviation. This study has allowed for the direct comparison of fuel cell powerplants that incorporate the conventional design rules regarding balance of plant sizing to those where the rules are derived via multi-disciplinary optimization. Results show that the aviation application places unique requirements on the fuel cell system that makes the optimal fuel cell system design very different than the conventional systems. In addition, the integrated design of the fuel cell, balance of plant, hydrogen storage, powertrain and airframe allows for the assessment of design tradeoffs among these components.

Additional results show that there exists a number of viable and high performance fuel cell unmanned aerial vehicle configurations. A baseline long-endurance fuel cell powered UAV is designed. The baseline configuration for this study is a high wing monoplane driven by traction propellers. The powerplant is a hydrogen/air polymer electrolyte membrane fuel cell which powers electric motors. Hydrogen is stored on board the aircraft using a variety of presently available technologies. The proposed mission is a low-altitude, long-endurance stationary orbit. The design includes a small, low-power payload representing remote sensing and/or communications equipment. The design sensitivity and robustness of the baseline design is assessed and discussed.

CHAPTER 6

ENERGY MANAGEMENT AND SUPERVISORY CONTROL OF FUEL CELL POWERED AIRCRAFT

6.1 Introduction

Hybridization has been proposed as a means to improve the performance of fuel cell powerplants for aircraft [41,94,120]. In general, hybridization can allow the power and energy demands of the fuel cell system to be isolated from those required of the aircraft. For example, a hybrid aircraft that must transition from cruise to climb can do so with the assistance of stored energy from an energy buffer. Decoupling the aircraft power demands from the fuel cell power demands may be able to improve the efficiency of the maneuver by allowing the fuel cell powerplant to maintain operation at near optimal conditions. Other means of improving the energy management of an aircraft through hybridization such as regenerative wind-milling, regenerative solar energy capture, and accessory load electrification are not considered in this study.

Aviation flight path optimization is an important and well developed field whose goal is the derivation of control strategies to improve the endurance or range of a variety of aircraft [96,98,99]. A majority of the studies of optimal periodic control have focused on gas turbine or internal combustion engine powerplants. For fuel cell powered aircraft it has primarily been considered in the contexts of thermal soaring for range extension [41], and diurnal flight paths for solar powered fuel cell aircraft [92,121]. In this study

we consider the more general problem of evaluating the effectiveness of flight path optimization for range and endurance optimization without external energy inputs.

In this work, energy management for hybrid fuel cell aircraft and flight path optimization for fuel cell aircraft are evaluated in simulation for their effect on the flight performance of a fuel cell powered aircraft. Two non-linear programming algorithms are implemented in order to determine the effectiveness and characteristics of an optimal energy management strategy for fuel cell powered aircraft. First, a dynamic programming algorithm is proposed with reduced order models of the fuel cell powerplant, aircraft dynamics and energy consumption. Next, a sequential quadratic programming routine is used to evaluate the possibility of extending endurance of fuel cell powered aircraft using flight path optimization. Simulation results with the optimal control strategies are presented for a variety of generic fuel cell aircraft missions. For comparison, optimal flight paths and energy management strategies are derived for an example aircraft powered by an internal combustion engine. Discussion focuses on an efficiency comparison of hybridization to flight path optimization and a discussion of regimes of effectiveness for both strategies.

6.2 Problem Formulation

The aircraft that are under consideration for this study are represented by a simplified model. Simplifications to the aircraft and powerplant models are applied to be able to isolate the phenomena of interest, specifically generalizeable and long period energy management behavior.

6.2.1. Aircraft Characteristics

To simply the problem of flight path optimization, the aircraft is constrained to a flight path in a vertical plane. The aircraft neither turns nor banks. Using a flat earth coordinate system the equations of motion of the aircraft are as follows [1].

$$\dot{h} = v \sin\gamma \tag{36}$$

$$\dot{v} = \frac{T\cos\alpha - D}{m} - g\sin\gamma \tag{37}$$

$$\dot{\gamma} = \frac{T\sin\alpha + L}{vm} - \frac{g}{v}\cos\gamma \tag{38}$$

Aircraft lift and drag are defined as:

$$L = \frac{1}{2}\rho v^2 S_w \left(C_{L,\alpha}\cdot\alpha + C_{L0}\right) \tag{39}$$

$$D = \frac{1}{2}\rho v^2 S_w \left(C_{D,\alpha}\cdot\alpha + C_{D0}\right) \tag{40}$$

The coefficients of lift and drag vary as a function of angle of attack. The mass and aerodynamic characteristics of the aircraft, presented in Table 15, are derived from a fuel cell powered aircraft design study conducted by the authors [16].

Table 13. Low fidelity aircraft model characteristics for energy management studies

Aircraft Model Characteristic	Value
$C_{L,\alpha}$	0.0979
C_{L0}	0.4818
$C_{D,\alpha}$	0.0029
C_{D0}	0.0229
S_w	1.078 m^2
m	12.51 kg
d	0.521 m
p	0.3683 m

6.2.2. Fuel Cell Powertrain Modeling

The fuel cell system is the primary power source for the fuel cell aircraft. A fuel cell is a direct electrochemical conversion device that converts reactants into products and electrical power. The fuel cell powerplant is modeled as a static polarization curve that represents the performance of the fuel cell stack and balance of plant systems. The performance of the fuel cell used in this study is based on direct hydrogen polymer electrolyte membrane fuel cell technology. This study assumes that the hydrogen reactant for the fuel cell powerplant is stored on board the aircraft in a compressed pressure vessel, and that the oxygen reactant is supplied from ambient air. The hydrogen consumption and fuel cell LHV efficiency as functions of fuel cell output power for the fuel cell system is shown in Figure 43 and Figure 44. These curves are based on fits to experimental system test data. They include the effects of plant energy consumption, hydrogen utilization, varying cathode stoichiometry and other static system loads. The fuel cell system output power is calculated as the product of fuel cell system voltage and current:

$$P_{FC} = V_{FC} \cdot I_{FC} \tag{41}$$

The LHV efficiency of the fuel cell is the ratio of fuel cell output power to the heating value of the hydrogen flow into the system.

$$\eta_{LHV} = \frac{P_{FC}}{q_{LHV} \cdot \dot{W}_{H2}} \tag{42}$$

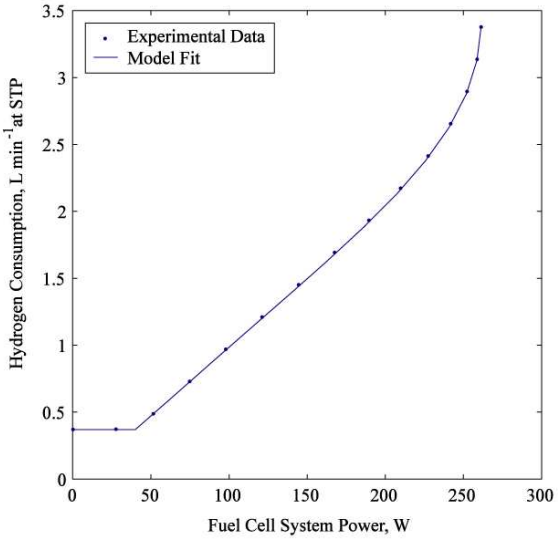

Figure 43. Fuel cell hydrogen consumption model

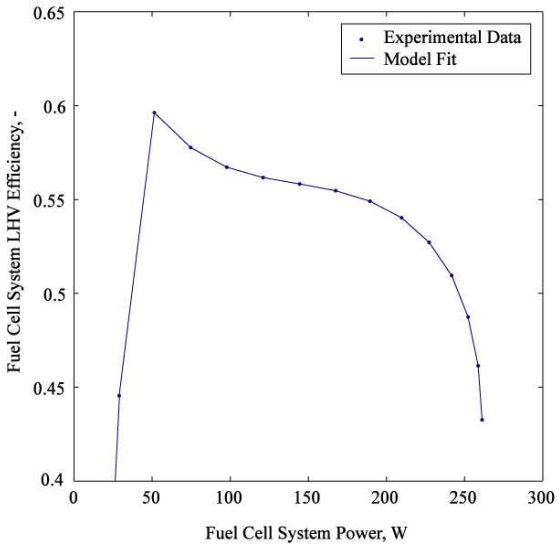

Figure 44. Fuel cell efficiency model

The dynamics of the fuel cell stack and balance of plant are not modeled as they are assumed to take place at a frequency much greater than the bandwidth of the aircraft and energy management controller.

The aircraft electric motor is modeled using a 3 layer perceptron neural network surrogate model trained using experimental data from dynamometer motor testing. The neural network model outputs the efficiency of the electric motor and motor controller as a function of output torque, input voltage and motor rotational speed. A subset of the electric motor surrogate model behavior is shown in Figure 45 and Figure 46. Motor efficiency is calculated as the ratio of mechanical output power to DC electrical input power:

$$\eta_{MOTOR} = \frac{\omega_{MOTOR} \cdot T_{MOTOR}}{V_{FC} \cdot I_{MOTOR}} \tag{43}$$

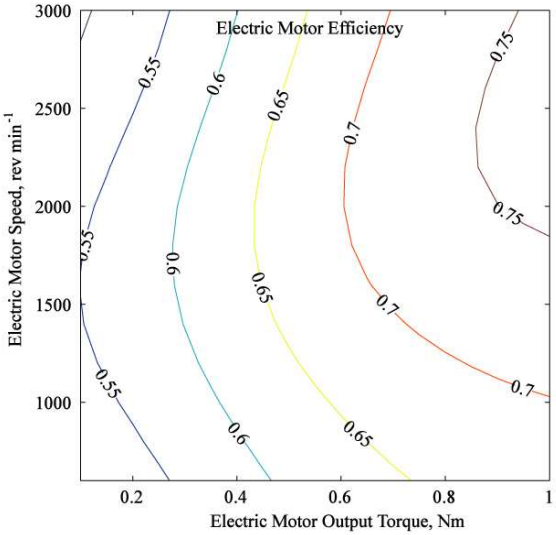

Figure 45. Electric motor efficiency map at motor input potential of 40V

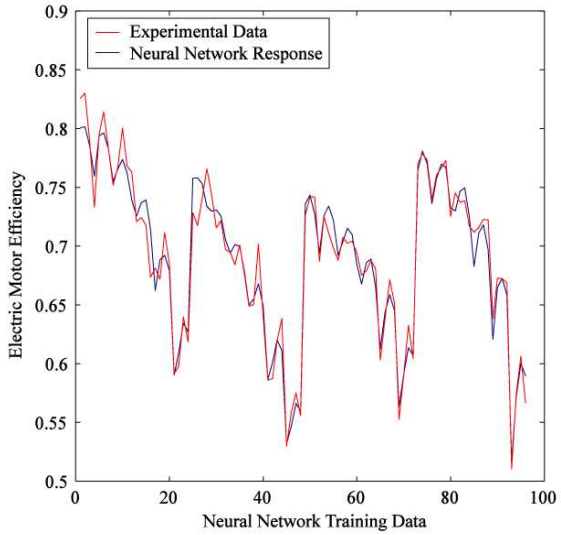

Figure 46. Electric motor model training data set

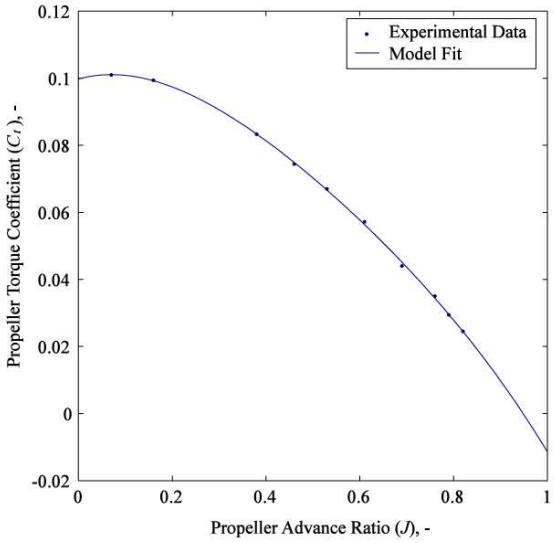

Figure 47. Propeller thrust coefficient model

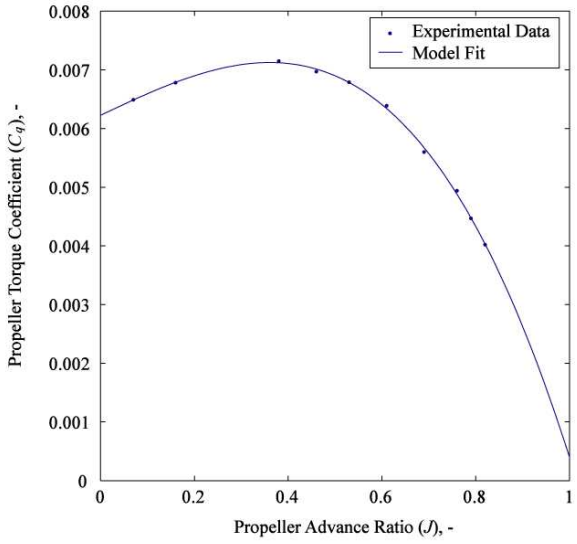

Figure 48. Propeller torque coefficient model

The propeller model is used to relate the electric motor torque to the aircraft thrust. The thrust, *T*, applied to the aircraft is defined by,

$$T = \rho\left(\frac{\omega}{2\pi}\right)^2 d^4 C_T \tag{44}$$

The propeller torque, Q, to be applied to the electric motor is determined from the software propeller model using the relation:

$$Q = \rho\left(\frac{\omega}{2\pi}\right)^2 d^5 C_q \tag{45}$$

Both the thrust and torque coefficients, C_q and C_T, are a function of the propeller advance ratio J, as shown in Figure 47 and Figure 48. The performance of the propeller is derived from wind tunnel test data [118].

$$J = \frac{v}{\left(\frac{\omega}{2\pi}\right)d} \tag{46}$$

6.2.3. Hybrid Energy Storage System Modeling

The hybrid energy storage system is modeled as a pack of 18650 lithium polymer battery cells. The open circuit voltage and internal resistance characteristics of each 18650 cell are derived from experimental data from the literature and are summarized in Figure 49 and Figure 50 [122]. The battery pack is assembled with each cell in electrical series so that when current into the battery has positive sign,

$$P_{batt} = V_{OC} I + I^2 R_{\text{int}} \tag{47}$$

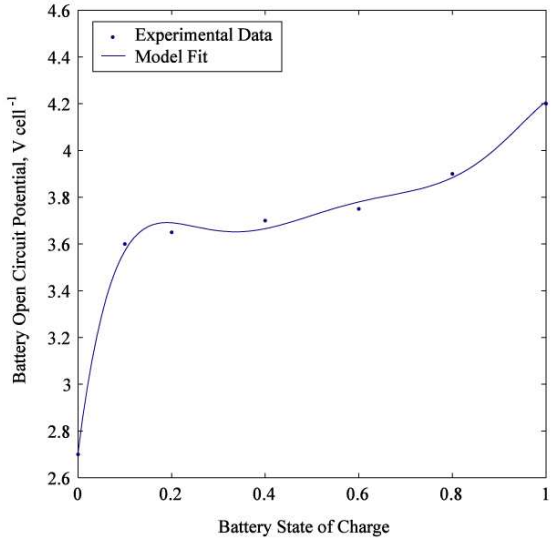

Figure 49. Lithium Ion battery open circuit voltage model

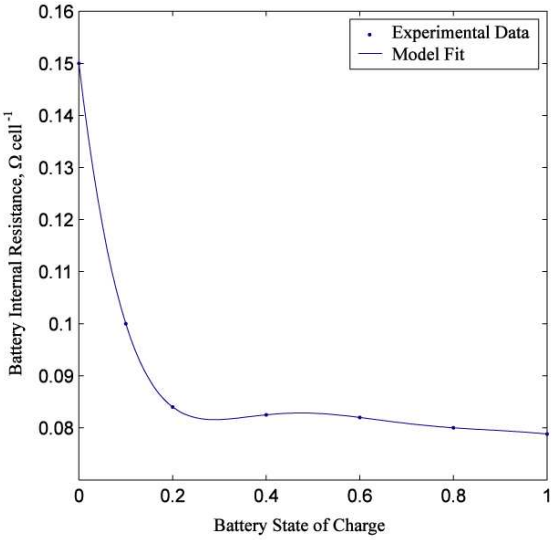

Figure 50. Lithium Ion battery internal resistance model

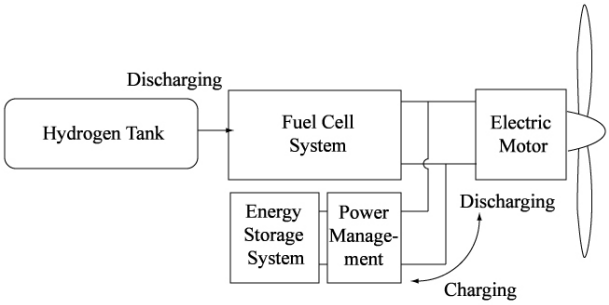

Figure 51. Hybrid electric fuel cell airplane diagram

Figure 51 shows a schematic of the aircraft powerplant. Between the battery pack and the fuel cell power bus is a power management system that allows the battery pack to discharge power to the fuel cell power bus and to charge from the power bus without requiring a matching of the fuel cell bus voltage and battery voltage. The power management device provides design freedom to specify the battery bus voltage and fuel cell bus voltage independently. The battery and fuel cell power sum to provide the electrical power to the electric motor such that

$$P_{FC} - P_{batt} = P_P \tag{48}$$

The battery model assumes that the battery coulombic efficiency is 100%, so that the state of charge can be defined as:

$$SOC = \frac{\int Idt}{C} \tag{49}$$

The battery capacity C = 12Ah. The battery energetic efficiency is defined by the ratio of the electrical energy that enters the battery to the energy extracted from the battery at constant state of charge. The energetic efficiency of the battery is less than 100% because of losses from ohmic losses during charging and discharging that are modeled using the battery internal resistance. The thermal state of the battery is not modeled.

6.2.4. Internal Combustion Engine Powertrain Modeling

In order to make a comparison between the energy management strategies for fuel cell powered aircraft and those of conventional internal combustion aircraft, we will

repeat the analyses with an internal combustion powerplant model. The internal combustion engine model is based on experimental testing of the UAV engine that powers Aerosonde [23]. The performance and efficiency of the internal combustion engine are shown in Figure 52 and Figure 53. This analysis assumes that the internal combustion engine does not idle and that it can be restarted instantly.

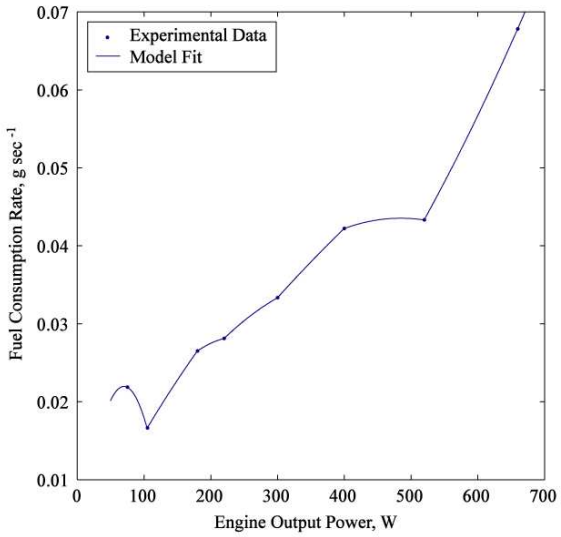

Figure 52. Internal combustion engine fuel consumption model

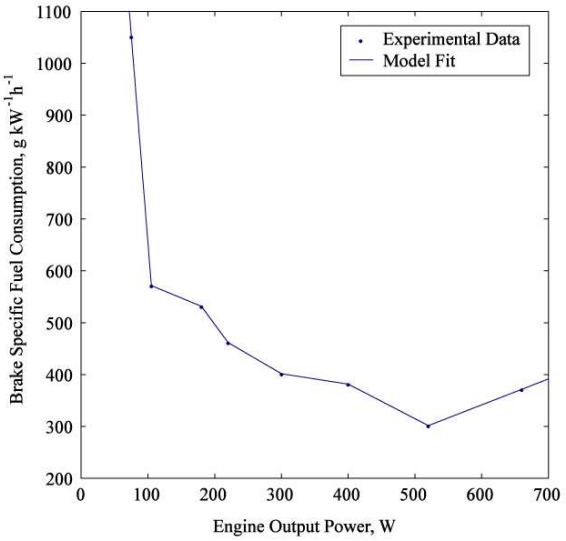

Figure 53. Internal combustion engine efficiency model

6.2.5. Energy Management Optimization Algorithms

Two nonlinear programming algorithms are used to determine the effectiveness of flight path optimization and hybridization as means to improve the performance of the fuel cell powered aircraft. First, a dynamic programming routine is used to determine the effectiveness of varying degrees of hybridization for varying aircraft flight profiles. Next a sequential quadratic programming routine is used to compare the effects of flight path optimization on both fuel cell powered and internal combustion engine powered aircraft.

Investigation I

In the first part of this study, a dynamic programming algorithm will be used to derive optimal battery/fuel cell power flows to as to optimize the endurance of the hybrid electric aircraft for predetermined flight paths. The resulting optimal energy consumptions can be compared among battery sizes and flight profiles to define optimal degrees of hybridization for fuel cell hybrid aircraft.

The aircraft can be described with the nonlinear system dynamics equation

$$\dot{S} = f(S, u, w) \tag{50}$$

The problem is then to determine the discrete control sequence,

$$u(k), k = 0,1,2...N-1 \tag{51}$$

that minimizes the objective function,

$$J = \sum_{k=0}^{N-1} g\left[S(k), u(k), w(k)\right], \tag{52}$$

subject to state and control constraints,

$$S(k) \in \Omega_S(k) \,|\, \{SOC_{\min} \le \Omega_S(k) \le SOC_{\max}\} \cap \{\Omega_S(0) = SOC_i\} \cap \{\Omega_S(N) = SOC_f\}$$
$$u(k) \in \Omega_u(k) \,|\, \{I_{b\min}[S(k)] \le \Omega_u(k) \le I_{b\max}[S(k)]\} \quad (53)$$

The objective function J is a summation of the fuel consumption at each stage $g(k)$, so that minimization of J maximizes aircraft endurance given a fixed fuel storage. The fuel consumption at each stage $g(k)$ is calculated from the set of equations (25-36) and the data in Figures 19-29 with $S(k)=SOC$, $u(k)=I_b$ and $w(k)=\gamma$ as inputs. The state of charge is constrained to remain within a recommended state of charge range where $SOC_{\min}$=20% and $SOC_{\max}$=90%. The initial and final states of charge (SOC_i and SOC_f) are constrained to ensure that the change in state of charge over the flight is zero. The battery current is constrained to remain within the battery charging current limits ($I_{b\max}$) and discharging current limits ($I_{b\min}$), which are calculated at each stage from the battery state of charge.

Investigation II

In the second part of this study, a sequential quadratic programming algorithm will be used to determine the effectiveness of flight path optimization for fuel cell powered aircraft. No hybrid energy storage is considered in this part of the study. The optimal flight path results for the fuel cell powered aircraft will be compared to results for an internal combustion powered aircraft.

This problem is posed as an optimal periodic endurance problem where the periodic flight of duration τ is split into two phases: a gliding flight phase (k=0), and a powered climb phase (k=1). The prototypical flight path is shown in Figure 1.

The aircraft and powerplant systems can be described with the nonlinear dynamic equation

$$\dot{y} = f(y, b) \tag{54}$$

$$y = \begin{bmatrix} v \\ \gamma \end{bmatrix} \tag{55}$$

$$b = \begin{bmatrix} \alpha \\ T \end{bmatrix} \tag{56}$$

The state variable y includes the velocity of the aircraft v and the flight path angle γ. The control variables are the propulsive thrust T and the aircraft angle of attack α. The problem is then to determine the discrete control sequence

$$b(k), k = 0,1, \tag{57}$$

that minimizes the objective function,

$$R = \sum_{k=0}^{1} \frac{g[y(k), b(k)]}{\tau}, \tag{58}$$

subject to state and control constraints,

$$\begin{matrix} y(k) \in \Omega_y(k) \,|\, \left\{ \begin{bmatrix} 0 \\ -\infty \end{bmatrix} \le \Omega_y(k) \right\} \\ b(k) \in \Omega_b(k) \,|\, \left\{ \Omega_b(k) \le \begin{bmatrix} \alpha_{\max} \\ \infty \end{bmatrix} \right\} \end{matrix}, \tag{59}$$

The objective function J is a summation of the fuel consumption at each stage $g(k)$ divided by the time τ required to complete the periodic flight cycle. As before, the fuel consumption is calculated from the set of equations (36-49) and the data in Figures 43-

53. The aircraft velocity is constrained to remain positive and the aircraft angle of attack is constrained to remain lower than stall.

6.3 Fuel Cell Aircraft Hybridization Results

This section compares the optimal energy management patterns for hybridized fuel cell powered aircraft by solving the problem as posed in the section labeled *Investigation I.* For each flight path we will derive the optimal energy management strategy so as to maximize the endurance of the aircraft over that flight. These investigations will allow for the assessment of the efficacy of hybridization as a means for improving aircraft performance over a variety of flight profiles. The flight profiles that will be presented here include steady level flight, steady level flight with random disturbances (as might result from the use of an autopilot speed controller), a cyclic power demand (as might result from orbiting flight with a steady wind), and a burst power demand (as might result from a high power takeoff).

6.3.1. Energy Management for Steady Level Flight

The flight path for this first experiment is a steady, level flight at 142W of DC powerplant output power. The size of the battery pack is varied by changing the number of batteries between 2 and 12. In each case, the most efficient energy management strategy for the fuel cell hybrid aircraft is to not use energy from the battery pack at all, as shown in Figure 54. These results are independent of the size of the battery pack.

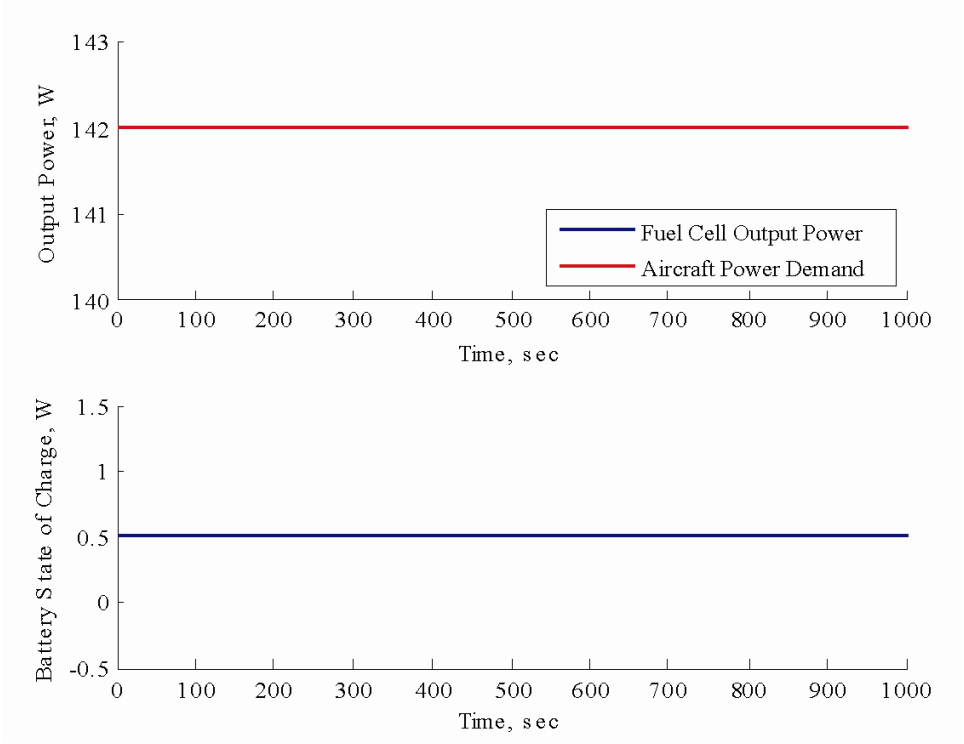

Figure 54. Optimal energy management strategy for hybrid fuel cell powered aircraft during steady flight

6.3.2. Energy Management for Level Flight with Random Disturbance

The flight path for this next experiment is a level flight at an average of 142W of DC powerplant output power. The literature has shown that modern autopilot UAV flight controllers can maintain a set airspeed against disturbances such as turbulence, steady winds, and aircraft dynamics with an uncertainty of 1.9% [123]. This corresponds to an 11.8W uncertainty in DC electric power required for flight for the example fuel cell aircraft. This uncertainty is modeled by a power trace with random deviations about the average cruise power of the aircraft.

As shown in Figure 55, the optimal energy management strategy for this flight path does not use the battery at all. Again, this result is independent of battery sizing.

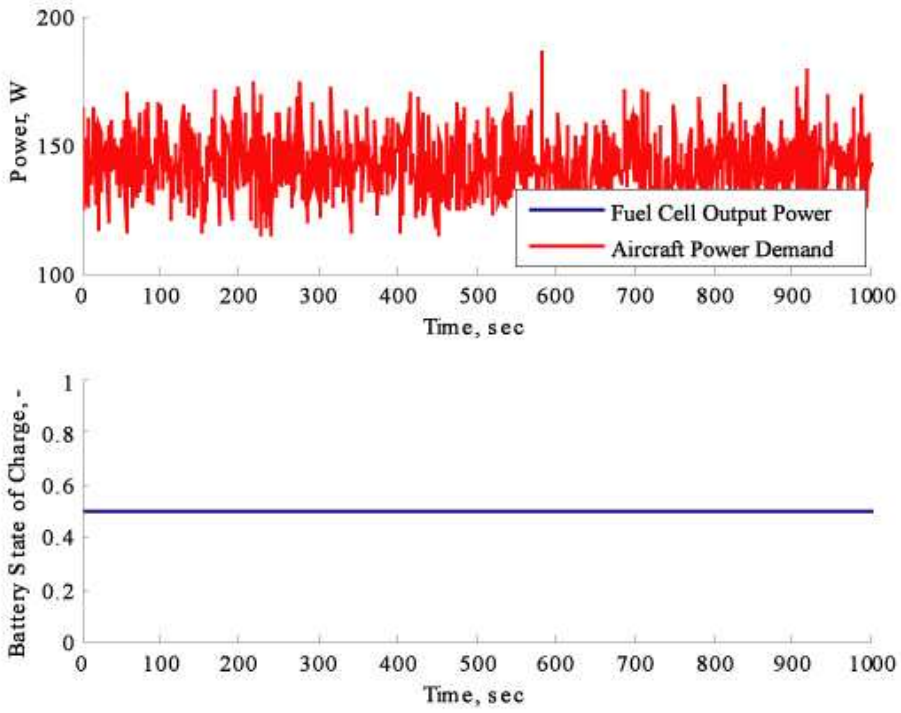

Figure 55. Optimal energy management strategy for hybrid fuel cell powered aircraft during turbulent level flight

6.3.3. Hybridization for Cyclical Power Missions and Level Flight

The flight path for this experiment includes a cyclic power demand on top of the steady state cruise power. Figure 56 shows the behavior of the optimal energy management strategy for this power demand cycle. As before, the optimal control strategy for the hybrid electric system is to not use the battery power at all.

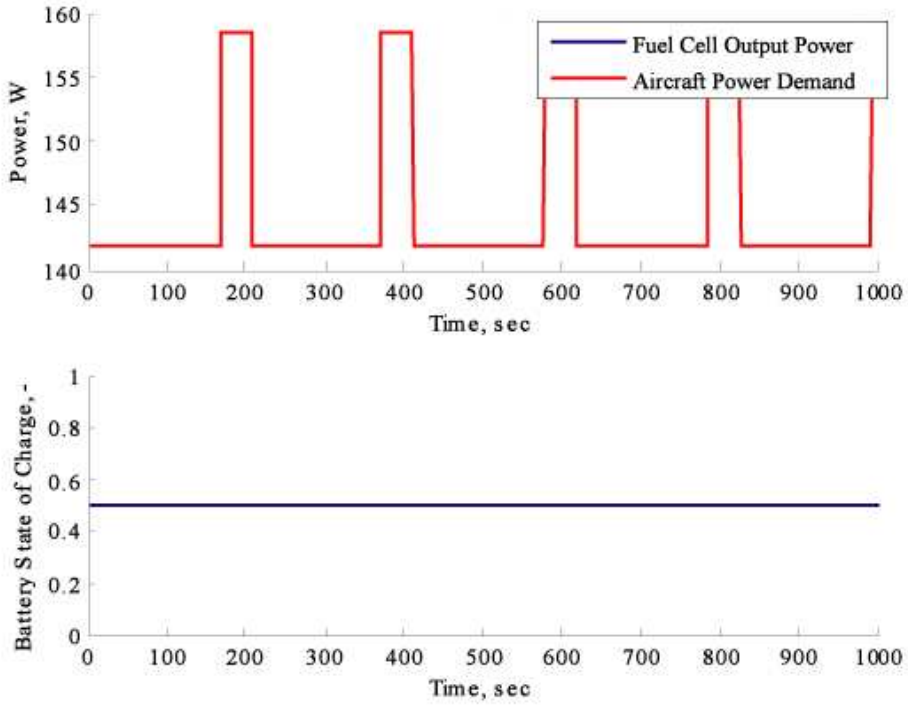

Figure 56. Optimal energy management strategy for hybrid fuel cell powered aircraft during level flight with cyclic power demands

6.3.4. Hybridization for Missions with a High Power Climb Followed by Steady Level Flight

The last flight path to be investigated represents the flight path of a UAV that has a large climb rate requirement. The power demand has a 500 second high power burst followed by a 500 second cruise.

When the initial and final states of charge are constrained so that the battery ends the cycle at the same state of charge as it began at, no battery power is used until the power demand becomes greater than the power that can be supplied by the fuel cell alone. This is shown in Figure 57(a) and (b). In Figure 57 (a), the optimal energy management strategy does not use the battery at all. Only, as in Figure 57 (b), when the aircraft power

demand becomes greater than the peak power of the fuel cell system (270 W), will the energy management strategy take power from the batteries in order to meet the power demand.

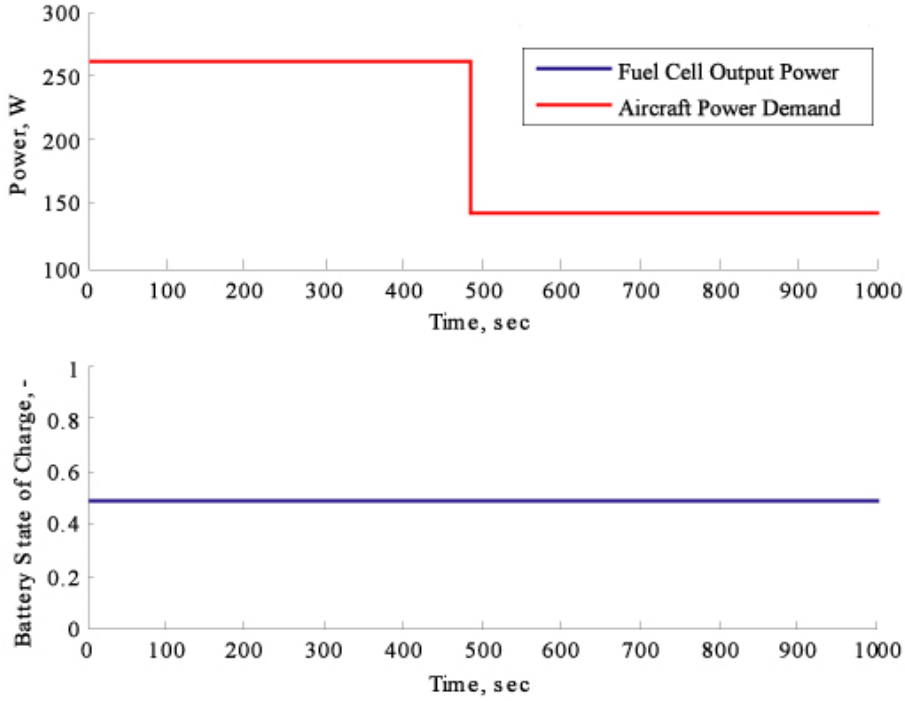

Figure 57. Optimal energy management strategy for hybrid fuel cell powered aircraft during level flight with burst power demands and a charge sustaining strategy

Of course, when the battery state of charge is allowed to deplete over the course of the cycle, the energy management strategy takes advantage of the energy available in the batteries to lessen the load on the fuel cell system and reduce its hydrogen consumption. This condition is shown in Figure 58.

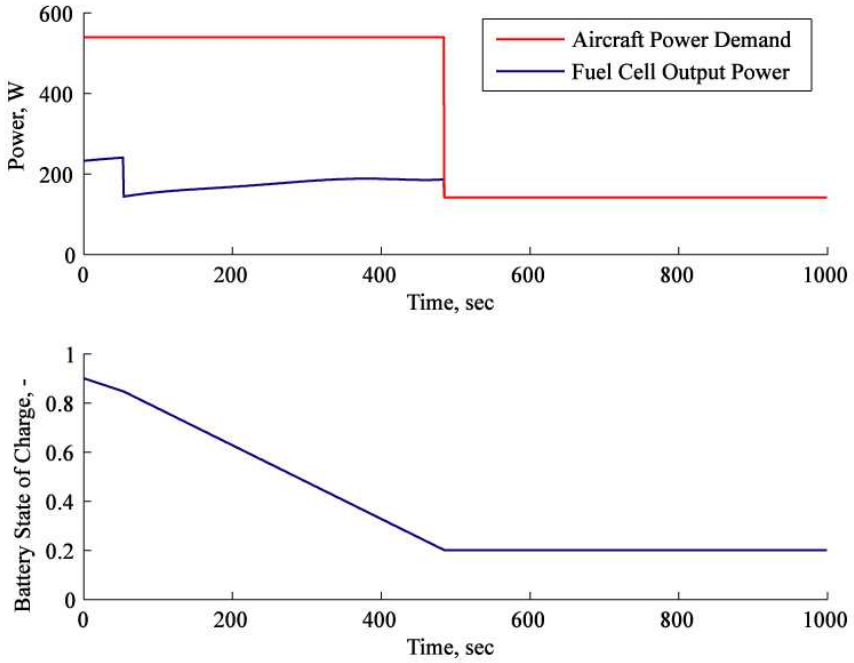

Figure 58. Optimal energy management strategy for hybrid fuel cell powered aircraft during level flight with burst power demands and a charge depleting strategy

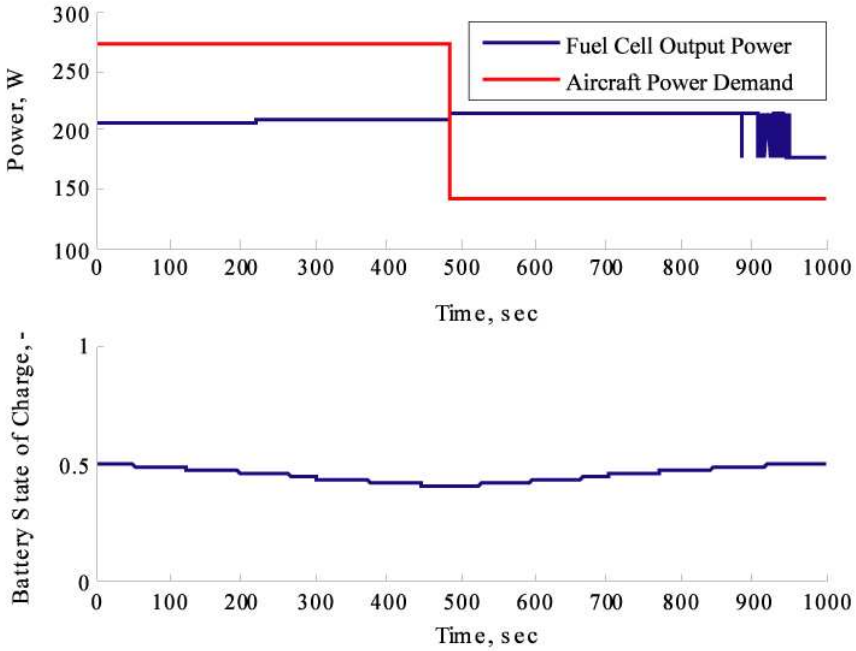

Figure 59. Optimal energy management strategy for hybrid fuel cell powered aircraft during level flight with burst power demands and a charge sustaining strategy

6.4 Fuel Cell Aircraft Flight Path Optimization Results

This section compares the characteristics of optimal flight patterns for un-hybridized fuel cell powered and internal combustion engine powered aircraft by solving the problem as posed in the section labeled ***Investigation II***. The result for each aircraft type is the optimal flight path trajectory which is defined by the velocity and flight path angle during the climb and glide phases.

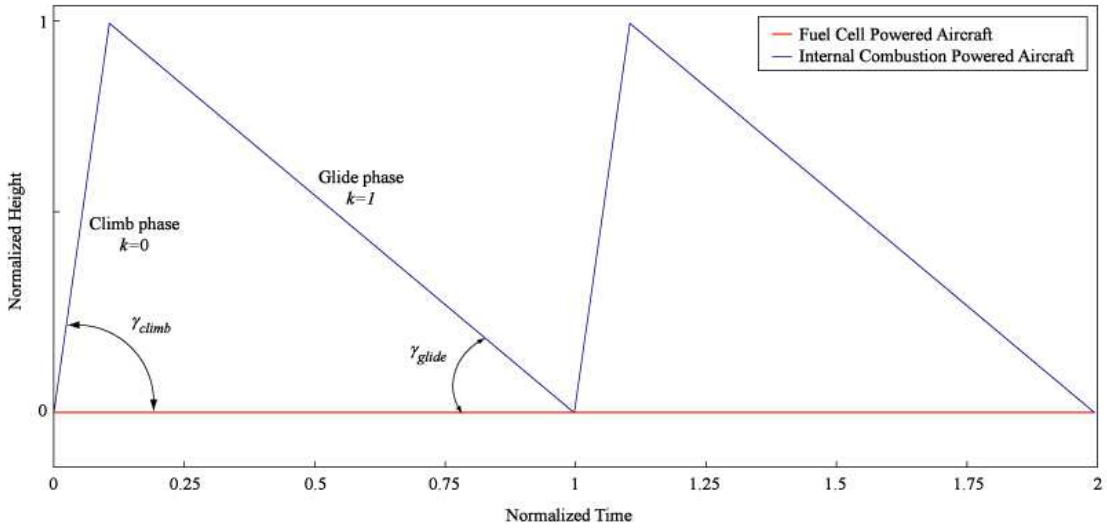

Figure 60. Optimal periodic flight paths for fuel cell and internal combustion powered aircraft

These results are presented in Figure 60. For the fuel cell powered aircraft, the optimal flight path for endurance is steady, level flight. Periodic climbing-gliding flight has no positive effect on the endurance of fuel cell powered aircraft. For the internal combustion powered aircraft the optimal flight path is a periodic optimal cruise where the flight is characterized by a γ_{climb} of 10 degrees followed by a gliding phase.

To numerically prove that the flight paths shown in Figure 60 are optimal flight paths,tFigure 61 shows that the period averaged fuel consumption for the fuel cell aircraft is minimized when the flight path angle is zero. This condition corresponds to steady, level flight.

Figure 62 shows the results of this same analysis for the internal combustion engine powered aircraft. The optimal flight path for the internal combustion engine powered aircraft is the periodic climb glide path shown in Figure 60. As can be seen in Figure 62, the optimal periodic flight path for the internal combustion engine requires a

flight path angle during climb (γ_{climb}) of 10 degrees to minimize fuel consumption. This corresponds to a climbing speed of 16.7 m s^{-1}, a gliding speed of 12.6 m s^{-1}, a gliding angle of -2.47 degrees, and a climbing/gliding duty cycle of 15.8%.

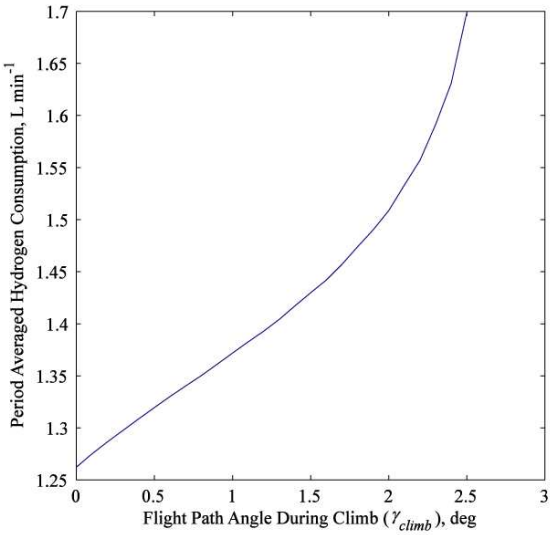

Figure 61. Fuel consumption versus flight path angle for fuel cell powered aircraft undergoing periodic flight

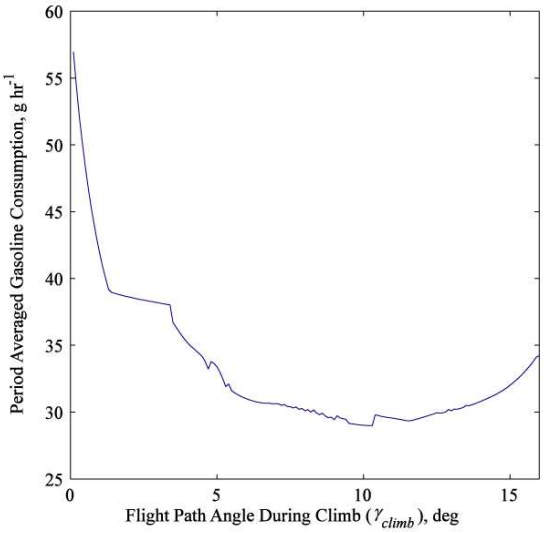

Figure 62. Fuel consumption versus flight path angle for internal combustion engine powered aircraft undergoing periodic flight

6.5 Discussion

There exists a natural connection between the concepts of hybridization and flight path optimization as both of these can be categorized as energy management strategies. In hybrid systems, the energy is stored as electrochemical energy. In aircraft under flight path optimization, the energy is stored as potential energy. In both cases they are strategies to improve the effectiveness of an aircraft for a particular mission through energy management.

The results of both *Investigation I* and *Investigation II* show that hybridization and flight path optimization do not improve the efficiency or endurance of fuel cell powered aircraft as they do for internal combustion powered aircraft.

These results suggest that if one were to construct a hybrid electric fuel cell powered aircraft, the aircraft efficiency would not be improved through energy management or flight path optimization. Instead the performance of the aircraft might be improved by allowing the batteries to provide takeoff power and designing the fuel cell powerplant for maximum endurance, unassisted by the hybrid system. To test the tradeoff between the improved efficiency of the hybridized aircraft fuel cell powerplant and the increased weight of the hybrid system components, we can use the design tools of Chapter 5.

6.6 Hybrid FCUAV Design Example

A hybrid, charge-depleting, fuel cell powered aircraft is designed that uses the battery system for takeoff and uses a fuel cell for long endurance cruise. The aircraft is designed by optimizing the aircraft for endurance with a reduced fuel cell powered climb rate. To deliver the 700W of power required to climb at 120m/min, 2.35kg of the 18650

lithium polymer battery cells are added to the aircraft mass. The architecture of the aircraft powerplant is shown in Figure 51. So as to allow comparison with the fuel cell powered UAV designed at the conclusion of Chapter 5, the hybrid aircraft is weight constrained to less than 20kg, climbs at 120 m/min and carry a 1 kg, 15W payload over a maximum endurance mission.

Table 14 compares the design characteristics and performance of the fuel cell powered aircraft and the fuel cell hybrid aircraft. Decoupling of the climb rate constraint from the endurance requirement allows the fuel cell hybrid aircraft to show much higher endurance than the conventional fuel cell powered UAV. Of course, the energy limitations of the batteries only allow the aircraft to climb for 18 minutes to an altitude of approximately 2100m. Despite that, the reduced power requirements of the fuel cell for the hybrid aircraft allows the downsizing of the fuel cell and the upsizing of the hydrogen tank. These effects work to increase the endurance of the aircraft from >22 hrs to > 47.5 hours.

Table 14. Fuel cell aircraft and hybrid fuel cell aircraft comparison

Aircraft Characteristic	Fuel Cell Powered Aircraft	Fuel Cell Hybrid Aircraft
Endurance, hrs	22.1	47.7
Climb rate, m min^{-1}	120	120
Payload mass, kg	1	1
Payload power, W	15	15
Hybrid battery mass, kg	0	2.35
Wing span, m	4.38	5.55
Powerplant and Energy Storage Specific Energy, Wh kg^{-1}	340	561
Hydrogen tank mass, kg	4.1	8.1
Number of fuel cells	50	31
Fuel cell active area, cm^2	35.8	35.1

6.7 Chapter Conclusions

This section of the research effort has allowed us to address research question 3, which is restated here:

Research Question 3*: What are the conditions where optimal fight path management and hybridization can improve the design performance of fuel cell powered aircraft?*

The results of this work show that energy management and flight path optimization is ineffective for fuel cell aircraft performing conventional steady long-endurance flight.

> ***Hypothesis 3.1****: Optimal energy management of a fuel cell powered aircraft will not improve the performance of fuel cell powered aircraft.*

In fact, energy management and hybridization of fuel cell aircraft work in unanticipated ways. The inclusion of a hybrid battery system does not improve the endurance or range of the fuel cell aircraft, given a fixed design and mission. There is no mechanism for the hybrid power system to improve the efficiency of the fuel cell powerplant during cruise. Instead, the hybridization allows for the decoupling of design requirements for the climb and cruise flight phases of the long endurance aircraft.

CHAPTER 7

DEVELOPMENT AND EXPERIMENTAL CHARACTERIZATION OF A FUEL CELL POWERED AIRCRAFT

7.1 Introduction

This section describes the characteristics and performance of a fuel cell powered unmanned aircraft constructed to allow for validation of the design methods and model presented in previous chapters. The aircraft features a 500 W polymer electrolyte membrane fuel cell with full balance of plant and compressed hydrogen storage incorporated into a custom airframe. Details regarding the design requirements, implementation and control of the aircraft are presented for each major aircraft system. The performances of the aircraft and powerplant are analyzed using data from flights and laboratory tests. The efficiency and component power consumption of the fuel cell propulsion system are measured at a variety of flight conditions. The performance of the aircraft powerplant is compared to other 0.5-1 kW-scale fuel cell powerplants in the literature and means of performance improvement for this aircraft are proposed. This work represents one of the first studies of fuel cell powered aircraft to result in a demonstration aircraft. As such, the results of this study are of practical interest to fuel cell powerplant and aircraft designers.

Figure 63. Fuel cell powered aircraft constructed for validation of design methodology

Based on the results of the previous sections of this dissertation, there exists a need for a comprehensive, documented development and performance analysis for a larger-scale fuel cell aircraft. To work towards this goal, the George Woodruff School of Mechanical Engineering, the Georgia Tech Research Institute and the Aerospace Systems Design Laboratory at the Georgia Institute of Technology Daniel Guggenheim School of Aerospace Engineering have designed and built the technology demonstrator fuel cell aircraft shown in Figure 1. The aircraft itself is novel as it is the largest fuel cell aircraft yet developed that is fueled by compressed hydrogen and the largest fuel cell aircraft whose design and test results are in the public domain.

This aircraft can serve as a platform for development and testing of fuel cell powerplants for aircraft and as a tool for validation of system design models and methodologies. The demonstrator aircraft is designed to comply with the specifications of the Academy of Model Aeronautics. This sets a maximum mass constraint for the aircraft at 24.9 kg and functionally limits the aircraft to testing at model aircraft runways.

This scale simplifies the licensing of the aircraft and is appropriate for an academic demonstration project.

The aircraft design was broken down into high-level conceptual and low-level detailed design tasks. The aircraft conceptual design was performed by assembling a series of contributing analyses into a higher level simulation of the fuel cell aircraft performance. The performance simulation is parameterized within a defined, discritized design space to allow variation in the aircraft configurations and subsystem specifications. Because of the high computational load associated with characterizing the design space, simplifying assumptions are built into the contributing analyses. Validation of the conceptual design is critical for ensuring its effectiveness. A more detailed breakdown of the conceptual and low-level design tasks is provided in references [12,14]. The aircraft was constructed based on the results of the detail design.

This section presents the low-level specifications and performance characteristics of the demonstration aircraft and its power and propulsion systems, as constructed. The fuel cell powerplant system design and aircraft design are presented with performance data that show the interaction between the fuel cell powerplant and vehicle. Flight and laboratory testing results are presented and means of performance improvements are discussed.

7.2 Powerplant System Description

For the demonstrator aircraft, the fuel cell is the only source of propulsive power. The fuel cell powerplant designed for use in the demonstrator aircraft is composed of the fuel cell stack, thermal management, air management, and hydrogen storage and management subsystems, as shown in Figure 64. These subsystems are controlled by an

ATMEGA32, 8-bit AVR microcontroller module (Atmega, San Jose, CA) that functions as both the powerplant controller and the aircraft data acquisition system.

A summary of the powerplant characteristics as constructed is presented in Table 15. The balance of plant configuration shown in Figure 64, which includes a dead-ended anode, liquid cooling, pressurized cathode and active air flow control, was chosen so that the powerplant incorporates the same subsystems that are required to control PEM fuel cell systems of much higher power. Although there are fuel cell systems with comparable power output that are passively controlled or incorporate simplified balance of plant systems, using a more complete balance of plant improves the applicability and generalization of the design tools developed and lessons learned for this project.

The following sections describe the components, design and specifications of the fuel cell powerplant subsystems.

Table 15. Fuel cell system characteristics

Powerplant Specification	*Value*
PEM Fuel Cell Stack	
Number of Cells	32
Cell Active Area	64 cm^2
Operating Temperature	60 C
Mass	4.96 kg
Hydrogen Storage	
Storage Pressure	31 MPa
Capacity	192 SL
Powerplant System	
Peak Output Power	465 W
Specific Electrical Energy	7.1 Wh/kg
Specific Electrical Power	52 W/kg

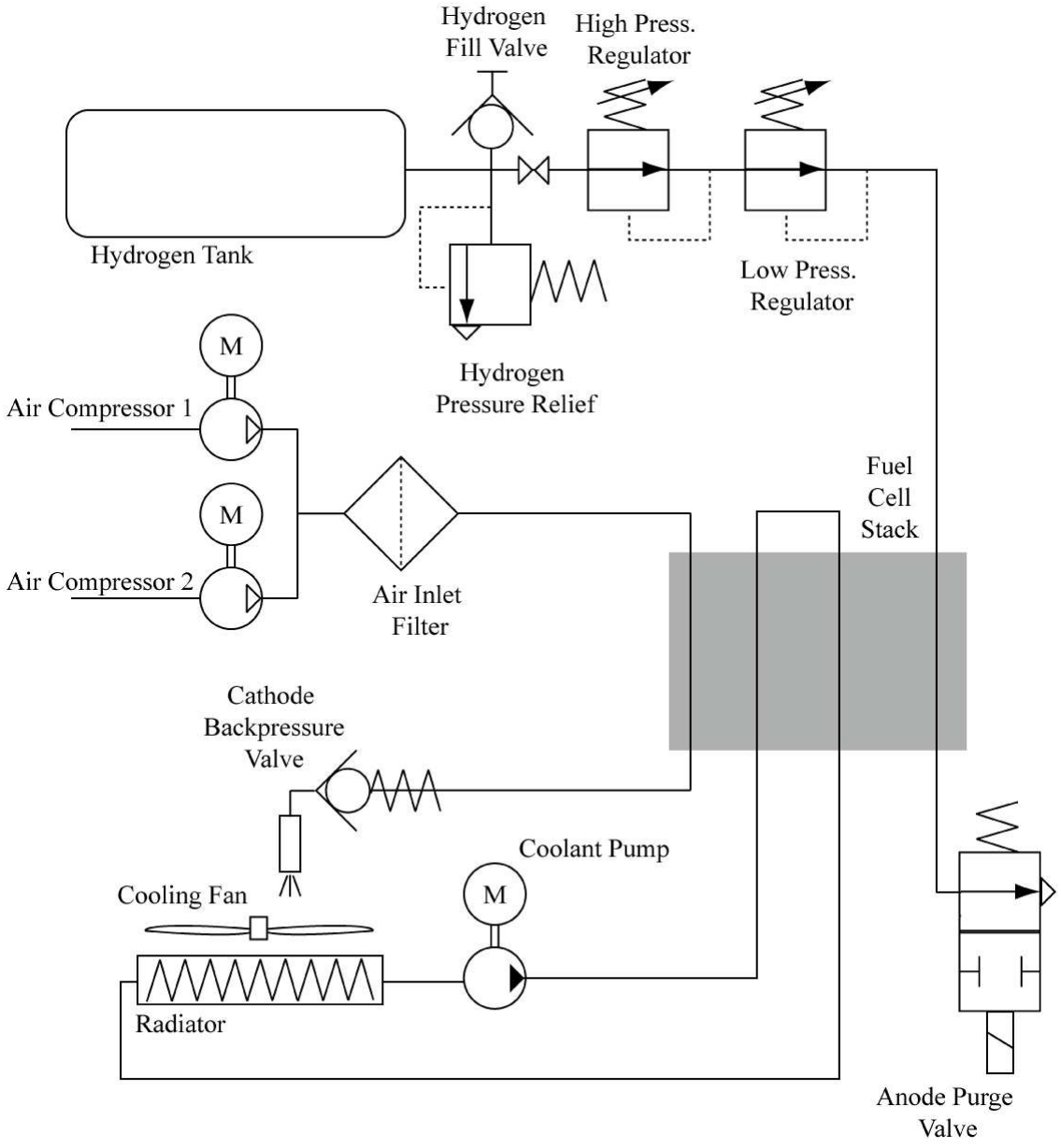

Figure 64. Fuel cell powerplant diagram

7.2.1. Fuel Cell Stack

The fuel cell stack converts the chemical energy of stored hydrogen and ambient oxygen to electricity. The fuel cell powerplant for the demonstrator fuel cell aircraft is derived from the 500 W 32-cell PEM self-humidified hydrogen-air fuel cell manufactured by BCS Technology Inc. (Bryan, TX). A photograph of the fuel cell stack

is shown in Figure 65. The fuel cell uses membranes from De Nora Inc. (Somerset, NJ) and a proprietary membrane electrode assembly production process designed to improve the water carrying capacity of the membrane [124]. The active area of each membrane electrode assembly is 64 cm^2. The graphite bipolar plates incorporate a triple-serpentine flow channel design, and liquid cooling channels. The fuel cell endplates are of a custom design to reduce the weight of the fuel cell and to simplify its mounting in the aircraft. The fuel cell stack performance without balance of plant loads is shown in Figure 66. The modifications to the stack that were required to incorporate the stack into the aircraft have no measurable effect on the electronic resistance or electrochemical performance of the stack.

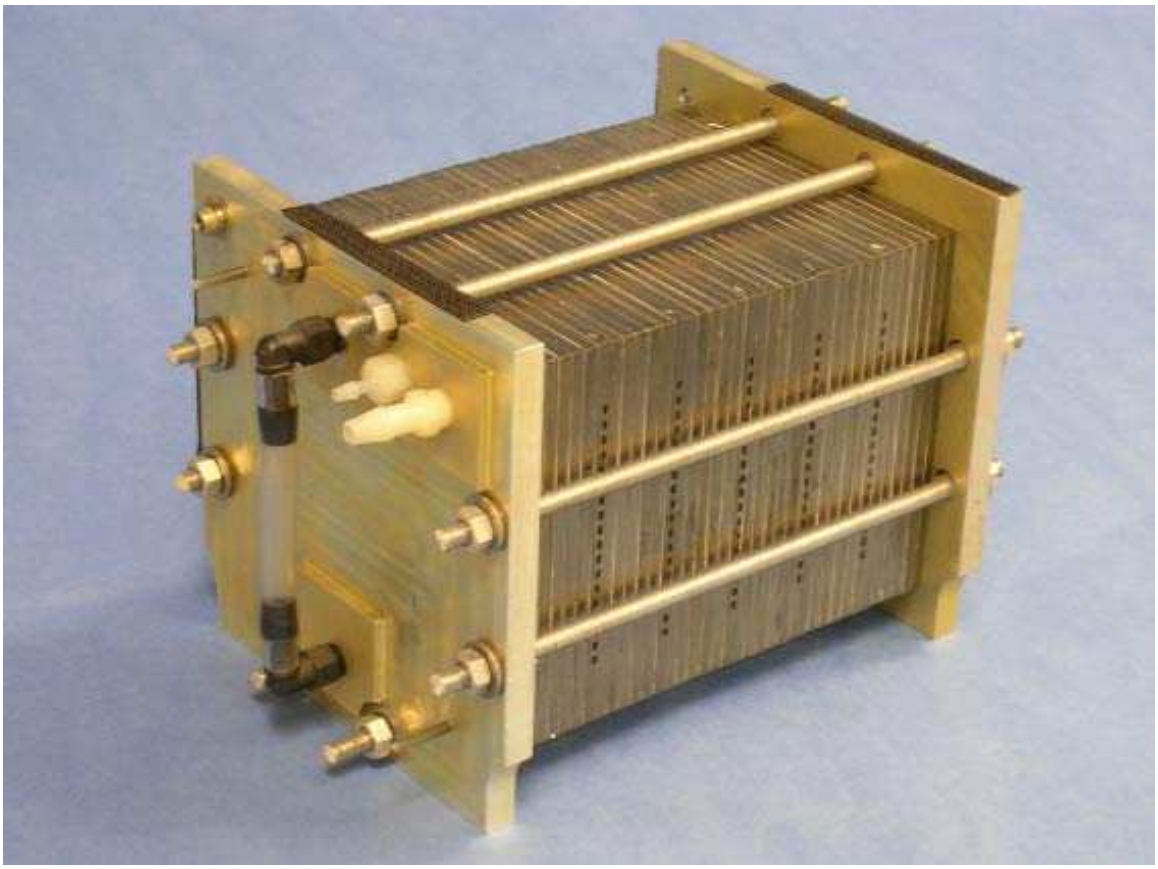

Figure 65. Customized 32-cell fuel cell stack

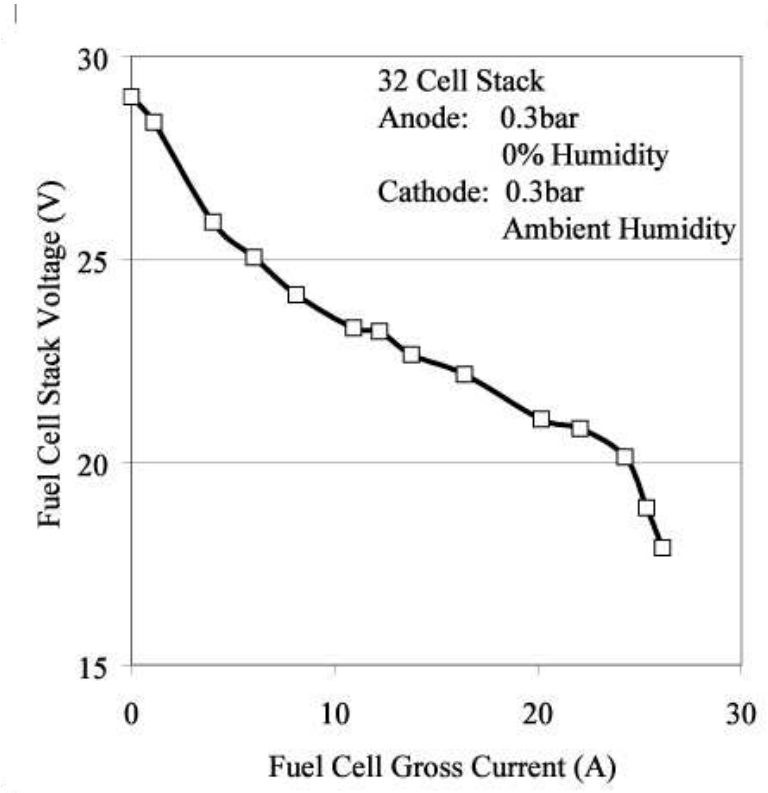

Figure 66. Fuel cell stack polarization curve

7.2.2. Temperature Control System

The purpose of the temperature control system is to maintain the temperature of the fuel cell stack within a range dictated by the fuel cell performance. When the fuel cell temperature is too low, the activation and mass transport overpotential is high. When the fuel cell temperature is too high (greater than approximately 65 C), the self-humidification function of the fuel cell begins to break down. The lack of liquid water decreases the protonic conductivity of the fuel cell membrane, degrading performance [125].

A liquid cooling circuit circulates deionized water through the fuel cell, water pump and radiator. There is no contact between the deionized water of the cooling circuit and the fuel cell reactants or product water. The water pump (Laing DDC, Chula Vista, CA) circulates 1.5 L/min of water at the pressure drop of the fuel cell, radiator and couplings.

The fuel cell radiator is constructed of internally finned aluminum tubing with carbon foam (Poco Graphite, 0.56 g/cc) providing the air to aluminum interface. A photograph of the radiator is shown in Figure 67. The carbon foam is cut into banks of fins and is pressed to the aluminum tubes. Air from the outside of the aircraft fuselage is ducted through the radiator by an 80 mm diameter, 3 W fan. The carbon foam is continuously wetted with the fuel cell product water to enable evaporative cooling of the radiator. Development of the custom carbon foam radiator resulted in a weight savings of 500 g and a power savings of 12 W when compared to conventional aluminum radiators.

Figure 67. Carbon foam radiator as implemented in demonstrator aircraft

7.2.3. Air management system

The air management system provides filtered and pressurized air to the cathode manifolds of the fuel cell with variable flow rate control. Variable flow rate control is particularly important in a self-humidified fuel cell system because of the risk of under-humidification at low current densities . For the self-humidified fuel cell, there are no humidification requirements for the reactant gases and the air enters the fuel cell at the ambient humidity ratio.

The 0.3 bar cathode pressure is regulated with a calibrated, spring loaded, ball check valve (Microchek 14B14B-5psi, Lodi, CA). Flow rate is controlled by pulse-width

modulation of two diaphragm compressors (T-Squared Manufacturing T202, Lincoln Park, NJ). These compressors are powered from the fuel cell bus voltage. By using two compressors, and turning one of the compressors off when low flow is required, higher high flow rates and lower low flow rates are achievable than is possible with a single compressor. Figure 68 shows the cathode stoichiometric ratio provided by the compressors as a function of the fuel cell output current. A cathode stoichiometry between 2.0 and 3.0 is recommended by the fuel cell manufacturer. For fuel cell system currents over 12 A, both compressors are used. Under 12 A, only one compressor is used. For fuel cell system currents under 5 A, the flow rate is constrained by the idle speed of the compressor, and the recommended stoichiometry cannot be achieved.

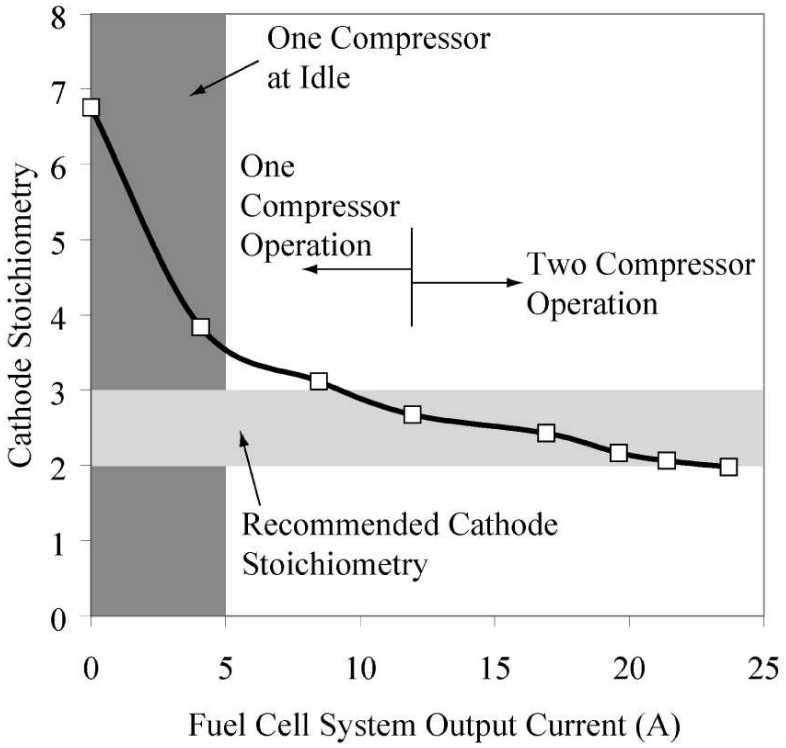

Figure 68. Cathode stoichiometry as a function of fuel cell system output current

7.2.4. Hydrogen Storage/Management System

For the demonstrator aircraft, hydrogen is stored on board of the aircraft in a carbon fiber/epoxy cylinder with aluminum tank liner (Luxfer Gas Cylinders P07A, Riverside, CA). The hydrogen tank has an internal volume of 0.74 L. Two inline single-stage regulators (Pursuit Marketing Inc., 40610, Des Plaines, IL and Airtrol Components Inc., ORS810, New Berlin, WI) regulate the hydrogen storage pressure of 310 bar down to the anode manifold delivery pressure of 0.3 bar. A solenoid purge valve (Asco Valve Inc., 407C1424050N, Florham Park, NJ) opens periodically to purge water and contaminants from the anode flow channels. The purge cycle period is an experimentally derived function of the fuel cell output current and is designed to maximize the voltage stability and hydrogen utilization of the stack. The purge cycle pulse width is 0.2 seconds. Figure 69 shows the experimentally measured dynamic behavior of the hydrogen flow rate and anode pressure during purge. Pressure and flow rate are measured using an inline flow meter (Omega Engineering Inc., FMA-1610A, Stamford, CT). The pressure droop during valve opening and the overshoot after valve closing are due to the regulator dynamics. Figure 70 shows the hydrogen utilization as a function of the fuel cell system output current. The hydrogen utilization is defined by the ratio of the purge hydrogen flow to the total hydrogen flow. Because the hydrogen purge cycle period is only a weak function of the current output of the fuel cell, the anode stoichiometry varies as a function of output current. The peak hydrogen utilization of the stack is 90% and occurs at peak current.

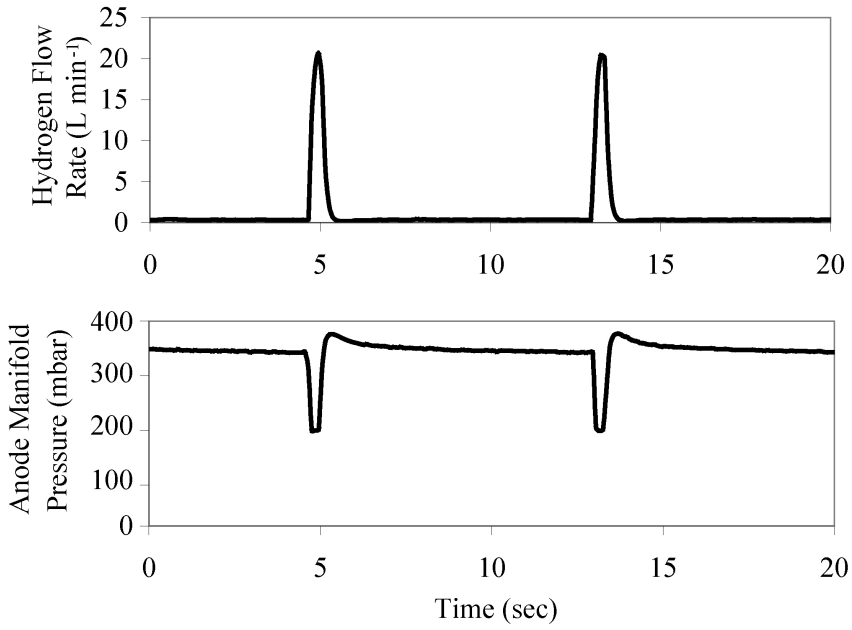

Figure 69. Dynamic behavior of hydrogen purge under idle conditions

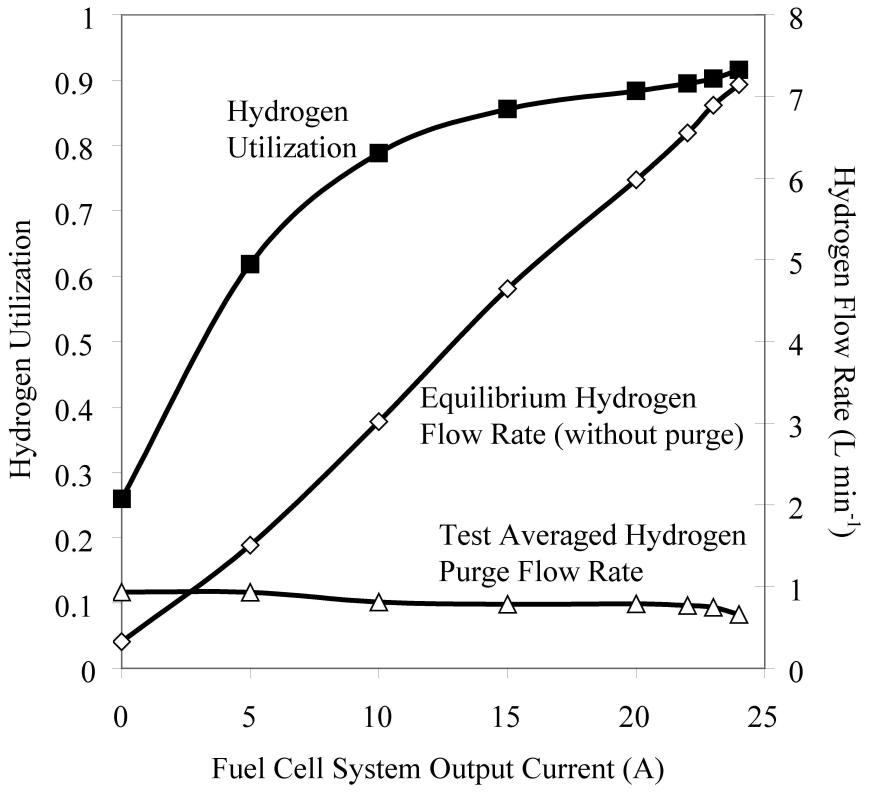

Figure 70. Hydrogen purge system behavior

7.3 Aircraft Description

The demonstrator aircraft is designed as a proof-of-concept without a defined payload or endurance requirement. The primary missions of the aircraft are to reliably demonstrate fuel cell powered flight, and gather high-quality repeatable data regarding the function of the aircraft and fuel cell systems. As such, the main requirements of the aircraft are robust flight performance, high stability and fast landing to takeoff turn around time. Even these broad performance requirements place limitations on the conceptual design of the aircraft. For instance, landing gear are used for the demonstrator aircraft despite their added weight and drag because they allow the aircraft to be reliably landed and redeployed without repair or reconfiguration.

The following sections describe the design requirements, and specifications of important aspects of an aircraft designed for use with a fuel cell powerplant.

7.3.1. Aerodynamics

To maximize the performance of the aircraft, the aircraft aerodynamic design is optimized by maximizing the propulsive efficiency of the fuel cell aircraft at cruise while applying design constraints on bank angle, climb rate and stall speed. These requirements push the aircraft design towards a design with high wing area and high aspect ratio. Table 16 lists some of the aerodynamic design characteristics of the demonstrator aircraft.

Table 16. Specifications of the demonstrator aircraft

Aircraft Specification	*Value*
Wing Area	188 dm^2
Aspect Ratio	23
Wing Span	6.58 m
Tail Area	45.5 dm^2
Length (nose to tail)	2.38 m
Mass	16.4 kg
Propeller Diameter	55.9 cm
Propeller Pitch	50.8 cm
Static Thrust / Weight	0.165
Cruise Airspeed	14.5 m/s

The wing is made up of a SD-7032 airfoil with varying taper and twist. The SD-7032 was chosen as compromise between high lift to drag ratio, high thickness ratio and excellent stall characteristics. Because the weight of the aircraft is dominated by the weight of the fuel cell system, the structural weight penalty that goes along with high wing area and aspect ratio is overcome by the improved lifting surface efficiency. The constraint on wing planform aspect ratio is set by a minimum Reynolds number constraint of Re=275,000 for the SD-7032 airfoil. To improve the span efficiency, taper and linear washout is added to the outer section of each wing.

A two view drawing of the demonstrator aircraft is shown in Figure 71. The demonstrator aircraft utilizes a pusher propeller design since a more aggressive rear fuselage taper can be facilitated with a pusher design. Aerodynamic simulation of the entire aircraft shows that the increased rear taper improves the aircraft lift to drag ratio by roughly 8%.

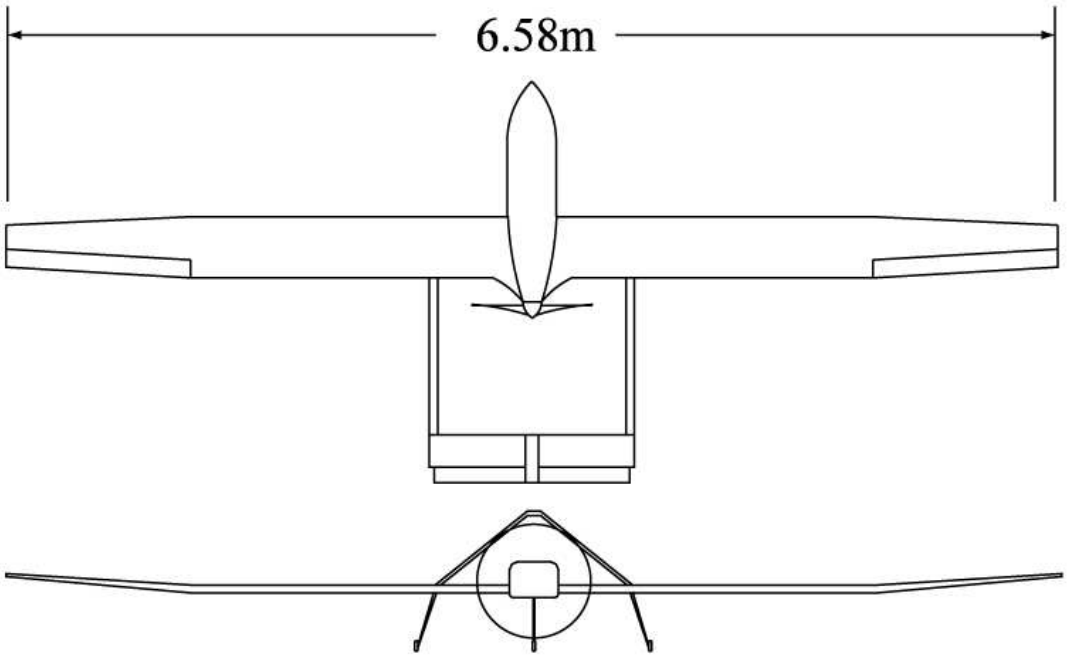

Figure 71. Two view drawing of fuel cell powered demonstrator aircraft

7.3.2. Aircraft Structures

The demonstrator aircraft is constructed from a tubular 6061-T6 aluminum space frame with a roll-wrapped carbon fiber tubular spar. The tail booms are constructed of roll-wrapped carbon fiber tubing, bonded to the spar with aluminum lugs. The fuselage is a non-structural fairing of fiberglass and Nomex honeycomb (Hexcel, Stamford, CT) construction. The wing and tail surfaces are balsa-sheeted polystyrene foam, covered with adhesive film (Monocote, Hobbico Inc., Champaign, IL) The main landing gear are machined out of 6061-T4 aluminum and the front gear is constructed of tubular fiberglass with a machined 6061-T6 fork.

7.3.3. Stability and Controls

Because the fuel cell aircraft has a much lower power to weight ratio compared to conventionally-powered small aircraft, the fuel cell demonstrator is designed for low-speed, stable, level flight with slow maneuvering. This corresponds to a stability number of 1 on the Cooper-Harper scale. The roll stability of the aircraft is set by incorporating polyhedral into the outboard section of the wing. Pitch and yaw stability is set by the size and angle of the "inverted vee" tail. Flaps are included to slow the aircraft for descent and landing.

7.3.4. Propulsion System

The propulsion system of the aircraft includes the electric motor, motor controller and propeller. The fuel cell provides power to the propulsion system at the fuel cell bus voltage. The aircraft is propelled by a single electric motor and propeller in a pusher configuration. Many of the components of the propulsion system are commercial off the shelf components, but they are specified and combined to maximize the efficiency of the aircraft at cruise.

Generally, the efficiency of the propulsion system increases with increasing propeller diameter and increasing advance ratio [126]. This pushes the propulsion system design towards large diameter propellers with high pitch that are turned by a slow-spinning, high torque motor. Propulsion system designs along this axis are only constrained by the current capacity of the fuel cell powerplant.

The propulsion electric motor (Hacker GmbH, C-50 13XL, Niederhummel, Germany) is a brushless, air cooled motor and incorporates a 6.7:1 planetary reduction between the motor and the propeller. The propeller specified is a 22 inch (56 cm)

diameter solid carbon-fiber two-bladed propeller with a pitch of 20 inches (51 cm) (Bolly LLC, 22x20, Elizabeth West, South Australia).

7.4 Aircraft and Powerplant Performance

Because of the low specific power of small scale fuel cell powerplants, the performance of the fuel cell demonstrator aircraft is power limited. The performance of the aircraft is therefore highly dependent on the weight and drag of the aircraft and on the performance of the fuel cell powerplant. In this section, the performance of the aircraft and power plant systems are analyzed using test data gathered from the demonstration aircraft.

7.4.1. Aircraft Weight Breakdown

Figure 72 shows the measured weight breakdown of the fuel cell demonstrator aircraft. The fuel storage and propulsion systems of the aircraft accounts for roughly 57% of the total aircraft weight. For all fuel cell aircraft designed or constructed to date, including this aircraft, the weight of the aircraft is dominated by the weight of the fuel cell and balance of plant [18,34,46-48,88]. For smaller fuel cell aircraft this effect occurs because many fuel cell components are heavy at such a small scale. For instance, the hydrogen tank used for the demonstrator aircraft is 1.4% hydrogen by weight. At larger scales, it is possible to manufacture tanks that are >12% hydrogen by weight [25]. Commercially available fuel cell systems at the 500 W scale are not generally intended for mobile applications, and are therefore not weight optimized.

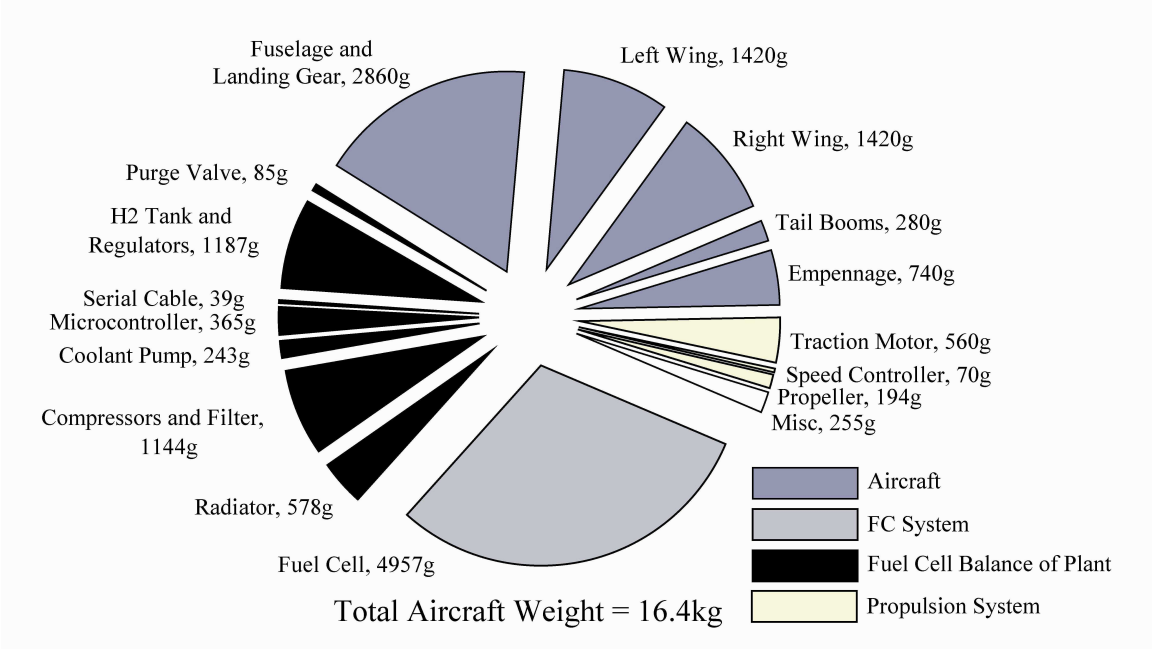

Figure 72. Weight breakdown for the fuel cell demonstrator aircraft

7.4.2. Flight Testing

Flight testing is an integral part of the project because it allows observation of the fuel cell powerplant under real-world operating conditions, it provides a functional test for all of the aircraft systems, and it allows for final validation of the models and assumptions used during design. Figure 73 shows some of the data collected during a short, high-performance circuit flight test. The flight test is divided into taxiing (0-27 sec), climb (27-72 sec), descent (72-110 sec) and landing (110-160 sec) sections. During the beginning of the taxi section, the airspeed and altitude are within measurement error of zero and the fuel cell is at its idling condition. At 10 seconds, the pilot begins to take off and the fuel cell goes to its maximum power condition. The aircraft accelerates and takes off. As the aircraft climbs, the airspeed and altitude increase as the fuel cell powerplant provides peak power. At the time of 88 seconds, the pilot lowers the motor

command and the aircraft begins to descend. At approximately 110 seconds, the aircraft touches down and coasts to a stop.

Figure 74 shows the behavior of the aircraft powerplant during a typical straight-line test flight. This data set is from a short, straight-line flight test of 80 seconds duration and 1200 m distance. The purpose of this test flight was aircraft trim and cruise testing. At the beginning of the flight, the aircraft is stationary on the airfield and the fuel cell is in a low-power idle condition. At a time of 3.7 seconds, the pilot begins to ramp up the current command and the propeller speed increases from the idle condition. The full-power propulsion system current and voltage is reached at 5.2 seconds. The air supply compressors are then controlled to supply their maximum airflow during the takeoff and climb portions of the flight test. At a time of 48 seconds, the aircraft stops its high power climb and begins to cruise. The aircraft cruises for 8-10 seconds and begins to descend and land after the 57 second mark.

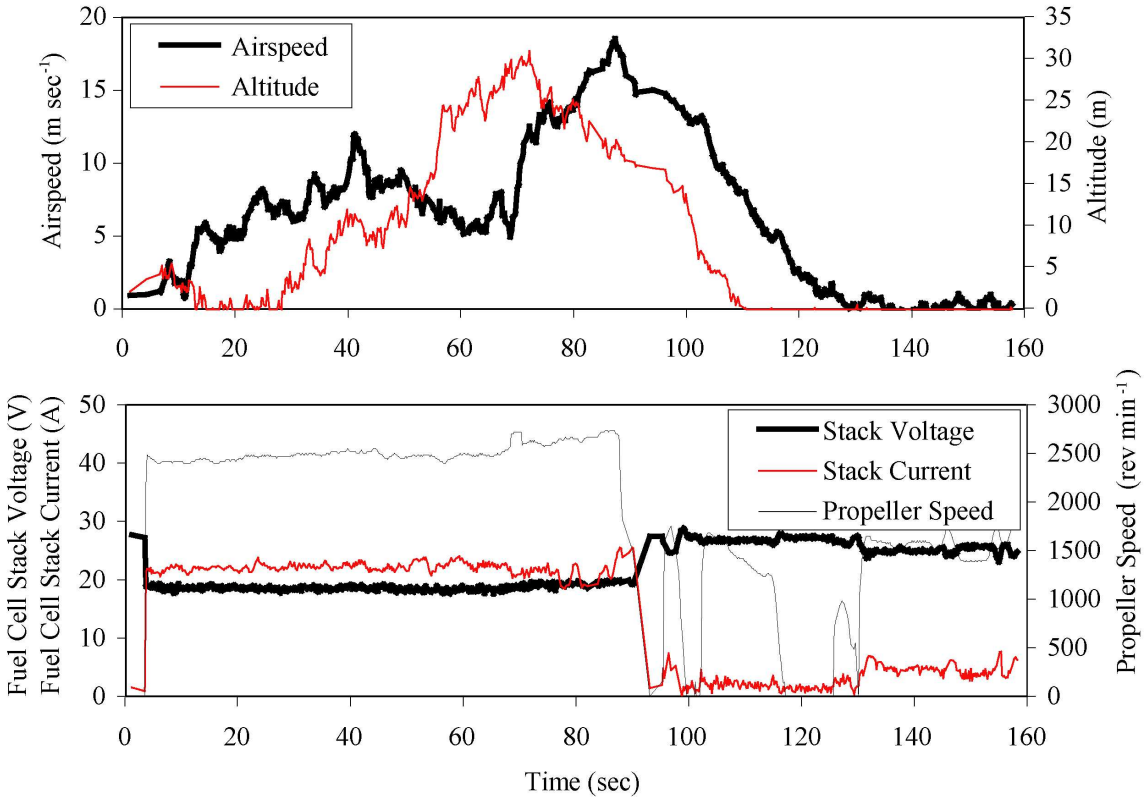

Figure 73. Representative flight test results for fuel cell powered circuit flight

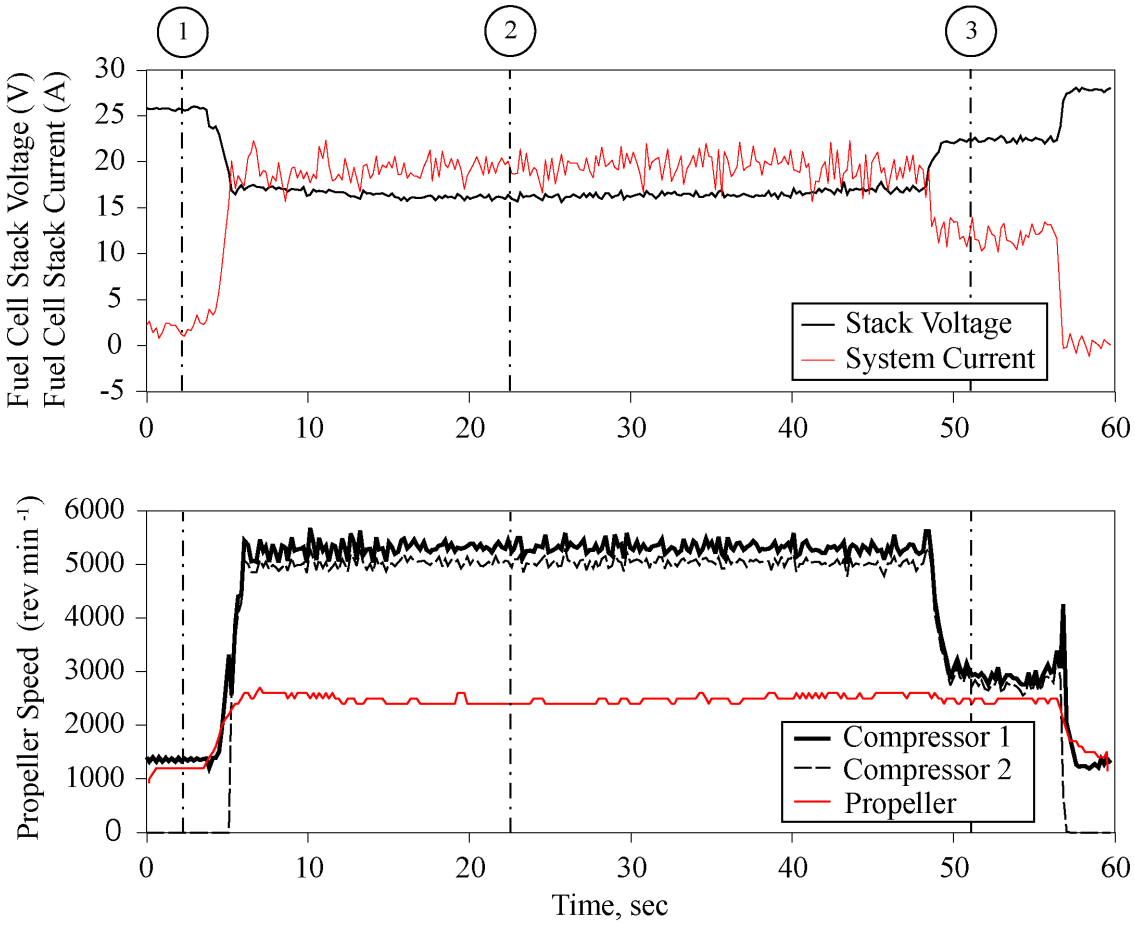

Figure 74. Representative flight test results for fuel cell powered straight-line flight

7.4.3. Component Power Consumptions

A number of points are labeled on Figure 74. These conditions represent the primary modes of use of the fuel cell powerplant in the UAV application. Point 1 corresponds to the idle condition. Point 2 is a high power condition that occurs during climbing and acceleration. Point 3 is the nominal cruise condition. In each case the performance and efficiency of the powerplant subsystems have been measured and analyzed in greater detail using the results of in-flight, bench-top and wind tunnel testing [118]. These results are presented as Sankey diagrams in Figure 75. Uncertainty analysis

is performed using the methods of Kline and McClintock [127] and uncertainties are represented using standard deviations.

At the idle condition the fuel cell is only producing the power required to idle the balance of plant and aircraft controls, as shown in Figure 75. Almost no net electricity is produced by the fuel cell powerplant as the standby power of the propulsion system is less than 1W. The input to the fuel cell powerplant is 1.26 Standard L/min of hydrogen gas. This flow has a lower heating value (LHV) of 227 W. As shown in Figure 75, the primary source of losses for the aircraft at idle is the anode purge. The time averaged LHV of the anode purge flow is 168 W. Very little electrical power is generated by the fuel cell because very little electrical power is required to run the balance of plant at idle. Only Compressor 1 is rotating to provide air to the fuel cell stack. This reduces the amount of power consumed by the fuel cell balance of plant to only 26 W.

During the acceleration and climb phase, Point 2 of Figure 74, the fuel cell powerplant is producing near its maximum power, as shown in Figure 76. The LHV of the input hydrogen flow is 1197 W, and the hydrogen utilization of the fuel cell is >88%. The net output power of the fuel cell powerplant is 323 W out of a maximum fuel cell output power of 465 W. The efficiency of the electric motor and motor controller is 74% and the efficiency of the propeller is 70%. The efficiency of the propeller is relatively low because of the low speed of the aircraft and low advance ratio at this flight condition. This leads to a relatively low propulsion system efficiency of 14%.

Finally, at the cruise condition, the aircraft is holding steady altitude of approximately 10m and a steady airspeed of 13.6 m/s. This cruise condition is faster and at a lower angle of attack than the calculated highest efficiency flight condition, but it is a

condition of steady level flight achieved during flight testing. At this condition, shown in Figure 77, the propulsive power of the aircraft is 84% of the propulsive power at Point 2. At cruise, the electric motor and motor controller is 66% efficient and the propeller is 80% efficient. When compared to the higher power condition, the efficiency of the electric motor is lower because it is functioning at a lower duty cycle, and the propeller efficiency is higher because it is functioning at a higher advance ratio. The total propulsion system efficiency from input hydrogen flow to propulsive power is 18%.

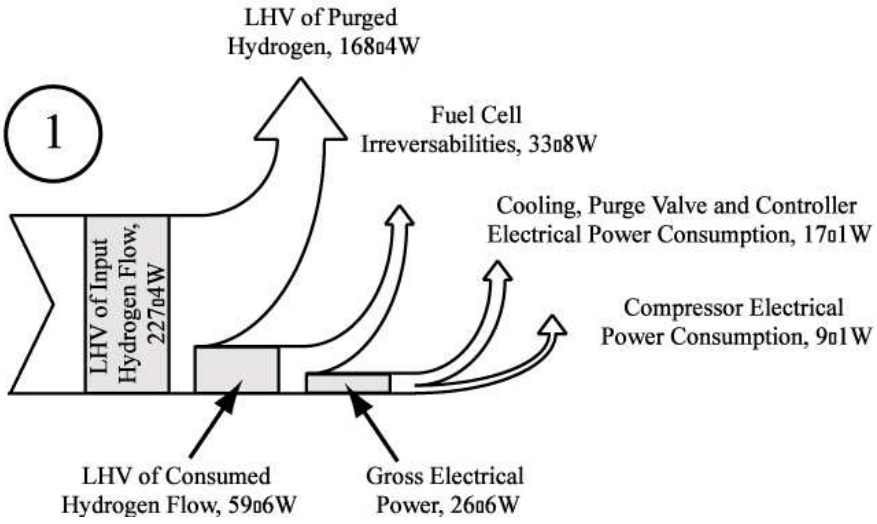

Figure 75. Propulsion system losses at the idle condition

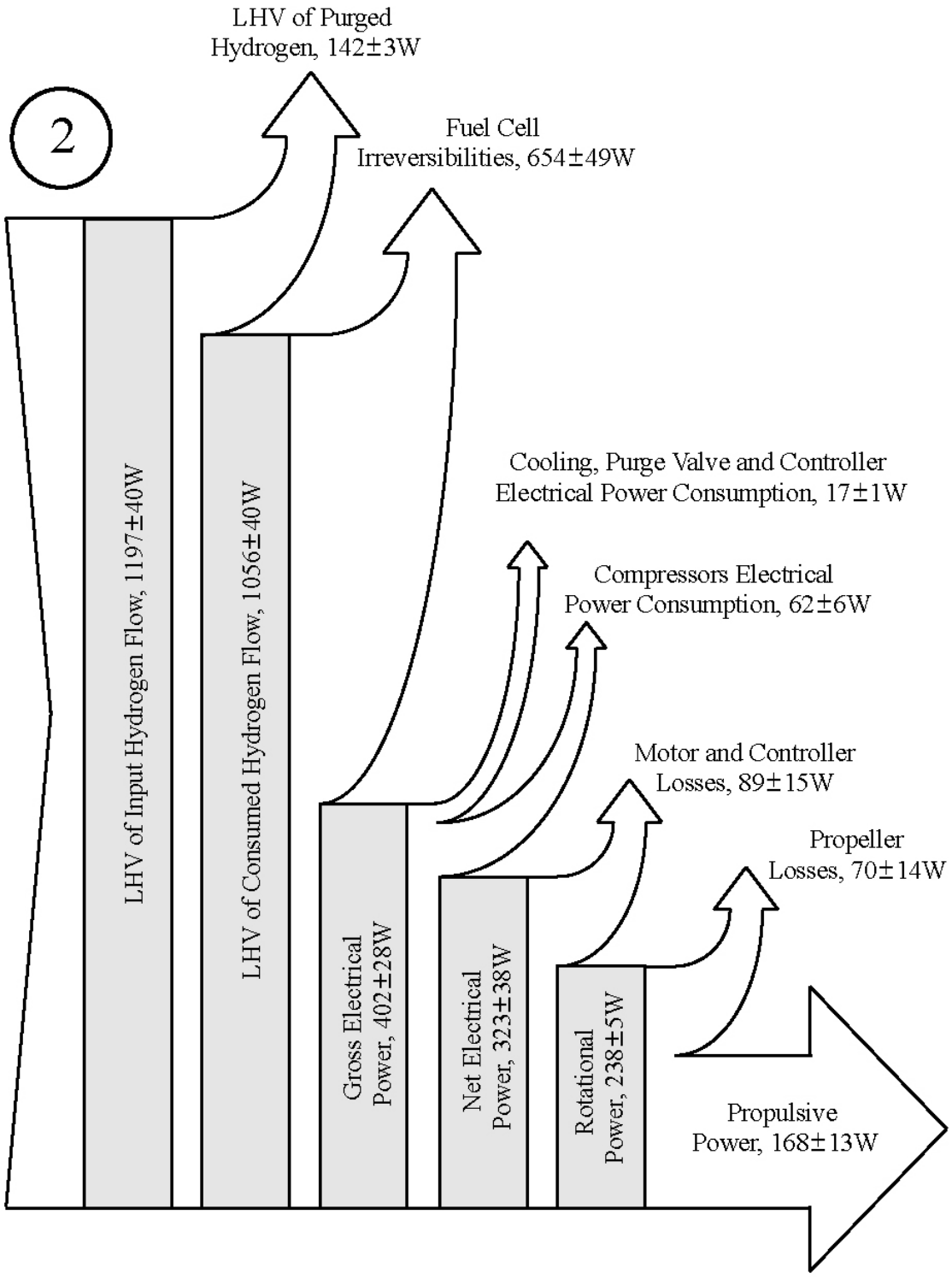

Figure 76. Propulsion system losses at the high power condition

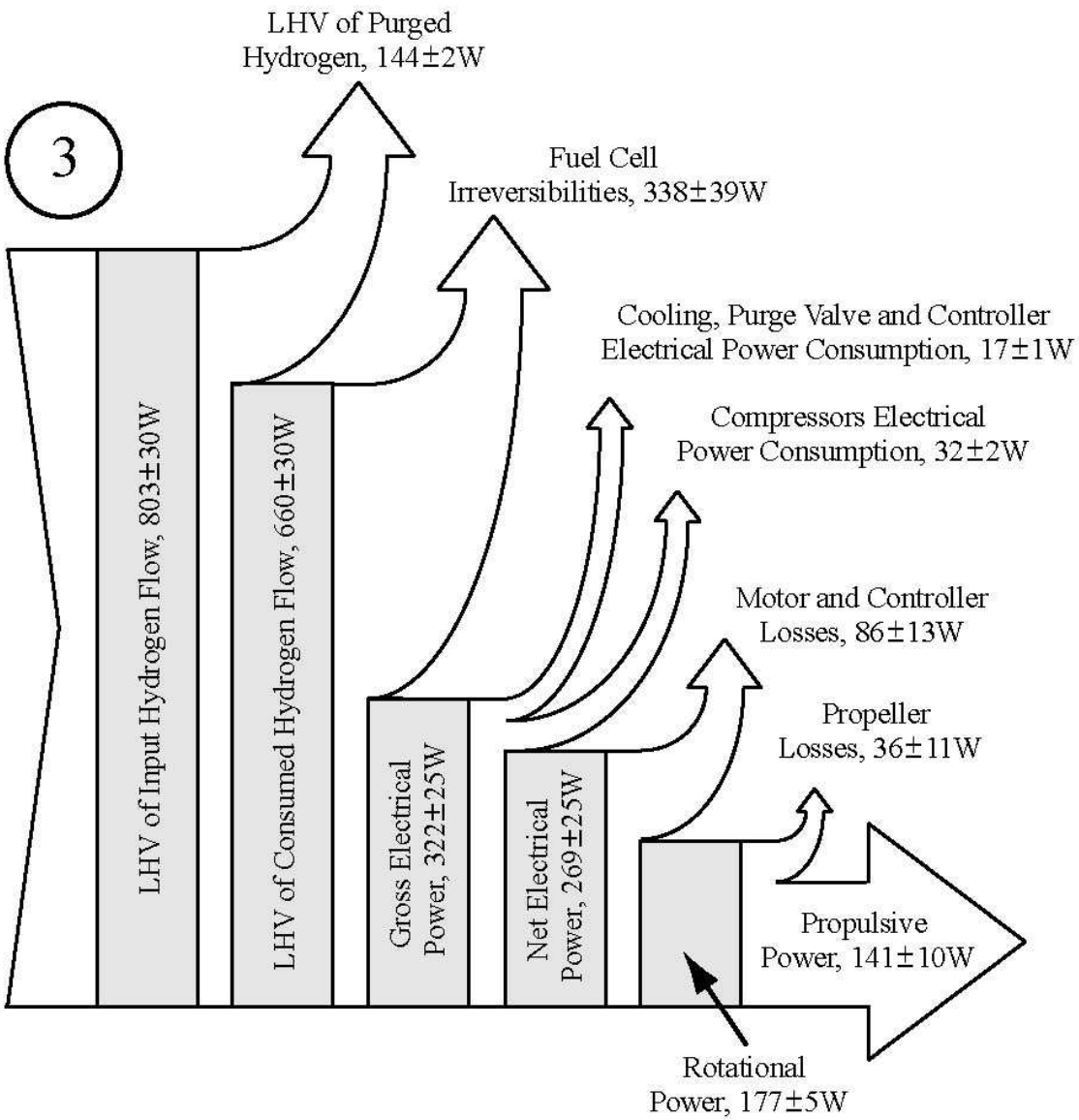

Figure 77. Propulsion system losses at the cruise condition

7.5 Results and Discussion

The results of the flight and laboratory testing show that the fuel cell aircraft has demonstrated the feasibility of fuel cell propulsion of small UAVs. The aircraft is capable of high power acceleration and climb as well as steady cruise flight. Based on the measured capacity of the on-board hydrogen tank (192 Standard L), the aircraft is capable of 43 min of cruising flight. At a constant tank size, the endurance of the aircraft is

limited by the efficiency of the propulsion system. The climb and acceleration rate of the aircraft is limited by the propulsive power output of the propulsion system. By reducing the losses or improving the efficiency of the propulsion system, the performance of the aircraft can be improved for all of these metrics.

In all of the flight conditions analyzed in the previous section, there are consistent sources of large losses. By increasing the hydrogen utilization to 99%, as has been possible in other applications [128], the endurance of the aircraft at cruise can be improved to roughly 52 min. The fuel cell powerplant is another large source of losses. The fuel cell powerplant converts 34% of the total hydrogen LHV to output electrical energy at cruise and 33% at high power. This efficiency is comparable to the 35% to 36% efficiency that has been reported for other small PEM fuel cells [128-130]. The balance of plant power consumption represents 15% of the gross electrical output power of the fuel cell at cruise. This compares favorably to the 20%-35% that has been reported in the literature [129-131]. The efficiency of the electric motor is much lower than was predicted by the models supplied by the motor manufacturer. An improved electric motor with efficiencies closer to 80% at cruise would improve the endurance and climb rate of the aircraft. Still the fuel to rotational energy efficiency of the fuel cell powerplant at cruise is 18% (in terms of hydrogen HHV). Again, this compares favorably to an efficiency of 13% for a 500W, 2-stroke combustion engine (in terms of the HHV of octane) [22,43]. The fixed pitch propeller requires a compromise between the propeller efficiency during low speed climb and during cruise. For this aircraft the propeller was chosen to maximize efficiency at cruise. A variable pitch propeller would allow for higher efficiency at both the cruise and high power flight conditions.

7.6 Conclusions

Fuel cell aircraft are an important application for fuel cells because fuel cells are an enabling technology for very long-endurance aircraft. To date, nearly all of the investigations into the design, construction, and performance of fuel cell aircraft have been primarily high-level and conceptual. The construction and experimental evaluation of a fuel cell aircraft has enabled the validation of design models using real-world performance data in addition to the evaluation and the demonstration of a new class of fuel cell vehicle. The results of this study have already been extended to studies of larger, more utilitarian, and much longer endurance aircraft.

The fuel cell demonstrator aircraft incorporates a 500 W PEM fuel cell powerplant with an advanced balance of plant including variable cathode flow rate control, liquid cooling, self-humidification and variable period anode purging. The aircraft structure and aerodynamics have been designed incorporating the opportunities and constraints of the fuel cell powerplant. Optimization of the aircraft and propulsion system has produced a stable and efficient experimental platform for evaluation of the fuel cell aircraft concept.

Low level analysis of the performance and efficiencies of the powerplant and propulsion components have allowed for identification of the sources of losses within the aircraft systems. A comparison of the propulsion system performance to the state of the art highlights mechanisms for improving the aircraft performance by improving subsystem performance.

The results of this study are very promising as a proof of the fuel cell aircraft concept. The fuel cell demonstrator aircraft has performed well in test flights and shows

the promise of fuel cell aircraft to accomplish new missions with improved effectiveness and environmental performance.

CHAPTER 8

HARDWARE IN THE LOOP SIMULATION OF A LONG ENDURANCE FUEL CELL UAV

8.1 Introduction

This chapter presents the design, development and test results for a hardware in the loop simulator. The hardware in the loop simulation results provide validation data to the validation tasks associated with Research Question 1 and Hypothesis 1.

To date, design validation and performance testing of UAV powertrains has been primarily performed through flight testing. For example, Kosmatka et al. [132], Tigner et al. [133], Bateman et al. [134], and the present authors [11] have used test flights to validate the powerplant and airframe design of prototype UAVs. Howard et al. performed powerplant testing using a half-scale model [135]. Compared to the flight testing methods described in the UAV literature, hardware in the loop (HiL) simulation can be a more effective tool for powertrain development and model validation. Rather than testing the components of an aircraft as a fully assembled aircraft system, HiL replaces portions of the aircraft hardware with software that can emulate the communication, kinetics and kinematics of the replaced systems. HiL testing is already extensively used for aviation and automotive controls software development [136,137].

HiL can provide significant benefits to the design, calibration, refinement and evaluation tasks of advanced UAV powerplant development. First, the components of the aircraft system that are modeled in software can be inexpensively and repeatedly

modified. If the propeller performance is modeled in software, analysis of the effects of propeller sizing can be done without repeatedly implementing and testing physical propeller hardware. Second, the components of the aircraft system that exist in hardware can be measured and controlled in great detail. Data acquisition systems that are not flight-worthy because of weight or size can be used for calibration and validation of system performance. Third, HiL allows the aircraft system to experience many of the dynamic operating conditions of flight without endangering costly hardware. Fusible links, translational hard stops or fail-safes can restrict the state of the HiL hardware to avoid catastrophic failure during system tuning. Finally, the testing conditions of HiL simulations can be tightly controlled to allow for repeatable performance benchmarking and system evaluation. For instance, laboratory control of ambient and simulated environmental conditions can enable the standard atmosphere still-air-range of the aircraft to be evaluated without performing actual flight tests.

This article presents a study of the performance of a fuel cell powered UAV using a HiL system. A proposed architecture for HiL simulation of UAVs is presented. The hardware, software and interface components of the HiL simulator are described. Sample experimental results from the HiL testing of the powertrain of a fuel cell powered UAV completing a long endurance mission are presented with uncertainty analysis. Discussion of the test results focuses on a comparison of the HiL results to static models and a performance comparison of various electrochemical and internal combustion powerplants. This study is novel in that it presents the experimental performance of long-endurance fuel cell powered aircraft.

8.2 Hardware in the Loop Simulation Architecture for UAV Powerplants

The design of HiL simulation architecture requires a tradeoff between the components of the HiL simulation that exist in hardware and the components that exist in software. Components for which accurate or scalable models exist can be modeled in software. Components whose performance we would like to analyze in detail can be modeled in hardware. By combining these attributes, HiL allows for the efficient, cost effective and flexible simulation of complex systems.

In this study, HiL simulation is used to evaluate the performance of a fuel cell powered UAV as it completes a specific mission. For a fuel cell UAV, the integrated powerplant and powertrain have been shown to be the primary source of aircraft performance uncertainty during design and development [16]. By using the actual powerplant and powertrain hardware during testing, the uncertainty associated with the performance simulation can be reduced. Conversely, the static performance of UAV airframes is well understood and can be accurately modeled by computer simulations [109]. Depending on the scalability and accuracy required of the computer simulation, the inputs to the software simulation can come from conceptual design algorithms, computational flow simulations or airframe flight tests.

For this study, the proposed HiL simulation architecture is shown in Figure 78. The simulation is composed of three parts: software simulation, hardware simulation and interface. The software simulation contains the aircraft flight path, as well as the models of the autopilot, aircraft and propeller. The hardware simulation contains all components of the energy storage system, powerplant, powertrain and control system, excluding the

propeller. The interface components actuate the hardware components and collect the inputs to the software simulation.

The arrows shown in Figure 78 show the direction of the signal and energy flows between the components of the HiL simulation. The input to the HiL simulation is the desired aircraft flight path in the form of an airspeed and altitude as a function of time. The error between the desired and actual flight path is input to the software autopilot simulation. The output of the autopilot simulation is a “throttle” command to the electric motor. The signal generator interface translates the command from the software simulation to a TTL PWM command sent to the electric motor hardware. The electric motor is physically coupled to both the fuel cell stack via a DC electrical bus, and to the dynamometer via a shaft coupling. The dynamometer provides the physical interface between the simulation hardware and software. The dynamometer applies a PI regulated torque to the electric motor based on the torque signal it acquires from the propeller simulation software. The inputs to the propeller simulation are the measured electric motor rotational speed and the simulated aircraft airspeed. Based on these inputs, the propeller simulation calculates the propeller torque and thrust. Propeller thrust is passed to the aircraft simulation, which calculates the dynamic states of the aircraft. At the top of the diagram, the fuel cell hardware is outside of the aircraft dynamics loop. The fuel cell controller regulates the temperature of the fuel cell stack by varying the fuel cell stack cooling fan speed. The hydrogen tank regulators regulate the hydrogen pressure delivered to the fuel cell stack.

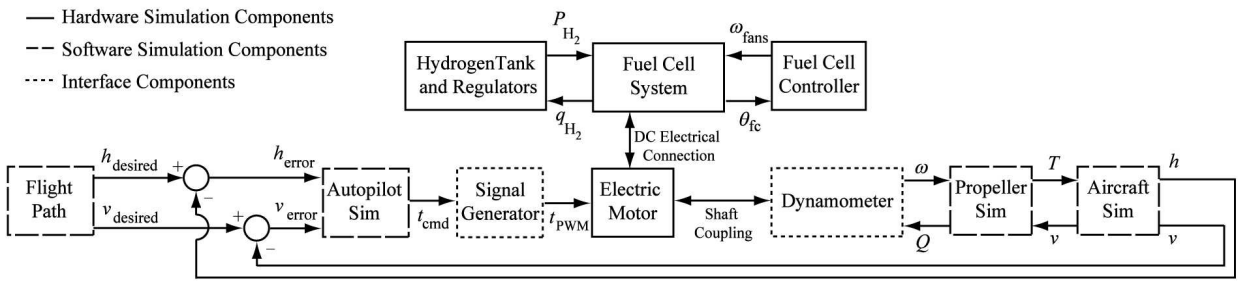

Figure 78. Schematic and control system causality flow chart for hardware in the loop simulation

8.3 Simulation Components

8.3.1. Simulation Hardware

The simulation hardware consists of the aircraft components that are under experimental evaluation. For this study this includes the hydrogen tank, regulators, fuel cell stack, fuel cell control system, and electric motor as shown in Figure 1. During the HiL tests, the fueling system and fuel cell powerplant are mounted to the laboratory bench top and are electrically connected to the other hardware.

The 300W fuel cell stack (Horizon Fuel Cells H300, Singapore) is the only source of electrical power for the aircraft components during testing. The stack is self-humidified, air cooled and requires only ambient cathode pressure. The stack is made up of 62 cells with 20cm^2 of active area per cell. As shown in Figure 1, the fuel cell control system controls the temperature of the stack (θ_{fc}) by dictating the speed of the cathode supply fans (ω_{fans}). This leads to a nonlinear and coupled relationship between cathode stoichiometry, membrane humidification and stack temperature. To statically quantify the performance of the fuel cell stack before HiL testing, the stack current was measured at constant voltage for 400 samples at a sampling frequency of 4Hz. Voltage steps were

taken every 100 seconds with the fuel cell stack under its normal thermal and stoichiometric control. The resulting polarization curve for the fuel cell system is shown in Figure 79 with a stack voltage model derived to fit the experimental data using the methods of Kulikovsky [68]. The fuel cell stack temperature is controlled by the fuel cell control system as a function of stack current. The resulting stack temperature varies between 32°C at low current to 52°C at high current.

For HiL testing, ultra-high purity hydrogen is supplied to the fuel cell using a laboratory hydrogen source. The hydrogen is delivered to the fuel cell anode at 34 kPa of gage pressure. A periodic anode purge is controlled to maintain a hydrogen utilization of >90%. The electrical power from the fuel cell powers the fuel cell control system, the aircraft flight controls (as simulated by a 12V 200mA load), payload (as simulated by a 12V 120mA load), and the propulsion electric motor (Neutronics 19102Y, San Diego, CA).

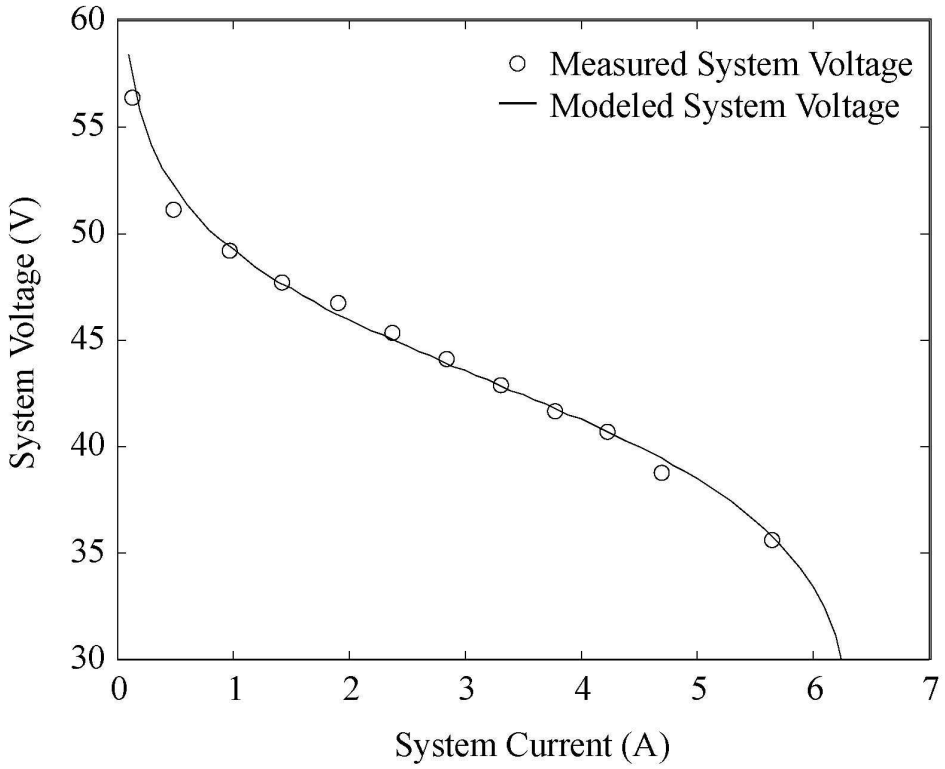

Figure 79. Measured and modeled Horizon H300 fuel cell system polarization curve

8.3.2. Interface Components

The interface components provide the physical and communication connections between the simulation software and the simulation hardware components.

A custom signal generator is the communication connection between the autopilot simulation and the hardware of the fuel cell powertrain. The signal generator consists of a PIC microcontroller that reads RS232 serial data from the autopilot simulation and outputs a pulse-width modulated signal to drive the inputs of the electric motor controller. The commands to the signal generator are updated at 4Hz.

The mechanical connection between the electric motor hardware and the propeller simulation software is made using a dynamometer developed for this application. A picture of the dynamometer is shown in Figure 80. The electric motor is held in a

bearing-suspended mount concentric to the motor rotational axis. During HiL testing, rotation of the motor mount is prevented by a strain gauged beam load cell which measures the torque output of the electric motor. The electric motor output shaft is coupled to the absorber and a tachometer via a flexible coupling. The absorber is a DC electrical generator whose output is current controlled by an electronic DC load (Hewlett-Packard 6050A, Palo Alto, CA). An analog tachometer measures the rotational speed of the electric motor shaft.

The bandwidth of the DC load is >1 kHz, potentially allowing dynamic simulation of the aircraft at very high bandwidth. For this investigation the dynamometer is controlled at a frequency of 4Hz, appropriate for modeling the aircraft flight dynamics and fuel consumption.

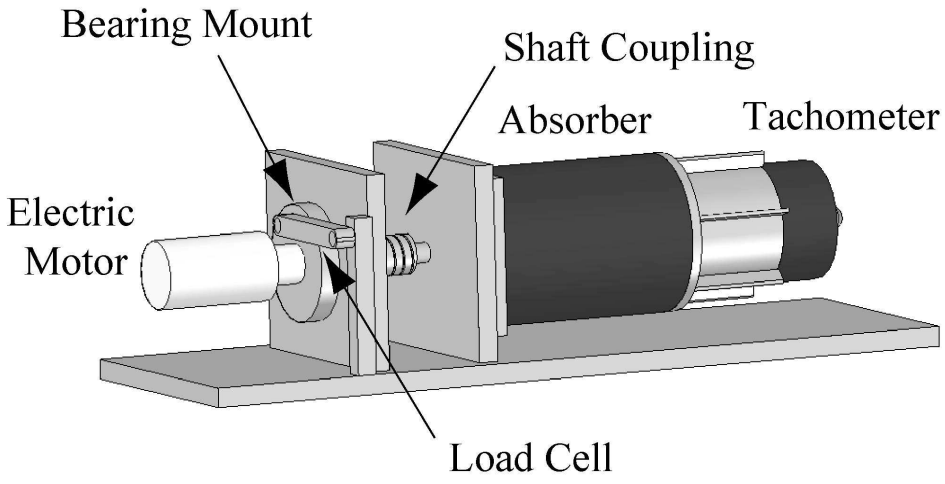

Figure 80. Diagram showing the dynamometer configuration and components

8.3.3. Simulation Software

The simulator software simulates the effects of the propeller, airframe and flight controller on the powertrain hardware.

The inputs to the propeller model are the airspeed of the aircraft and the rotation speed of the electric motor shaft. The outputs of the propeller model are the thrust produced by the propeller and the torque applied to the electric motor [1]. The thrust, *T*, applied to the aircraft is defined by,

$$T = \rho\left(\frac{\omega}{2\pi}\right)^2 d^4 C_T \tag{60}$$

The propeller torque, *Q*, to be applied to the electric motor is determined from the software propeller model using the relations:

$$Q = \rho\left(\frac{\omega}{2\pi}\right)^2 d^5 C_q \tag{61}$$

Both the thrust and torque coefficients, C_q and C_T, are a function of the propeller advance ratio,

$$J = \frac{v}{\left(\frac{\omega}{2\pi}\right)d} \tag{62}$$

Airspeed (v) is calculated from the dynamic model of the aircraft.

The input to the aircraft dynamic model is the thrust from the propeller. The outputs are aircraft airspeed and altitude. The aircraft model assumes a flat-earth coordinate system and coordinated turns. The equations of motion of the aircraft are [1]:

$$\dot{h} = v\sin\gamma \tag{63}$$

$$\dot{v} = \frac{T\cos\alpha - D}{m} - g\sin\gamma \tag{64}$$

$$\dot{\gamma} = \frac{T\sin\alpha + L}{mv}\cos\phi - \frac{g}{v}\cos\gamma \tag{65}$$

Aircraft lift and drag are defined as:

$$L = \frac{1}{2}\rho v^2 S_w C_L \tag{66}$$

$$D = \frac{1}{2}\rho v^2 S_w C_D \tag{67}$$

The coefficients of lift and drag vary as a function of angle of attack.

The states of the model are the propeller speed, ω, aircraft altitude, h, airspeed, v, and climb path angle, γ. The angle of attack, α, and bank angle, ϕ, are static control parameters that are determined by the aircraft flight controller. The propeller and aircraft simulation are run on the control computer and the thrust and velocity of the aircraft are updated at 4Hz.

8.3.4. Simulated Flight Path Definition

The aircraft is programmed to fly a virtual mission that consists of four segments: takeoff, climb, a long-endurance orbit and landing. The simulated flight path emulates the path of a generic long-endurance remote sensing mission. The flight path is shown in Figure 81.

The takeoff segment begins with the states of the aircraft, $h = v = \gamma = \omega = 0$. The aircraft attitude is fixed so that $\alpha = \phi = 0$. As the flight simulation begins, the electric motor accelerates providing thrust to the simulated aircraft. An additional drag term due

to rolling friction $D_{rr} = mgC_{rr}$ is added to (8) while the aircraft is contact with the ground. When the aircraft reaches the cruise velocity of the aircraft in flight, the autopilot controller rotates the aircraft to $\alpha > 0$ and the aircraft simulation takes flight.

During the climb segment the aircraft attitude is fixed so that $\phi = 0$ and $\alpha = 6$ deg. The aircraft controller holds the aircraft velocity constant through elevator deflection, leading to a dynamic $\dot{h}$ of between 30 and 40 m/min. The aircraft climbs to an altitude of 100 m before transitioning to cruising flight. The long endurance segment consists of a cruising flight path which circles slowly over a target. The aircraft executes a coordinated turn of radius 1000 m at constant $\alpha = 7.4$ deg. The airspeed is controlled to be constant and the motor throttle regulates altitude. The aircraft orbits over its target until the hydrogen tank is nearly empty and then begins the landing segment.

The landing segment is modeled as a spiral gliding descent from the cruise altitude. The aircraft reaches the ground $h = 0$ at approximately the same location where the takeoff began.

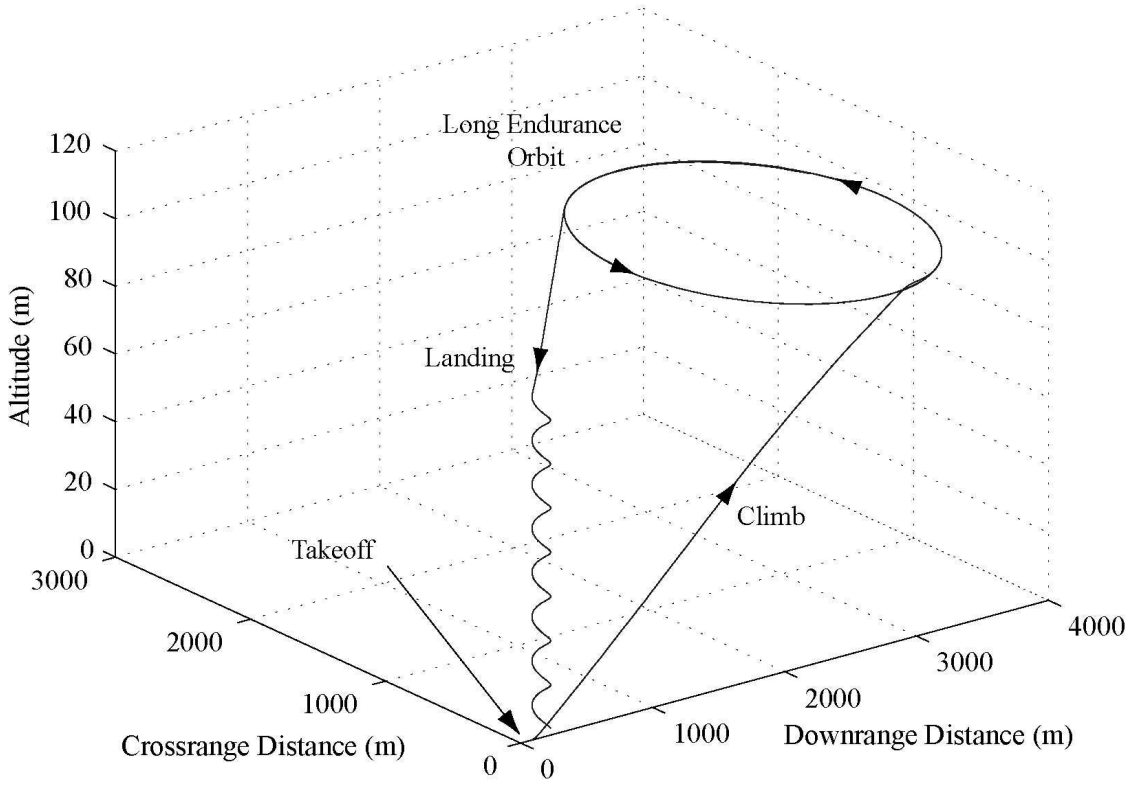

Figure 81. Long endurance flight path

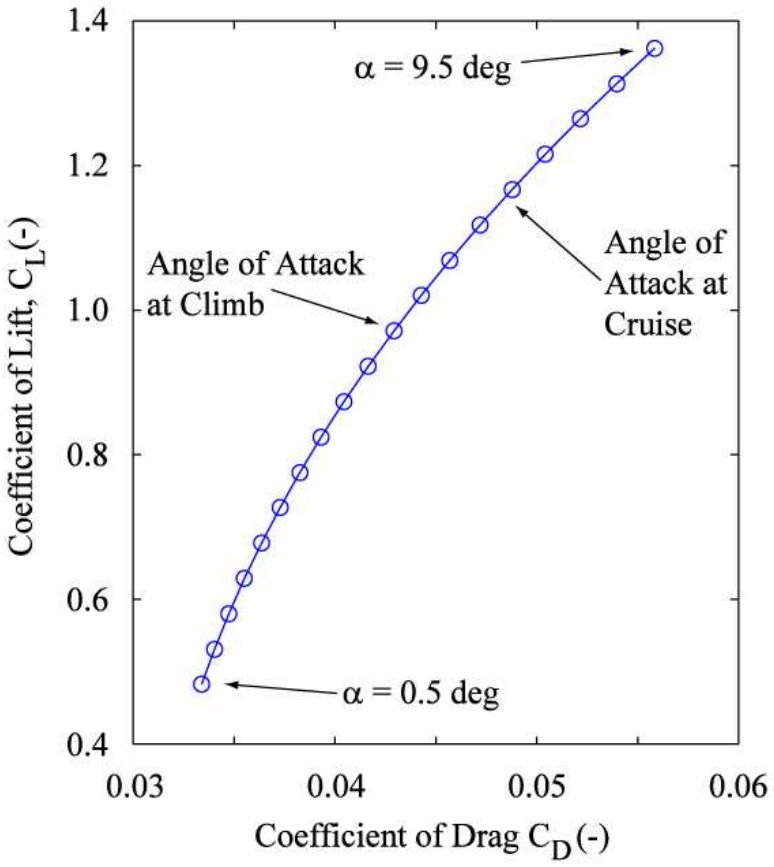

Figure 82. Aerodynamic characteristics of the airframe under HiL test

8.3.5. Aircraft Description

The aircraft considered in this study is a fuel cell powered, propeller driven, UAV. The airframe consists of a low straight wing monoplane with an aerodynamic design based on a fuel cell demonstrator aircraft which was successfully flown in 2006 [11]. The aerodynamic characteristics of the aircraft are modeled using a potential flow analysis [109] with experimental corrections and are presented in Figure 82. The cruise and climb angles of attack are chosen as a compromise between higher airframe

efficiency at higher angles of attack and proximity to the estimated stall point at a fuselage angle of attack of $\alpha = 9.5$ deg.

A summary of the aircraft characteristics is presented in Table 1. Compressed hydrogen is stored on-board the aircraft in a composite overwrapped pressure vessel (Carleton Technologies PN6109, Orchard Park, NY) at a maximum pressure of 31 MPa. The propeller (Landing Products 20.5x14.5, Woodland, CA) has a diameter of 52.1 cm and a nominal pitch of 35.6 cm. The aerodynamic performance of the propeller is modeled using Goldstein's vortex theory of propellers [16]. The inputs to the propeller software model are shown as a function of advance ratio in Figure 83.

A data acquisition system monitors and records the conditions of operation of the test equipment, hardware and software. The principal measured signals with their associated closed-loop uncertainty at cruise are presented in Table 2. All uncertainties are presented as standard deviations, and are propagated using the methods of [127]. For the purposes of this study, the aircraft and propeller models are treated as deterministic and accurate.

Table 17. Characteristics of the simulated aircraft

Aircraft Characteristic	Value
Gross Takeoff Mass	12.51 kg
Hydrogen Fuel Mass	205.8 g
Powerplant and Tank Mass	7.40 kg
Cruise Lift to Drag Ratio	24
Wing Area	1.078 m^2

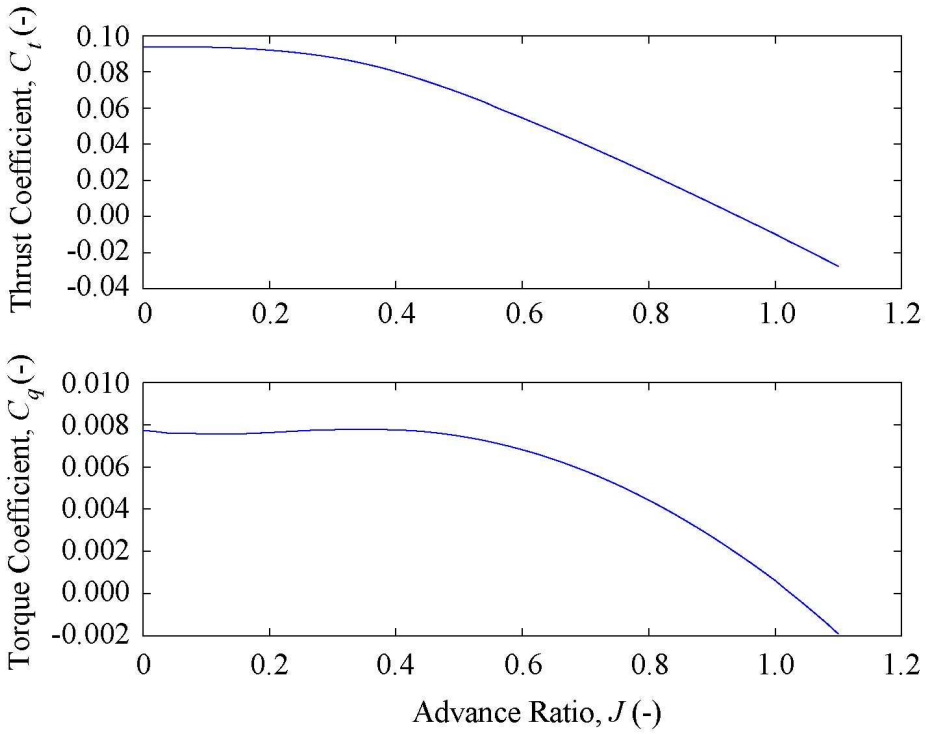

Figure 83. Propeller performance specifications

8.4 Experimental Results

8.4.1. Flight Simulation Results

HiL testing was performed in controlled laboratory environment at a constant 23°C and 37% relative humidity. Cathode flow rate is a constant 200 L/min for the duration of the HiL test.

Figure 84 shows the performance of the aircraft hardware simulation as it completes a subset of the simulated flight. At a time of 0.002 hrs, the fuel cell current increases and the fuel cell voltage decreases as the aircraft begins the takeoff segment of the flight test. The simulated aircraft begins to climb after it reaches takeoff speed. The hydrogen consumption of the powerplant increases with increasing fuel cell stack current. The periodic purges of the fuel cell anode are visible as spikes in the hydrogen flow rate.

At a time of 0.065 hrs, the simulated aircraft has reached its cruising altitude of 100 m, and the aircraft enters the cruise segment of the flight test. The fuel cell voltage increases and the current decreases as the power output of the powerplant decreases to match the cruise power of the aircraft. After the climbing flight segment, the aircraft cruises at steady level flight conditions.

Figure 85 shows the behavior of the aircraft powerplant for the entirety of the long endurance flight. During the long endurance cruise, the aircraft flies at steady speed and altitude. After the early voltage excursions associated with the takeoff and climbing flight segments, there is a slight decrease in the measured output voltage of the fuel cell stack over the remainder of the test. The fuel cell voltage decreases from the short period value of 46 V, to a steady state average of 39.6 V. This result is analyzed more completely in the Discussion section.

The actual duration of the HiL flight simulation is 22.75 hours. After this period, the aircraft has consumed all of hydrogen carried on board. The experimental endurance of the aircraft for this HiL experiment is 22.75 ± 0.64 hours, which includes experimental uncertainty.

Table 18. Values and uncertainty for the primary data acquired during testing

Measured Signal	Nominal Value at Cruise	Total Uncertainty	Percentage Uncertainty	Sampling Period
Fuel Cell System Current	3.56 A	0.207 A	5.82%	0.25 sec
Fuel Cell System Voltage	40.04 V	0.454 V	1.13%	0.25 sec
Motor Output Torque	0.43 N m	0.005 N m	1.27%	0.25 sec
Motor Rotational Speed	235.3 rad sec^{-1}	6.32 rad sec^{-1}	2.68%	0.25 sec
Hydrogen Flow Rate	1.54 L min^{-1}	0.042 L min^{-1}	2.75%	0.05 sec

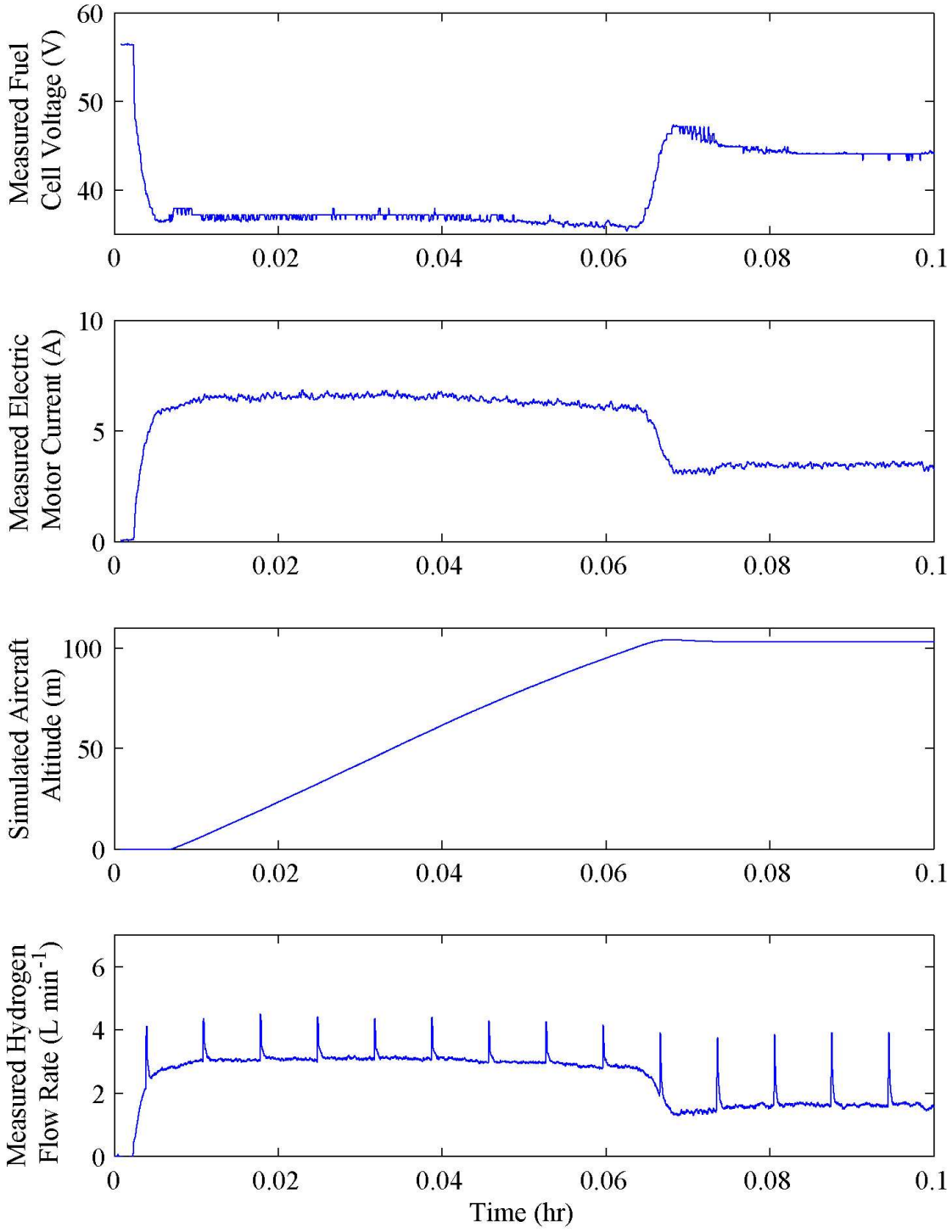

Figure 84. Hardware simulation performance during takeoff and climb flight segments

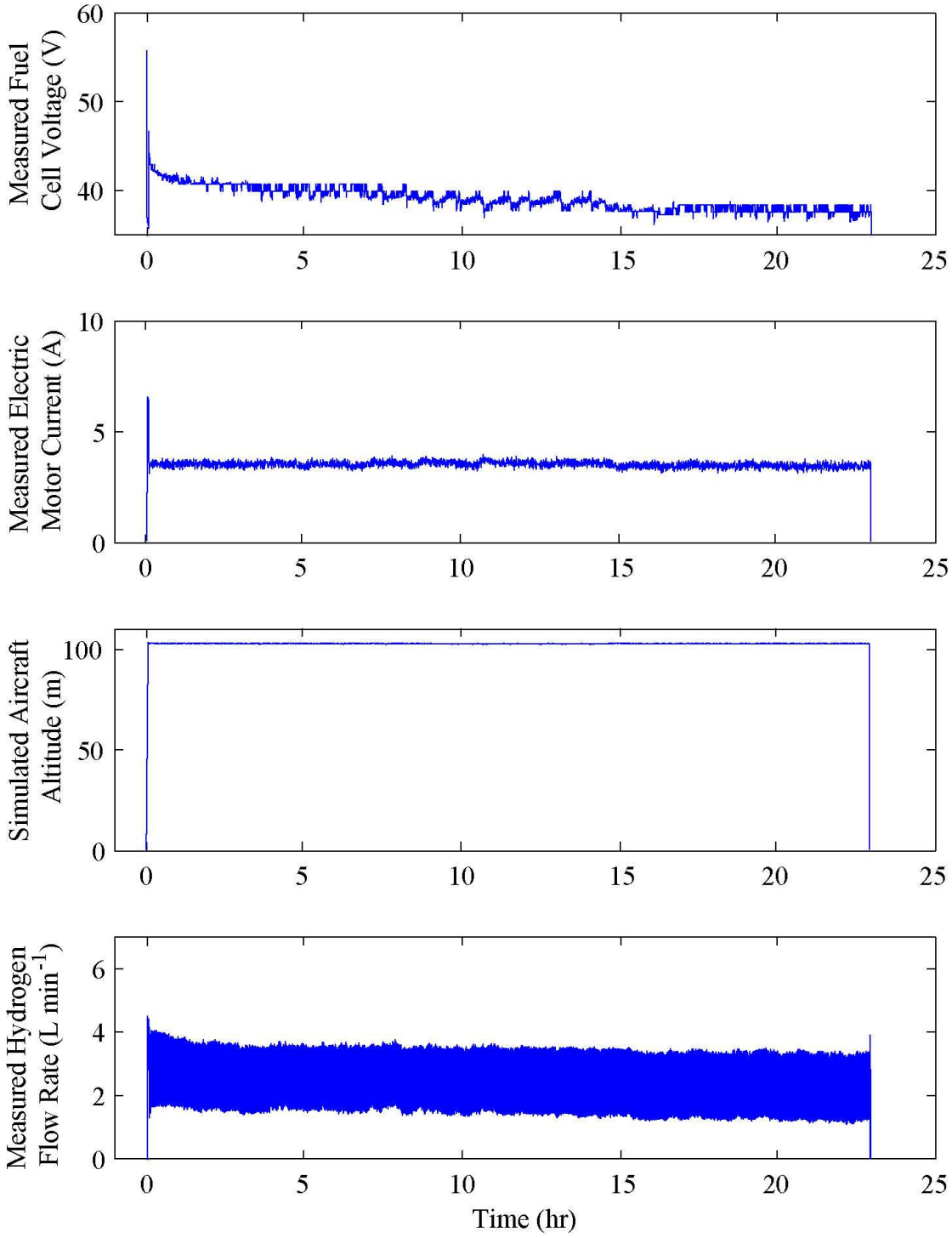

Figure 85. Hardware simulation performance during the entire long endurance flight

8.4.2. Powertrain Performance at Cruise

During cruise, the efficiencies of the powerplant and powertrain have a large influence on the performance and endurance of the aircraft. One of the primary advantages of HiL testing is that detailed control system tuning and data acquisition can be performed under flight conditions. Figure 86 shows a detailed breakdown of the power consumption and output of each major powerplant and powertrain component. Each power flow is labeled with its measured or simulated uncertainty over 10000 samples of the cruise flight segment. This is the same conditions of flight as shown in Table 2.

The power input to the fuel cell stack is a flow of hydrogen gas. This flow has a lower heating value of 120.1 MJ/kg, equivalent to an average power of 307 ± 8W. Approximately 10% of the flow of hydrogen is released unreacted to the environment from the periodic purging of the anode manifold. The electrical output power of the fuel cell is split between the payload and balance of plant and the electric motor. The conversion efficiency of the fuel cell system from hydrogen flow to DC electrical power is 52% ± 8%. The electric motor converts electrical power to rotational power at 71% ± 4%. The propeller simulation finds that the propeller is 69% ± 3% efficient at cruise, producing 70 ± 3W of propulsive power.

HiL simulation allows for the detailed measurement and tuning of the powerplant performance in ways that are not possible during flight testing.

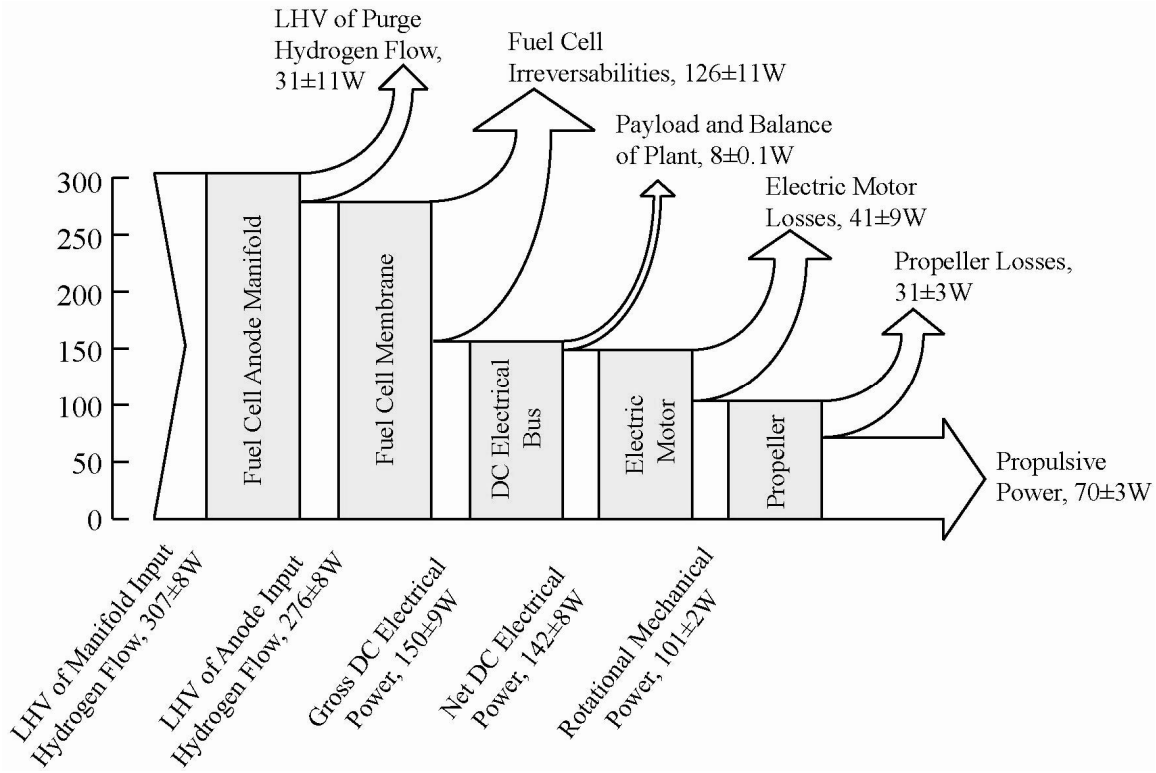

Figure 86. Propulsion system losses at the cruise condition

8.5 Discussion

8.5.1. Dynamic Powerplant Performance

Advanced UAV powerplant systems often exhibit unmodeled dynamics, performance uncertainty, or tunable control systems. In these cases, HiL testing allows for the evaluation of system performance in earlier stages of aircraft development. This section of the discussion will discuss the unmodeled dynamics of the fuel cell powerplant during HiL simulation.

Many of the fuel cell powerplant system design studies performed to date rely on a static fuel cell polarization curve to represent the performance of the fuel cell stack. A static polarization curve, such as is shown in Figure 2, contains intrinsic assumptions regarding stoichiometry, membrane water content, ambient conditions and stack

temperature. The dynamic behavior of fuel cell stacks is often different than their static behavior in ways that can affect the effectiveness of a fuel cell system design.

Figure 87 shows the voltage and current of the fuel cell system during the long endurance fuel cell HiL test. At idle, the fuel cell stack operates at low current and 56 V at point 1. As the aircraft accelerates and takes off, the fuel-cell performance tracks the polarization curve to the high current, low voltage condition at point 2. Near point 2, the aircraft is climbing and the fuel cell stack is operating at approximately 6.7A and 38V. At this condition, the current and voltage of the fuel cell system are higher during the HiL test than under the static experimental test. This suggests that the conditions of use of the fuel cell during the HiL test are causing the fuel cell system to momentarily outperform its steady state performance. It is hypothesized that the low stack temperature (relative to the static tests of Figure 2) reduces the evaporation rate at the cathode allowing more liquid water to remain in the stack, reducing the stack overpotential.

After the climb segment, the power required by the aircraft decreases as it enters the cruise segment. The fuel cell system moves to a current of 3.2 A and a voltage of 47 V at point 3. For a short period after the high current operation, the voltage is higher than the modeled steady-state operating voltage of the fuel cell stack. This reduction in overpotential occurs because the fuel cell stack is at a higher measured operating temperature (see Figure 11) and higher water content than steady state. Over the course of the next hours, the system settles along a line of constant power into an operating point at lower voltage and higher current at point 4. This increase in overpotential could be due to changes in membrane water content [138], catalyst oxidation [139], high frequency current requirements from the electric motor controller, or other uncontrolled

effects. The voltage dynamics of the fuel cell system under HiL testing are consistent and repeatable, as shown in Figure 89.

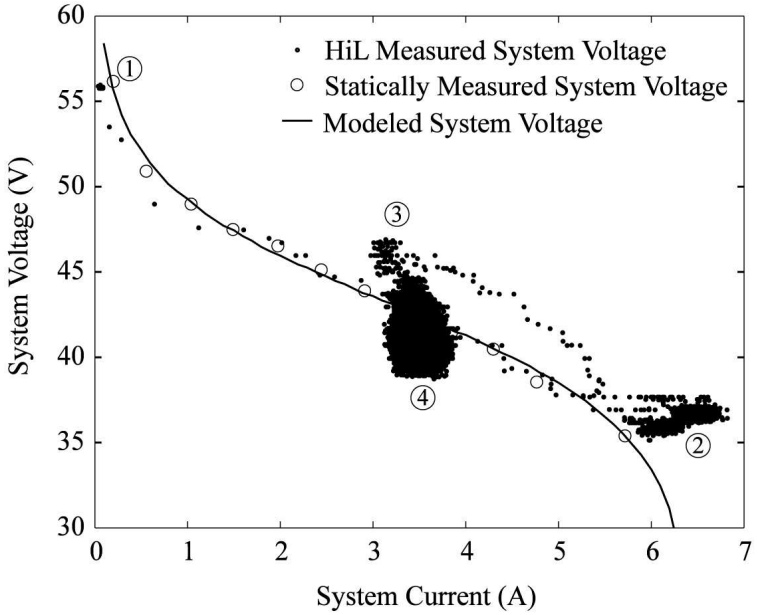

Figure 87. Measured and modeled Horizon H300 fuel cell system polarization curve for a long endurance HiL test

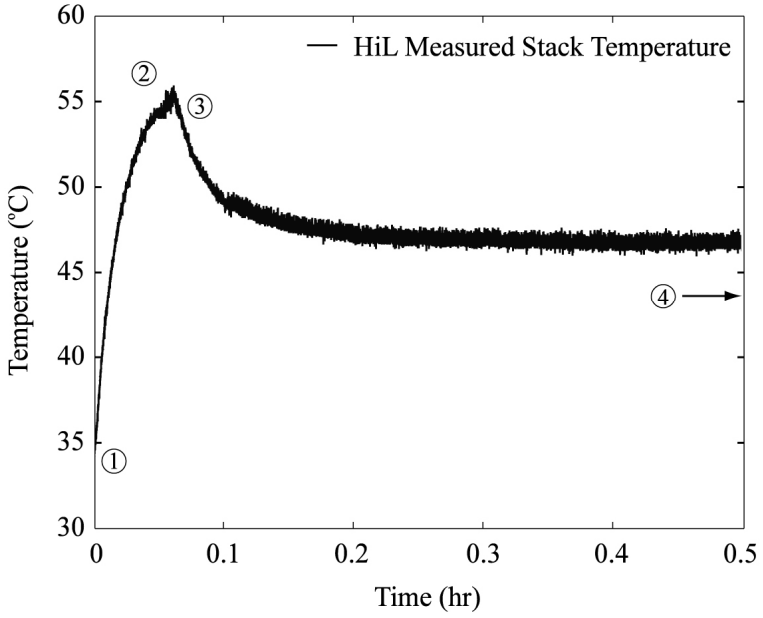

Figure 88. Measured fuel cell stack temperature for first portion of long endurance HiL test. Labels correspond to labels from Figure 10.

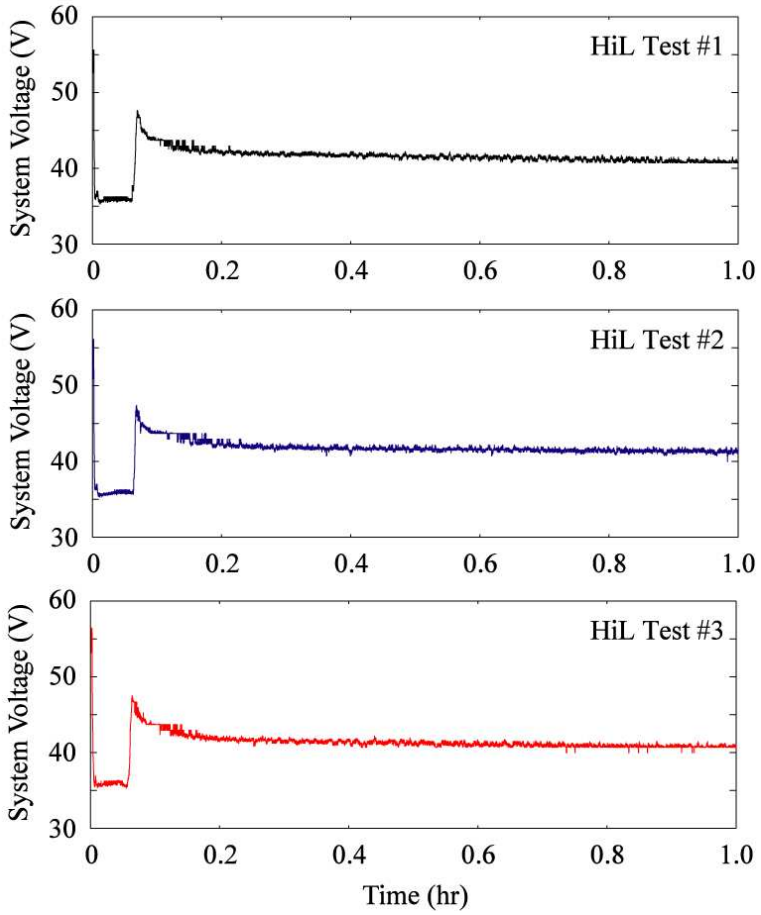

Figure 89. Comparison of fuel cell stack dynamics among subsequent long endurance HiL tests showing excellent repeatability

These unmodeled dynamics have a considerable effect on the performance of the aircraft. For instance, the lower than predicted stack voltage during cruise reduces the efficiency of the fuel cell powerplant and reduces the endurance of the aircraft system. As shown in Figure 85, the stack performs components of the long endurance test at a voltage as low as 39.0 V instead of its predicted voltage of 42.3 V. In the hydrogen/air fuel cell system, the efficiency of the fuel cell stack is defined as,

$$\eta_{stack} = \frac{V}{n_{\text{cells}} E^{\circ}} \tag{68}$$

Using (9) the efficiency of the fuel cell stack as predicted from the static polarization curve is 54%. Under HiL testing, the efficiency of the stack is as low as 51%, reducing the performance and endurance of the aircraft system.

By quantifying the unmodeled performance of the fuel cell stack, HiL simulation allows the aircraft designer to assess the real-world performance of the aircraft system. In addition, the effect of unmodeled operating conditions, environmental variables, and component degradation can all be assessed repeatably without constructing and testing entire aircraft systems.

8.5.2. UAV Powerplant Performance Comparison

Conceptual studies and simple calculations have been used to compared the theoretical performance of numerous electrochemical and internal combustion powerplants in the UAV application [14,43]. The results of this study now provide us with a designed, constructed and tested PEM fuel cell powerplant whose performance can be used to compare the performance of UAV powerplant technologies, using similar results from the literature. This section of the discussion will present a first order analytical comparison between the performance of aircraft incorporating various UAV energy storage technologies.

Using Newton's laws, a simplified range equation for unconventional powerplants can be derived where aircraft weight is constant,

$$ds = \int \frac{dE}{T} \tag{69}$$

For steady level flight, $T=D$ and $L=mg$,

$$s = \left(\frac{E}{D}\right) = \left(\frac{L}{D}\right)\left(\frac{E}{L}\right) = \left(\frac{E}{m}\right)\left(\frac{C_L}{gC_D}\right) \tag{70}$$

A similar approach can be followed to derive a simplified endurance equation for unconventional powerplants. For an aircraft at steady level flight,

$$T = \frac{C_D}{C_L}W \tag{71}$$

Rearranging (7) with $W=L$,

$$v = \left(\frac{W}{\frac{1}{2}\rho S_w C_L}\right)^{\frac{1}{2}} \tag{72}$$

The propulsive output energy is the integral of the propulsive output power. Under the assumption that the weight of the aircraft changes negligibly over the course of the flight,

$$E = \int_0^t \frac{C_D}{C_L} W \left(\frac{W}{\frac{1}{2}\rho S_w C_L}\right)^{\frac{1}{2}} dt = \frac{C_D t}{\sqrt{\frac{1}{2}\rho S_w}}\left(\frac{W}{C_L}\right)^{\frac{3}{2}} \tag{73}$$

Solving for the aircraft endurance,

$$t = \left(\frac{E}{m^{\frac{3}{2}}}\right)\left(\frac{\left(\frac{1}{2}\rho S_w\right)^{\frac{1}{2}} C_L^{\frac{3}{2}}}{g^{\frac{3}{2}} C_D}\right) \tag{74}$$

To compare the range and endurance performance of the fuel cell powered aircraft to other electrochemical energy storage technologies we can compare the quantities $\left(\frac{E}{m}\right)$ and $\left(\frac{E}{m^{3/2}}\right)$.

To construct a comparison to the variable mass internal combustion powerplant, we can numerically integrate (14) under the assumption of constant airspeed *v*, with varying mass *m*, a controllable angle of attack α, and the aircraft aerodynamic characteristics shown in Figure 5.

These comparisons assume that the airframe mass is the same for each technology. Electric motor mass (283g), fuel mass and fuel tankage mass (5% of fuel mass) are included where appropriate. For all powerplants, propeller efficiency is a constant 69% and for all electric powerplants, motor efficiency is a constant 71%. Each powerplant is sized to have the same take-off weight as the HiL aircraft. For the internal combustion engine, the payload and aircraft control power is produced assuming an alternator of 80% efficiency. The specifications of the energy storage subsystems are from the literature or from the results of the fuel cell UAV HiL tests. By designing an aircraft using these assumptions, these energy storage subsystem performance metrics can be translated into aircraft-level performance metrics $\left(\frac{E}{m}\right)$ and $\left(\frac{E}{m^{3/2}}\right)$. Equations (70) and (74) can then be used to calculate the range and endurance of the designed aircraft.

The first result of this analysis is shown in the first three rows of Table 3. The second column shows that the specific energy of the HiL PEM fuel cell energy storage system is significantly higher than the specific energy of both Zinc-Air batteries and Lithium Polymer batteries. This translates into higher aircraft performance metrics and

higher aircraft endurance and range for the PEM fuel cell powered UAV. In other words, using commercially available compressed hydrogen storage and fuel cell systems, a small-scale hydrogen fueled PEM UAV can enable longer range and endurance than other electrochemical energy storage systems, including zinc-air and lithium-polymer batteries. For long-endurance or long-range applications where electrically-powered UAVs are preferred, the fuel cell powerplant offers the highest performance.

The second result of this analysis is a comparison of the performance of the fuel cell aircraft to the performance of the internal combustion engine aircraft, as shown in the final row of Table 3. The comparison shows that the specific energies, endurance and range of the internal combustion aircraft are approximately equal to those of the PEM fuel cell aircraft. This result suggests that the scale of the HiL aircraft is near the crossover point for comparing these technologies in the long endurance and long range UAV application. Although further development will improve the performance of both the PEM fuel cell powerplant and the internal combustion engine, this analysis provides a basis for validated comparison of powerplant hardware at the scale of the designed and tested fuel cell UAV.

Table 19. Comparison of electrochemical powerplants for long range and long endurance missions in small scale aircraft

Powerplant Type	Energy Storage Subsystem Specifications	$\left(\frac{E}{m}\right)$	$\left(\frac{E}{m^{3/2}}\right)$	Calculated Range (s) using (70)	Calculated Endurance (t) using (74)
HiL Hydrogen PEM Fuel Cell	448 DC Wh kg^{-1}	124.9 Wh kg^{-1}	35.3 Wh $kg^{-3/2}$	1100 km	24.1 hr
Zinc Air Battery	350 DC Wh kg^{-1} [42]	101.4 Wh kg^{-1}	28.7 Wh $kg^{-3/2}$	894 km	19.6 hr
Lithium Polymer Battery	166 DC Wh kg^{-1} [33]	48.1 Wh kg^{-1}	13.6 Wh $kg^{-3/2}$	423 km	9.3 hr
Small Internal Combustion Engine	0.3 kg hr^{-1}@105W [43]	124.7 Wh kg^{-1}	35.2 Wh $kg^{-3/2}$	1083 km	23.8 hr

8.6 Conclusions

The development of advanced powerplants for UAVs will allow for improved performance in long endurance or long range applications. The successful design and system optimization of these powerplants is highly dependent on the reduction of performance uncertainty early in the design process. HiL testing allows for repeatable, reliable and detailed evaluation of UAV powerplants without the implementation of extraneous aircraft systems as is required by conventional flight testing.

This article proposes an architecture for HiL simulation of a UAV powerplant for system-level performance, range and endurance testing. For this study, the UAV powertrain hardware is embedded within the main aircraft dynamics loop and the energy storage hardware is coupled to the simulation by a DC electrical bus. Interface between the software simulation of the aircraft dynamics and the powerplant hardware is performed by a torque- and speed-controlled dynamometer and signal conditioning hardware. The architecture and components used for this HiL simulation of a PEM fuel cell powered UAV can be adapted to a variety of electric powerplant technologies.

Testing of the climb performance and endurance of a PEM fuel cell powered UAV is performed by simulating the flight of the aircraft over a generic long-endurance remote sensing mission. The aircraft exhibits a measured climb rate of up to 40 m min^{-1} and a flight endurance of 22.75 ± 0.64 hours, validating the viability and performance of this fuel cell powered aircraft. Measurements of the power flows within the aircraft powerplant quantify the efficiencies and losses of each major powerplant component.

With the increasing complexity of advanced UAV powerplants can come increasing performance uncertainty. HiL simulation allows for the quantitative assessment of the

responses of the powerplant to the conditions of use and environment that will be encountered during flight. The performance of a highly passive fuel cell system under real world conditions is assessed and compared to static models. The aircraft-level performance of the PEM fuel cell powerplant used in this study is then compared to state of the art electrochemical energy storage technologies and internal combustion engines. The fuel cell powerplant constructed for this study can outperform other available electrochemical energy storage technologies in key metrics for long endurance or long range missions. Its performance in these key metrics is comparable to the performance of an internal combustion engine powerplant.

CHAPTER 9

CONCLUSIONS

9.1 Conclusions

This dissertation has defined and completed a series of tasks to address the primary research challenges associated with the modeling, design and energy management of fuel cell systems for aircraft. New subsystem models of fuel cell powerplants for aircraft are shown to be validateable, within the fidelity requirements of a proposed fuel cell UAV design process. The proposed design process is application-integrated, optimizeable, multidisciplinary and allows for the definition of families of high performance fuel cell powered aircraft. The scope of the modeling and design tools are defended through comparison to design tools with simplified fuel cell subsystem models and design tools with simplified application models. In each case, the full design model shows significant performance benefits over these simplifications which are representative of the state of the art. The role of hybridization and flight path optimization for fuel cell powered aircraft is explored and charge-depleting hybridization strategy for takeoff is shown to be the most beneficial form of energy management for FC UAVs.

This research has defined conceptual design requirements and tradeoffs for fuel cell systems for small-scale aircraft. Fuel cell powered aircraft are an important application of fuel cell technology with research demands coming from fuel cell and aviation industries, research institutions and governmental entities. The design studies performed for this dissertation are novel in that they are the only studies that take a

rigorous multi-disciplinary, complex systems approach to the design of aviation fuel cell systems. The tools of complex system analysis are required for these design problems because advanced fuel cell systems are highly constrained, inadequately modeled and they can incorporate a high degree of uncertainty in parameters and design goals. Within the more specific domain of aeronautical engineering, these are the first optimization-based studies of fuel cell powerplants for fuel cell powered aircraft. These design studies have shows significant performance improvements are available for the design of fuel cell powerplants for aircraft through utilization of the newly developed design techniques. Table 20 shows a comparison between the most capable published fuel cell UAV design available at the present (the AeroVironment *Puma*), and the results of this dissertation design study. The HiL fuel cell UAV that has been built and tested in hardware outperforms the state of the art fuel cell aircraft in terms of endurance by more than a factor of 2. The conceptual designs improve the performance of the state of art by more than a factor of 2 again, in terms of endurance.

Table 20. Design comparison between state of the art, developed fuel cell aircraft and conceptual fuel cell aircraft designs

Design Characteristic	AeroVironment *Puma* [51]	HiL FCUAV [Ch.8]	Conceptual FCUAV[Ch.5]	Conceptual FC Hybrid UAV[Ch.6]
Powerplant Type	Fuel Cell	Fuel Cell	Fuel Cell	Fuel Cell
Empty Endurance	9 hrs	23 hrs	25.2 hrs	47.7 hrs
Climb Rate	?	~50 m/min	120 m/min	120 m/min
Gross Take-off Mass	5.7 kg	12.5 kg	20 kg	20 kg
Wing Span	2.6 m	2 m	4.4 m	5.55 m

The work performed for this dissertation has demonstrated the feasibility of the fuel cell aircraft in concept and in engineering practice. The fuel cell aircraft constructed

for this dissertation is the largest compressed hydrogen UAV built to date and is currently the only fuel cell aircraft whose design and test results are in the public domain. When constructed, the hardware in the loop aircraft designed for this dissertation will be the longest endurance fuel cell aircraft built to date. The emphasis on validation and hardware development will be of use to the fuel cell and aircraft communities to evaluate the near- and long-term feasibility of fuel cell powered aircraft.

This research has refined many of the tools of complex system analysis that have been used in the design of "revolutionary" aerospace vehicles, and applied these tools to integrated fuel cell system and powerplant design. These tools include multidisciplinary optimization, system sensitivity analysis, uncertainty propogation and nonlinear programming for hybrid powerplant and flight path optimization. By bringing these techniques to stages of design beyond conceptual design, these research efforts have resulted in new methods and case studies for making decisions under uncertainty, guiding complex system validation procedures and demonstrating on-design performance.

9.2 Research Contributions of this Dissertation

The primary contributions of this dissertation are presented below:

- A survey of existing fuel cell powered aviation literature;
- A set of fuel cell sub-system models that can be assembled into a fuel cell system which are application integrated, scalable, parametric, optimizeable, validated and can be used for conceptual design of fuel cell systems;
- A tool for conceptual design that allows for the synthesis of application-optimal fuel cell systems. The conceptual design tool is shown to exhibit

improvements over conventional design rules and over sub-system-level optimized solutions;

- A quantitative and general mathematical assessment of flight path optimization and hybridization for their benefit to the performance of fuel cell hybrid aircraft;
- The first published design process and flight test results for a fuel cell powered aircraft;
- An architecture for, and demonstration of hardware-in-the loop simulation of fuel cell powerplants for aircraft. Test results from hardware showing aircraft performance greater than electrochemical powerplants and internal combustion powerplants at the scale of the tested UAV.

9.3 Future Work

This dissertation involves the development of advanced techniques and a deeper understanding of the design of fuel cell systems for unconventional applications. As such, the models and methods developed for this research effort are widely applicable to efforts other than fuel cell powered aircraft. The emphasis on long-endurance, high energy applications is appropriate, since this is a metric at which hydrogen powered fuel cells can outperform other means of electrical energy storage. There are a wide number of potential fuel cell applications that would benefit from the advanced design techniques applied in this work. Underwater unmanned vehicles, automobiles, spacecraft and mobile power supplies are just some of the applications where fuel cells powerplant design and control will be strongly constrained by requirements of the application. The development of methodologies for fuel cell system modeling, design and optimization

that will improve the performance of fuel cells in these other applications should be investigated.

This research has assumed a compressed hydrogen storage fuel cell aircraft because of the near term viability of such a solution. A structured means for design optimization and comparison of hydrogen storage systems for the fuel cell UAV application is required to facilitate cross-technology performance comparisons. The next investigations will focus on characterization for parametric design of the primary technologies for hydrogen storage: compressed hydrogen gas, low and high pressure liquid hydrogen, low and high pressure metal hydride, and low pressure chemical hydrides. Conceptual design studies will characterize and compare the performance of the integrated fuel cell/hydrogen storage/aircraft systems. Proof-of-concept fuel cell UAVs should be constructed from the most promising system designs.

APPENDIX A

DETAIL DESIGN FOR FUEL CELL POWERED DEMONSTRATION AIRCRAFT

This section describes the detailed design of the fuel cell powerplant for the fuel cell powered demonstration aircraft referenced throughout this dissertation. The detail design requirements for this particular aircraft are defined. The details of the modeling, design and function of the fuel cell and balance of plant systems are described in detail.

A1.1 Design Requirements Generation

The purpose of the power generation and propulsion system of a fuel cell-powered aircraft is to provide energy to the propulsive, accessory and payload systems with appropriate efficiency and robustness. This section describes the requirements for the power and propulsion system as determined through an understanding of the tradeoffs present within the fuel cell demonstrator airplane design.

As discussed above, fuel cell powerplants are characterized by low specific power (W/kg). Aircraft specific power (or power-to-weight ratio) is commonly used as a high-level indicator of aircraft climb rate, bank angle, payload capability and performance. The mismatch between the characteristics of the powerplant and the requirements of the vehicle provides strict limits on the power consumption and weight of the powerplant systems, so as to maximize aircraft specific power. Fuel cell-powered aircraft are therefore characterized by high efficiency airframes, low weight structures, high

efficiency propulsion systems, low power payloads and low-margin, highly constrained designs.

As such, an integrated design process was required to successfully design a functional fuel cell powered aircraft. The process for design of the fuel cell powered aircraft was broken down into a high-level, low-fidelity conceptual design task and a lower-level, higher-fidelity detail design task. First, the aircraft was designed conceptually using high-level simulations of the aircraft and powerplant. An aircraft performance metric (Q) was chosen that incorporates a weighted average of the aircraft takeoff distance, climb rate, range and endurance. The coefficients (b_i) of a 2nd-degree response surface equation of the form:

$$, \quad Q = b_0 + \sum_{i=1}^{3} b_i x_i + \sum_{i=1}^{3} b_{ii} (x_i)^2 + \sum_{i=1}^{2} \sum_{j=2}^{3} b_{ij} (x_i x_j) \tag{A1}$$

were fit to the aircraft performance dataset as a function of the powerplant design inputs (x_i). These design inputs include propulsion system efficiency, mass, frontal area and accessory load. This response surface equation model of the aircraft performance was used to communicate the design requirements of the fuel cell propulsion system to the propulsion system design task.

Table 21. Aircraft performance sensitivities to power and propulsion system performance

	Aircraft Performance Metric Sensitivities				
Power and Propulsion System Performance Metric	Takeoff Distance	Climb Rate	Range	Endurance	Composite Aircraft Performance Sensitivity
System Efficiency	-1.9	3.6	1.2	1.2	2.0
System Frontal Area	0.4	-0.6	-0.2	-0.2	-0.4
System Accessory Load	1.9	-3.6	-1.2	-1.2	-2.0
System Mass	2.0	-2.1	-0.9	-0.7	-1.4

Using response surface equations to communicate design objectives from the conceptual design task to the detail design task allows the detail designer to understand the high-level effect of low-level design decisions. In this case, the response surface equations can be solved efficiently to determine the effect that changes in the powerplant design will have on the aircraft as a whole, without having to rerun the conceptual design process. The sensitivity of the aircraft to propulsion system design can be assessed and the design requirements of the propulsion system can be prioritized. For this aircraft the sensitivity of the aircraft performance metrics to the propulsion system design is presented in Table 21. Both the sensitivities of the considered aircraft performance metrics and the composite performance metric (Q) are shown.

Based on this low-order analysis, the requirements of the power and propulsion system specific to fuel cell aircraft, in the order of importance to maximize aircraft specific power are:

1) Minimization of balance of plant, accessory, and payload power consumption
2) Optimization of propulsion system efficiency
3) Minimization of system mass
4) Minimization of system frontal area

These requirements must be met under whatever static and dynamic flight conditions the aircraft experiences.

The power and propulsion systems of the fuel cell demonstrator aircraft have been designed to meet these requirements within the normal engineering constraints of budget and component availability. In the following sections, the architecture and detailed function of the power and propulsion systems are described for the fuel cell powered

aircraft. The performance of the subsystems is evaluated using the proposed design requirements.

A1.2 Controls and DAQ Development

The aircraft systems are broken down into fuel cell, balance of plant, payload, propulsion and aircraft control systems. A diagram showing the interactions of the components of the aircraft is presented in Figure 90. All components are powered primarily from the fuel cell power bus, although the aircraft control system has a battery backup. The pilot controls the aircraft from the ground control radio and the aircraft systems react to the pilot's control signals. There is no buffering of pilot commands, no aircraft autonomy, and no maneuver preplanning, at present. The aircraft system controller coordinates the control of the fuel cell and balance of plant based on the control inputs from the pilot and acts as a data acquisition system for the aircraft. Data regarding the performance of the aircraft and powerplant are transmitted wirelessly to the ground station data acquisition system (DAQ), where they are logged by a ground-based computer.

Figure 91 shows the flow chart of the aircraft control algorithm. The primary functions of the aircraft controller are data acquisition, aircraft mode control, compressor airflow control, thermo-static control of the fans, and control of the anode purge valve. Details of the data acquisition hardware, functions and wiring are provided in Table 22 and Table 23.

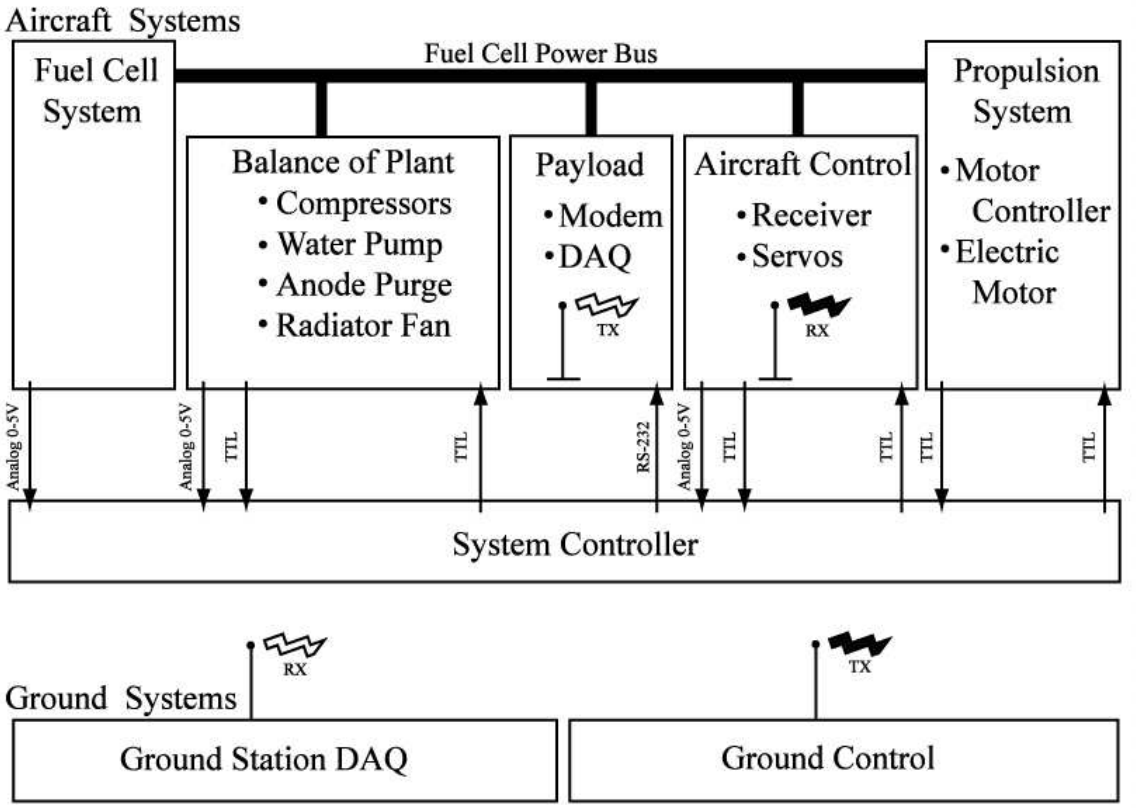

Figure 90. System diagram showing power and signal communication between modules

Table 22. Wiring spreadsheet and sensor list for fuel cell A/D converter and system controller

Analog to Digital Converter					
Analog Input Channel	***Signal Name***	***Signal Type***	***Signal Range***	***Connects to***	***Comment***
AIN0	Barometer	Analog	2.5-4.0V	Barometer	
AIN1	Pitot Tube	Analog	0.25-4.25V	Differential Pressure Sensor	http://www.allsensors.com/datasheets/commercial_temp/amp_med.pdf
AIN2	Strain Gauge	Analog	0-5V	Strain Gauge Signal Amplifier	http://www.transducertechniques.com/EBB-Load-Cell.cfm
AIN3	Coolant Temperature	Analog	0-5V	Thermistor Voltage Divider	
AIN4	Fuel Cell Temperature	Analog	0-5V	Thermistor Voltage Divider	
AIN5	Outside Temperature	Analog	0-5V	Thermistor Voltage Divider	
AIN8	Fuel Cell Voltage	Analog	0-5V	Voltage Divider	
AIN9	Balance of plant current	Analog	2.5-4.0V	Fuel Cell Current Sensor	http://www.tamuracorp.com/clientuploads/pdfs/engineeringdocs/L07P_S05.pdf
AIN10	Current Sensor	Analog	2.5-4.0V	Fuel Cell Current Sensor	http://www.tamuracorp.com/clientuploads/pdfs/engineeringdocs/L07P_S05.pdf
MicroController					
Digital Input Channel	***Signal Name***	***Signal Type***	***Signal Range***	***Connects to***	***Comment***
none	Mode Control	Digital	TTL	Mode Switch	http://www.nkkswitches.com/pdf/MtogglesBushing.pdf
PD2	Compressor 1 Speed	Digital	TTL	Compressor #1 Encoder	http://www.pennmotion.com/part_num_database/pdf/9234S005.pdf
PD3	Motor speed	Digital	TTL	Hall sensor on Motor Shaft	
PB2	Compressor 2 Speed	Digital	TTL	Compressor #2 Encoder	http://www.secomtel.com/UpFilesPDF/PDF/Agilent/PDF_DOCS/ISONCONT/02_MOTN/2_40_45.pdf
Output Channel	***Signal Name***	***Signal Type***	***Signal Range***	***Connects to***	***Comment***
PD4	Thermostatic Fan Control	TTL	0-5V	Fan Control MOSFET #5	http://www.nteinc.com/specs/2300to2399/pdf/nte2395.pdf
PD7	Compressor #1 PWM	TTL	0-5V	Compressor 1 Control MOSFET #3	http://www.nteinc.com/specs/2300to2399/pdf/nte2395.pdf
PB3	Compressor #2 PWM	TTL	0-5V	Compressor 2 Control MOSFET #4	http://www.nteinc.com/specs/2300to2399/pdf/nte2395.pdf
PD5	H2 Purge Valve Control	TTL	0-5V	Purge Valve MOSFET #2	http://www.nteinc.com/specs/2300to2399/pdf/nte2395.pdf
PD6	Water Pump On/Off	TTL	0-5V	Pump Motor Mosfet #1	http://www.nteinc.com/specs/2300to2399/pdf/nte2395.pdf

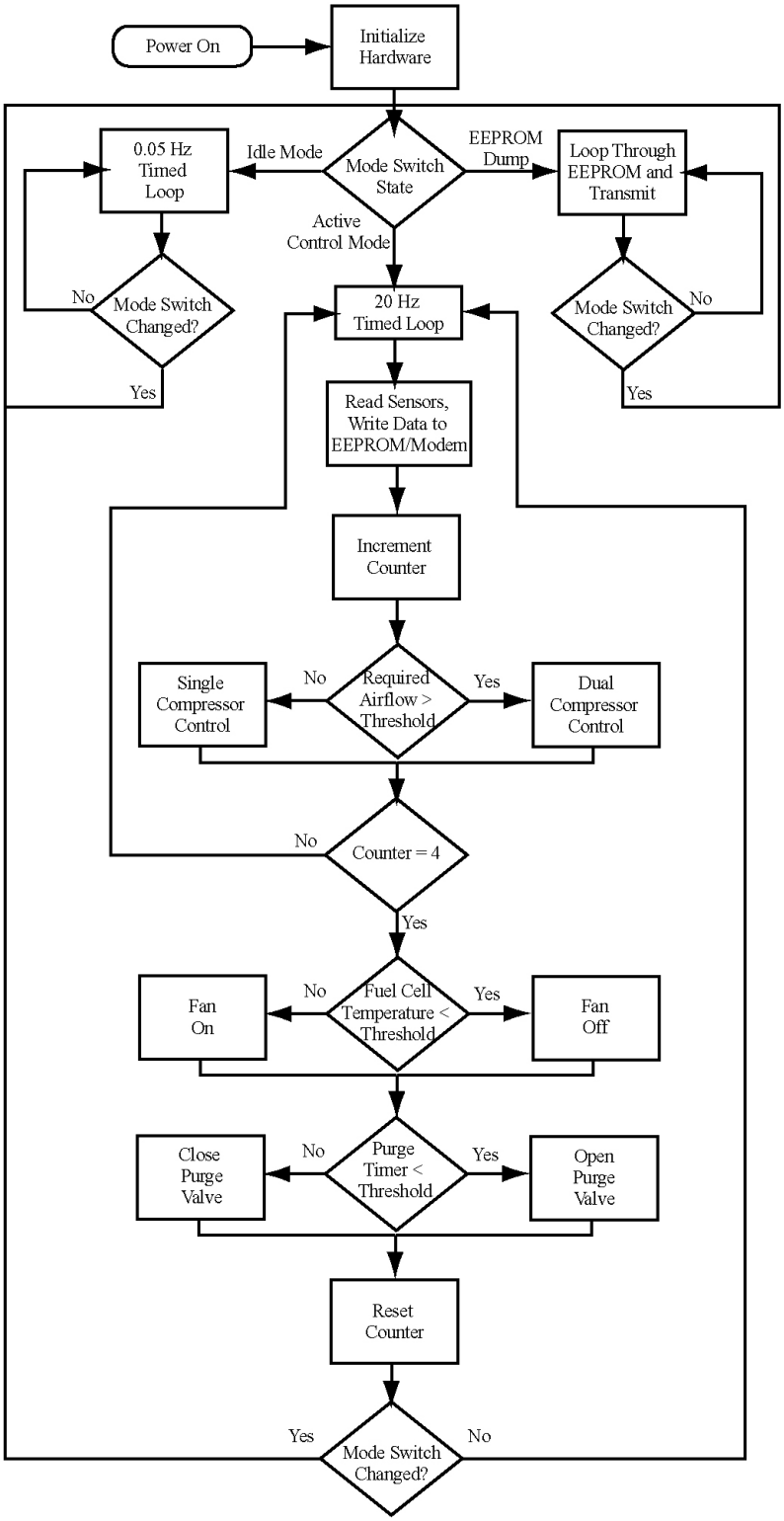

Figure 91. Flow chart of the system control algorithm

Table 23. Wiring connections for fuel cell system controller

Connector	*# of pins*	*Pin number*	*On-Board Connection*	*Off-Board Connection*
Connector 1	24	1	+5V bus	Pitot tube connector Pin1
Connector 1	24	2	GND	Pitot tube connector Pin2
Connector 1	24	3	AIN1	Pitot tube connector Pin3
Connector 1	24	4	GND	NC
Connector 1	24	5	+5V Bus	Fuel Cell Temp Thermistor
Connector 1	24	6	AIN4	Fuel Cell Temp Thermistor
Connector 1	24	7	+5V Bus	Modem Power
Connector 1	24	8	GND	Modem Ground
Connector 1	24	9	+5V Bus	Outside Temp Thermistor
Connector 1	24	10	A/D Converter Channel 3	Outside Temp Thermistor
Connector 1	24	11	Rs232 DI	Modem DI
Connector 1	24	12	RS232 DO	Modem DO
Connector 1	24	13	+5V bus	Strain Gauge Signal Amplifier Pin1
Connector 1	24	14	GND	Strain Gauge Signal Amplifier Pin2
Connector 1	24	15	AIN2	Strain Gauge Signal Amplifier Pin3
Connector 1	24	16	GND	Strain Gauge Signal Amplifier Pin4
Connector 1	24	17	+5V Bus	Coolant Temp Thermistor
Connector 1	24	18	AIN3	Coolant Temp Thermistor
Connector 1	24	19	+5V bus	Prop Speed Sensor Pin1
Connector 1	24	20	GND	Prop Speed Sensor Pin2
Connector 1	24	21	PD7	Prop Speed Sensor Pin3
Connector 1	24	22	GND	Prop Speed Sensor Pin4
Connector 1	24	23	NC	NC
Connector 1	24	24	NC	NC
Connector	***# of pins***	***Pin number***	***On-Board Connection***	***Off-Board Connection***
High Current Lug 1	1	1	Current Sensor Positive In	Fuel Cell Positive Current Collector
High Current Lug 2	1	1	Current Sensor Positive Out	Electric Motor
High Current Lug 3	1	1	Ground	Fuel Cell Negative Current Collector
Connector	***# of pins***	***Pin number***	***On-Board Connection***	***Off-Board Connection***
Connector 2	24	1	+5V bus	Motor 1 Encoder Pin 4
Connector 2	24	2	GND	Motor 1 Encoder Pin 1
Connector 2	24	3	PB1	Motor 1 Encoder Pin 5
Connector 2	24	4	NC	NC
Connector 2	24	5	MOSFET 4 Drain	Compressor 1 GND
Connector 2	24	6	+FC Bus	Compressor 1 V+
Connector 2	24	7	MOSFET 2 Drain	H2 Purge Valve Control GND
Connector 2	24	8	+FC Bus	H2 Purge Valve Control V+
Connector 2	24	9	MOSFET 1 Drain	Water Pump GND
Connector 2	24	10	+FC Bus	Water Pump V+
Connector 2	24	11	MOSFET 3 Drain	Fan GND
Connector 2	24	12	+FC Bus	Fan V+
Connector 2	24	13	+5V bus	Motor 2 Encoder Pin 4
Connector 2	24	14	GND	Motor 2 Encoder Pin 1
Connector 2	24	15	PB0	Motor 2 Encoder Pin 5
Connector 2	24	16	NC	NC
Connector 2	24	17	NC	NC
Connector 2	24	18	+FC Bus	NC
Connector 2	24	19	NC	NC
Connector 2	24	20	+FC Bus	NC
Connector 2	24	21	NC	NC
Connector 2	24	22	+FC Bus	NC
Connector 2	24	23	MOSFET 1 Drain	Compressor 2 GND
Connector 2	24	24	+FC Bus	Compressor 2 V+

A1.3 Fuel Cell Air Supply Controls Development

The purpose of the compressor control system is to maximize the efficiency of the fuel cell system by maintaining the proper cathode stoichiometry under dynamic operating conditions while minimizing the compressor power consumption. The compressor control is implemented in the “Single Compressor Control” and “Dual Compressor Control” blocks shown in Figure 91.

The compressor control pneumatic system is made up of two independently actuated diaphragm compressors, and a passive ball and spring pressure regulator. Each compressor is driven by a brushed DC electric motor, and has a maximum output of 15 L/min of air. The voltage applied to the compressor motor is controlled by pulse width modulation of a power MOSFET, connected to the ground leg of the motor power leads. Switching losses in the motors and MOSFETs are minimized by specifying the speed constant of the compressor motor so that the compressor is at full flow rate at the fuel cell maximum power operating voltage with the MOSFET nearly always on, as defined by:

$$k \cdot \dot{Q}_{\text{air\_max}} \approx \omega_m > K_v \left(V_{\text{fc\_max}} - V_{MOSFET} \right) \tag{A2}$$

The voltage losses in the MOSFET are represented by V_{MOSFET} and K_v is the DC motor back EMF constant.

To minimize the power consumption of the compressor system, a primary and a secondary compressor are used. For flight conditions where less than 15L/min of air are required, the secondary compressor is turned off and only the primary compressor is used to meet the airflow requirements. For flight conditions where more than 15L/min of air are required, both compressors are run at the same speed to meet the airflow requirements. The compressor switching takes place in the "Required Airflow > Threshold" block of the control algorithm shown in Figure 91.

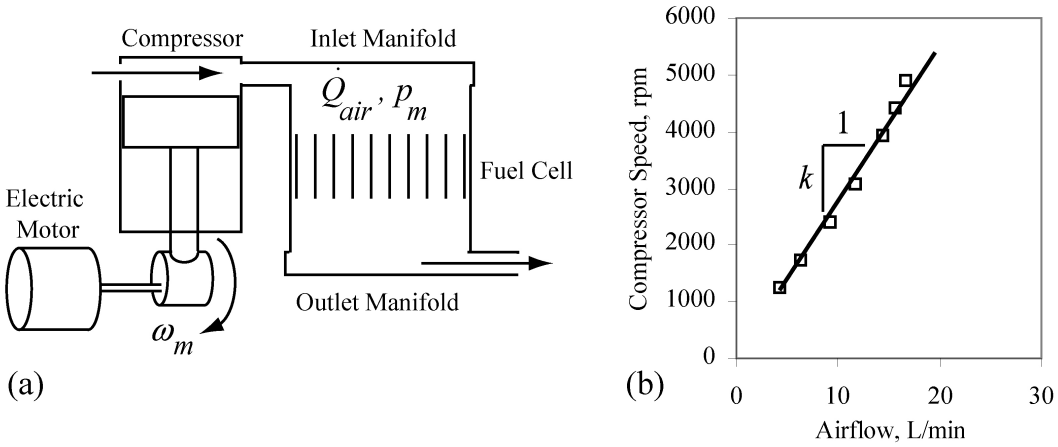

Figure 92 (a) Schematic of low pressure fuel cell cathode with positive displacement air compressors, (b) Performance of positive displacement compressors

To design the compressor controller, a model of the air management system was constructed. Compressor controllers available in the literature are derived for much larger fuel cells and do not model positive displacement compressors [72]. A diagram of the modeled system is shown in Figure 92(a). Because the compressors are positive displacement pumps, the air flow rate is a linear function of the motor speed, which is a linear function of the applied motor voltage (V_m) and K_v:

$$\dot{Q}_{air} = k \cdot \omega_m = k \cdot K_v \cdot V_m \tag{A3}$$

This assumption is validated with experimental data, as shown in Figure 92 (b). Where R is the universal gas constant and RFC is the linearized resistance of the fuel cell air channels, the air manifold dynamics simplify to:

$$\frac{dp_m}{dt} = \frac{\mathrm{R}\theta_{\mathrm{fc}}}{V_{im}}\left(k \cdot \omega_m - \frac{p_m}{R_{FC}}\right) \tag{A4}$$

At the low cathode pressure, small inlet manifold volume (V_{im}), and constant temperature (θ_{fc}) of the fuel cell under consideration, the single eigenvalue of this equation is stable, very fast and will remain uncompensated. The time electrical and mechanical time constants of the motor/compressor pair are on the order of 1 millisecond and 10 milliseconds respectively, and will also remain uncompensated. The constitutive equations of the compressor system are therefore simplified into an algebraic relation between the voltage applied to the compressor motor and the airflow rate to the fuel cell. The pressure of the fuel cell is passively regulated by the cathode backpressure valve.

A block diagram of the low-level compressor control routine is shown in Figure 93. This block diagram represents the control system under the "Single Compressor Control" and "Dual Compressor Control" blocks shown in Figure 91. The input to the control system is the fuel cell output current, sensed with a hall-effect current sensor, and the fuel cell output voltage, sensed with a voltage divider. A non-linear feedforward (FF) command is used to overcome plant hysteresis and to minimize steady state error. The feedforward gain (K_{flow}) converts the fuel cell current into a desired compressor speed using (4) and the following equation:

$$\dot{Q}_{air} = \lambda_c \frac{nI}{4F}\left(MW_{O2}\right)\frac{1}{0.23} \tag{A5}$$

The compressor controller is programmed to maintain a cathode stoichiometry of approximately λ_c>2.0 under all conditions. A conventional discrete proportional integral controller is implemented to control around a desired compressor speed and to compensate for any unmodeled dynamics. The integrator term is suppressed for all conditions except for low-flow compressor idle conditions. At idle, the integrator term is

allowed to saturate to reduce integrator windup. The pilot's current command signal incorporates a 15 A/sec slew rate limit.

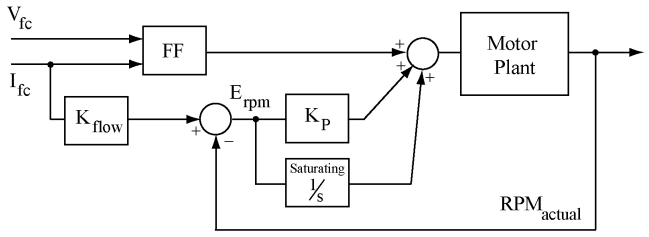

Figure 93 Signal flow diagram of the fuel cell compressor controller

Figure 94 shows the dynamic behavior of the fuel cell balance of plant and controller during takeoff acceleration of the aircraft. The current and speed signals are unfiltered and acquired at 40Hz, the sampling and control frequency of the compressor control algorithm. The cathode stoichiometry is calculated for each data point. When the current to the motor increases with the pilot's command, the fuel cell controller ramps up the speed of the compressors (including the start from rest of Compressor 2) to maintain the cathode stoichiometry at >2.0. When the fuel cell stoichiometry is less than 1.0, the performance and lifetime of the fuel cell will go down. This shows that the compressor controller can dynamically control the stoichiometry of the fuel cell cathode using the algorithm derived above.

Figure 95 shows the dynamic behavior of the of the fuel cell balance of plant and controller during bench testing. This plot shows that the controller has the ability to meet the airflow requests of the fuel cell at a variety of current draws.

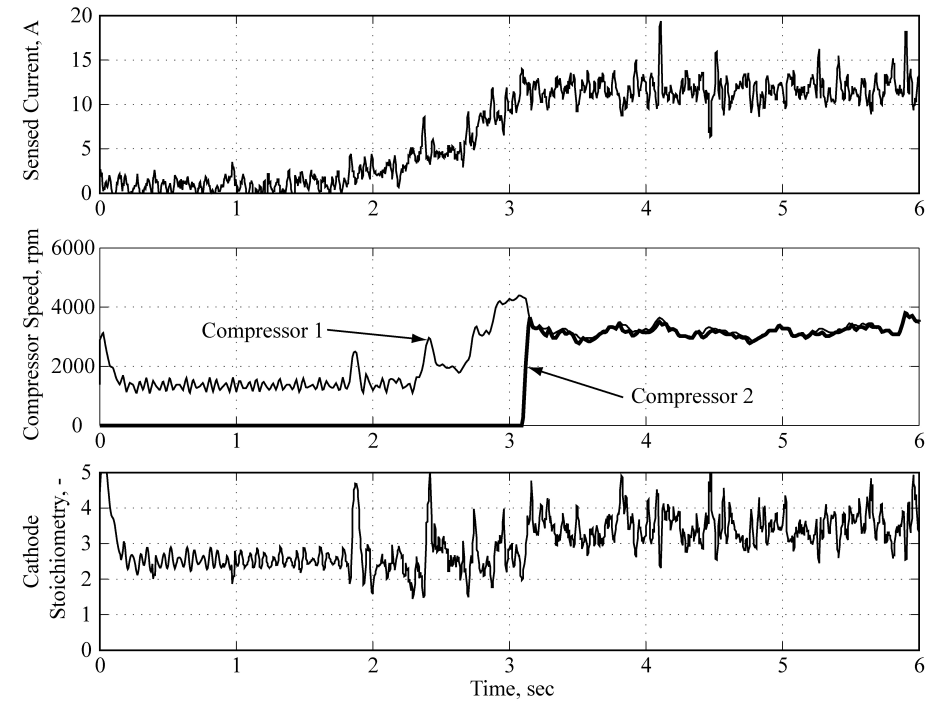

Figure 94. Dynamic performance of the compressor control system during flight testing

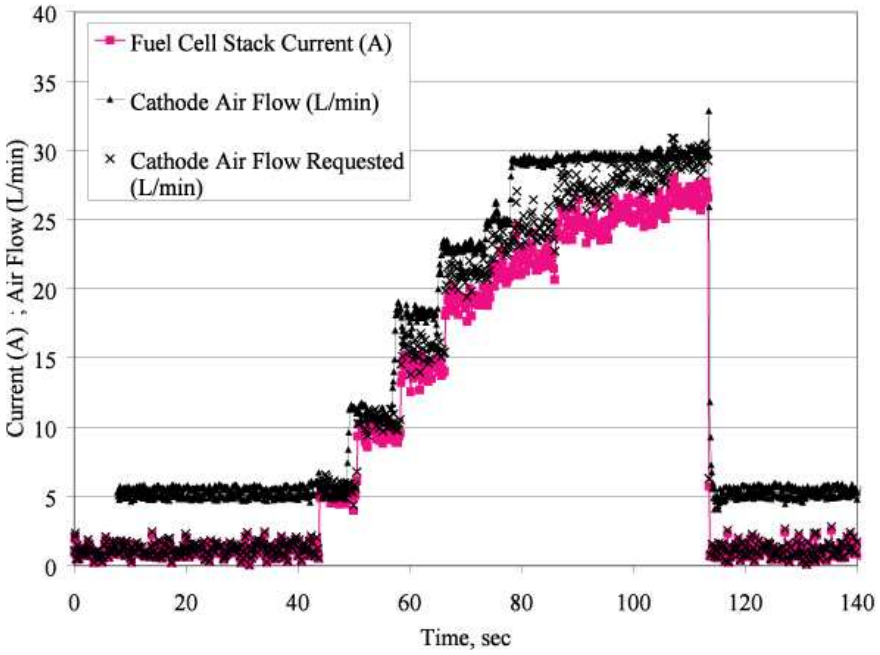

Figure 95. Dynamic performance of the compressor control system during benchtop testing

A1.4 Hydrogen Storage Systems Development

Portable fuel cells are often supplied with hydrogen from a portable hydrogen storage vessel. The most commercially available hydrogen storage systems for portable fuel cells use either high pressure compressed hydrogen storage, metal-hydride hydrogen storage units, or chemical hydride hydrogen storage systems. Both metal-hydride and compressed hydrogen storage systems were implemented during the development of the fuel cell powered aircraft. Schematic representations of these powerplants are shown in Figure 96 and Figure 97.

To fully control the hydrogen input to the fuel cell stack its pressure and flow rate must be actively controlled. For our example system, hydrogen is supplied to the fuel cell stack from a high pressure composite overwrapped pressure vessel. The operating pressure of the hydrogen tank is 31 MPa. Anode manifold pressure control is achieved through a dual inline regulator setup. Dual regulators are necessary to minimize the supply pressure effect, the variation of regulator output pressure with changing regulator pressure. Single stage diaphragm regulators act as a passive proportional pressure controller. When the input pressure changes the output pressure changes in response. Common regulator specifications for supply pressure effect are 1:100, that is the output pressure will vary by 10kPa for each 1MPa change in supply pressure. By placing two regulators in series the supply pressure effect is reduced to 1:10000, or about 3kPa maximum variation. Hydrogen flow rate is controlled using a normally closed solenoid purge valve. The purge valve operates with a constant purge pulse width and variable purge cycle period. The hydrogen flow rate through the anode purge valve can be

represented by a first-order system with a time constant, τ_c, of 0.3 sec as shown in Figure 69.

$$q_{H2} = q_{\max}\left(1 - e^{-t/\tau_c}\right) \tag{A6}$$

The measured volume of the hydrogen input manifold, 96 anode serpentine channels (32 cells, 3 channels per cell), the hydrogen output manifold and the anode purge valve is 24mL. Using the first order anode manifold model, we can solve for the purge pulse width that purges a volume of hydrogen equal to the volume of the anode manifold.

$$v_{\text{purge}} = q_{\max}\left(t - \tau_c + \tau_c e^{-t/\tau_c}\right) \tag{A7}$$

When the purge valve pulse width is set to 0.35 sec, the entire internal volume of the anode manifold is replaced with each anode purge.

The purge cycle period is derived from the desired hydrogen utilization. For fuel cells operated on neat hydrogen, hydrogen utilizations of greater than 99% are desirable and achievable. Hydrogen utilization is defined as the ratio of the volume of hydrogen consumed electrochemically to the volume of hydrogen purged.

$$U = \frac{v_{\text{consumed}}}{v_{\text{purge}} + v_{\text{consumed}}} \tag{A8}$$

Assuming that the hydrogen lost to leaks and hydrogen crossover is negligible, the volume of hydrogen consumed since the last purge event, v_{consumed}, can be calculated at each controller clock cycle from the fuel cell stack current and Faraday's Law.

$$v_{\text{consumed}} = \sum_{k=1}^{n} T \frac{n_{\text{cells}} I}{4F} \left(\frac{MW_{H_2}}{\rho_{H_2}} \right) \tag{A9}$$

The purge cycle period is over when $v_{\text{consumed}} \geq \frac{U}{1-U} v_{\text{purge}}$, or when an arbitrarily large period of time has passed (i.e. the fuel cell is at idle conditions). Figure 102 shows the hydrogen utilization of the example fuel cell system as a function of stack output current. At low currents, the hydrogen management controller purges the anode every 30 seconds. At currents higher than 1A, the controller (labeled 'GTRI controller') is able to maintain hydrogen utilization at approximately 90%. The stock controller for the Horizon fuel cell stack does not utilize this same controller logic.

The combination of a passive pressure control system and an active flow control system controls all of the states of the hydrogen management system with a bandwidth of 0.21 seconds.

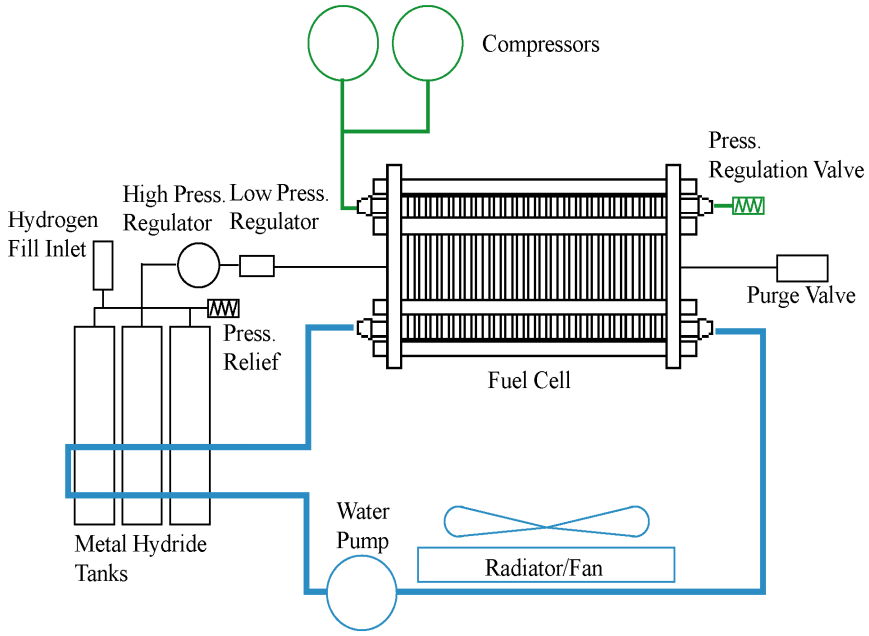

Figure 96. Schematic showing components of the 1st generation metal hydride fuel cell powerplant

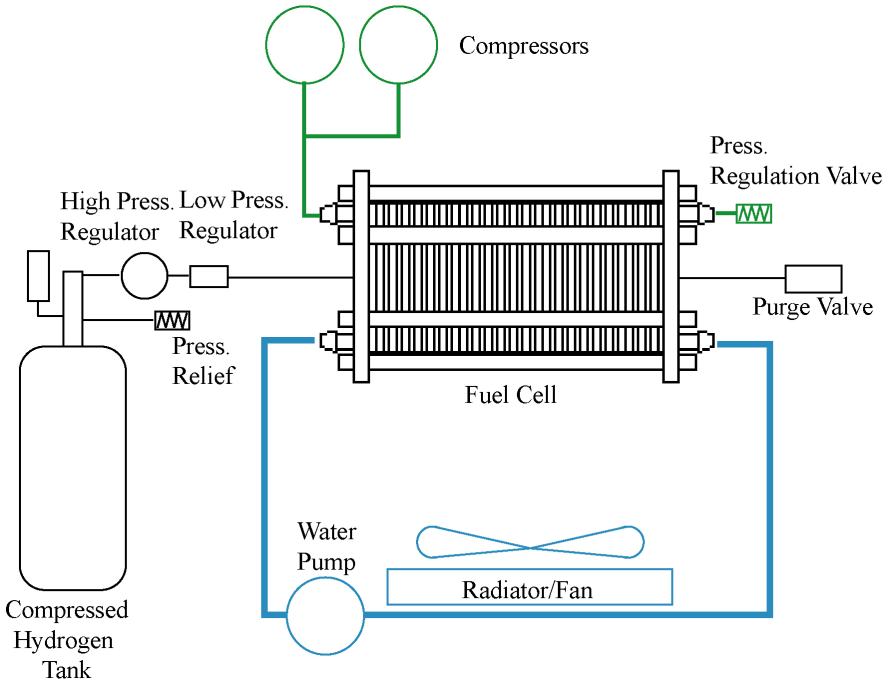

Figure 97. Schematic showing components of the 2nd generation compressed hydrogen fuel cell powerplant

A1.5 Other Balance of Plant Systems Development

The fuel cell is cooled by pumping distilled water through cooling channels in the fuel cell bipolar plates. The cooling water pump is driven by a DC brushed motor. In order to maintain a constant flow rate, the voltage applied to the DC motor is regulated by a switching DC/DC converter. The high startup loads of the water pump that would ordinarily overload the DC/DC converter are handled by using a RC soft-start circuit to limit the startup current required of the DC/DC converter. A circuit diagram of the soft-start and a diagram of the controlled soft-start sequence are shown in Figure 98. The purpose of the soft-start circuit is to minimize the size, weight, and electrical losses associated with the DC/DC converter while meeting the start-up current requirements of the water pump.

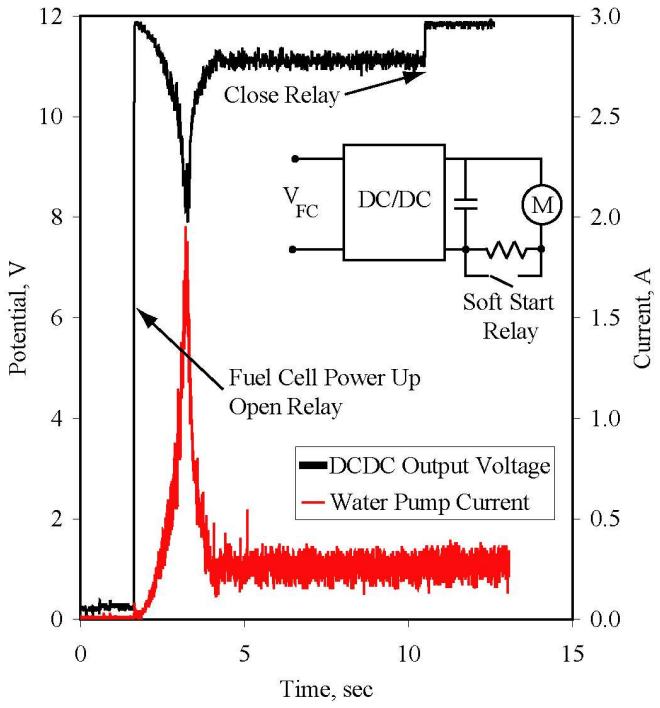

Figure 98. Experimental performance data for the DC/DC converter during water pump startup

The radiator for the fuel cell aircraft was the subject of a considerable development effort. The aluminum, brass and custom carbon foam radiators shown in Figure 99 were constructed and tested in order to determine the best physical configuration and technology. All three radiators are tested with and without evaporative cooling. Figure 100 presents the results, showing that the carbon foam radiators reject more heat per unit of radiator mass than the brass radiators. The *Carbon Foam II* radiator rejects roughly the same amount of heat as the *Carbon Foam I* radiator but because of the lower air side pressure losses, the power consumption of the *Carbon Foam II* radiator is much lower. *Carbon Foam II* radiator was chosen as the radiator to be used in the FC UAV and is shown as built in Figure 67.

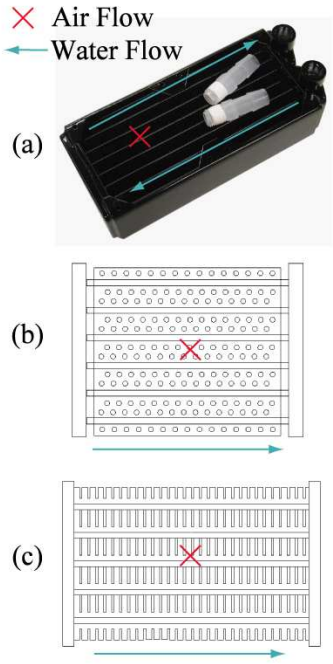

Figure 99. Radiator configurations tested for use in the FC UAV demonstration aircraft (a) *Brass Radiator,* (b) *Carbon Foam I* radiator with 0.125 in. pin hole fins, (c) *Carbon Foam II* radiator with 0.0625 in. rectangular fins

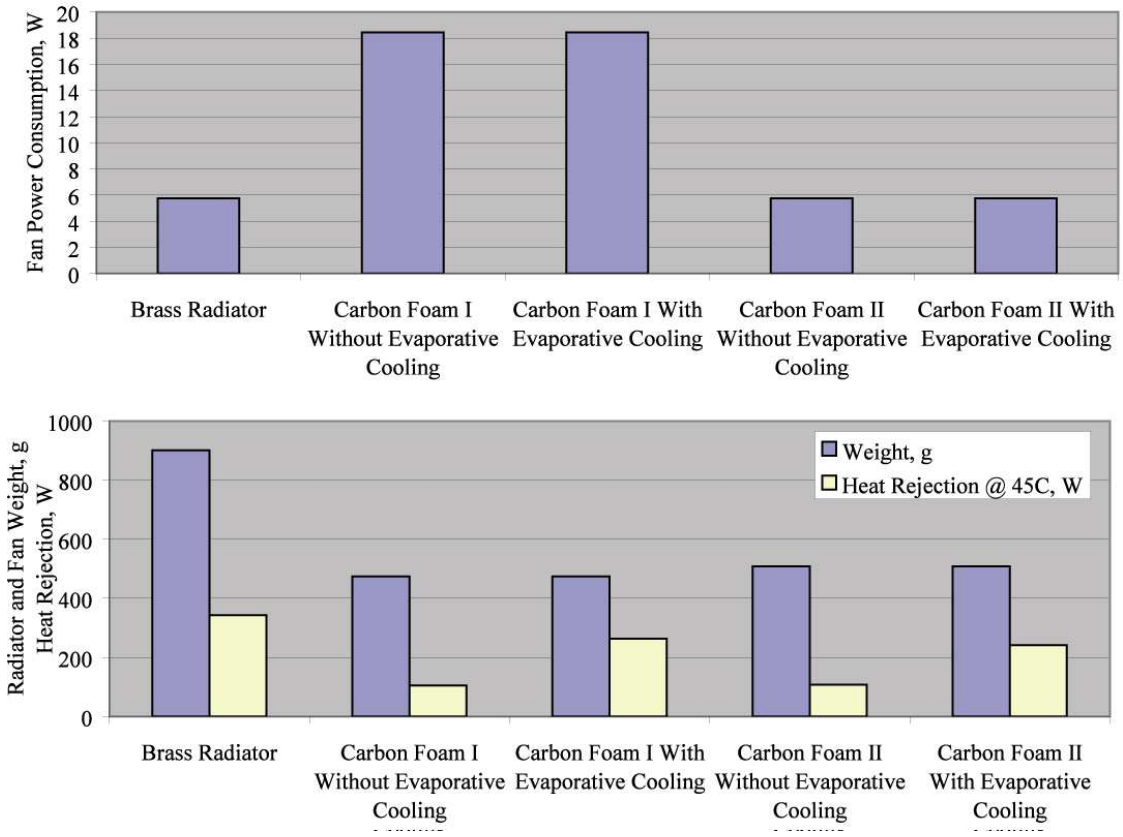

Figure 100. Comparison of experimental radiator performances

APPENDIX B

DETAIL DESIGN FOR HIL TEST EQUIPMENT AND HIL FUEL CELL POWERPLANT

This section describes the design of the fuel cell powerplant and hardware-in-the-loop test equipment. The detail design and development of the fuel cell system, HiL test equipment and calibration data are provided.

A2.1 Fuel Cell System Development

The Horizon 300 fuel cell stack is supplied with a controller that controls the state of the stack fans, the purge valve, and the stack on-off operation. This stock Horizon controller is not designed for mobile applications and was redesigned. The new (GTRI) controller controls the state of the anode purge valve and stack fans as a function of the current output of the stack and the temperature of the stack. The controller also serves as a data acquisition system that can measure stack temperature, current and voltage and can output intermediate control variables in real time at a frequency of 8 Hz. This section describes the function, calibration and performance of the GTRI controller for the Horizon H300 stack.

The stock H300 controller controls the temperature setpoint of the fuel cell stack as a function of the current output of the fuel cell stack. This relationship as measured using the stock H300 controller is shown in Figure 101. A linear fit to the stock temperature setpoint vs. stack current is implemented in the GTRI controller. The

behavior of the new controller is shown in Figure 101. The GTRI controller shows improved temperature regulation behavior compared to the Horizon controller.

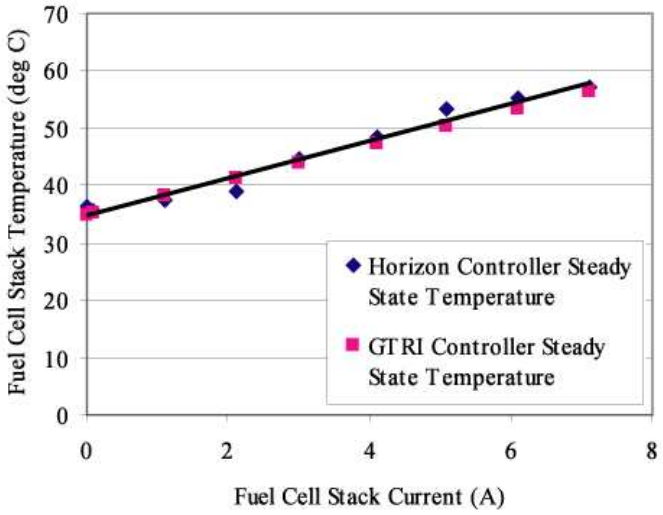

Figure 101. Fuel cell thermal set point calibration

The stock H300 controller controls the anode purge valve using a constant purge pulse width and a constant purge cycle period. This algorithm leads to hydrogen utilization that varies as a function of the fuel cell stack current. An improved algorithm which is described in Section A.1.3 is implemented in the GTRI controller. This algorithm controls directly for hydrogen utilization and is demonstrated to allow for a much wider region of high hydrogen utilization, as shown in Figure 102

To measure the temperature of the stack, an NTC thermistor voltage divider was used. NTC thermistors have a non-linear resistance vs. temperature curve, requiring the use of a two-part linear curve fit. The fits and resulting calibrations are shown in Figure 103.

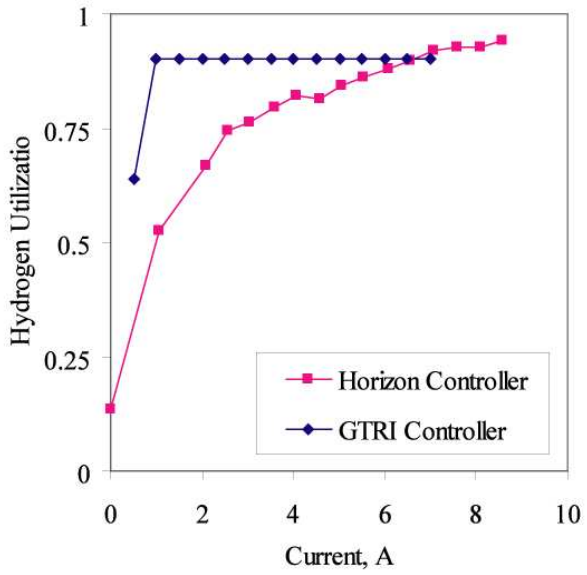

Figure 102. Hydrogen utilization of H300 fuel cell stack

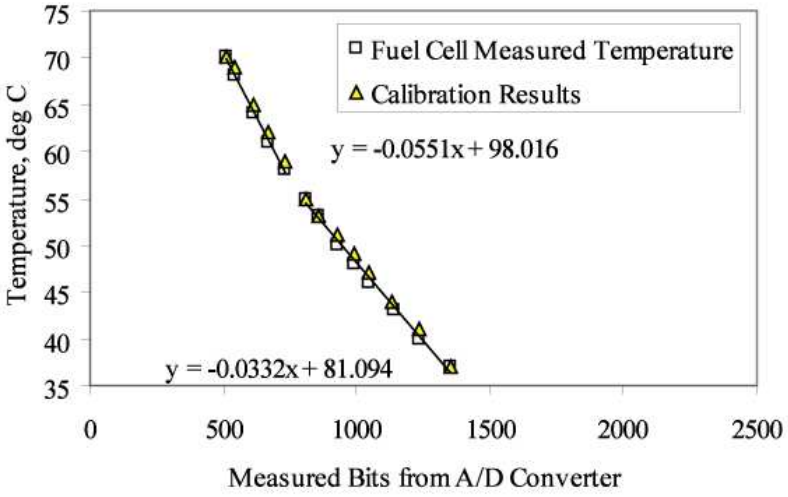

Figure 103. GTRI controller thermistor calibration

The current of the H300 stack is measured using an inductive current sensor. The measured current output and calibration curves for the current sensor are shown in Figure 104.

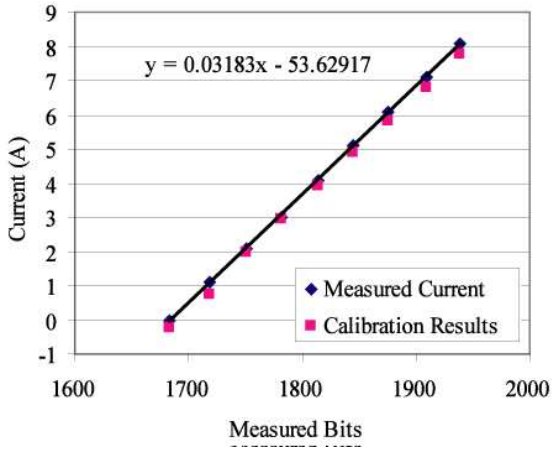

Figure 104. GTRI controller current sensor calibration

The constructed GTRI controller can perform both control and data acquisition tasks for the fuel cell system during both flight testing and HiL testing. A sample of the output data from the GTRI controller data acquisition system are shown in Figure 105. This test shows the start up of the stack . At a current of 4A, the desired temperature of the stack is approximately 48C, as shown in Figure 101. The GTRI controller successfully regulates the stack temperature at slightly above 48C.

Figure 106 shows the comparison between the performance of the fuel cell system without the balance of plant and controller loads and the fuel cell system with the balance of plant and controller loads of the GTRI fuel cell system controller. There is a significant reduction in the performance of the fuel cell when control loads are included. This increase in overpotential is hypothesized to be due to the unsteady loads that are placed on the fuel cell from the DC/DC converters and MOSFETs that are used in the control system hardware, but further investigation is warranted.

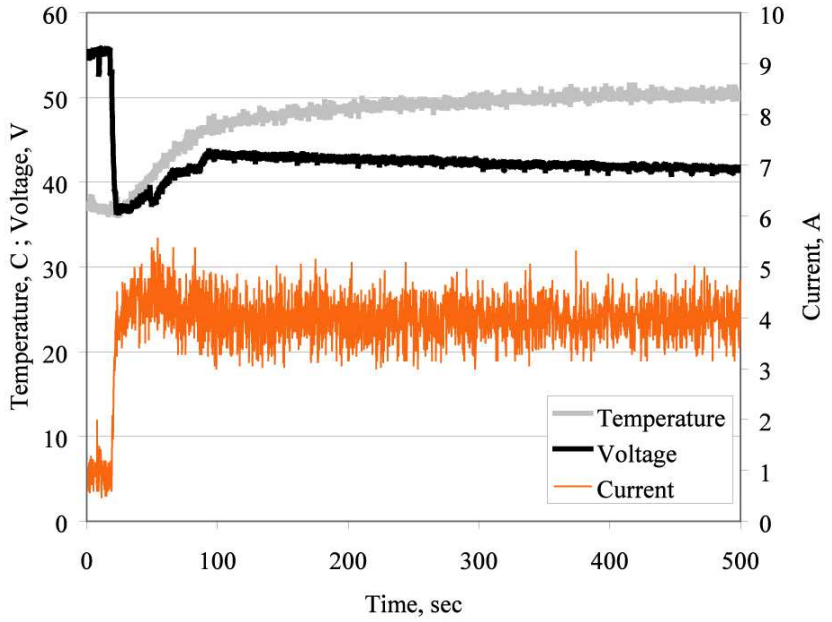

Figure 105. Sample data acquisition results from Horizon H300 with GTRI controller

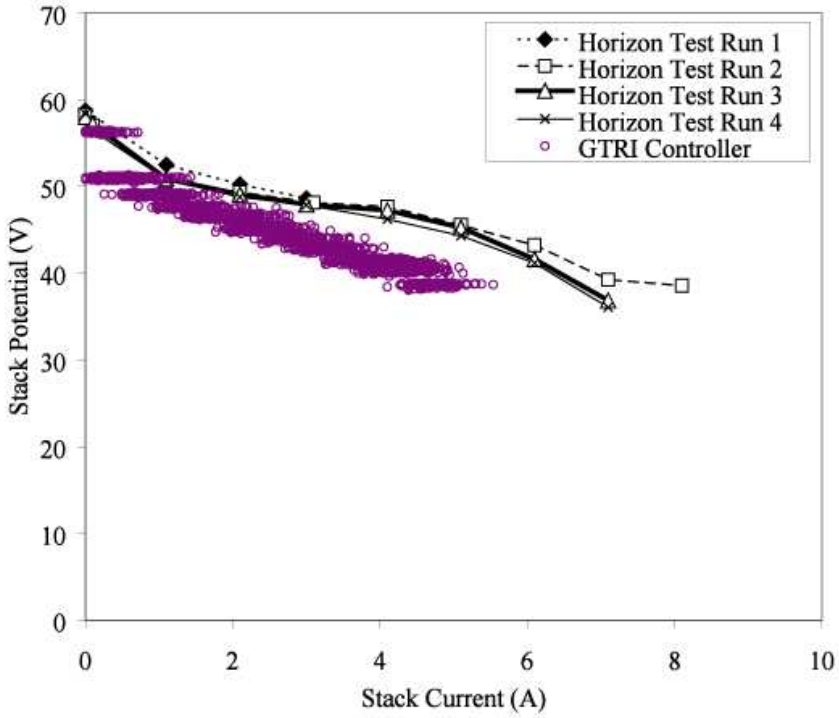

Figure 106. Comparison of fuel cell polarization curves with and without control hardware

A2.2 HiL Detail Development

AB.2.1. Hardware Development

The hardware of the HiL dynamometer is made up of the electric motor, torque measurement mechanism, coupling and absorber. The electric motor is bolted to a bearing-mounted motor mount whose rotation is constrained by the torque measurement mechanism. The CAD drawing of the motor mount is shown in Figure 107. The motor is mounted to surface A and the bearing is mounted to the outside of surface B. The stiction torque in the bearing negligible at < $3x10^{-3}$ Nm. Heating of the bearing is undetectable.

The absorber for the dynamometer is an off-the-shelf DC motor coupled to the aircraft electric motor. The absorber has a voltage constant of 0.02 V/rpm. The HP 6050A electronic load has a maximum input potential of 60V, leading to a maximum rotational speed of the motor and of the dynamometer of 3000 rpm. This constraint limits the conditions of use of the HiL system. The specification of an absorber with a lower voltage constant would improve the speed range of the HiL system.

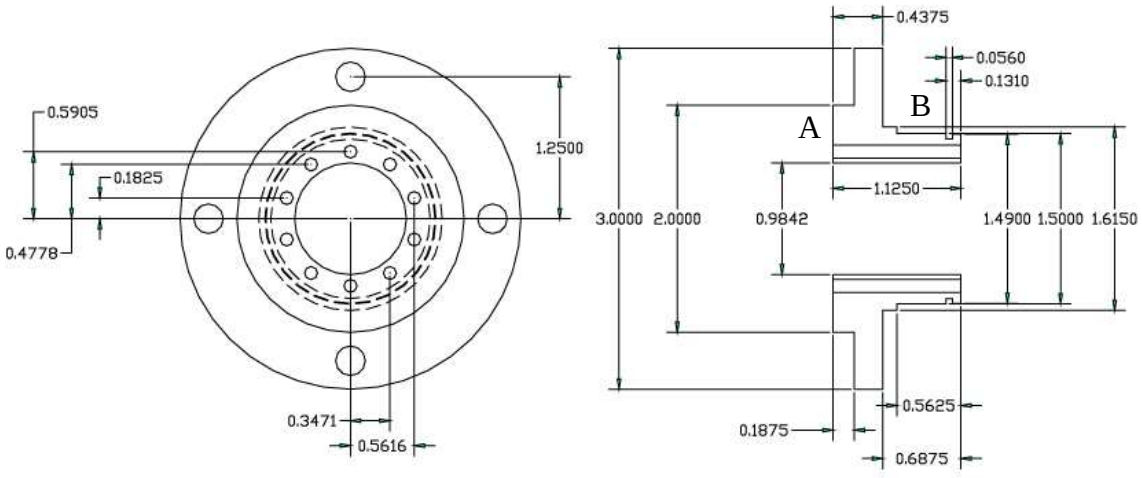

Figure 107. CAD drawing of the HiL motor mount

The HiL simulator is a dynamic dynamometer and as such, the dynamic properties of the motor coupling, and absorber should be similar to the dynamic properties of the propeller and couplings that are actually present in the aircraft. If the inertias of these components are of the same order of magnitude, then we can be confident that the acceleration and deceleration of the dynamometer is not putting unrealistic dynamic loads on the electric motor. The inertia of the absorber was estimated to be approximately 1.8×10^{-4} kg m^2 from the product literature of a similar motor. The inertia of the propeller was calculated by cutting up a propeller and numerically integrating the masses of the sections to estimate the total propeller inertia, as shown in Table 24. The total inertia of the propeller is 1.9×10^{-3} kg m^2, approximately an order of magnitude greater than the absorber inertia. This analysis suggests that no extraneous loads will be placed on the electric motor during testing due to a difference in inertia between the dynamometer and the actual propeller.

Table 24. Tabulation of propeller inertia for Bolly 22x20 carbon fiber propeller

Propeller Section	Section center of gravity location (in)	Section center of gravity location (m)	Section Mass (g)	Inertia Contribution (kg m^2)
0	0	0	60.4	1.94838E-05
1	1.5	0.0381	14.5	2.10483E-05
2	2.5	0.0635	8.74	3.52419E-05
3	3.5	0.0889	7.52	5.94321E-05
4	4.5	0.1143	6.42	8.3874E-05
5	5.5	0.1397	5.92	0.000115535
6	6.5	0.1651	5.05	0.000137653
7	7.5	0.1905	4.28	0.000155322
8	8.5	0.2159	2.99	0.000139372
9	9.5	0.2413	2.11	0.000122856
10	10.5	0.2667	1.16	8.25095E-05
			Prop Mass (kg)	Propeller Inertia (kg m^2)
			0.17778	0.001925174

AB.2.2. Software Development

The software components of the HiL system are the software models of the aircraft, and the software dynamometer controls including electric motor pulse-width modulated (PWM) control, dyno load control and data acquisition. The software models of the aircraft are presented in detail in Chapter 8. This section will concentrate on the other functions of the HiL software.

The electric motor is speed controlled by the aircraft autopilot simulator via a PWM signal that is transmitted by serial from the HiL simulation computer to the dynamometer microcontroller. The dynamometer microcontroller translates the serial command into a TTL PWM command that is transmitted to the electric motor controller. The electric motor speed controller is a variable gain digital proportional controller.

The dynamometer current load is proportional to the absorber torque load, which is equal to the torque applied to the electric motor. The absorber torque is controlled open-loop with a feedforward analog signal supplied to the analog control input of the HP 6050 electronic load. The calibration between the load command to the load sensor (in grams) and the PWM input to the D/A converter is shown in Figure 108.

The signals acquired by the HiL dynamometer data acquisition system are described with sensor specifications in Table 25.

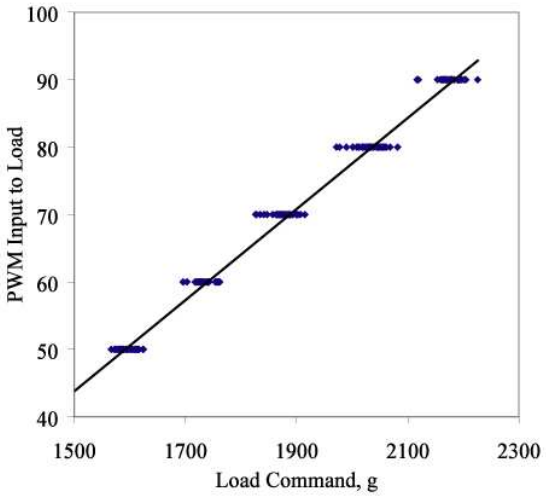

Figure 108. Static feedforward calibration for dynamometer load control

Table 25. Signals acquired by HiL dynamometer data acquisition system

Signal Name	*Sensor Location*	*Transducer*	*Signal Type*
Fuel Cell Net Current	Dynamometer	06709, Simpson, Lac du Flambeau, WI	Analog
Fuel Cell Voltage	Dynamometer	Voltage Divider	Analog
Electric Motor Speed	Dynamometer	Brushed Tachometer	Analog
Electric Motor Torque	Dynamometer	EBB-10, Transducer Techniques, Temecula, CA	Analog
Hydrogen Flow Rate	Dynamometer	FMA-1610A, Omega Engineering, Stamford, CT	RS-232

REFERENCES

[1] Rogers, J.L., "DeMAID/GA: An enhanced design manager's aid for intelligent decomposition," AIAA Paper 96-4157, Sep. 1996.

[2] Sobieszczanski-Sobieski, J., "Sensitivity analysis and multidisciplinary optimization for aircraft design: Recent advances and results," *Journal of Aircraft* Vol. 27, No. 2, 1990.

[3] Borggard, J., and Burns, J., "A PDE sensitivity equation method for optimal aerodynamic design," NASA CR 198349, Jun. 1996.

[4] Mavris, D.N., DeLaurentis, D.A., Bandte, O., and Hale, M.A., "A Stochastic Approach to Multi-disciplinary Aircraft Analysis and Design," AIAA Paper 98-0912, Jan. 1998.

[5] Delucchi, M., "Hydrogen fuel cell vehicles," University of California Davis, Institute for Transportation Studies Report 92-14, Sep. 1992.

[6] Moore, R.M., Gottesfeld, S., and Zelenay, P., "A fuel control strategy that optimizes the efficiency of a direct-methanol fuel cell in an automotive application," Society of Automotive Engineers Paper 1999-01-2913, Aug. 1999.

[7] Crumm, A., "Solid Oxide Fuel Cell Systems," *Proceedings of the Fuel Cell Seminar,* Honolulu, HI, Nov. 2006.

[8] Perry, M.L., and Fuller, T.F., "A historical perspective of fuel cell technology in the 20th century," *Journal of The Electrochemical Society,* Vol. 149, No. 7, pp. S59-S67, 2002.

[9] Prater, K., “Solid polymer fuel cell developments at Ballard,” *Journal of Power Sources*, Vol. 37, 1992, pp. 181-188.

[10] Moffitt, B.A., Bradley, T.H., Parekh, D.E., and Mavris, D., “Design and Performance Validation of a Fuel Cell Unmanned Aerial Vehicle.” AIAA Paper 2006-0823, Jan 2006.

[11] Bradley, T. H., Moffitt, B., Thomas, R. W., Mavris, D. and Parekh, D. E., 2006. “Test Results for a Fuel Cell-Powered Demonstration Aircraft,” Society of Automotive Engineers Paper 2006-01-3092, Nov 2006.

[12] Bradley, T.H., Moffitt, B., Mavris, D., and Parekh, D.E., “Development and Experimental Characterization of a Fuel Cell Powered Aircraft,” *Journal of Power Sources*, Vol. 171, 2007, pp. 793-801.

[13] Moffitt, B.A., Bradley, T.H., Parekh, D.E., and Mavris, D.N., “Design space exploration of small-scale PEM fuel cell unmanned aerial vehicle,” AIAA Paper 2006-7701, Sep. 2006.

[14] Bradley, T.H., Moffitt, B.A., Parekh, D.E., and Mavris, D., “Validated Modeling and Synthesis of Medium-scale PEM Fuel Cell Aircraft,” *4th International ASME Conference on Fuel Cell Science, Engineering and Technology*, Irvine, CA, Jun. 2006.

[15] Moffitt, B A., Bradley, T.H., Parekh, D.E., and Mavris, D. “Vortex propeller model generation and validation with uncertainty analysis for UAV design.” AIAA Paper 2008-406, Jan. 2008.

[16] Moffitt, B., Bradley, T.H., Mavris, D., and Parekh, D.E., "Reducing Design Error of a Fuel Cell UAV through Variable Fidelity Optimization," AIAA Paper 2007-7793, Sep. 2007.

[17] Bradley, T. H., Moffitt, B. A., Fuller, T., Parekh, D. E., and Mavris, D. "Hardware in the loop performance simulation for a fuel cell unmanned aerial vehicle," submitted to *AIAA Journal of Propulsion and Power,* 2008.

[18] Wentz, W.H., and Mohamed, A.S., "Preliminary design considerations for zero greenhouse gas emission airplanes," *SAE Transactions Journal of Aerospace*, vol. 113 No. 1, 2004, pp. 1-16.

[19] Wickenheiser, T.J., Sehra, A.K., Seng, G.T., Freeh, J.E. and Berton, J.J., "Emissionless aircraft: Requirements and challenges," AIAA Paper 2003-2810, July 2003.

[20] Royal Commission on Environmental Pollution, The environmental effects of civil aircraft in flight, 2002.

[21] Penner, J.E., Lister, D., Griggs, D.J. , Dokken, D.J., and McFarland M., Aviation and Global Atmosphere, Cambridge University Press, 1999.

[22] Cadou, C., Moulton, N., and Menon, S., "Performance measurement and scaling in small internal combustion engines," AIAA Paper 2003-671, Jan. 2003.

[23] Hendrickson, S.P., "A miniature powerplant for very small, very long range autonomous aircraft," Insitu Group, Bingen, Washington, 1999.

[24] HATZ Motorenfabrik GmbH, "1B20 Engine Specification Sheet," http://www.hatz-diesel.de/index.php?id=72&L=1, Accessed Jul. 2008.

[25] Mitlitsky, F., Myers, R. and Weisberg, A.H. “Lightweight pressure vessels and unitized regenerative fuel cells,” *Proceedings of the 1996 Fuel Cell Seminar*, Kissimmee, Florida, Nov. 1996.

[26] Aceves, S.M., Berry, G.D., and Rambach, G.D., “Insulated pressure vessels for hydrogen storage on vehicles,” *International Journal of Hydrogen Energy*, Vol. 23, No. 1, 1998, pp. 583-591.

[27] Peschka, W., Liquid Hydrogen, Fuel of the Future. Springer-Verlag. Vienna, Austria, 1998.

[28] Sullivan, R.M., Palco, J.L, Tornabene, R.T., Bednarcyk, B.A., Powers, L.M, Mital, S.K., Smith, L.M., Wang, X.-Y.J., and Hunter, J.E., “Engineering analysis studies for preliminary design of lightweight cryogenic hydrogen tanks in UAV applications,” NASA/TP-2006-214094, 2006.

[29] US Department of Energy, “Hydrogen, fuel cells and infrastructure technologies plan: Multi-year research development and demonstration plan”, 2007.

[30] Schaffer, S., “Development update on Delphi's SOFC system,” SECA Program Review, Boston, MA, 2004.

[31] Dillon, R., Srinivasan. S., Arico, A.S., and Antonucci, V., “*International activities in DMFC R&D: Status of technologies and potential applications*,” in Fuel Cells Compendium (Brandon, N.P., and Thompsett, D., Ed.), Elsevier Science, 2005.

[32] Venturi, M., Kallio, E., Smith. S., Baker, J., and Dhand, P., “Recent results on liquid fuelled APU for truck application,” *SAE Transactions*, Vol. 112, No. 2, 2003, pp. 11-17.

[33] Sanyo Electric Company Ltd., “Lithium polymer rechargeable batteries,” Product Literature, October 10, 2002.

[34] Himansu, A., Freeh, J.E., Steffen, C.J., Tornabene, R.T., and Wang, X.-Y.J., “Hybrid solid oxide fuel cell/gas turbine system design for high altitude long endurance aerospace missions,” NASA/TM-2006-214328, 2006.

[35] Howe, D., Aircraft Conceptual Design Synthesis, Professional Engineering Publishing Ltd. UK, 2005.

[36] EG&G Technical Services, Fuel Cell Handbook, 7th Ed. U.S. Department of Energy, Morgantown, West Virginia, 2004.

[37] Haraldsson, K., Alvfors, P., “Effects of ambient conditions on fuel cell vehicle performance,” *Journal of Power Sources* Vol. 145, 2005, pp. 298-306.

[38] Pratt, J.W., Brouwer, J., and Samuelsen, G.S., “Performance of Proton Exchange Membrane Fuel Cell at High-Altitude Conditions,” *Journal of Propulsion and Power*, Vol. 23, No. 2, 2007, pp. 437-444.

[39] Hauf, T. Schulte, P., Alheit R. and Schlager, H. “Rapid vertical trace gas transport by an isolated midlatitude thunderstorm,” *Journal of Geophysical Research*, Vol. 100, No. D11, pp. 22,957 - 22,970.

[40] Sundstrom, O., and Stefanopoulou, A., “Optimum battery size for fuel cell hybrid electric vehicle – Part I,” *Journal of Fuel Cell Science and Technology* Vol. 4, 2007, pp. 167-175.

[41] Herwerth, C., Chiang, C., Ko, A., Matsuyama, S., Choi, SB., Mirmirani, M., Gamble, D., Arena, A., Koschany A., Gu, G., and Wankewycz, T., “Development

of a Small Long Endurance Hybrid PEM Fuel Cell Powered UAV," Society of Automotive Engineers Paper 2007-01-3930, Sep. 2007.

[42] Putt, R., Naimer, N., and Atwater. T., "Fourth Generation Zinc-Air Batteries," *Proceedings of the 41st Power Sources Conference*, Philadelphia, PA, Jun. 2004.

[43] Menon, S., Moulton, N., and Cadou, C., "Development of a Dynamometer for Measuring Small Internal-Combustion Engine Performance," *Journal of Propulsion and Power*, Vol. 23, No. 1, 2007, pp. 194-202.

[44] Velev, O. "Summary of fuel cell projects: Aerovironment 1997-2007." *National Hydrogen Association Fall 2007 Topical Forum*, Charlotte, SC, Oct. 2007.

[45] AeroVironment Press Release, "AeroVironment flies world's first liquid hydrogen-powered UAV," Jun. 2005.

[46] Scheppat, B. "Betriebsanleitung fuer das brennstoff-zellenbetriebene Modellflugzeug," Fachhochschule Wiesbaden, 2004.

[47] Kellogg, J., "Fuel cells for micro air vehicles," *Joint Service Power Exposition*, Tampa, Florida, May 2005.

[48] California State University Press Release, "Cal State L.A.'s fuel-cell plane passes key flight test," Sep. 2006.

[49] Deutsches Zentrum fuer Luft- und Raumfahrt Press Release, "Erfolgreicher erstflug des Hyfish," April 3, 2007.

[50] Kwon, S., "PEM fuel cell system for UAV," Available online at http://rocket.kaist.ac.kr/03_sub_08.htm

[51] "AeroVironment's unmanned aircraft achieves record flight," *Fuel Cells Bulletin*, Vol. 2007, No. 8, 2007, p. 8.

[52] Freeh, J.E., Pratt, J.W., and Brouwer, J., ”Development of a Solid-Oxide Fuel Cell/Gas Turbine Hybrid System Model for Aerospace Applications,” NASA TM 2004-213054.

[53] Breit, J and Szydlo-Moore, J., “Fuel cells for commercial transport airplanes needs and opportunities,” AIAA Paper 2007-1390, Jan. 2007.

[54] Anderman, M., “Brief assessment of improvements in EV battery technology since the BTAP June 2000 report.” California Air Resources Board, 2003.

[55] Sexton, E.D. and Olson, J.B. “Coulombic efficiency of a sealed, thin plate, spiral lead-acid battery,” *Proceedings of the Thirteenth Annual Battery Conference on Applications and Advance*s, Long Beach, California, Jan. 1998.

[56] Burke, K.A., “High energy density regenerative fuel cell systems for terrestrial applications,” NASA/TM-1999-209429, 1999.

[57] Burke, K.A. “Unitized regenerative fuel cell development,” NASA/TM-2003-212739, 2003.

[58] Noll, T.E., Brown J.M., Perez-Davis M.E., Ishmael, S.D., Tiffany G.C. and Gaier M., “Investigation of the Helios Prototype Aircraft Mishap Volume I Mishap Report,” NASA, Jan. 2004.

[59] Chang, B., Johnson, D.W., Garcia, D.P., Akupca, I.J., Scullin, V.J., and Bents D.J., “Regenerative Fuel Cell Test Rig at Glenn Research Center,” NASA TM 2003-212375.

[60] Friend, M.G., Daggett, D.L., “Fuel cell demonstrator airplane,” AIAA Paper 2003-2868, Jul. 2003.

[61] Kohout, L.L., Schmitz, P.C., “Fuel cell proplulsion systems for an all-electric personal air vehicle.” AIAA Paper 2003-2867, Jul. 2003.

[62] Brewer, G.D., Hydrogen Aircraft Technology, CRC Press, Boca Raton, Florida, 1991.

[63] Dunn J., “Fuel cell aircraft applications,” *Portable Fuel Cell Conference September* Boston, Massachusetts, Sep. 2002.

[64] Dorange, C., “Boeing Successfully Flies Fuel Cell-Powered Airplane,” Boeing News Release, Apr. 2008.

[65] Amphlett, J.C., Baumert, R.M., Mann, R.F., Peppley, B.A., Roberge, P.R., and Harris, T.J., “Performance Modeling of the Ballard Mark IV Solid Polymer Electrolyte Fuel Cell: I Mechanistic Model Development,” *Journal of the Electrochemical Society*, Vol. 142, No. 1, 1995, pp. 1-8.

[66] Amphlett, J.C., Baumert, R.M., Mann, R.F., Peppley, B.A., Roberge, P.R. and Rodrigues A., “Parametric modelling of the performance of a 5kw proton exchange membrane fuel cell stack.” *Journal of Power Sources*, Vol. 49, 1994, pp. 349-356.

[67] Pisani, L., Murgia, G., Valentini, M. and D’Aguanno, B., “A new semi-empirical approach to performance curves of polymer electrolyte fuel cells,” *Journal of Power Sources*, Vol. 108, 2002, pp.192-203.

[68] Kulikovsky, A.A., “The effect of stoichiometric ratio on the performance of a polymer electrolyte fuel cell,” *Electrochimica Acta*, Vol. 49, No. 4, 2004, pp. 617-25.

[69] Amphlett, J.C., Mann, R.F., Peppley, B.A., Roberge, P.R. and Rodrigues, A., "A model predicting transient responses of proton exchange membrane fuel cells," *Journal of Power Sources*, Vol. 61, 1996, pp. 193-188.

[70] Morner, S.O. and Klein, S.A, "Experimental evaluation of the dynamic behavior of an air-breathing fuel cell stack," *Journal of Solar Energy Engineering*, Vol. 123, 2001, pp. 225-231.

[71] Philipps, S.P. and Ziegler, C., "Computationally efficient modeling of the dynamic behavior of a portable PEM fuel cell stack," *Journal of Power Sources* Vol. 180, 2008. pp. 309–321.

[72] Pukrushpan, J.T., Stefanopoulou, A.G., and Peng, H., Control of Fuel Cell Power Systems, Springer (2004).

[73] Rodatz, P., Paganelli, G., and Guzzella, L., "Optimizing air supply control of a PEM fuel cell system," *American Control Conference*, Denver CO Jun. 2003, pp 2043-2048.

[74] Gelfi, S., Stefanopoulou A.G., Pukrushpan, J.T. and Peng, H., "Dynamics of low-pressure and high-pressure fuel cell air supply systems," *American Control Conference*, Denver CO, Jun. 2003. pp 2049-2054.

[75] Cunningham, J.M., Hoffman, M.A., Moore R.M., and Friedman, D.J, "Requirements for a Flexible and Realistic Air Supply Model for Incorporation into a Fuel Cell Vehicle (FCV) System Simulation," Society of Automotive Engineers Paper 1999-01-2912, Aug. 1999.

[76] Grujicic, M., Chittajallu, K.M., Law, E.H., and Pukrushpan, J.T., "Model-based control strategies in the dynamic interaction of air supply and fuel cell,"

Proceedings of the Institution of Mechanical Engineers Part A: Journal of Power and Energy, Vol. 218, No. 7, 2004, pp. 487-499.

[77] Friedman, D.J., Eggert, A., Badrinarayanan, P., and Cunningham, J., "Balancing stack, air supply and water/thermal management demands for an indirect methanol PEM fuel cell system," Society of Automotive Engineers Paper 2001-01-0535, Mar. 2001.

[78] Cao, J. and Djilali, N. "Computational Simulation of Water Transport in PEM Fuel Cells Using an Improved Membrane Model", *10th Canadian Hydrogen Conference*, Quebec City, May 2000, pp. 447-456.

[79] Sun, J., and Kolmanovsky, I., "Load governor for fuel cell oxygen starvation protection: a robust nonlinear reference governer approach," *IEEE Transactions on Control Systems Technology*, Vol. 13, No. 6, Nov. 2005, pp. 911-919.

[80] Frangopoulos, C.A., and Nakos, L.G., "Development of a model for thermoeconomic design and operation optimization of a PEM fuel cell system," *Energy* Vol. 31, 2006, pp. 1501–1519.

[81] Kim, M.-J., and Peng, H., "Power management and design optimization of fuel cell/battery hybrid vehicles," *Journal of Power Sources* Vol. 165, 2007, pp. 819-32.

[82] Na, W., and Gou, B., "The efficient and economic design of PEM fuel cell systems by multi-objective optimization," *Journal of Power Sources* Vol. 166, 2007, pp. 411–418.

[83] Calise, F., Dentice d' Accadia, F., Vanoli, M., and von Spakovsky, M.R., "Single-level optimization of a hybrid SOFC–GT power plant," *Journal of Power Sources* Vol. 159, 2006, pp. 1169–1185.

[84] Xue, D., Dong, Z., "Optimal fuel cell system design considering functional performance and production costs," *Journal of Power Sources* Vol. 76, 1998, pp. 69–80.

[85] Ahluwalia, R.K., Doss, E.D., and Kumar, R., "Performance of High-Temperature Polymer Electrolyte Fuel cell Systems," *Journal of Power Sources*, Vol. 117, 2003, pp. 45-60, 2003.

[86] Cunningham, J., Personal Communication, April 2, 2008.

[87] Roskam, J., Airplane Design Part VI: Preliminary Calculation of Aerodynamic, Thrust and Power Characteristics, DAR Corporation, Lawrence, Kansas, 2000.

[88] Kohutt, L.L., and Schmitz, P.C., "Fuel cell propulsion systems for an all-electric personal air vehicle," NASA TM-2003-212354, 2003.

[89] Nickol, C.L., Guynn, M.D., Kohout, L.L., and Ozoroski, T.A., "High altitude long endurance air vehicle analysis of alternatives and technology requirements development," AIAA Paper 2007-1050, Jan. 2007.

[90] Romeo, G., Frulla, G., Cestino, E., and Corsino G., "HELIPLAT: Design, aerodynamic, structural analysis of long-endurance solar-powered stratospheric platform," *Journal of Aircraft* Vol. 41, No. 6, 2004, pp. 1505-1520.

[91] Colozza, A., "Initial Feasibility Assessment of a High Altitude Long Endurance Airship," NASA/CR-2003-212724.

[92] Youngblood, J., and Talay, T., “Solar powered airplane design for long-endurance, high altitude flight,” AIAA Paper 1982-0811, May 1982.

[93] Youngblood, J. W., Talay, T. A., and Pegg, R. J., “Design of Long-Endurance Unmanned Airplanes Incorporating Solar and Fuel Cell Propulsion,” AIAA Paperj 84-1430, Jun. 1984.

[94] Choi, T.P., Soban D.S., and Mavris, D.N., “Creation of a Design Framework for All-Electric Aircraft Propulsion Architectures,” AIAA Paper 2005-5549, Aug. 2005.

[95] Baldock, N., and Mokhtarzadeh-Dehghan, M.R., “A study of solar-powered, high-altitude unmanned aerial vehicles,” *Aircraft Engineering and Aerospace Technology: An International Journal*, Vol. 78, No. 3, 2006, pp. 187–193.

[96] Qu, Y.C., and Zhao, Y.J., “Energy-Efficient Trajectories of Unmanned Aerial Vehicles Flying through Thermals,” *Journal of Aerospace Engineering*, Vol. 18, No. 2, 2005, pp. 84-92.

[97] Menon, P.K., Sweriduk, G.D., Bowers, A.H., “A study of near-optimal endurance maximizing periodic cruise trajectories,” AIAA Paper 2005-6046, Aug. 2005..

[98] Speyer, J.L., Dannemiller, D., and Walker D., “Periodic Optimal Cruise of an Atmospheric Vehicle.” *Journal of Guidance*, Vol. 8, No. 1, pp. 31-38, 1985.

[99] Chen, R.H., and Speyer, J.L., “Improved Endurance of Optimal Periodic Flight,” *Journal of Guidance, Control and Dynamics*, Vol. 30, No. 4, 2007, pp. 1123-33.

[100] Guzzella, L, and Amstutz, A., “CAE Tools for Quasi-Static Modeling and Optimization of Hybrid Powertrains,” *IEEE Transactions on Vehicular Technology*, Vol. 48, No. 6, 1999, pp. 1762-1769.

[101] O'Keefe, M.P., Markel, T., "Dynamic programming applied to investigate energy management strategies for plug-in HEV," NREL/CP-540-40376, 2006.

[102] W. L. Gore & Associates, Inc. "Gore Primea 58 Series Membranes," Product Literature, 2003.

[103] Colozza, A.J., "Hydrogen storage for aircraft applications overview," NASA/CR—2002-211867, 2002.

[104] Lark, R. F., "Recent advances in lightweight, filament-wound composite pressure vessel technology," *Energy Technology Conference*, Houston, TX, Sept. 1977.

[105] Shigley, J., Mischke, C. and Budynas, R. Mechanical Engineering Design. 7th Edition, McGraw-Hill, New York.

[106] Kulkarni, S. V., and Zweben, C. H., Composites in pressure vessels and piping. American Society of Mechanical Engineers, New York, 1977.

[107] Harris, J., Grande, R. and Higgins, M., "Ultralight propellant tank for NASA space technology 5," AIAA Paper 2003-4608, Jul. 2003.

[108] McQuarrie, D. A., and Simon, J. D., Physical Chemistry: A Molecular Approach, University Science Books, Sausalito, CA 1997.

[109] Phillips, W.F., and Snyder, D.O., "Modern adaptation of Prandtl's classic lifting-line theory," *Journal of Aircraft*, Vol. 37, No. 4, 2000, pp. 662-670.

[110] Lyon, C.A., Broeren, A.P., Giguere, P., Gopalarathnam, A., Selig, M.S., Summary of Low-Speed Airfoil Data: Volume 3, SoarTech Publications, Virginia Beach, Virginia: 1997.

[111] Goldstein, S., "On the Vortex Theory of Screw Propellers," *Proceedings of the Royal Society of London*, Series A. Vol. 123, No. 792, pp. 440-495, 1929.

[112] Lowry, J. T., Performance of Light Aircraft, AIAA Education Series, Reston, Virginia, 1999.

[113] Vanderplaats, G.N., Numerical Optimization Techniques for Engineering Design, McGraw Hill, New York, 1984.

[114] McDonald, R., "Error Propagation and Metamodeling for a Fidelity Tradeoff Capability in Complex Systems Design," PhD Dissertation, Georgia Institute of Technology, 2006.

[115] Ninness, B., and Goodwin, G.C., "Estimation of model quality," *Automatica*. Vol. 31, No. 12, 1995, pp. 1771-1797.

[116] Pederson, K., Emblemsvag, J., Bailey, R., Allen, J.K., and Mistree, F., "The 'Validation Square' – Validating Design Methods," American Society of Mechanical Engineers Paper DETC2000/DTM-14579, Nov. 2000.

[117] Grande, R., "Composite Pressure Vessel Product List," Carleton Technologies Inc., 2007.

[118] Merchant, M., and Miller, L.S., "Propeller performance measurement for low Reynolds number UAV applications," AIAA Paper 2006-1127, Jan. 2006.

[119] ImSAR LLC, "NanoSAR – World's smallest SAR," 2008. http://www.imsar.net/NanoSAR%20Flyer_03_08.pdf

[120] Choi, T.P., "A recourse-based solution approach to the design of fuel cell aeropropulsion systems," PhD Dissertation, Georgia Institute of Technology, 2008.

[121] Keidel, B., "Auslegung und Simulation von hochfliegenden, dauerhaft stationierbaren Solardrohnen," PhD Dissertation, Technischen Universität München, 2000.

[122] Zhang S.S., Xu K., and Jow T.R., “Charge and discharge characteristics of a commercial LiCoO2-based 18650 Li-ion battery,” *Journal of Power Sources*, Vol. 160, 2006, pp. 1403–1409.

[123] Schmalle III, D.G., Dingus, B.R and Reinholtz, C. “Development and application of an autonomous unmanned aerial vehicle for precise aerobiological sampling above agricultural fields,” *Journal of Field Robotics* Vol. 25, No. 3, 1008, pp. 133–147.

[124] Dhar, H.P., “Near ambient unhumidified solid polymer fuel cell,” US Patent No. 5,242,764, September 7, 1993.

[125] Zawodzinki, T.A., Derouin, C., Radzinski, S., Sherman, R.J., Smith, V.T., Springer, T.E., and Gottesfeld, S., “Water uptake by and transport through Nafion 117 membranes,” *Journal of the Electrochemical Society* Vol. 140, 1993, pp. 1041-1047.

[126] Phillips, W.F., Mechanics of Flight, John Wiley and Sons, Inc., Hoboken, New Jersey, 2004.

[127] Kline, S.J., and McClintock, F.A., “Describing Uncertainties in Single-Sample Experiments,” *Mechanical Engineering*, Vol. 75, 1953, pp. 3-7.

[128] Hwang, J.J., Wang, D.Y., and Shih, N.C., “Development of a lightweight fuel cell vehicle,” Journal of Power Sources, Vol. 141, 2005, pp. 108–115.

[129] Hwang, J.J., Wang, D.Y., Shih, N.C., Lai, D.Y. and Chen, C.K., "Development of fuel-cell-powered electric bicycle," Journal of Power Sources, Vol. 133, 2004, pp. 223–228.

[130] Susai, T., Kawakami, A., Hamada, A., Miyake, Y., and Azegami, Y., "Development of a 1 kW polymer electrolyte fuel cell power source," *Journal of Power Sources*, Vol. 92, 2001, pp. 131-138.

[131] Atwood, P., Gurski, S., Nelson, D.J., and Wipke, K.B., "Degree of hybridization modeling of a fuel cell hybrid electric sport utility vehicle," Society of Automotive Engineers Paper 2001-01-0236, Mar. 2001.

[132] Kosmatka, J.B., "Development of a long-range small UAV for atmospheric testing." AIAA Paper 2007-2234, Apr. 2007.

[133] Tigner, B., Meyer, M.J., Holden, M.E., Rawdon, B.K., Page, M.A., Watson, W., and Kroo, I. "Test techniques for small scale research aircraft," AIAA Paper 98-2726, Jun. 1998

[134] Bateman, T.A., Nelson, J.D., and Argrow, B.M., "A low-cost rapid construction unmanned aircraft design." AIAA Paper 2007-2703, May 2007.

[135] Howard, R.M., Tanner, J.C., and Lyons, D.F., "Flight test of a half-scale unmanned air vehicle." *Journal of Aircraft*, Vol. 28, No. 12, 1991, pp. 843-8.

[136] Mackall, D.A., "Qualification needs for advanced integrated aircraft," NASA TM-86731, 1985.

[137] Fathy, H.K., Filipi, Z.S., Hagena, J., and Stein, J.L., "Review of hardware-in-the-loop simulation and its prospects in the automotive area." *Proceedings of SPIE*, Vol. 6228E, 2006, pp. 1-20.

[138] Hamelin, J., Agbossou, K., Laperriere, A., Laurencelle, F., and Bose, T.K., "Dynamic behavior of a PEM fuel cell stack for stationary applications," *International Journal of Hydrogen Energy*, Vol. 26, 2001, pp. 625-629.

[139] Bi W., Gray, G.E. and Fuller, T.F., "PEM fuel cell Pt/C dissolution and deposition in Nafion electrolyte," *Electrochemical and Solid-State Letters*, Vol. 10, No. 5, 2007, pp B101.